VNIVERSITAT DE VALÈNCIA

Some Aspects of Chiral Perturbation Theory and Neutrino Physics

Tesis Doctoral

Doctorado en Física

Mayo 2017

Mehran Zahiri Abyaneh

IFIC - Universitat de València - CSIC
Departament de Física Teòrica

Director: Antonio Pich Zardoya

To My Mother and Deceased Father

Antonio Pich Zardoya,
catedrático de la Universidad de Valencia,

CERTIFICA:

Que la presente memoria "Some Aspects of Chiral Perturbation Theory and Neutrino Physics" ha sido realizada bajo su dirección en el Instituto de Física Corpuscular, centro mixto de la Universidad de Valencia y del CSIC, por Mehran Zahiri Abyaneh y constituye su Tesis para optar al grado de Doctor en Física.

Y para que así conste, en cumplimiento de la legislación vigente, presenta en el Departamento de Física Teórica de la Universidad de Valencia la referida Tesis Doctoral, y firma el presente certificado.

Valencia, a 30 de Mayo de 2017.

Antonio Pich Zardoya

Contents

Introduction

The advent of Spontaneous Symmetry Breaking (SSB) by Yoichiro Nambu [1]–[3] from Superconductivity to the particle physics community was the beginning of an era, whose consequences are still fruitful. SSB is a phenomenon where a symmetry in the basic laws of physics appears to be broken. For example, when an standing straight rod which has the rotational symmetry, that is, it looks the same from any horizontal direction, is pressurized from the top, it will bend in some direction, and the rotational symmetry is lost. Since all directions are equivalently probable to be chosen for bending, one says the symmetry is broken spontaneously. There are many examples of SSB in Quantum mechanics and solid state physics. For example, ferro-magnets, rotational invariance in crystals, etc.

In the language of Quantum Field Theory (QFT), a system is said to possess a symmetry that is spontaneously broken if the Lagrangian describing the dynamics of the system is invariant under these symmetry transformations, but the vacuum is not [4]. Since, the vacuum has many intrinsic degrees of freedom, SSB can play an important role and as the universe expands and cools down, several SSB phase transitions from states of higher symmetries to lower ones might have happened. In fact, this is the ultimate dream of the particle physics community to realize, what was the original symmetry of nature, before any SSB took place.

The SSB can happen in two ways that is, the symmetry which is broken can be global or local, which has completely different consequences. We will here describe briefly both types of SSB and then will consider some examples of each in coming chapters. Lectures about the phenomenon of spontaneous symmetry breaking of a global symmetry and how the situation changes in the presence of a local gauge symmetry can be found in refs. [5, 6].

First a recount of the history as Nambu describes it himself [1], *One day before publication of the BCS paper, Bob Schrieffer, still a student, came to Chicago to give a seminar on the BCS theory in progress ... I was very much disturbed by the fact that their wave function did not conserve electron number. It did not make sense ... At the same time I was impressed by their boldness and tried to understand the problem.* So, the main reason which led him to the idea was the fact that, as it turns out, in the BCS model of superconductivity [7], the quasi

particles introduced by Bogoliubov [8] and Valatin [9](BV), which are the building blocks of the Cooper pairs, seem not to have a definite charge. This means that the electric charge is not conserved which leads to problems for electromagnetic phenomena like the Meissner effect. Therefore, he introduced the notion of a massless spin–zero collective mode; to be called later on the Nambu–Goldstone (NG) boson; that appears due to the spontaneously broken continuous gauge symmetry and rescues the charge conservation [2]. This is an example of the SSB for a local symmetry or as Weinberg puts it [10], *A superconductor is simply a material in which electromagnetic gauge invariance is spontaneously broken.*

Soon after the introduction of the notion of the spontaneously broken continuous local symmetry in superconductors, due to the similarity of the BV equation to the Dirac equation, Nambu and Jona-Lasinio (NJL) transported the BCS theory to nuclear physics [3]. In this case, the axial symmetry as an approximately conserved *global* symmetry in flavor space, is spontaneously broken. Therefore, the nucleon mass is generated by an SSB of chirality, and the pion is the NG boson of this symmetry breaking. In the limit of exact conservation, the pion will become massless and the proton and the neutron masses will also become the same.

On the other hand, in 1962 Goldstone showed [11] that spontaneous breaking of a global symmetry in a relativistic field theory results in massless spin-zero bosons. According to the Goldstone theorem: *if a theory has a global symmetry of the Lagrangian, which is not a symmetry of the vacuum, then there must exist one massless boson, scalar or pseudoscalar, associated to each generator which does not annihilate the vacuum and having its same quantum numbers. These modes are referred to as Nambu-Goldstone bosons or simply as Goldstone bosons.*

So, the NJL model is an example of SSB, where the Goldstone theorem applies. It was the first model to introduce pion as a Nambu-Goldstone boson of the broken chiral symmetry in QCD, but not the last one. In fact, it suffers from lack of confinement and is nonrenormalizable in four space–time dimensions. Therefore, this model is regarded as an effective theory for the QCD, which needs to be UV completed. There are other effective theories to describe dynamics of mesons like Chiral perturbation Theory (ChPT), which we will discuss in detail later on, after introducing the notion of effective field theories in general. We will also discuss a work related to ChPT.

Back to the history, after Goldstone's prediction of massless modes, the problem was that apart from the pions in nuclear physics, they were excluded experimentally in QFT and therefore, at the time the application of SSB to the QFT was not clear. In fact, solution to this problem also came from the solid state

community. The year before Goldstone published his paper, Philip Anderson had pointed out [12] that, in a superconductor where the local gauge symmetry is broken spontaneously, the Goldstone (plasmon) mode becomes massive due to the gauge field interaction and is effectively eaten by the photon to become a finite-mass longitudinal mode (Meissner effect), despite the gauge invariance. But, he did not discuss any relativistic model and so, since Lorentz invariance was a crucial ingredient of the Goldstone theorem, he did not demonstrate that NG modes could be evaded.

Finally, following the work of Goldstone, Anderson and Nambu, in 1964 realistic models with Lorentz invariance and non-Abelian gauge fields were formulated by Higgs and others [13,14]. They showed that in the case when a gauge symmetry is broken spontaneously, the Goldstone's theorem does not apply and another mechanism comes to rescue, the so-called Higgs mechanism [13]. *The would-be Goldstone bosons associated to the global symmetry breaking do not manifest explicitly in the physical spectrum but instead they combine with the massless gauge bosons and as a result, once the spectrum of the theory is built up on the asymmetrical vacuum, there appear massive vector particles. The number of vector bosons that acquire a mass is precisely equal to the number of these would-be-Goldstone bosons.* This led Glashow–Weinberg–Salam (GWS) [15–17] to develop the electroweak theory as a part of the Standard Model of particle physics (SM). We will describe the SM of Electroweak (EW) interactions in the next chapter and will present two works related to the Higgs mechanism later on, in the framework of the neutrino physics.

As a side note, Higgs also predicted that due to this SSB a new scalar mode will appear in the particle spectrum of the theory, nowadays known as the Higgs boson. This was finally detected in 2012 in the Large Hadron Collider at CERN. But ironically, the only Higgs boson to be discovered experimentally before 2012 was also detected in solid state physics as an unexpected feature of the Raman spectrum of $NbSe2$, an oscillation of the amplitude of the superconducting gap [18],

The outline of this thesis is the following. In chapter 1 we will discuss the Standard Model of electroweak interactions, which is also relevant to neutrino physics. The chapter 2 briefly introduces the notion of effective field theories and discusses symmetries of the QCD Lagrangian in the flavor space. Afterwards, it introduces the ChPT as an effective field theory. A prologue to the paper on ChPT is given at the end of this chapter. In chapter 3, using the information from previous chapters, the neutrino physics is considered, where the Renormalization Group (RG) equations for neutrino parameters are also discussed. A prologue to

the two papers, related to neutrino physics, is given at the end of this chapter. The three papers constituting the bulk of the thesis are presented subsequently.

Bibliography

[1] Y. Nambu, Nobel Lecture, December 8, (2008).

[2] Y.Nambu, Phys. Rev. **117**, 648 (1960), Y. Nambu, Phys. Rev. Lett. **4**, 380 (1960).

[3] Y. Nambu and G. Jona-Lasinio, Phys. Rev. **122**, 345 (1961); Phys. Rev. **124**, 246 (1961).

[4] M. J. Herrero, arXiv:9812242 [hep-ph]

[5] R. Brout, hep-th/0203096.

[6] F. Englert, arXiv:1204.5382 [hep-th].

[7] J. Bardeen, L. N. Cooper, and J. R. Schrieffer, Phys. Rev. **108**, 1175 (1957).

[8] N. N. Bogoliubov, J. Exptl. Theoret. Phys. (U.S.S.R.)**34** (1958), 58.

[9] G. Valatin, Nuovo Cimento **7**, 843 (1958).

[10] S. Weinberg, The Quantum Theory of Fields, vol. **II**, Cambridge University Press, Cambridge, (1996).

[11] J. Goldstone, A. Salam and S. Weinberg, Phys. Rev. **127**, 965 (1962).

[12] P. W. Anderson, Phys. Rev. **130** (1963) 439. doi:10.1103/PhysRev.130.439

[13] P.W. Higgs, Phys. Rev. Lett. **13**, 508 (1964)

[14] F. Englert and R. Brout, Phys. Rev. Lett. **13**, 321 (1964).

[15] S.L.Glashow, Nucl. Phys. **22**, 579 (1961).

[16] A. Salam, Conf. Proc. C **680519**, 367 (1968).

[17] S. Weinberg, Phys. Rev. Lett. **19**, 1264 (1967).

[18] P. B. Littlewood and C. M. Varma, Phys. Rev. B. **26**, 4883 (1982)

1. The Standard Model of Particle Physics

The Standard Model of particle physics is one of the most successful models in modern physics, based on the gauge group $SU(3)_C \times SU(2)_L \times U(1)_Y$, which describes the fundamental building blocks of nature and their interactions. It includes strong interactions under $SU(3)_C$, and weak interactions and the electromagnetic interactions, unified in the EW interaction under the gauge group $SU(2)_L \times U(1)_Y$. A pedagogical review to the SM as a gauge theory can be found in Ref. [1].

The SM describes three out of the four fundamental interactions, but not gravity. All of these interactions are mediated by the exchange of particles, called gauge bosons. The mediator of the electromagnetic interaction is the photon, for the strong interaction they are called gluons, and the weak interaction is mediated by massive vector bosons called W and Z bosons. On the other side, the SM contains three generations of fermions, each including two quarks and two leptons. The particle content of the SM and the corresponding quantum numbers are shown below

$$1^{st} \text{ family: } \psi_{L_1^l} = \begin{pmatrix} \nu_e \\ e^- \end{pmatrix}_L, \psi_{R_1^l} = e_R^-, \psi_{L_1^q} = \begin{pmatrix} u \\ d \end{pmatrix}_L, \psi_{R_1^q} = u_R, d_R$$

$$2^{nd} \text{ family: } \psi_{L_2^l} = \begin{pmatrix} \nu_\mu \\ \mu^- \end{pmatrix}_L, \psi_{R_2^l} = \mu_R^-, \psi_{L_2^q} = \begin{pmatrix} c \\ s \end{pmatrix}_L, \psi_{R_2^q} = c_R, s_R$$

$$3^{rd} \text{ family: } \psi_{L_3^l} = \begin{pmatrix} \nu_\tau \\ \tau^- \end{pmatrix}_L, \psi_{R_3^l} = \tau_R^-, \psi_{L_3^q} = \begin{pmatrix} t \\ b \end{pmatrix}_L, \psi_{R_3^q} = t_R, b_R$$

where the upper index l (q) stands for quark (lepton) and the anti particles also have to be added. As it can be seen, there is no right handed counterpart for

neutrinos in the SM. The SM particles have certain quantum numbers, under $SU(2)_L \times U(1)_Y$ transformations, which are listed in the following table.

	T	T_3	Y	Q
ν_e	$1/2$	$1/2$	-1	0
$e_{_L}$	$1/2$	$-1/2$	-1	-1
$e_{_R}$	0	0	-2	-1
$u_{_L}$	$1/2$	$1/2$	$1/3$	$2/3$
$d_{_L}$	$1/2$	$-1/2$	$1/3$	$-1/3$
$u_{_R}$	0	0	$4/3$	$2/3$
$d_{_R}$	0	0	$-2/3$	$-1/3$

(1.1)

Where the Hypercharge Y, and the electric charge Q, of these particles are related via

$$Q = \frac{Y}{2} + T_3 \,. \tag{1.2}$$

The Lagrangian of the EW Theory in a generic form can be written as [2]

$$\mathcal{L}_{SM} \equiv \mathcal{L}_0 + \mathcal{L}_G + \mathcal{L}_{SSB} + \mathcal{L}_Y \,.$$

The $\mathcal{L}_0$ is the kinetic term for fermions. After implementing the local gauge invariance the normal derivative transforms into the covariant derivative

$$D_\mu \;\equiv\; \partial_\mu - i g_s \mathbf{G}_\mu - i\, g\, \mathbf{W}_\mu - i\, g' \frac{Y}{2} B_\mu \,,$$

where $\mathbf{W}_\mu = W^a_\mu \sigma_a/2$, $\mathbf{G}_\mu = G^a_\mu \lambda_a/2$. G^a_μ, W^a_μ and B_μ are the gauge fields of $SU(3)_C$, $SU(2)_L$ and $U(1)_Y$ respectively and λ_a are the Gell–Mann matrices. Also, g_s, g and g' are the corresponding gauge couplings. Then $\mathcal{L}_0$ takes the form [1]

$$\mathcal{L}_0 \;=\; \sum_{q,l} \sum_{L,R} \sum_{j=1}^{3} i\, \overline{\psi}_j(x)\, \gamma^\mu\, D_\mu \psi_j(x) \,, \tag{1.3}$$

where ψ is a generic notation for quarks and lepton fields introduced above. In the rest of the thesis the sum over fermion field ψ is understood to be for all families and both chiralities, unless it is stressed. $\mathcal{L}_G$ is constructed by adding the gauge invariant kinetic terms for the gauge fields

$$\mathcal{L}_G = -\tfrac{1}{4} G^a_{\mu\nu} G^{\mu\nu}_a - \tfrac{1}{4} W^a_{\mu\nu} W^{\mu\nu}_a - \tfrac{1}{4} B_{\mu\nu} B^{\mu\nu} \;\;,$$

which is written in terms of the field strength tensors,

$$G^a_{\mu\nu} = \partial_\mu G^a_\nu - \partial_\nu G^a_\mu + g_s f^{abc} G^b_\mu G^c_\nu \,,$$

$$W^a_{\mu\nu} = \partial_\mu W^a_\nu - \partial_\nu W^a_\mu + g\epsilon^{abc} W^b_\mu W^c_\nu \,,$$
$$B_{\mu\nu} = \partial_\mu B_\nu - \partial_\nu B_\mu$$

and $f^{abc}(\epsilon^{abc})$ are the structure constants for the $SU(3)(SU(2))$ groups. The conserved charges for $SU(3), SU(2)$ and $U(1)$ are called color, weak isospin and hypercharge.

The Higgs Mechanism

In this section we describe the $\mathcal{L}_{SSB} + \mathcal{L}_Y$ part of the Lagrangian (1), which is the part related to the SSB. As was described earlier, due to the requirement of the gauge invariance, the bosons and fermions of the SM should be massless. However, this is not what we observe in nature. Therefore, they get mass via the Higgs mechanism, where the EW symmetry gets spontaneously broken to the electromagnetic $U(1)_{\rm em}$ group due to a non-vanishing vacuum expectation value (vev) of a scalar doublet, namely, the Higgs field.

Hence, one introduces an additional field Φ (the Higgs field), that interacts with the gauge sector in a gauge and Lorentz invariant manner and whose self-interactions, must produce the wanted breaking, $SU(2)_L \times U(1)_Y \to U(1)_{\rm em}$. This happens by Φ attaining a non zero vacuum expectation value $\langle 0|\Phi|0\rangle \neq 0$.

The SSB of the EW theory is based on the following Lagrangian

$$\begin{aligned} \mathcal{L}_{SSB} &= (D_\mu \Phi)^\dagger (D^\mu \Phi) - V(\Phi) \\ V(\Phi) &= -\mu^2 \Phi^\dagger \Phi + \lambda (\Phi^\dagger \Phi)^2 \; ; \; \lambda > 0 \end{aligned}$$

where,

$$\Phi = \begin{pmatrix} \phi^+ \\ \phi_0 \end{pmatrix} . \tag{1.4}$$

Here Φ is a fundamental complex doublet with hypercharge $Y(\Phi) = 1$ and $V(\Phi)$ is the simplest renormalizable potential.

There are two possibilities for the v.e.v. $< 0|\Phi|0 >$ that minimizes the potential $V(\Phi)$, Fig. 1.1, depending if $-\mu^2 > 0$, or $-\mu^2 < 0$.

1) $(-\mu^2) > 0$: The minimum is at:

$$< 0|\Phi|0 >= 0 \,. \tag{1.5}$$

The vacuum is symmetric and therefore no symmetry breaking occurs.

2) $(-\mu^2) < 0$: Which is the interesting case, there are infinite degenerate vacua which can break the $SU(2)_L \times U(1)_Y$. The simplest choice which also respects the $U(1)_{em}$ of the vacuum is:

$$< 0|\Phi|0 >= \begin{pmatrix} 0 \\ \frac{v}{\sqrt{2}} \end{pmatrix} \; ; \quad v \equiv \sqrt{\frac{\mu^2}{\lambda}} \, . \tag{1.6}$$

The physical spectrum is built by performing 'small oscillations' around

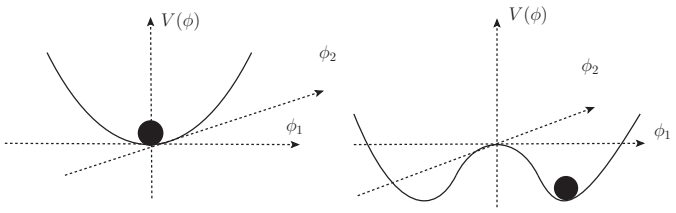

Figure 1.1: The Higgs potential. The diagram on the left belongs to the case 1 (1.5) and the diagram on the right to the case 2 (1.6), where the continuous symmetry in the $\phi_1 - \phi_2$ plane can break in infinite different directions.

this vacuum. These are parametrized by

$$\Phi(x) = \exp\left(i\frac{\vec{\xi}(x)\vec{\sigma}}{v}\right)\begin{pmatrix} 0 \\ \frac{v+H(x)}{\sqrt{2}} \end{pmatrix} , \tag{1.7}$$

where $\vec{\xi}(x)$ and $H(x)$ are small fields. Then, the $\vec{\xi}(x)$ fields are gauged away, and the kinetic piece of the scalar Lagrangian leads, after diagonalization, to the mass term of the gauge bosons and the Higgs boson H

$$\begin{aligned} (D_\mu \Phi')^\dagger (D^\mu \Phi') &= \left(\frac{g^2 v^2}{4}\right) W_\mu^+ W^{\mu -} + \frac{1}{2}\left(\frac{(g^2+g'^2)v^2}{4}\right) Z_\mu Z^\mu + ... \\ V(\Phi') &= \frac{1}{2}(2\mu^2)H^2 + ... \end{aligned} \tag{1.8}$$

and we get finally the tree level predictions:

$$\begin{aligned} M_W &= \frac{gv}{2}\,,\; M_Z = \frac{\sqrt{g^2+g'^2}v}{2}\,, \\ M_H &= \sqrt{2}\mu\,. \end{aligned} \tag{1.9}$$

The physical $W^{\pm}$, Z and A fields are linear combinations of the original W and B fields:

$$\begin{aligned} W^{\pm}_{\mu} &= \frac{W'^1_{\mu} \mp i W'^2_{\mu}}{\sqrt{2}}, \\ Z_{\mu} &= c_w W'^3_{\mu} - s_w B'_{\mu}, \\ A_{\mu} &= s_w W'^3_{\mu} + c_w B'_{\mu}, \end{aligned} \tag{1.10}$$

where θ is the Weinberg angle $\tan\theta = g'/g$. As can be seen the photon has remained massless.

Now, by rewriting the SSB part of the above Lagrangian as

$$\mathcal{L}_{SBS} + \mathcal{L}_Y \rightarrow \mathcal{L}_H^{\rm free} + \mathcal{L}_H^{\rm int} + \dots\,,$$

where

$$\mathcal{L}_H^{\rm free} = \tfrac{1}{2}\partial_\mu H \partial^\mu H - \tfrac{1}{2} M_H^2 H^2\,,$$

one finds the self interaction terms of the Higgs field as well as its interactions with gauge bosons and the fermion fields to be

$$\begin{aligned} \mathcal{L}_H^{\rm int} = &-\frac{M_H^2}{2v}H^3 - \frac{M_H^2}{8v^2}H^4 - \frac{m_f}{v}\overline{\psi}H\psi + M_W^2 W^+_\mu W^\mu - \left(1 + \frac{2}{v}H + \frac{1}{v^2}H^2\right) \\ &+ \frac{1}{2}M_Z^2 Z_\mu Z^\mu \left(1 + \frac{2}{v}H + \frac{1}{v^2}H^2\right)\,, \end{aligned} \tag{1.11}$$

where ψ stands for the fermion field (see relation (1.3)). The masses of the fermions of all three generations come from the Yukawa Lagrangian

$$\begin{aligned} \mathcal{L}_Y = &-\lambda^{(d)}_{ij}\left(\bar{u}, \bar{d}\right)_{L\,i} \Phi d_{R\,j} - \lambda^{(u)}_{ij}\left(\bar{u}, \bar{d}\right)_{L\,i} \Phi^{\rm c}\, u_{R\,j} \\ &- \lambda^{(l)}_{ij}\left(\bar{\nu}_l, \bar{l}\right)_{L\,i} \Phi\, l_{R\,j} + \text{h.c.}\,, \end{aligned} \tag{1.12}$$

where λ_{ij} are the Yukawa couplings, Φ is defined in (1.4) and u, d and l are the quarks and charged leptons fields in the so-called flavour basis. Also $\Phi^{\rm c} = i\sigma_2\phi^*$ which carries hypercharge -1. After the SSB this takes the form

$$\mathcal{L}_Y \;=\; -\,(1+\frac{H}{v})\,\left\{\bar{d}_L M_d\, d_R + \bar{u}_L M_u\, u_R + \bar{l}_L M_l\; l_R\right\}\,. \tag{1.13}$$

As can bee seen, neutrinos remain massless because no Yukawa term can be written for them, since there are no right-handed components.

The matrices M are not diagonal, but can be diagonalized with two unitary matrices U and W such that

$$M_u = U_u^\dagger M_{u_d} W_u \qquad M_d = U_d^\dagger M_{d_d} W_d \qquad M_l = U_l^\dagger M_{l_d} W_l\;. \tag{1.14}$$

Then the mass eigen–states of the quarks and lepton fields become

$$\begin{aligned} d'_L &= U_d d_L \qquad u'_L = U_u u_L \qquad l'_L = U_l l_L \\ d'_R &= W_d d_R \qquad u'_R = W_u u_R \qquad l'_R = W_l l_R\,. \end{aligned} \tag{1.15}$$

This transformation on the fields introduces flavour mixing in the charged current (CC) interactions

$$\mathcal{L}_{\rm CC} \;=\; -\frac{g}{2\sqrt{2}}\,\left\{W_\mu^\dagger\,\left[\bar{u}'_i\gamma^\mu(1-\gamma_5)V_{ij}d'_j \;+\; \bar{\nu}'_l\gamma^\mu(1-\gamma_5)l'\right] \;+\; \text{h.c.}\right\}\,, \tag{1.16}$$

where $V = U_u U_d^\dagger$ is the Cabibbo-Kobayashi-Maskawa (CKM) matrix [3, 4].

Since in the SM neutrinos are massless, there is no need to define a CKM type matrix for the leptonic sector because in that case one can always redefine the neutrino flavours, so that $\bar{\nu}_L l_L = \bar{\nu}_L U_l^\dagger l'_L = \bar{\nu}'_L l'_L$. But, when they are assumed to be massive a similar procedure as for the quarks will be assumed which, will be discussed in the next chapters.

Shortcomings of the SM

Although the SM is very successful, we know that it cannot be the final description of nature. Despite its very accurate predictions, there are a number of observations that do not fall within the scope of what the SM can describe. The most overwhelming problem of the SM is the fact that

it does not contain gravity. Apart from this, the SM does not have a viable dark matter candidate and is not capable of describing the baryon asymmetry of the Universe in a satisfactory way.

Another issue which is more relevant to our work is that there are no neutrino masses in the model. On the other hand, it is necessary to give mass to neutrinos to describe neutrino oscillations, a phenomenon that will be treated extensively in the next chapter. In this case there will appear a mixing in the lepton sector similar to that in the quark sector described above.

One could give the Dirac type of mass to the neutrinos by introducing a right handed degree of freedom to the SM similar to the charged leptons. Also, one could introduce a dimensional five operator, which gives the Majorana mass to the left handed neutrinos (see next chapter). However, both of these scenarios are beyond the SM, even though the Higgs mechanism is at work in both cases.

To conclude, even though the SM has been utterly successful in describing particle interactions, an underlying model is necessary to be a theoretical model consistent with these observations and to be able to produce the same results as the SM ones in the energy range that it is applicable.

Bibliography

[1] A. Pich, arXiv:0705.4264 [hep-ph].

[2] M.J.Herrero, arXiv:9812242 [hep-ph]

[3] M. Kobayashi and T. Maskawa, Prog. Theor. Phys.,**49**, 652 (1973).

[4] N. Cabibbo, Phys. Rev. Lett. **10**, 531 (1963).

2. Effective Field Theories and ChPT

The basic premise of all the effective theories is that dynamics at low energies (or large distances) do not depend on the details of the dynamics at high energies (or short distances) [1, 2]. For example, if we want to study the motion of a macroscopic object, a ball, we will not care at all about the internal dynamics of the molecules, atoms, nuclei or quarks. These will not macroscopically produce any significant modification. The reason is that the macroscopic object lives at scales (meters) widely separated from e.g. the quarks' ones ($\simeq 10^{-15}$ meters).

When we say low energy physics we mean those processes that happen at an energy smaller than a certain scale Λ. The value of such a scale depends on the particular system we study. Low-energy physics can be described using an effective Lagrangian that contains only a few degrees of freedom, ignoring additional degrees of freedom present at higher energies. This is clearly an approximation to the problem, which can always be improved adding corrections induced by the neglected energy scales. Eventually we will need to check that a more complete description including all the degrees of freedom (both heavy or light) gives the same outcomes as the effective theory, at least approximately.

In fact, there is a theorem ascribed to Weinberg which states [6]: For a given set of asymptotic states, perturbation theory with the most general Lagrangian containing all the terms allowed by the assumed symmetries will yield the most general S-matrix elements consistent with analyticity, perturbative unitarity, cluster decomposition and the assumed symmetries. In other words, regardless of the underlying theory, when the degrees of freedom and the symmetries relevant to the energy scale at hand are known, the effective Lagrangian built based on them will address the same physics of the underlying theory. So, when studying a specific phenomenon, it is

necessary to isolate the most relevant ingredients from the rest, so that one can obtain a simple description without having to understand everything.

Let us show how an effective field theory is built up. As we said, one must find a good set of variables to describe the dynamics of the system under study, which means one must select the relevant degrees of freedom. Thus we select the fields we want to include in our description and build up the Lagrangian starting from them. To do this we find out the symmetries of the system and write down all the operators invariant under those symmetries. The resulting Lagrangian is a sum of operators O_i [1]

$$\mathcal{L} = \sum_i C_i O_i \,. \tag{2.1}$$

The operators O_i are built out of the fields and their derivatives and the constants C_i are couplings. They determine how important the operator they multiply is.

We are already facing a problem in (2.1). In principle there is no limit to the number of operators satisfying the symmetries we have required. But we can not calculate the probability amplitudes with an infinite number of operators. However dimensional analysis offers us a way out. The Lagrangian density has dimension four in power of masses thus each term $C_i O_i$ in the sum (2.1) must have dimension four. This means that if the dimension of the operator O_i is d_i, then the coupling C_i must have dimension $-d_i + 4$.

There is another striking feature in (2.1) that we have not observed yet. The operators O_i contain only the light degrees of freedom, the light fields. However, this Lagrangian must also contain the information of the heavy degrees of freedom. These information can only be encoded then in the C_i which therefore must somehow depend on the high energy scales, so on Λ.

This last consideration, together with the dimensional analysis done before, leads us to assume that the C_i couplings scale as

$$C_i \simeq \frac{1}{\Lambda^{d_i-4}} \,. \tag{2.2}$$

This assumption imposes an ordering in the operators of (2.1). If O_i has a large dimension $d_i (d_i > 4)$ the corresponding coupling C_i is small. This means that the dynamics predicted by that term of the Lagrangian are suppressed and therefore can be neglected at a first approximation. The operators of (2.1) are thus ordered according to their dimensions. The

larger the dimension of O_i the less important the corresponding term of $\mathcal{L}$ is. As a consequence also the observables calculated in the effective field theory framework will be ordered in an expansion of terms of increasing importance. We stress that while the form of the operators O_i in (2.1) can be inferred by the symmetries and the field content, we do not have any information on the couplings C_i. We need phenomenology to infer their values.

Matching in Effective Field Theories

In this section we go through an important subject in effective field theories namely matching, which we will use in future work on neutrino physics as well. Following the above discussions it should be clear that a theory that describes interactions at a given energy and below, should not depend directly on the dynamics at higher energies. In fact due to the Appelquist-Carazzone theorem [3] it is vital to use the effective theory for calculating the evolution of the parameters below the high mass scale, to get meaningful results. This theorem states that heavy particles decouple at energies much smaller than their masses, so that physics is independent of them at these energies, except for the possible appearance of effective operators.

A very subtle point is in order here that is, in perturbation theory, the observables can be expressed in terms of Feynman loop diagrams where the integration is carried out to infinity. Consequently, contributions from all energies are present even in the low-energy observables. Therefore, one should properly define, what one means under the statement low-energy and be able to track down the effect of the high energy theory in the low energy one via the couplings of the effective theory, as stated above. This task is done by a process called matching.

One starts at a very large scale, that is with a very high renormalization scale μ. At this energy the physics is described by a set of fields χ, describing the heaviest particles of mass M, and a set of light particle fields ϕ, describing all the lighter particles. The Lagrangian has the form [4]

$$\mathcal{L} = \mathcal{L}_{\chi,\phi} + \mathcal{L}_{\phi}\,, \tag{2.3}$$

where $\mathcal{L}_{\phi}$ contains all the terms that depend only on the light fields and $\mathcal{L}_{\chi,\phi}$ is everything else. One then runs parameters of the theory down with

respect to the energy and until the heavy particle with mass M shows up, this evolution is described by the renormalization group. However, when μ goes below the mass, then one should change to a new effective theory without the heavy particle, changing the parameters of the theory. The Lagrangian of the effective theory below M has the form

$$\mathcal{L}_\phi + \delta\mathcal{L}_\phi \,, \tag{2.4}$$

where $\delta\mathcal{L}_\phi$ is the part that contains all the changes. This can be seen schematically in Fig. 2.1 We shall illustrate this phenomena via a toy model

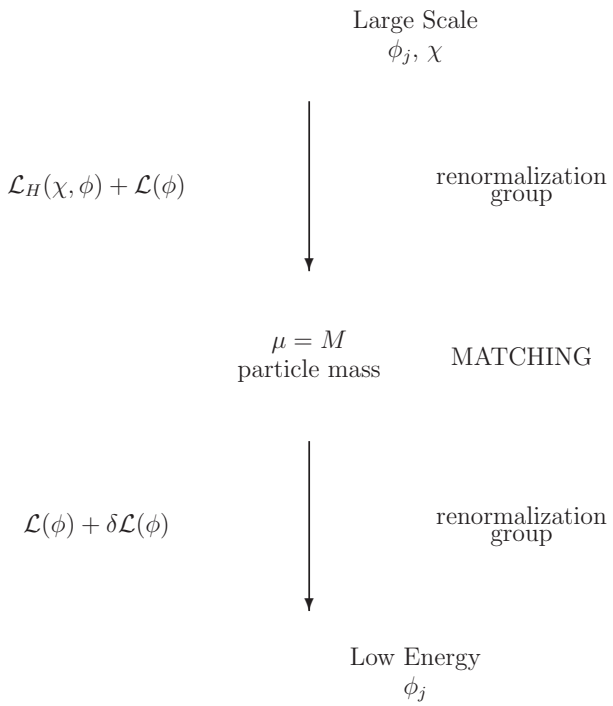

Figure 2.1: An schematic illustration of a matching calculation [4]

example here. We start with the high energy Lagrangian

$$\mathcal{L} = \frac{1}{2}(\partial\phi)^2 - \frac{m^2}{2}\phi^2 - \frac{M^2}{2}\chi^2 - \frac{g}{2}\phi^2\chi\,, \tag{2.5}$$

where ϕ and χ denote the light and heavy fields with masses m and M, respectively. Consider the scattering process $\phi(p_1)\phi(p_2) \to \phi(p_3)\phi(p_4)$ at the energies $E \sim m \ll M$ where the dynamics of the light field is described by the following effective Lagrangian

$$\mathcal{L}_{eff} = \frac{1}{2}C_0(\partial\phi)^2 - \frac{1}{2}C_1\phi^2 - \frac{1}{4!}C_2\phi^4\,. \tag{2.6}$$

Here C_0, C_1 and C_2 are the Wilson coefficients of the effective Lagrangian which contain the information from the high energy theory. One can expand these coefficients as

$$C_0 = C_0^{(0)} + C_0^{(1)} + \ldots \quad C_1 = C_1^{(0)} + C_1^{(1)} + \ldots \quad C_2 = C_2^{(0)} + C_2^{(1)} + \ldots\,, \tag{2.7}$$

where the upper index indicates the corresponding loop order. At the matching scale $\mu = M$, both Lagrangians should lead to the same dynamics that is, all the scattering amplitudes should be identical. First we check this for the tree level amplitudes which are shown in Fig. 2.2.

The amplitude from the Lagrangian (2.5) is

$$\mathcal{M} = i3\frac{g^2}{M^2} + O(M^{-4})\,, \tag{2.8}$$

while for the effective theory it is given by

$$\mathcal{M}^0_{eff} = -iC_2^{(0)}\,, \tag{2.9}$$

from which one can conclude

$$C_2^{(0)} = -3\frac{g^2}{M^2} + O(M^{-4})\,, \tag{2.10}$$

at the tree level. Also at this level $C_0^{(0)}=1$ and $C_1^{(0)}=m^2$ by comparing propagators of ϕ in both theories.

At one loop things are a bit more involved as shown in Fig. 2.3. The two upper diagrams of this figure after renormalizing lead to the following

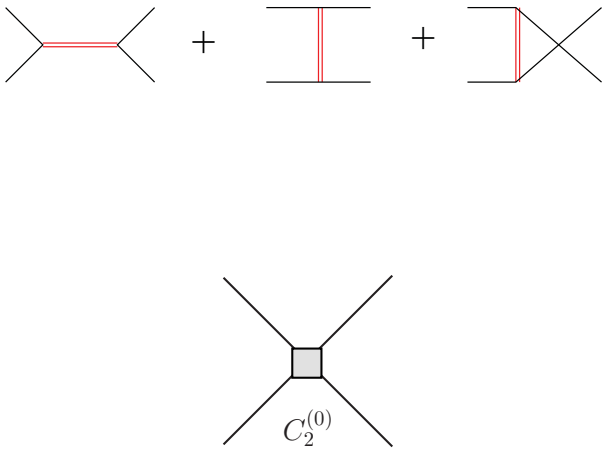

Figure 2.2: The tree-level scattering amplitude for the process $\phi\phi \to \phi\phi$ in the model described by the Lagrangian given in Eq. (2.5) (up), and by the Lagrangian (2.6) (down). In the upper figure the single and double lines correspond to the light and heavy fields, respectively.

amplitude [5]

$$\begin{aligned}\mathcal{M}_R &= i\frac{g^2(\mu)}{(4\pi)^2}\Big[\frac{3}{2}\frac{m^2(\mu)}{M^2}\ln(\frac{m^2(\mu)}{M^2}) - \frac{1}{2}\frac{m^2(\mu)}{M^2} + 1 + \frac{1}{2}\frac{p^2}{M^2} \\ &- \ln(\frac{M^2}{\mu^2})\Big]\,, \end{aligned} \tag{2.11}$$

with $m(\mu)$ and $g(\mu)$ as the running mass and coupling in the original theory and the index $_R$ stands for renormalized. Doing the same calculations for the effective Lagrangian one finds

$$\begin{aligned}\mathcal{M}_{eff,R} &= i\frac{3}{2}\frac{g_{eff}^2(\mu)}{(4\pi)^2}\frac{m_{eff}^2(\mu)}{M^2}\Big[\ln(\frac{m_{eff}^2(\mu)}{\mu^2}) - 1\Big] \\ &- iC_1^{(1)}(\mu) + ip^2C_0^{(1)}(\mu)\,. \end{aligned} \tag{2.12}$$

Now, demanding the two amplitudes to match at $\mu = M$ one finds the Wilson coefficients of the effective theory to be

$$C_0^{(1)} = \frac{1}{2}\frac{g^(M)}{(4\pi)^2 M} \qquad C_1^{(1)} = -\frac{g^2(M)}{(4\pi)^2}\left(1 + \frac{m^2(M)}{M^2}\right). \tag{2.13}$$

Since both theories have similar IR behavior, the IR divergent logarithms cancel in the process of matching as can be seen from the above relations. In fact this is a general property of all effective theories. Also the $C_2^{(1)}$ coefficient should be derived from another matching shown in the Fig. 2.4 [5].

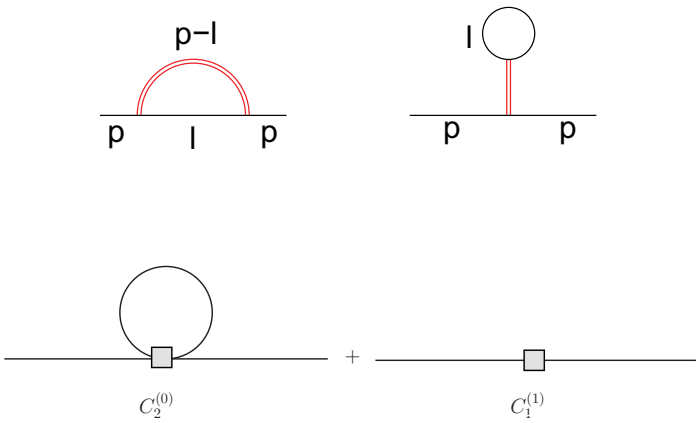

Figure 2.3: The self-energy of the light particle at one loop in the model described by the Lagrangian given in Eq. (2.5)(up), and by the Lagrangian (2.6) (down).

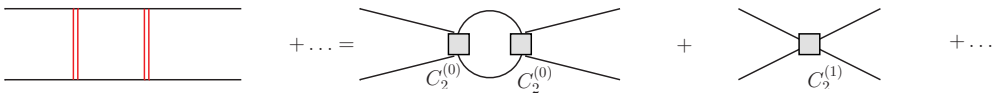

Figure 2.4: The second set of diagrams for one loop matching conditions.

Finally, putting every thing together and using these Wilson coefficients, after the field redefinition

$$\phi \to \phi \sqrt{1 - \frac{1}{2}\frac{g_{eff}^2(\mu)}{(4\pi)^2 M^2}}\,, \tag{2.14}$$

one can write the effective Lagrangian as

$$\mathcal{L}_{eff} = \frac{1}{2}(\partial\phi)^2 - \frac{1}{2}\bar{m}_{eff}^2(\mu)\phi^2 - \frac{1}{4!}\bar{g}_{eff}(\mu)\phi^4\,, \tag{2.15}$$

where

$$\begin{aligned} \bar{m}_{eff}^2(\mu) &= m_{eff}^2(\mu) - \frac{g_{eff}^2(\mu)}{(4\pi)^2}\left(1 + \frac{m_{eff}^2(\mu)}{M^2}\right) - \frac{1}{2}\frac{g_{eff}^2(\mu) m_{eff}^2(\mu)}{(4\pi)^2 M^2} \\ \bar{g}_{eff}(\mu) &= -3\frac{g_{eff}^2(\mu)}{M^2} + (3+a)\frac{g_{eff}^4(\mu)}{(4\pi)^2 M^4}\,, \end{aligned} \tag{2.16}$$

where a comes from the contribution of the Fig. 2.4. So, in the context of an example, we have seen how the effects of physics at high energy scale appear in the low energy theory via the couplings.

QCD and the Chiral Lagrangian

Equipped with the previous discussions, we go ahead to the case of QCD at low energies. We know that in some cases it can be extremely difficult to extract useful predictions in a theory even when the Lagrangian is well-known. The usual way to calculate physical observables from the Lagrangian is through the use of perturbation theory. This means that if the coupling that governs the interaction is smaller than 1 it is possible to order the different contributions to physical observables in terms of increasing powers in the couplings and thus in decreasing order of importance. To obtain a prediction it is therefore sufficient to add enough contributions to this perturbative expansion.

On the other hand, we know that quarks and gluons are confined within hadrons and their dynamics is described by the $SU(3)_C$ of the SM. Due to the fact that QCD is a renormalizable theory, the properties of confinement and asymptotic freedom can be explained by seeing the evolution of the

coupling constant $\alpha_s(E)$ with the energy involved thanks to the equations of the renormalization group. It is observed that $\alpha_s(E)$ decreases as the energy E increases. Then QCD ceases to be perturbative at low energies because the interactions are very strong and calculating any observable is impossible. This is where hadrons are the relevant degrees of freedom, not quarks and gluons. Unfortunately, a transformation that links the Lagrangian of QCD and its parameters with the properties of the hadronic states is not known. A widely used method of dealing with the problem has been through effective theories. In the case of QCD at low energies, this theory is called Chiral Perturbation Theory (ChPT) [6, 7]. Some good reviews on the subject can be found in Refs. [1, 8].

Let us first show the QCD Lagrangian. Due to the fact that three quarks, u, d and s are much lighter than the c, b and t, one can write the QCD Lagrangian only for light degrees of freedom as

$$\mathcal{L} = \sum_{j=u,d,s} \bar{\psi}_j (i\gamma^\mu \partial_\mu + g_s \mathbf{G}^\mu \gamma_\mu - m)\psi_j - \frac{1}{4} G^a_{\mu\nu} G_a^{\mu\nu} \,. \tag{2.17}$$

For completeness we should also add a term as $\theta G_{\mu\nu} G_{\alpha\beta} \epsilon^{\mu\nu\alpha\beta}$ to this Lagrangian, which is also called the θ–term. The numerical value of the coupling θ is very small ($\theta < 10^{-10}$). A lot of interesting physics arises from such a term. However we will not consider its effects in here, since it is beyond the scope of this thesis. For more detailed explanations we recommend [8].

One can define the left handed and right handed fermion fields as

$$\psi_L = \frac{1}{2}(1 - \gamma_5)\psi \,, \qquad \psi_R = \frac{1}{2}(1 + \gamma_5)\psi \,. \tag{2.18}$$

and $\psi = \psi_L + \psi_R$. The QCD Lagrangian when written in terms of ψ_L and ψ_R writes

$$\begin{aligned} \mathcal{L} = & \sum_{j=u,d,s} \bar{\psi}_{L_j} (i\gamma^\mu \partial_\mu + g_s \mathbf{G}^\mu \gamma_\mu)\psi_{L_j} + \bar{\psi}_{R_j} (i\gamma^\mu \partial_\mu + g_s \mathbf{G}^\mu \gamma_\mu)\psi_{R_j} \\ & - m\bar{\psi}_{L_j}\psi_{R_j} - m\bar{\psi}_{R_j}\psi_{L_j} - \frac{1}{4} G^a_{\mu\nu} G_a^{\mu\nu} \,. \end{aligned} \tag{2.19}$$

If one drops the mass terms the Lagrangian will be invariant under the following transformations in the flavor space

$$\psi_L \to g_L \psi_L \qquad \psi_R \to g_R \psi_R \,, \tag{2.20}$$

where $(g_L, g_R) \in SU(3)_L \times SU(3)_R$. Hence, the massless Lagrangian of QCD is said to have $SU(3)_L \times SU(3)_R = G$ symmetry or the chiral symmetry in the flavor space. Of course, quarks are massive and the chiral symmetry is not realized fully in nature and for the three lightest quarks u, d, s, it could be assumed to hold approximately. In this scenario, the masses of the light quarks play the role of the symmetry breaking parameters whose magnitude is a measure for the extent to which chiral symmetry is broken explicitly. However, as this symmetry is not visible in the spectrum of light hadrons, it should be spontaneously broken in nature due to some spontaneous symmetry breaking (SSB) mechanism. This leads to the global symmetry $SU(3)_L \times SU(3)_R = G$ to be reduced to the subgroup $H = SU(3)_V$.

Now, the Goldstone theorem [9] dictates that the difference between the original number of generators and the final ones, should have turned into Goldstone bosons. In the case at hand the number of Goldstone bosons is 8. As the chiral symmetry is also broken explicitly due to the quark masses in the QCD Lagrangian, the bosons could be recognized as the pseudo–scalar mesons, which have acquired a small mass due to this explicit symmetry breaking.

In QCD the global chiral symmetry is broken via the strong underlying interactions, which lead to a quark condensate. This condensate made up of a quark and an anti-quark is the order parameter and the corresponding SSB is said to be a dynamical symmetry breaking.

The next step is to show how external fields are included into the QCD Lagrangian.

External Fields

This was introduced in [10] to simplify the calculations and to include interactions like the electromagnetic and some of the weak ones. Furthermore it allows to perform calculations maintaining the chiral symmetry throughout.

We consider again the Lagrangian for three-flavor QCD dropping the mass terms and the gluon tensor field $G_{\mu\nu}$. But we incorporate now also a few new fields called external fields (or sources).

$$\begin{aligned}\mathcal{L} = & \sum_{i,j=u,d,s} \bar{\psi}_{iL}(i\gamma^\mu\partial_\mu + g_s\mathbf{G}^\mu\gamma_\mu)\psi_{iL} + \bar{\psi}_{iR}(i\gamma^\mu\partial_\mu + g_s\mathbf{G}^\mu\gamma_\mu)\psi_{iR} \\ & - \bar{\psi}_{iL}(s-ip)_{ij}\psi_{jR} - \bar{\psi}_{iR}(s+ip)_{ij}\psi_{jL} + \bar{\psi}_{iL}\gamma^\mu(v_\mu - a_\mu)_{ij}\psi_{jL} \\ & + \bar{\psi}_{iR}\gamma^\mu(v_\mu + a_\mu)_{ij}\psi_{jR}\,. \end{aligned} \tag{2.21}$$

In (2.21) there are four new fields $s = s^a\lambda_a/2, p = p^a\lambda_a/2, v_\mu = v_\mu^a\lambda_a/2, a_\mu = a_\mu^a\lambda_a/2$. These depend on the space-time coordinates and are Hermitian 3×3 matrices. Chiral symmetry for the massless QCD Lagrangian is a global symmetry, but thanks to these new sources it is possible to promote it to a local symmetry for the Lagrangian in (2.21). We assume the operators $(g_L, g_R) \in SU(3)_L \times SU(3)_R$, depending now on the space-time coordinates, to act on the fields as

$$\begin{aligned} \psi_L \to g_L\psi_L\,, \quad \psi_R \;&\to\; g_R\psi_R\,, \quad (s+ip) \to g_R(s+ip)g_L^\dagger \\ l_\mu = (v_\mu - a_\mu) \;&\to\; g_L l_\mu g_L^\dagger - i\partial_\mu g_L g_L^\dagger\,, \\ r_\mu = (v_\mu + a_\mu) \;&\to\; g_R r_\mu g_R^\dagger - i\partial_\mu g_R g_R^\dagger\,. \end{aligned} \tag{2.22}$$

By plugging the transformation rules (2.22) in (2.21) it is possible to show that the Lagrangian (2.21) is invariant under local chiral transformations. This is due to the particular transformations of the fields l_μ and r_μ.

Then, for example, the gauge fields of electroweak interactions can be automatically included as external fields by the substitution

$$\begin{aligned} l_\mu &= eQA_\mu + \frac{g_2}{cos\theta_W}\left(T_z - \sin^2\theta_W\right)Z_\mu + \frac{g_2}{\sqrt{2}}\left(W_\mu^+ T_+ + W_\mu^- T_-\right)\,, \\ r_\mu &= eQA_\mu - \frac{g_2}{cos\theta_W}\sin^2\theta_W Z_\mu\,, \end{aligned} \tag{2.23}$$

with e, g_2 and θ_W, the electromagnetic coupling constant, the gauge coupling constant of $SU(2)_L$ and the weak mixing angle, respectively. Also

$$Q = \frac{1}{3}\begin{pmatrix} 2 & 0 & 0 \\ 0 & -1 & 0 \\ 0 & 0 & -1 \end{pmatrix}\,,$$

and

$$T_z = \frac{1}{2}\begin{pmatrix} 1 & 0 & 0 \\ 0 & -1 & 0 \\ 0 & 0 & -1 \end{pmatrix},$$

$$T_+ = \begin{pmatrix} 0 & V_{ud} & V_{us} \\ 0 & 0 & 0 \\ 0 & 0 & 0 \end{pmatrix},$$

with V_{ij} the elements of the CKM matrix.

For example if we identify the field v_μ with a photon field eQA_μ, we can recover the electromagnetic interactions. Furthermore the field s provides us with a very elegant way to include also the quark masses. We can indeed identify

$$s = M = \begin{pmatrix} m_u & 0 & 0 \\ 0 & m_d & 0 \\ 0 & 0 & m_s \end{pmatrix}. \tag{2.24}$$

To understand how an effective theory, using the expansion in powers of momenta can actually describe dynamics of the Goldstone bosons correctly, forgetting about the underlying theory, we digress to the Linear Sigma model as an example.

Non-Linear Sigma Model

Let's start with the linear sigma model Lagrangian

$$\mathcal{L} = \frac{1}{2}\partial^\mu \boldsymbol{\phi}^T \cdot \partial_\mu \boldsymbol{\phi} - \lambda\left(\boldsymbol{\phi}^T \cdot \boldsymbol{\phi} - \nu^2\right)^2, \tag{2.25}$$

where the vector field $\boldsymbol{\phi} = (\phi_1, ..., \phi_N)$ is an N-component real scalar field. The potential has its minimum at $|\phi| = v$. The set of field configurations that satisfy this equation is known as vacuum manifold and in this example is the set of points $\boldsymbol{\phi} = (\phi_1, ..., \phi_N)$ which satisfy $\phi_0^2 = \phi_1^2 + ... + \phi_N^2 = \nu^2$. This Lagrangian has a global $O(N)$ symmetry under which ϕ transforms as an $O(N)$ vector. We assume that among an infinite number of ground states that satisfy this condition, one of them is chosen dynamically so that $\boldsymbol{\phi}_0 = (0, 0, .., \nu)$. Hence, the symmetry is spontaneously broken to the subgroup $H \equiv O(N-1)$. This leads to the generation of $N-1$ Goldstone bosons according to the Goldstone theorem [9], which are taken to be π^i.

Expanding around this minimum and switching to polar coordinates, one finds

$$\phi = (\rho + \nu) \exp(i \sum_{i}^{(N-1)} \frac{\sigma^i \cdot \pi^i}{\nu}) \begin{pmatrix} 0 \\ 0 \\ . \\ . \\ . \\ 1 \end{pmatrix} , \tag{2.26}$$

where σ_i are the Pauli matrices. Plugging back into the above Lagrangian, one ends up with

$$\begin{aligned} \mathcal{L} &= \frac{1}{2}\partial_\mu\rho\partial^\mu\rho - \lambda(\rho^2 + 2\nu\rho)^2 + \frac{1}{2}(\nu+\rho)^2 \\ &\times [\partial_\mu \exp(-i \sum_{i}^{(N-1)} \frac{\sigma^i \cdot \pi^i}{\nu})\partial^\mu \exp(i \sum_{i}^{(N-1)} \frac{\sigma^i \cdot \pi^i}{\nu})]_{NN} , \end{aligned} \tag{2.27}$$

where $[]_{NN}$ is the NN element of the matrix. Then assuming that in the low energy limit the ρ field is absent [11], one finds the corresponding effective Lagrangian of the non-linear sigma model to be

$$\mathcal{L}_{eff} = \frac{1}{2}\nu^2 [\partial_\mu \exp(-i \sum_{i}^{(N-1)} \frac{\sigma^i \cdot \pi^i}{\nu})\partial^\mu \exp(i \sum_{i}^{(N-1)} \frac{\sigma^i \cdot \pi^i}{\nu})]_{NN} . \tag{2.28}$$

It can be seen that the coupling is proportional to momentum and the π field has remained massless. Now the stage is set to introduce the ChPT.

ChPT

As was mentioned before, in the low energy domain a thorough analysis of the QCD dynamics in terms of quarks and gluons is a highly non perturbative problem. A description in terms of the hadronic states seems more adequate. We have seen that there are 8 pseudo-Goldstone bosons arising from the SSB of chiral symmetry identified with the pseudo scalar mesons. Notice that there is a mass gap separating these pseudo-scalars from the rest of the hadronic spectrum, the next particle in mass, the ρ meson, being away from the octet. This allows us to build an effective field theory con-

taining only the Goldstone bosons as degrees of freedom, like the non-linear sigma model, and basically forgetting about the quarks and gluons.

To construct an effective theory of strong interactions at low energies one would build an effective Lagrangian for a process happening at a scale $p \ll \Lambda$, using a expansion in powers of p/Λ where Λ is the cut–off of the model to be around 1 GeV and p is the momenta. Then the Lagrangian could be organized as a series of growing powers of momenta, i.e. of derivatives as

$$\mathcal{L} = \mathcal{L}_2 + \mathcal{L}_4 + ...\mathcal{L}_{2n} \,, \tag{2.29}$$

where the subscript indicates the number of derivatives. The most important contribution to a given amplitude comes from the tree level Lagrangian, $\mathcal{L}_2$. The next to leading order Lagrangian is $\mathcal{L}_4$ and so on.

The most general Lagrangian invariant under Lorentz and chiral transformations at the lowest order has the form [7]

$$\mathcal{L}_2 = \frac{F_0^2}{4} Tr(D_\mu U^\dagger D^\mu U) + \frac{F_0^2}{4} Tr(U\chi^\dagger + \chi U^\dagger) \,, \tag{2.30}$$

where F_0 is the pion decay constant, $\chi = 2B_0(s + ip)$ and B_0 is a constant related to the chiral quark condensate. U is the $SU(3)$ matrix, written in terms of the meson fields as

$$U = \exp(\frac{i\sqrt{2}}{F_0}\phi) \,, \tag{2.31}$$

where

$$\phi = \begin{pmatrix} \frac{1}{\sqrt{2}}\pi^0 + \frac{1}{\sqrt{6}}\eta & \pi^+ & K^+ \\ \pi^- & -\frac{1}{\sqrt{2}}\pi^0 + \frac{1}{\sqrt{6}}\eta & K^0 \\ K^- & \bar{K}^0 & -\frac{2}{\sqrt{6}}\eta \end{pmatrix} .$$

The covariant derivative is

$$D_\mu U = \partial_\mu U - i r_\mu U + i U l_\mu \,, \tag{2.32}$$

with left and right fields l_μ and r_μ.

As we discussed above, the effective Lagrangian can be written in terms of a sum of Lagrangians ordered by the dimensions of their operators. In ChPT after the $O(p^2)$ Lagrangian we can decide to go to higher order and build up the $O(p^4)$ one containing operators of dimension 4. The Lagrangian of

the order p^4 has the form [7]

$$\begin{aligned}\mathcal{L}_4 &= L_1\langle D_\mu U^\dagger D^\mu U\rangle^2 + L_2\langle D_\mu U^\dagger D_\nu U\rangle\langle D^\mu U^\dagger D^\nu U\rangle \\ &+ L_3\langle D^\mu U^\dagger D_\mu U D^\nu U^\dagger D_\nu U\rangle + L_4\langle D^\mu U^\dagger D_\mu U\rangle\langle \chi^\dagger U + \chi U^\dagger\rangle \\ &+ L_5\langle D^\mu U^\dagger D_\mu U(\chi^\dagger U + U^\dagger\chi)\rangle + L_6\langle \chi^\dagger U + \chi U^\dagger\rangle^2 + L_7\langle \chi^\dagger U - \chi U^\dagger\rangle^2 \\ &+ L_8\langle \chi^\dagger U\chi^\dagger U + \chi U^\dagger\chi U^\dagger\rangle - iL_9\langle F^R_{\mu\nu} D^\mu U D^\nu U^\dagger + F^L_{\mu\nu} D^\mu U^\dagger D^\nu U\rangle \\ &+ L_{10}\langle U^\dagger F^R_{\mu\nu} U F^{L\mu\nu}\rangle\,. \end{aligned} \tag{2.33}$$

with non-Abelian field strengths

$$\begin{aligned} F^R_{\mu\nu} &= \partial^\mu r^\nu - \partial^\nu r^\mu - i[r^\mu, r^\nu]\,, \\ F^L_{\mu\nu} &= \partial^\mu \ell^\nu - \partial^\nu \ell^\mu - i[\ell^\mu, \ell^\nu]\,. \end{aligned} \tag{2.34}$$

Each of the operators in (2.30) and (2.33) can contain in principle as many mesons as wanted. These arise from the expansions of the U matrix. As a consequence we can draw infinitely many Feynman diagrams. We clearly cannot calculate contributions from an infinite set of diagrams. One might wonder whether with ChPT we can predict any quantity at all.

Luckily also the Feynman diagrams, as the Lagrangians, can be ordered in a systematic way according to the expected size of their contributions. This is once again done through a power counting of the momenta in the different parts of the diagram. Thus if we want to calculate an observable we first must decide at which order in the momentum expansion we want to stop to get the desired precision. Then we calculate as many diagrams as needed. The procedure is illustrated in Fig 2.5. A vertex from $\mathcal{L}_2$ in (2.30) counts as two powers of momenta since it has two derivatives or M^2. Also, because of the mathematical form of the propagator $1/(p^2 - M^2)$ an internal line counts as $1/p^2$. Finally, the loop integration gives a power of p^4. We will use these rules in our calculations when computing the local and non-local Green functions (see next sections).

As can be seen, the expansion in ChPT is organized in powers of momenta p and mass. When one wants to calculate an observable one needs to take matrix elements of the operators in the Lagrangian. From the previous discussions, the coefficient of an operator with d derivatives behaves as $1/\Lambda^{(d-4)}$. Therefore the effect of a d derivatives vertex is of order $p^d/\Lambda^{(d-4)}$ and at an energy small compared to Λ, the more derivatives are involved the smaller is the contribution to the matrix element. Hence, the contri-

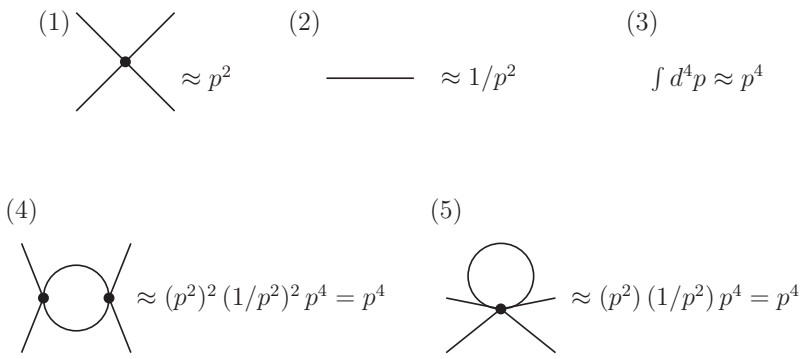

Figure 2.5: The upper part diagrams show the power counting rules. The lower diagrams are loop diagrams [12].

bution from (2.33) is smaller than the one of (2.30). Notice that in the Lagrangian (2.30) and (2.33) the external fields appear as well. The fields l and r count as a derivative so as momentum, while s and p contribute as p^2.

The couplings in (2.30) and (2.33) have the role in ChPT of the C_i in (2.1) and one needs to infer their values from experiments. In order to identify from which physical observables one can find out their values, one must look at the operators they multiply and check which are the processes they are responsible for.

At the lowest order $\mathcal{O}(p^2)$, the effective ChPT Lagrangian $\mathcal{L}_2$ depends only on two low-energy couplings. The next to leading order Lagrangian, $\mathcal{L}_4$, which includes couplings of $\mathcal{O}(p^4)$, introduces seven (ten) additional coupling constants for the two (three) quark flavors case [7].

Predictions of the $\mathcal{O}(p^2)$ and $\mathcal{O}(p^4)$ chiral Lagrangians are in very good agreement with experimental observations. Some examples can be found in Refs. [1, 8]. Now, phenomenological precision obliges us to go to the next–to–next–to leading order or $\mathcal{O}(p^6)$. This task was accomplished in Refs. [13]

and [14]. Through the use of partial integration, the equations of motion, Bianchi identities and the Cayley-Hamilton relations for SU(n) matrices, the authors of Ref. [13] managed to write down a basis of operators for $\mathcal{L}_6$ in the even-intrinsic-parity sector for $n = 2$ ($n = 3$) light flavors consisting of 90(53) terms plus 4(4) contact terms. For the sake of completeness we have shown the terms of the $O(p^6)$ Lagrangian in the Appendix.

To be able to construct these operators, we introduce a new notation which will be more appropriate for our calculations. We define

$$\begin{aligned} u_\mu &= i\{u^\dagger(\partial_\mu - ir_\mu)u - u(\partial_\mu - i\ell_\mu)u^\dagger\} \\ \chi_\pm &= u^\dagger\chi u^\dagger \pm u\chi^\dagger u\,, \end{aligned} \tag{2.35}$$

where

$$u = \exp\left(\frac{i}{\sqrt{2}F_0}\phi\right)\,, \tag{2.36}$$

is the Goldstone matrix field, $r_\mu = v_\mu + a_\mu$ and $\ell_\mu = v_\mu - a_\mu$. The Lagrangian of lowest order takes the form

$$\mathcal{L}_2 = \frac{F_0^2}{4}\left\langle u_\mu u^\mu + \chi_+\right\rangle\,. \tag{2.37}$$

To go to higher orders like $O(p^6)$ one will need additional operators [13]

$$\begin{aligned} f_\pm^{\mu\nu} &= uF_L^{\mu\nu}u^\dagger \pm u^\dagger F_R^{\mu\nu}u\,, \qquad \nabla_\lambda f_\pm^{\mu\nu}\,, \\ h_{\mu\nu} &= \nabla_\mu u_\nu + \nabla_\nu u_\mu\,, \\ \chi_{\pm\mu} &= u^\dagger D_\mu\chi u^\dagger \pm uD_\mu\chi^\dagger u = \nabla_\mu\chi_\pm - \frac{i}{2}\{\chi_\mp, u_\mu\}\,, \end{aligned} \tag{2.38}$$

with $D_\mu\chi = \partial_\mu\chi - ir_\mu\chi + i\chi l_\mu$. The covariant derivative

$$\nabla_\mu X = \partial_\mu X + [\Gamma_\mu, X]\,, \tag{2.39}$$

is defined in terms of the chiral connection

$$\Gamma_\mu = \frac{1}{2}\{u^\dagger(\partial_\mu - ir_\mu)u + u(\partial_\mu - i\ell_\mu)u^\dagger\}\,. \tag{2.40}$$

The matrices u_μ, $f_\pm^{\mu\nu}$, $h_{\mu\nu}$ and $\nabla_\lambda f_\pm^{\mu\nu}$ are also traceless.

The First paper (see Chapter 4)

Motivation

So as it was stated, the number of the operators in the $\mathcal{O}(p^6)$ chiral Lagrangian increases significantly, compared to the lower order Lagrangians and the pattern shows that by going to higher orders, this number will increase even more. The question is, now that one has to deal with such a large number of terms, does one know for sure that there is no redundancy in the Lagrangian? In other words, is the minimality of this Lagrangian proved?

In recent years, an additional relation among the operators in the basis of [13] for the $n = 2$ case was proven [15], where no additional manipulations but those already used in [13] were required. This showed that the derivation of an algorithm to exhaust all possible algebraic conditions among the $\mathcal{L}_6$ operators imposed by partial integration, equations of motion, Bianchi identities and, particularly, Cayley-Hamilton relations, is a nontrivial task.

Therefore, the question about the minimality of the $\mathcal{O}(p^6)$ chiral Lagrangian is proper and, to the best of our knowledge, remains unanswered. It is our aim to describe a method that provides necessary conditions for the existence of additional relations between the operators of the $\mathcal{L}_6$ Lagrangian.

By doing so one could be sure that is not dealing with unnecessary operators in calculations and also, one will not have to go through experiments to extract the value of redundant coupling constants. Needless to say that, even if one has resources to do so, it is not practical because many of the operators contribute to processes in the lowest approximation which are phenomenologically irrelevant [13].

Based on what we said before, our aim is not to find the possible algebraic conditions among the $\mathcal{L}_6$ operators using the common approach to the problem. In fact, we know that processes with up to 6 mesons legs or two vector or axial-vector currents are far off experimentally which means, for practical purposes it would be enough to check the minimality of the Lagrangian up to this approximation and not to the operator level. Besides that, if one can reach this level of precision, the task of checking the minimality at the operator level will be hugely simplified. So, we have chosen to check the minimality of the basis of the $\mathcal{O}(p^6)$ Lagrangian up to this ap-

proximation. This has allowed us to develop a mechanism which, although computationally involved, is straightforward and with automatization can be generalized to any number of basis.

Furthermore, to simplify the calculations and establish the method (see below), we have chosen to work in the chiral $SU(2)$ flavor limit, without external scalar or pseudo scalar sources. That is, we only have pions as pseudo scalar mesons and we also set all the masses equal to zero. Of course, when the method is established, one can generalize it to the case of $SU(3)$ flavor including the masses as well.

The Method

To answer the question of the minimality of the order p^6 chiral Lagrangian, instead of using the algebraic conditions (used in [13]) we analyze the Green functions built from arbitrary linear combinations of the operators in the basis and demand them to vanish for an arbitrary kinematic configuration. Then, if we find some relations between the operators involved in the process, we can say these operators are not independent (it is explained below via an example). On the other hand, if the method allows for new relations, it cannot immediately answer the question about the minimality of the set, but it has the advantage that it gives the precise form that the (potential) new relations among the operator must have.

The method involves the computation of tree-level Green functions of order p^6. Despite being tree-level, the large number of operators in $\mathcal{L}_6$ and their involved Lorentz structure, containing vertices with up to six derivatives, produce rather long expressions. The latter can nevertheless be handled easily with the help of computer tools, and the method lends itself easily to automatization.

The general structure of the $\mathcal{O}(p^6)$ ChPT Lagrangian, in the $n = 3$ case reads [13, 14]

$$\mathcal{L}_6^{\mathrm{SU(3)}} = \sum_{i=1}^{90} C_i \mathcal{O}_i + 4 \text{ contact terms} , \tag{2.41}$$

which for the $n = 2$ case, in which we are interested, becomes [13, 14]

$$\mathcal{L}_6^{\mathrm{SU(2)}} = \sum_{i=1}^{53} c_i \mathcal{P}_i + 4 \text{ contact terms} , \tag{2.42}$$

where $\mathcal{P}_i$ and $\mathcal{O}_i$ are the basis elements and c_i and C_i are the corresponding low energy constants. As we said, we work in the chiral limit without external scalar and pseudo scalar sources. This leaves us with $27+2$ of the $53+4$ operators.

In this limit, v_μ and a_μ, the external vector and axial sources respectively, are general traceless 2×2 matrices

$$v_\mu = \begin{pmatrix} v_{11} & v_{12} \\ v_{21} & -v_{11} \end{pmatrix}_\mu \qquad \text{and} \qquad a_\mu = \begin{pmatrix} a_{11} & a_{12} \\ a_{21} & -a_{11} \end{pmatrix}_\mu . \tag{2.43}$$

It should be mentioned that we do not confine ourselves to the Standard Model vector and axial currents, but allow for the parametrization of other possible beyond-the-Standard-Model currents. Also, the matrix ϕ in the two flavor-case collects the pion fields,

$$\phi = \begin{pmatrix} \frac{1}{\sqrt{2}}\pi^0 & \pi^+ \\ \pi^- & -\frac{1}{\sqrt{2}}\pi^0 \end{pmatrix} . \tag{2.44}$$

On the other hand, as we work in the chiral limit and since quark masses are introduced in the ChPT meson amplitudes through the scalar matrix s, then we can put $s=0$. In addition we also set $p=0$ and therefore, we can drop all operators containing the χ tensor in what follows.

Now, to check the independency of the basis of the Lagrangian in this specific limit, we are going to find the solutions of the following relation

$$\sum_{i=1} c_i \mathcal{P}_i = 0 \quad . \tag{2.45}$$

So, we demand that the matrix elements which include these operators to vanish

$$\langle 0|\, T\, \phi(x_1)\phi(x_2)\dots f_1(y_1)f_2(y_2)\dots \Big(\int d^4x \sum_i \alpha_i\, \mathcal{P}_i(x)\Big)|0\rangle = 0\,, \tag{2.46}$$

where, α_i are real or complex numbers, ϕ an arbitrary number of pion fields and $f_i = v,\, a,\, s,\, p$ external field sources. Therefore, by calculating the amplitude in terms of the coefficients c_i and the Lorentz invariants; which in general can have any value as we are assuming an arbitrary kinematic configuration; and demanding it to vanish, we are able to find the relations

between the operators contributing to each matrix element, if there exist any.

To demonstrate how our method works in a crystal clear manner, we will explain it using an example, step by step. That is the decay of an off-shell photon to four pions, π^+, π^- and two π^0, which we denote symbolically as $\langle\gamma^* 4\pi\rangle$. The Feynman diagrams belonging to this Green function at order p^6 are shown in Figs. 2.6 and 2.7. As can be seen, there exist two types of diagrams, those without internal pion lines, which we call local, and those with a pion propagator, which we call non-local. The local diagrams only include the p^6 Lagrangian. The non–local diagrams consist of two vertices of which, one is of order p^6 and the other p^2 but still, the whole diagram remains of order p^6, following the laws of power counting described in Fig. 2.5. We work in the momentum space for the sake of convenience and take all the momenta to be incoming. Using the energy momentum conservation, we are able to write one momentum in term of the others. Then, we have 4 independent momenta, p_1, p_2, p_3 and p_4 and one polarization vector, ϵ belonging to the photon field. By taking the pion fields to be on-shell, we can eliminate the momentum squared via the on-shell condition, $p_i^2 = 0$. Therefore, we have 10 different Lorentz invariants, $p_1\cdot\epsilon$, $p_1\cdot p_2$, $p_1\cdot p_3$, $p_1\cdot p_4$, $p_2\cdot\epsilon$, $p_2\cdot p_3$, $p_2\cdot p_4$, $p_3\cdot\epsilon$, $p_3\cdot p_4$ and $p_4\cdot\epsilon$, in terms of which the amplitudes are written. Operators which contribute to the local amplitude are $\mathcal{P}_1, \mathcal{P}_3, \mathcal{P}_{27}, \mathcal{P}_{28}$, $\mathcal{P}_{36}$, $\mathcal{P}_{37}$, $\mathcal{P}_{38}$, $\mathcal{P}_{51}$ and $\mathcal{P}_{53}$. On the other hand, the contribution to the non-local amplitude comes from the $O(p^2)$ Lagrangian as well as the operators $\mathcal{P}_{51}$ and $\mathcal{P}_{53}$ of the $O(p^6)$ Lagrangian. In the non-local case, both Lagrangians can contribute to each vertex.

The total amplitude in this case is too large to be shown here. However, after calculating the total amplitude, we multiply the contribution of each operator by an arbitrary coefficient, α_i, and adding up all contributions, demand the whole amplitude to vanish. This will lead to a set of coupled equations to be solved to find the α_is. The set of equations to be solved in

this case has the general form

$$
\begin{aligned}
&8\,(-6c_{27}-24c_{51})=0,\\
&6\,(-12c_1+12c_2+12c_3+6c_{36}+6c_{38}-8c_{51})=0,\\
&8\,(-12c_2-24c_3+6c_{36}-4c_{51})=0,\\
&\quad .\\
&\quad .\\
&\quad .\\
&16\,(-6c_3+9c_{27}-6c_{28}+3c_{36}-3c_{37}+9c_{38}+9c_{51}-3c_{53})=0,\\
&16\,(12c_1-12c_2-6c_3+3c_{28}-9c_{36}-9c_{38}+25c_{51}-3c_{53})=0,\\
&\ 8\,(-12c_3+6c_{38}-2c_{51}-2c_{53})=0,\\
&16\,(2c_{51}-2c_{53})=0,\\
&\ 8\,(6c_{51}-2c_{53})=0,\\
&18\,(-24c_1+24c_2+30c_3-3c_{27}+9c_{36}+15c_{37}-21c_{38}-5c_{51}-c_{53})=0,\\
&14\,(12c_2+6c_3-3c_{27}+3c_{36}-9c_{38}-c_{51}-c_{53})=0,\\
&14\,(-12c_2-6c_3+3c_{27}-3c_{36}+9c_{38}+c_{51}+c_{53})=0,\\
&\quad .\\
&\quad .\\
&\quad .
\end{aligned}
\tag{2.47}
$$

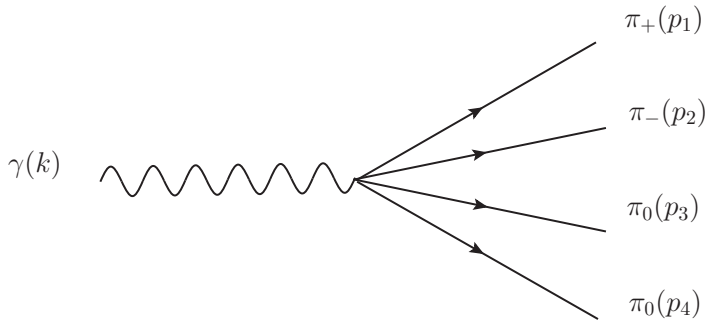

Figure 2.6: The local diagram.

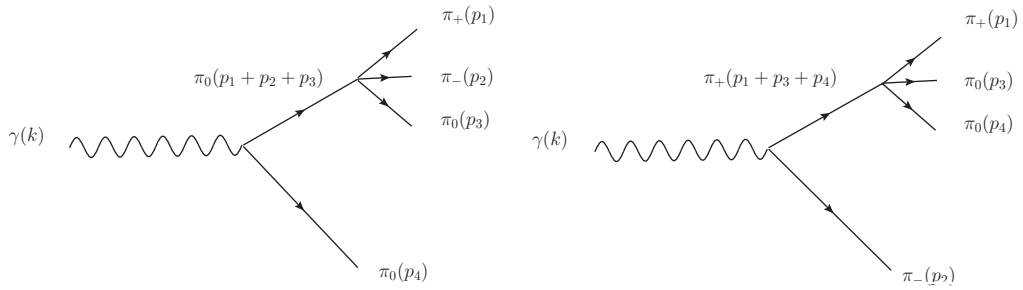

Figure 2.7: The non-local diagrams.

Now, if some of the operators are not independent, we will find some relations between the given coefficients as explained before. Obviously, doing this calculation without automatization is not practical. After solving all these equations together, one will find the following relations between the operators involved in this process.

Results

The combination of matrix elements

$$\langle vv\rangle,\ \langle vaa\rangle,\ \langle vv\,2\pi\rangle,\ \langle aa\,2\pi\rangle,\ \langle v\,4\pi\rangle,\ \langle 6\pi\rangle\,, \tag{2.48}$$

already involve all the operators in the limit we are cheking that is the $SU(2)$ with $s = p = 0$. However, operators P_{45} and P_{55} only appear in $\langle vaa\rangle$ and hence we need another matrix element namely $\langle vva\pi\rangle$ to which P_{45} contributes in order to fix it completely. Therefore, as a whole one needs to calculate seven Green functions.

Combining the equations for c_i found for the different Green functions we get

$$
\begin{aligned}
& c_{38} = c_{50} = c_{52} = c_{55} = c_{56} = 0\,, \\
& c_1 \Big(8\,\mathcal{P}_1 - 2\,\mathcal{P}_2 + 6\,\mathcal{P}_3 - 20\,\mathcal{P}_{24} + 8\,\mathcal{P}_{25} + 12\,\mathcal{P}_{26} - 16\,\mathcal{P}_{28} - 3\,\mathcal{P}_{29} + 3\,\mathcal{P}_{30} \\
& \qquad - 6\,\mathcal{P}_{31} + 12\,\mathcal{P}_{32} - 3\,\mathcal{P}_{33} + 8\,\mathcal{P}_{36} - 8\,\mathcal{P}_{37} - 11\,\mathcal{P}_{39} + 5\,\mathcal{P}_{40} + 14\,\mathcal{P}_{41} \\
& \qquad - 8\,\mathcal{P}_{42} - 9\,\mathcal{P}_{43} + 3\,\mathcal{P}_{44} - 3\,\mathcal{P}_{45} - 6\,\mathcal{P}_{51} - 6\,\mathcal{P}_{53} \Big) = 0 \\
+\, & c_{27} \Big(8\,\mathcal{P}_{27} + 8\,\mathcal{P}_{28} - 2\,\mathcal{P}_{29} + 2\,\mathcal{P}_{30} - 4\,\mathcal{P}_{31} + 8\,\mathcal{P}_{32} - 2\,\mathcal{P}_{33} - 2\,\mathcal{P}_{39} + 2\,\mathcal{P}_{40} \\
& \qquad + 4\,\mathcal{P}_{41} - 2\,\mathcal{P}_{43} + 2\,\mathcal{P}_{44} - 2\,\mathcal{P}_{45} - 4\,\mathcal{P}_{51} - 4\,\mathcal{P}_{53} \Big) = 0\,, \qquad (2.49)
\end{aligned}
$$

which holds for whatever values of c_1 and c_{27}. In other words, the two linear combinations among the operators $\mathcal{P}_i$ between parenthesis must vanish independently. It leads to

$$
\begin{aligned}
& 4\,\mathcal{P}_{27} + 4\,\mathcal{P}_{28} - \mathcal{P}_{29} + \mathcal{P}_{30} - 2\,\mathcal{P}_{31} + 4\,\mathcal{P}_{32} - \mathcal{P}_{33} - \mathcal{P}_{39} + \mathcal{P}_{40} + 2\,\mathcal{P}_{41} \\
& \qquad - \mathcal{P}_{43} + \mathcal{P}_{44} - \mathcal{P}_{45} - 2\,\mathcal{P}_{51} - 2\,\mathcal{P}_{53} = 0\,, \qquad (2.50)
\end{aligned}
$$

$$
\begin{aligned}
& 8\,\mathcal{P}_1 - 2\,\mathcal{P}_2 + 6\,\mathcal{P}_3 - 20\,\mathcal{P}_{24} + 8\,\mathcal{P}_{25} + 12\,\mathcal{P}_{26} - 12\,\mathcal{P}_{27} - 28\,\mathcal{P}_{28} + 8\,\mathcal{P}_{36} - 8\,\mathcal{P}_{37} \\
& \qquad - 8\,\mathcal{P}_{39} + 2\,\mathcal{P}_{40} + 8\,\mathcal{P}_{41} - 8\,\mathcal{P}_{42} - 6\,\mathcal{P}_{43} = 0\,. \qquad (2.51)
\end{aligned}
$$

But, these relations were already shown to exist analytically in Refs. [15,16]. Therefore, using our method we have concluded that these are the only operator relations which can exist in the limit we have studied and the original basis of 27 measurable terms plus 2 contact terms written in [13] in the even-intrinsic-parity sector has 25+2 independent terms. Also, the fact that they are proved analytically as well, confirms our method. The point is, even if the two relations had not been proved analytically, our method would be useful to be sure that up to this approximation there are two relations and to be sure that they hold at the operator level.

Appendix

monomial (Y_i)	SU(n)	SU(3)	SU(2)	contributes to
$\langle u \cdot u h_{\mu\nu} h^{\mu\nu} \rangle$	1	1	1	$\pi\pi \to \pi\pi$
$\langle u \cdot u \rangle \langle h_{\mu\nu} h^{\mu\nu} \rangle$	2	2		$\pi\pi \to \pi\pi$
$\langle h_{\mu\nu} u_\rho h^{\mu\nu} u^\rho \rangle$	3	3	2	$\pi\pi \to \pi\pi$
$\langle h_{\mu\nu} u_\rho \rangle \langle h^{\mu\nu} u^\rho \rangle$	4			$\pi\pi \to \pi\pi$
$\langle h_{\mu\nu} \left(u_\rho h^{\mu\rho} u^\nu + u^\nu h^{\mu\rho} u_\rho \right) \rangle$	5	4	3	$\pi\pi \to \pi\pi$
$\langle h_{\mu\nu} u_\rho \rangle \langle h^{\mu\rho} u^\nu \rangle$	6			$\pi\pi \to \pi\pi$
$\langle (u \cdot u)^2 \chi_+ \rangle$	7	5	4	$\pi\pi \to \pi\pi$
$\langle (u \cdot u)^2 \rangle \langle \chi_+ \rangle$	8	6		$\pi\pi \to \pi\pi$
$\langle u \cdot u \rangle \langle u \cdot u \chi_+ \rangle$	9	7		$\pi\pi \to \pi\pi$
$\langle u \cdot u \rangle^2 \langle \chi_+ \rangle$	10			$\pi\pi \to \pi\pi$
$\langle u \cdot u u_\mu \chi_+ u^\mu \rangle$	11	8		$\pi\pi \to \pi\pi$
$\langle u \cdot u u_\mu \rangle \langle \chi_+ u^\mu \rangle$	12	9		$\pi\pi \to \pi\pi$
$\langle \chi_+ u_\mu u_\nu u^\mu u^\nu \rangle$	13	10	5	$\pi\pi \to \pi\pi$
$\langle \chi_+ \rangle \langle u_\mu u_\nu u^\mu u^\nu \rangle$	14	11		$\pi\pi \to \pi\pi$
$\langle \chi_+ u_\mu u_\nu \rangle \langle u^\mu u^\nu \rangle$	15			$\pi\pi \to \pi\pi$
$\langle \chi_+ \rangle \langle u_\mu u_\nu \rangle^2$	16			$\pi\pi \to \pi\pi$
$\langle \chi_+ h_{\mu\nu} h^{\mu\nu} \rangle$	17	12	6	$\langle \pi\pi \rangle$
$\langle \chi_+ \rangle \langle h_{\mu\nu} h^{\mu\nu} \rangle$	18	13		$\langle \pi\pi \rangle$
$\langle u \cdot u \chi_+^2 \rangle$	19	14	7	$\langle \pi\pi \rangle$
$\langle u \cdot u \chi_+ \rangle \langle \chi_+ \rangle$	20	15	8	$\langle \pi\pi \rangle$
$\langle u \cdot u \rangle \langle \chi_+^2 \rangle$	21	16		$\langle \pi\pi \rangle$
$\langle u \cdot u \rangle \langle \chi_+ \rangle^2$	22			$\langle \pi\pi \rangle$
$\langle \chi_+ u_\mu \chi_+ u^\mu \rangle$	23	17	9	$\langle \pi\pi \rangle$
$\langle \chi_+ u_\mu \rangle^2$	24	18		$\langle \pi\pi \rangle$
$\langle \chi_+^3 \rangle$	25	19	10	$\langle \pi\pi \rangle$
$\langle \chi_+^2 \rangle \langle \chi_+ \rangle$	26	20	11	$\langle \pi\pi \rangle$
$\langle \chi_+ \rangle^3$	27	21		$\langle \pi\pi \rangle$
i $\langle \chi_- \{ h_{\mu\nu}, u^\mu u^\nu \} \rangle$	28	22	12	$\pi\pi \to \pi\pi$
i $\langle \chi_- h_{\mu\nu} \rangle \langle u^\mu u^\nu \rangle$	29	23		$\pi\pi \to \pi\pi$

Table 2.1:

monomial (Y_i)	SU(n)	SU(3)	SU(2)	contributes to
i $\langle h_{\mu\nu}u^\mu u^\nu\rangle\langle\chi_-\rangle$	30	24		$\pi\pi\to\pi\pi$
i $\langle h_{\mu\nu}u^\mu\chi_- u^\nu\rangle$	31	25	13	$\pi\pi\to\pi\pi$
i $\langle h_{\mu\nu}u^\mu\rangle\langle\chi_- u^\nu\rangle$	32			$\pi\pi\to\pi\pi$
$\langle u\cdot u\chi_-^2\rangle$	33	26	14	$\pi\pi\to\pi\pi$
$\langle u\cdot u\chi_-\rangle\langle\chi_-\rangle$	34	27	15	$\pi\pi\to\pi\pi$
$\langle u\cdot u\rangle\langle\chi_-^2\rangle$	35	28		$\pi\pi\to\pi\pi$
$\langle u\cdot u\rangle\langle\chi_-\rangle^2$	36			$\pi\pi\to\pi\pi$
$\langle u_\mu\chi_- u^\mu\chi_-\rangle$	37	29	16	$\pi\pi\to\pi\pi$
$\langle u_\mu\chi_-\rangle^2$	38	30		$\pi\pi\to\pi\pi$
$\langle\chi_-^2\chi_+\rangle$	39	31	17	$\langle\pi\pi\rangle$
$\langle\chi_+\rangle\langle\chi_-^2\rangle$	40	32	18	$\langle\pi\pi\rangle$
$\langle\chi_+\chi_-\rangle\langle\chi_-\rangle$	41	33	19	$\langle\pi\pi\rangle$
$\langle\chi_+\rangle\langle\chi_-\rangle^2$	42			$\langle\pi\pi\rangle$
i $\langle\chi_-\{\chi_{+\,\mu}, u^\mu\}\rangle$	43	34	20	$F_S^\pi(t)$
i $\langle\chi_-\rangle\langle\chi_{+\,\mu}u^\mu\rangle$	44	35	21	$F_S^\pi(t)$
i $\langle\chi_{+\mu}\rangle\langle\chi_- u^\mu\rangle$	45	36		$F_S^\pi(t)$
$\langle\chi_{-\mu}\rangle^2$	46	37		$\langle SS\rangle$
$\langle\chi_{+\mu}\chi_+^\mu\rangle$	47	38	22	$\langle SS\rangle$
$\langle\chi_{+\mu}\rangle^2$	48	39	23	$\langle SS\rangle$
$\langle(u\cdot u)^3\rangle$	49	40	24	$\pi\pi\to 4\pi$
$\langle(u\cdot u)^2\rangle\langle u\cdot u\rangle$	50	41		$\pi\pi\to 4\pi$
$\langle u\cdot u\rangle^3$	51			$\pi\pi\to 4\pi$
$\langle u\cdot uu_\mu u\cdot uu^\mu\rangle$	52	42		$\pi\pi\to 4\pi$
$\langle u\cdot uu_\mu\rangle^2$	53	43		$\pi\pi\to 4\pi$
$\langle u\cdot uu_\mu u_\nu u^\mu u^\nu\rangle$	54	44	25	$\pi\pi\to 4\pi$
$\langle u\cdot uu_\mu u_\nu\rangle\langle u^\mu u^\nu\rangle$	55			$\pi\pi\to 4\pi$
$\langle u\cdot u\rangle\langle u_\mu u_\nu\rangle^2$	56			$\pi\pi\to 4\pi$
$\langle u\cdot u\rangle\langle u_\mu u_\nu u^\mu u^\nu\rangle$	57	45		$\pi\pi\to 4\pi$
$\langle u_\mu u_\nu u_\rho u^\mu u^\nu u^\rho\rangle$	58	46	26	$\pi\pi\to 4\pi$
$\langle u_\mu u_\nu u_\rho\rangle^2$	59			$\pi\pi\to 4\pi$
$\langle u_\mu u_\nu u_\rho u^\mu u^\rho u^\nu\rangle$	60	47		$\pi\pi\to 4\pi$
$\langle u_\mu u_\nu u_\rho\rangle\langle u^\mu u^\rho u^\nu\rangle$	61			$\pi\pi\to 4\pi$

Table 2.1:

monomial (Y_i)	SU(n)	SU(3)	SU(2)	contributes to
$\langle u_\mu u_\nu\rangle\langle u_\rho u^\mu u^\rho u^\nu\rangle$	62			$\pi\pi \to 4\pi$
$\langle u_\mu u_\nu\rangle\langle u^\mu u_\rho\rangle\langle u^\nu u^\rho\rangle$	63			$\pi\pi \to 4\pi$
i $\langle f_{+\mu\nu}\{u\cdot u, u^\mu u^\nu\}\rangle$	64	48		$\gamma^* \to 4\pi$
i $\langle u\cdot u\rangle\langle f_{+\mu\nu}u^\mu u^\nu\rangle$	65	49		$\gamma^* \to 4\pi$
i $\langle f_{+\mu\nu}u_\rho u^\mu u^\nu u^\rho\rangle$	66	50	27	$\gamma^* \to 4\pi$
i $\langle f_{+\mu\nu}u^\mu u\cdot u u^\nu\rangle$	67	51	28	$\gamma^* \to 4\pi$
i $\langle f_{+\mu\nu}\{u_\rho, u^\mu u^\rho u^\nu\}\rangle$	68	52		$\gamma^* \to 4\pi$
i $\langle f_{+\mu\nu}u_\rho\rangle\langle u^\mu u^\nu u^\rho\rangle$	69			$\gamma^* \to 4\pi$
i $\langle f_{+\mu\nu}[u^\mu, u_\rho]\rangle\langle u^\nu u^\rho\rangle$	70			$\gamma^* \to 4\pi$
$\langle u\cdot u f_{+\mu\nu}f_+^{\mu\nu}\rangle$	71	53	29	$\gamma\gamma \to \pi\pi$
$\langle u\cdot u\rangle\langle f_{+\mu\nu}f_+^{\mu\nu}\rangle$	72	54		$\gamma\gamma \to \pi\pi$
$\langle f_{+\mu\nu}u_\rho f_+^{\mu\nu}u^\rho\rangle$	73	55	30	$\gamma\gamma \to \pi\pi$
$\langle f_{+\mu\nu}u_\rho\rangle^2$	74			$\gamma\gamma \to \pi\pi$
$\langle f_{+\mu\nu}f_+^{\mu\rho}u^\nu u_\rho\rangle$	75	56	31	$\gamma\gamma \to \pi\pi$
$\langle f_{+\mu\nu}f_+^{\mu\rho}u_\rho u^\nu\rangle$	76	57	32	$\gamma\gamma \to \pi\pi$
$\langle f_{+\mu\nu}f_+^{\mu\rho}\rangle\langle u^\nu u_\rho\rangle$	77	58		$\gamma\gamma \to \pi\pi$
$\langle f_{+\mu\nu}\left(u_\rho f_+^{\mu\rho}u^\nu + u^\nu f_+^{\mu\rho}u_\rho\right)\rangle$	78	59	33	$\gamma\gamma \to \pi\pi$
$\langle f_{+\mu\nu}u_\rho\rangle\langle f_+^{\mu\rho}u^\nu\rangle$	79			$\gamma\gamma \to \pi\pi$
$\langle f_{+\mu\nu}u^\nu\rangle\langle f_+^{\mu\rho}u_\rho\rangle$	80	60		$\gamma\gamma \to \pi\pi$
$\langle \chi_+ f_{+\mu\nu}f_+^{\mu\nu}\rangle$	81	61	34	$\langle VV\rangle$
$\langle \chi_+\rangle\langle f_{+\mu\nu}f_+^{\mu\nu}\rangle$	82	62		$\langle VV\rangle$
i $\langle f_{+\mu\nu}\{\chi_+, u^\mu u^\nu\}\rangle$	83	63		$F_V^\pi(t),\ K_{l3}$
i $\langle \chi_+\rangle\langle f_{+\mu\nu}u^\mu u^\nu\rangle$	84	64		$F_V^\pi(t),\ K_{l3}$
i $\langle f_{+\mu\nu}u^\mu\chi_+u^\nu\rangle$	85	65	35	$F_V^\pi(t),\ K_{l3}$
$\langle f_{-\mu\nu}\left(h^{\nu\rho}u_\rho u^\mu + u^\mu u_\rho h^{\nu\rho}\right)\rangle$	86	66	36	K_{l4}
$\langle f_{-\mu\nu}h^{\nu\rho}\rangle\langle u^\mu u_\rho\rangle$	87	67	37	K_{l4}
$\langle f_{-\mu\nu}u^\mu\rangle\langle h^{\nu\rho}u_\rho\rangle$	88	68		K_{l4}
$\langle f_{-\mu\nu}\left(u^\mu h^{\nu\rho}u_\rho + u_\rho h^{\nu\rho}u^\mu\right)\rangle$	89	69	38	K_{l4}
$\langle u\cdot u f_{-\mu\nu}f_-^{\mu\nu}\rangle$	90	70	39	$K_{l4\gamma}$
$\langle u\cdot u\rangle\langle f_{-\mu\nu}f_-^{\mu\nu}\rangle$	91	71		$K_{l4\gamma}$
$\langle f_{-\mu\nu}u_\rho f_-^{\mu\nu}u^\rho\rangle$	92	72	40	$K_{l4\gamma}$

Table 2.1:

monomial (Y_i)	SU(n)	SU(3)	SU(2)	contributes to
$\langle f_{-\mu\nu}u_\rho\rangle^2$	93			$K_{l4\gamma}$
$\langle f_{-\mu\nu}f_-^{\mu\rho}u^\nu u_\rho\rangle$	94	73	41	$K_{l4\gamma}$
$\langle f_{-\mu\nu}f_-^{\mu\rho}u_\rho u^\nu\rangle$	95	74	42	$K_{l4\gamma}$
$\langle f_{-\mu\nu}f_-^{\mu\rho}\rangle\langle u^\nu u_\rho\rangle$	96	75		$K_{l4\gamma}$
$\langle f_{-\mu\nu}\left(u_\rho f_-^{\mu\rho}u^\nu + u^\nu f_-^{\mu\rho}u_\rho\right)\rangle$	97	76	43	$K_{l4\gamma}$
$\langle f_{-\mu\nu}u_\rho\rangle\langle f_-^{\mu\rho}u^\nu\rangle$	98			$K_{l4\gamma}$
$\langle f_{-\mu\nu}u^\nu\rangle\langle f_-^{\mu\rho}u_\rho\rangle$	99	77		$K_{l4\gamma}$
i $\langle f_{+\mu\nu}[f_-^{\nu\rho},h_\rho^\mu]\rangle$	100	78	44	$\pi\to l\nu\gamma$
i $\langle f_{+\mu\nu}[f_-^{\nu\rho},f_{-\rho}^\mu]\rangle$	101	79	45	$\langle VAA\rangle$
$\langle\chi_+f_{-\mu\nu}f_-^{\mu\nu}\rangle$	102	80	46	$\langle AA\rangle$
$\langle\chi_+\rangle\langle f_{-\mu\nu}f_-^{\mu\nu}\rangle$	103	81		$\langle AA\rangle$
$\langle f_{+\mu\nu}[f_-^{\mu\nu},\chi_-]\rangle$	104	82	47	$\pi\to l\nu\gamma$
i $\langle f_{-\mu\nu}[\chi_-,u^\mu u^\nu]\rangle$	105	83	48	K_{l4}
i $\langle f_{-\mu\nu}u^\nu\rangle\langle u^\mu\chi_-\rangle$	106	84		K_{l4}
$\langle f_{-\mu\nu}\{\chi_+^\mu,u^\nu\}\rangle$	107	85	49	$\langle VAA\rangle$
$\langle\chi_+^\mu\rangle\langle f_{-\mu\nu}u^\nu\rangle$	108	86		$\langle VAA\rangle$
$\langle\nabla_\rho f_{-\mu\nu}\nabla^\rho f_-^{\mu\nu}\rangle$	109	87	50	$\langle AA\rangle$
i $\langle\nabla_\rho f_{+\mu\nu}[h^{\mu\rho},u^\nu]\rangle$	110	88	51	$F_V^\pi(t),\ K_{l3}$
i $\langle\nabla^\mu f_{+\mu\nu}[f_-^{\nu\rho},u_\rho]\rangle$	111	89	52	$\pi\to l\nu\gamma^*$
i $\langle\nabla^\mu f_{+\mu\nu}[h^{\nu\rho},u_\rho]\rangle$	112	90	53	$F_V^\pi(t),\ K_{l3}$
contact terms				
$\langle D_\mu\chi D^\mu\chi^\dagger\rangle$	113	91	54	
i $\langle F_{L\mu\nu}F_L^{\mu\rho}F_{L\rho}^\nu\rangle + L\to R$	114	92	55	
$\langle D_\rho F_{L\mu\nu}D^\rho F_L^{\mu\nu}\rangle + L\to R$	115	93	56	
additional contact term for $SU(3)$				
$\det(\chi)$ + h.c.		94		
additional contact term for $SU(2)$				
$\langle D_\mu\chi D^\mu\widetilde{\chi}\rangle$ + h.c.			57	

Table 2.1: $\mathcal{O}(p^6)$ operators in the basis of [13]. The label in the first column refers to the numbering scheme used in the latter reference. The last column indicates the simplest Green function to which the operator contributes. Also, $u\cdot u$ stands for $u_\mu u^\mu$.

Bibliography

[1] A. Pich, Rept. Prog. Phys. **58**, 563 (1995).

[2] D. B. Kaplan, arXiv:nucl-th/0510023 [nucl-th].

[3] T. Appelquist, J. Carazzone, Phys. Rev. **D11**, 2856 (1975).

[4] H. Georgi, Annu. Rev. Nucl. Part. Sci. **43**, 209 (1993).

[5] V. llisie, Concepts in Quantum Field Theory A Practitioner's Toolkit, Springer (2016).

[6] S. Weinberg, Physica A **96**, 327 (1979).

[7] J. Gasser and H. Leutwyler, Ann. Phys. (N.Y.) **158** , 142 (1985), Nucl, Phys, B **250**, 465 (1985).

[8] S. Scherer, Adv. Nucl. Phys. **27**, 277 (2003).

[9] J. Goldstone, A. Salam and S. Weinberg, Phys. Rev. **127**, 965 (1962).

[10] J. Gasser and H. Leutwyler, Nucl. Phys. B **250**, 465 (1985).

[11] A. V. Manohar, In *Lake Louise, 274 (1995) [hep-ph/9508245].

[12] J. Bijnens, Prog. Part. Nucl. Phys. **58** (2007) 521, arXiv:hep-ph/0604043.

[13] J. Bijnens, G. Colangelo and G. Ecker, JHEP **9902**, 020 (1999) [hep-ph/9902437].

[14] H. W. Fearing and S. Scherer, Phys. Rev. D **53**, 315 (1996) [hep-ph/9408346].

[15] C. Haefeli, M. A. Ivanov, M. Schmid and G. Ecker, arXiv:0705.0576 [hep-ph].

[16] P. Colangelo, J. J. Sanz-Cillero and F. Zuo, JHEP **1211**, 012 (2012) [arXiv:1207.5744 [hep-ph]].

3. Neutrino physics and Renormalization Group Equations

The first sign of neutrinos appeared via the study of the nuclear beta decay in the 1920s

$$n \to p + e^- + \overline{\nu}_e \,. \tag{3.1}$$

Normally the energy of the electron in the final state is expected to be given as $E_e = M_i - M_f$, but the experiments showed that the energy of the electron covers a continuous range from m_e to the maximum allowed value. Many people tried to explain this phenomenon and even Niels Bohr went as far as questioning the energy conservation principle. Finally in 1930 Wolfgang Pauli proposed that the missing energy could be taken away by a new particle, which had not been observed to that date, with spin 1/2 and zero electric charge. These new particles, called neutrinos, remained unobserved until 1956 when Reines and Cowan detected them [1]. Further studies showed that neutrinos were chiral particles and led to the V-A nature of weak interactions, to which neutrinos contribute. Later on muon neutrinos were discovered via the interaction $\pi^{\pm} \to \mu^{\pm} + \nu$ and it was demonstrated by L. Lederman, M. Schwarz and J. Steinberger in 1962 that the type of neutrino involved in this process was ν_μ. Finally, the neutrino belonging to the third lepton τ was also discovered in July 2000 by the *DONUT* collaboration [2]. Even though at the beginning neutrinos were assumed to be massless and the SM was constructed with massless neutrinos, oscillation experiments have shown that neutrinos are massive. Therefore in coming sections we describe the experimental bounds on the neutrino masses and introduce the models which can accommodate the mass of neutrinos.

Limits on the Neutrino masses

To measure the neutrino mass directly one can use the kinematics to put an upper bound on it. Taking into account that ν_1, ν_2 and ν_3 are primary mass components of ν_e, ν_μ and ν_τ respectively, the upper limits on the $\bar{\nu}_e$ mass from different experiments read [6]

$$m_{\nu_e} < 2.2 \text{ e}V \qquad [7] \quad \text{at} \quad 2\sigma\,. \tag{3.2}$$

If one assumes that neutrinos are Majorana, then the neutrinoless double beta decay experiments should be studied. A double beta decay experiment can be described via the Feynman diagram in the Fig. 3.1, while the neutrinoless double beta decay experiment is showed in Fig. 3.2, which is sometimes called the lobster diagram.

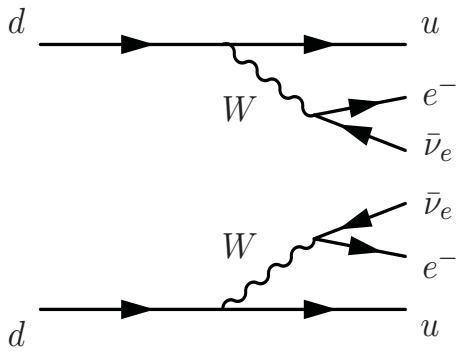

Figure 3.1: The Feynman diagram for the double beta decay experiment [6]

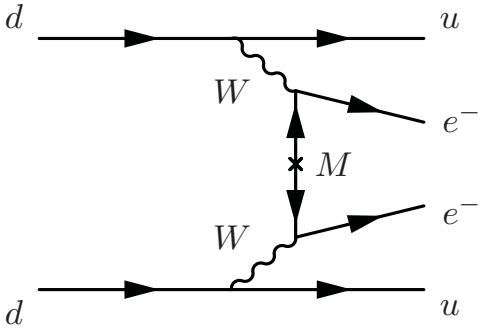

Figure 3.2: The Feynman diagram for the neutrinoless double beta decay experiment, the lobster diagram [6]

The expression for the effective neutrino mass in neutrinoless double beta decay is

$$M_{e\,e} \equiv \mid \sum_j U_{ej}^2 m_j \mid , \tag{3.3}$$

which is a function of mixing angles and phases and the upper limit is $M_{ee} \leq 0.4$ eV [5].

Also, there are some bounds from cosmological observations on the neutrino masses which are model dependent. Combining the Cosmic Microwave Background (CMB) data of the WMAP experiment with supernovae data and data on galaxy clustering one can obtain an upper limit on the sum of neutrinos masses. Depending on the model complexity and the input data used one obtains (up to 2σ) [8]:

$$\sum_j m_j \leq (0.3 - 1.3)\ \mathrm{e}V\,. \tag{3.4}$$

Assuming the validity of the ΛCDM (Cold Dark Matter) model, and using the Planck experiment data on the CMB temperature power spectrum anisotropies, polarization and gravitational lensing effects, the Planck Collaboration reported the following updated upper limit on the sum of the neutrino masses (up to 2σ) [9, 10]

$$\sum_j m_j \leq 0.57\ \mathrm{e}V\,. \tag{3.5}$$

Now that the limits on neutrino masses are known, we go ahead to consider the consequences of massive neutrinos.

Neutrino mass and See-saw mechanism

First we will review some basic properties of the Dirac equation and its solutions. We know that a Dirac spinor can be written in the form

$$\Psi = \psi_L + \psi_R\,, \tag{3.6}$$

where ψ_L and ψ_R represent the left chiral and right chiral fermion fields, respectively. This can be seen more clearly by introducing the projection operator

$$P_L = \frac{1-\gamma_5}{2} \qquad \text{and} \qquad P_R = \frac{1+\gamma_5}{2}\,, \tag{3.7}$$

which has the effect

$$\begin{aligned} P_L\Psi &= \psi_L\,, \\ P_R\Psi &= \psi_R\,, \\ \overline{\Psi}P_L &= \overline{\psi_R}\,, \\ \overline{\Psi}P_R &= \overline{\psi_L}\,. \end{aligned} \tag{3.8}$$

These projectors are useful for massless as well as massive Dirac particles.

Another useful operator is the charge conjugation operator which is defined for the fermion field as follows

$$\psi^{\mathrm{c}} = \mathcal{C}\bar{\psi}^T = \mathcal{C}\gamma_0\psi^*\,, \tag{3.9}$$

where $\mathcal{C} = i\gamma_0\gamma_2$. In correspondence with the aforementioned properties of the ψ one should note that

$$(\psi_L)^{\mathrm{c}} = (\psi^{\mathrm{c}})_R \qquad \text{and} \qquad (\psi_R)^{\mathrm{c}} = (\psi^{\mathrm{c}})_L\,. \tag{3.10}$$

This property can be interesting in the case that

$$\begin{aligned} \psi_L &= (\psi_R)^{\mathrm{c}}\,, \\ \psi_R &= (\psi_L)^{\mathrm{c}}\,, \end{aligned} \tag{3.11}$$

which, neglecting a possible phase factor, boils down to

$$\psi^{\mathrm{c}} = \psi\,. \tag{3.12}$$

This is the definition of a Majorana field.

The See-saw mechanism

Using the above definitions one can define two types of masses for fermions namely, the Dirac mass and the Majorana mass. The Dirac mass term reads

$$\mathcal{L}_D = -M_D(\overline{\psi}_R\psi_L + \overline{\psi}_L\psi_R)\,. \tag{3.13}$$

Also, taking into account the properties of the operator $\mathcal{C}$, the Majorana mass term takes the form

$$\mathcal{L}_M = -\frac{1}{2}M_L(\overline{\psi_L^c}\psi_L + \overline{\psi_L}\psi_L^c) - \frac{1}{2}M_R(\overline{\psi_R^c}\psi_R + \overline{\psi_R}\psi_R^c)\,, \tag{3.14}$$

where the notation $\psi_{L(R)}^c = (\psi_{L(R)})^c$ is in use. It is worthwhile to mention that both of the above mass terms violate the chiral symmetry, while the Majorana mass term violates the lepton number symmetry as well.

Both of these masses can be used to write a general fermion mass term

$$\begin{aligned}\mathcal{L}_{Mass} &= -\frac{1}{2}M_L\overline{\psi_L^c}\psi_L - \frac{1}{2}M_R\overline{\psi_R^c}\psi_R - M_D\overline{\psi_R}\psi_L + h.c. \\ &= -\frac{1}{2}\overline{\Psi_L^c}M\Psi_L + h.c.\,,\end{aligned} \tag{3.15}$$

with

$$\Psi_L = \begin{pmatrix} \psi_L \\ \psi_R^c \end{pmatrix} \qquad \text{and} \qquad M = \begin{pmatrix} M_L & M_D \\ M_D & M_R \end{pmatrix}. \tag{3.16}$$

To diagonalize this matrix we define

$$U = \begin{pmatrix} \cos\theta & \sin\theta \\ -\sin\theta & \cos\theta \end{pmatrix} \qquad \text{and} \qquad \Psi_L = U\begin{pmatrix} \chi_{L1} \\ \chi_{L2} \end{pmatrix}. \tag{3.17}$$

Then

$$\begin{pmatrix} M_1 & 0 \\ 0 & M_2 \end{pmatrix} = \begin{pmatrix} \cos\theta & -\sin\theta \\ \sin\theta & \cos\theta \end{pmatrix}\begin{pmatrix} M_L & M_D \\ M_D & M_R \end{pmatrix}\begin{pmatrix} \cos\theta & \sin\theta \\ -\sin\theta & \cos\theta \end{pmatrix}, \tag{3.18}$$

where the masses are real but can be positive or negative. Demanding the off diagonal terms to vanish one finds the mixing angle to be

$$\tan 2\theta = \frac{2M_D}{M_R - M_L}\,. \tag{3.19}$$

Now, the diagonalized mass term reads

$$\mathcal{L}_{dig} = -\frac{1}{2}M_1\overline{\chi_{1L}^c}\chi_{1L} - \frac{1}{2}M_2\overline{\chi_{2L}^c}\chi_{2L} + h.c.\,, \tag{3.20}$$

which describes two Majorana fields with masses M_1 and M_2 and the eigenvalues become

$$M_{1,2} = \frac{M_R + M_L}{2} \pm \sqrt{\frac{(M_L - M_R)^2}{4} + M_D^2}\,. \tag{3.21}$$

So far we have considered the fermion fields in general but, the Majorana mass term is allowed only for electrically neutral particles since otherwise it would violate charge conservation. Therefore, it is belived that the only candidates to have a Majorana mass in the SM are neutrinos.

Moreover, in the context of the SM the Majorana mass for the left handed neutrinos is not allowed due to the $SU(2)$ gauge invariance. This can be cured via the Higgs mechanism by introducing the dimension 5 Weinberg operator

$$\mathcal{L}_\kappa = \frac{\kappa_{gf}}{\Lambda}\, \overline{\ell^c_{\mathrm{L}c}}^{\,g} \varepsilon^{cd} \phi_d \; \ell^f_{\mathrm{L}b} \varepsilon^{ba} \phi_a + \mathrm{h.c.}\,. \tag{3.22}$$

This is an effective Lagrangian where; based on what we said about the effective Lagrangians in the previous chapter; the effect of the heavy degrees of freedom is given by Λ and κ_{gf} is a complex symmetric matrix. Also, l_L is the left handed lepton field of the SM and Φ is the standard model Higgs doublet. After the SSB the neutral component of the Higgs field will get the vacuum expectation value $\langle \Phi_0 \rangle = v/\sqrt{2}$ with $v = 246$ GeV. When the Higgs field gets the vev this term becomes a Majorana mass term for the left handed neutrinos. The only issue with this operator is that it is not renormalizable. In a fundamental theory it should be generated by "integrating out" some heavier new states. One way to provide this is the See-saw mechanism.

If one adds singlet right handed neutrinos to the SM, they can get the Majorana mass, which in principle can be very heavy. Also, a Dirac mass term could be created via the Lagrangian (3.13). Hence, following the above calculation, writing

$$\Psi_L \;\; = \begin{pmatrix} \nu_L \\ \nu^{\mathrm{c}}_R \end{pmatrix} \tag{3.23}$$

instead of (3.16), taking $M_L = 0$ and the limit $M_R \gg M_D$, the eigenvalues (3.21) belong to two Majorana neutrinos, one which is very heavy and

another one which is very light such that

$$M_1 \simeq -\frac{M_D^2}{M_R}\,,$$
$$M_2 \simeq M_R\,, \tag{3.24}$$

where the minus sign can be absorbed by a phase redifinition [11]. The corresponding eigenstates read

$$\chi_{1L} \simeq \nu_L - \frac{M_D}{M_R}\nu_R^{\rm c}\,,$$
$$\chi_{2L} \simeq \nu_R^{\rm c} + \frac{M_D}{M_R}\nu_L\,. \tag{3.25}$$

Which are approximately the left handed fields defined above, but with a small admixture of order $\frac{M_D}{M_R}$. Now, if one assumes M_D to be around 100 GeV which corresponds to the EW scale, taking M_R to be around 10^{14} GeV, then $M_1 = 0.1$ eV which is compatible with the upper limit of the left handed neutrino masses. This is the essence of the Type-1 See-saw mechanism.

Another interesting limit to consider is when $M_L = M_R = 0$ and $M_D \neq 0$. In this case, the mixing angle is maximal $\theta = \pi/4$ and the eigenstates become

$$\chi_{1L} = \frac{1}{\sqrt{2}}(\nu_L - \nu_R^{\rm c})\,,$$
$$\chi_{2L} = \frac{1}{\sqrt{2}}(\nu_L + \nu_R^{\rm c})\,, \tag{3.26}$$

which shows that a Dirac fermion can be written in terms of two Majorana fermions with identical masses. For the case of $M_D = 0$, the rotation matrix is the identity.

In short, in type one See-saw one adds singlet right handed neutrinos to the SM and using the Higgs field one can create a Dirac mass. At the same time, the right handed neutrino can get a Majorana mass term, which can be very large in principle compared to the Higgs vev. This will lead to a mass matrix which after diagonalization leads to a light left handed mass term. In type two See-saw, there are no right handed neutrinos and instead,

one writes down the Majorana mass term directly using a new $SU(2)$ triplet scalar field. The new triplet, combined with the two left handed doublets of leptons, will lead to a singlet under the group transformations. Finally, the type three See-saw is similar to type one with a fermion triplet replacing the right handed neutrinos. Different types of the See-saw are shown in the Fig. 3.3. It should be stressed that all of these variants of the See-saw mechanism boil down to the Weinberg operator, when the heavy degrees of freedom are integrated out.

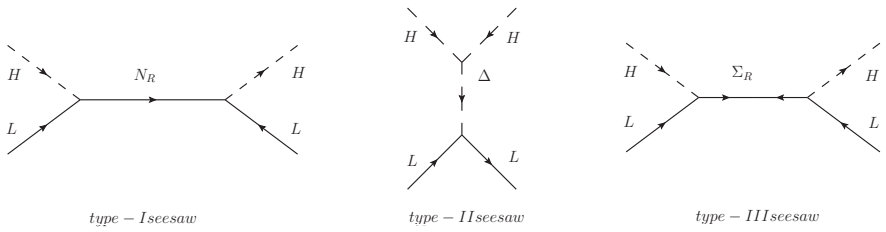

Figure 3.3: See-saw different scenarios

In fact, the nature of neutrinos is still unknown and they can be of Dirac or Majorana type. There are many ongoing experiments [3]– [5] to test this point however, we take both to be equally probable. Therefore, one of our projects deals with Majorana neutrinos and the other with Dirac neutrinos (next sections).

Neutrino oscillations in vacuum

As Bruno Pontecorvo [12] predicted many years ago, when neutrinos are massive the flavor mixing will happen for neutrinos in vacuum. We know that the weak eigenstates of quarks are related to the mass eigenstates by the CKM matrix [13]

$$\begin{pmatrix} d' \\ s' \\ b' \end{pmatrix} = V^{CKM} \begin{pmatrix} d \\ s \\ b \end{pmatrix} \quad . \tag{3.27}$$

As it was discussed in chapter 1, the same thing happens for the lepton sector, when neutrinos are massive, that is

$$\begin{pmatrix} \nu_e \\ \nu_\mu \\ \nu_\tau \end{pmatrix} = U^{PMNS} \begin{pmatrix} \nu_1 \\ \nu_2 \\ \nu_3 \end{pmatrix} \ , \tag{3.28}$$

where U_{PMNS} stands for Pontecorvo-Maki-Nakagawa-Sakata unitary matrix [12, 14]. Now, since it is not practical to measure the mass of neutrinos at least for the time being, one has to write the amplitudes in term of all mass eigenstates and due to the fact that each state evolves with a different phase, one will inevitably face oscillations in flavor space. We will elaborate more on this in coming paragraphs. Writing

$$|\nu_\eta\rangle = \sum_i U^*_{\eta i} |\nu_i\rangle \, , \tag{3.29}$$

one can write a well defined flavor state in terms of mass states, at a distance L from the production point, and at a time t after production in the following form

$$|\nu_\eta(t, L)\rangle = \sum_j U^*_{\eta j} e^{-iE_j t + ip_j L} |\nu_j\rangle \, , \tag{3.30}$$

where $E_i = \sqrt{p^2 + m_i^2}$. Calculating the amplitude for the transition from one flavor state to another, using $\langle \nu_j | \nu_i \rangle = \delta_{ij}$, one finds

$$\begin{aligned} M(\nu_A \to \nu_B; t, L) &= \langle \nu_B | \nu_A(t, L) \rangle \\ &= \sum_{j,k} U^*_{Aj} U_{Bk} e^{-iE_j t + ip_j L} \langle \nu_k | \nu_j \rangle \\ &= \sum_j U^*_{Aj} U_{Bj} e^{-iE_j t + ip_j L} \, . \end{aligned} \tag{3.31}$$

By squaring the amplitude one finds the probability of the transition to be

$$P(\nu_A \to \nu_B; t, L) = \sum_{j,k} U^*_{Aj} U_{Bj} U_{Ak} U^*_{Bk} e^{-i(E_j - E_k)t + i(p_j - p_k)L} \,. \tag{3.32}$$

Since we do not know when precisely each neutrino is produced, therefore we should integrate over time

$$\begin{aligned} P(\nu_A \to \nu_B; L) &= \frac{1}{N} \int dt |P(\nu_A \to \nu_B; t, L)|^2 \\ &= \frac{1}{N} \sum_{j,k} U^*_{Aj} U_{Bj} U_{Ak} U^*_{Bk} e^{i(p_j - p_k)L} \delta(E_j - E_k) \\ &\simeq \sum_{j,k} U^*_{Aj} U_{Bj} U_{Ak} U^*_{Bk} e^{-i\frac{\Delta m^2_{jk} L}{2E}} \,, \end{aligned} \tag{3.33}$$

where N is a normalization constant and the approximation

$$p_i = \sqrt{E_i^2 - m_i^2} \simeq E_i - \frac{m_i^2}{2E_i} \simeq E - \frac{m_i^2}{2E} \,, \tag{3.34}$$

has been used in the limit $p \to E$. As it can be seen, the probability depends on the energy E the distance L and the mass squared difference $\Delta m^2_{jk} = m^2_j - m^2_k$, not the absolute masses.

Two flavor case

To be more specific, we consider the case of two flavor oscillations [6]. Let's assume the oscillation takes place between the electron and muon neutrino flavors. Ignoring the Majorana phases for the case of the Majorana neutrino one has

$$\begin{pmatrix} \nu_e \\ \nu_\mu \end{pmatrix} = \begin{pmatrix} \cos\theta & \sin\theta \\ -\sin\theta & \cos\theta \end{pmatrix} \begin{pmatrix} \nu_1 \\ \nu_2 \end{pmatrix} . \tag{3.35}$$

Assuming that the initial state is an electron neutrino it can be written in terms of the mass states as follows

$$|\nu(t=0)\rangle = |\nu_e\rangle = \cos\theta |\nu_1\rangle + \sin\theta |\nu_2\rangle \,. \tag{3.36}$$

Then the probability takes the form

$$P(\nu_e \to \nu_\mu; L) = \sin^2 2\,\theta \sin^2[\frac{\Delta m^2_{12} L}{4E}]\,, \tag{3.37}$$

which depends on the neutrino energy E and the mass difference ($\Delta m^2_{12} = m^2_1 - m^2_2$), also called the solar mass Δm^2_{sol}. The other mass square difference which appears in the three flavor case ($\Delta m^2_{23} = m^2_2 - m^2_3$) is also called the atmospheric mass Δm^2_{atm}, see Fig. 3.4. For the three generation case, the mixing matrix parameters which are the three angles have already been measured but the CP phase remains undetermined. Apart from this, it is not known which is the hierarchy of the masses, normal (NH) or inverted (IH), as represented in Fig. 3.4

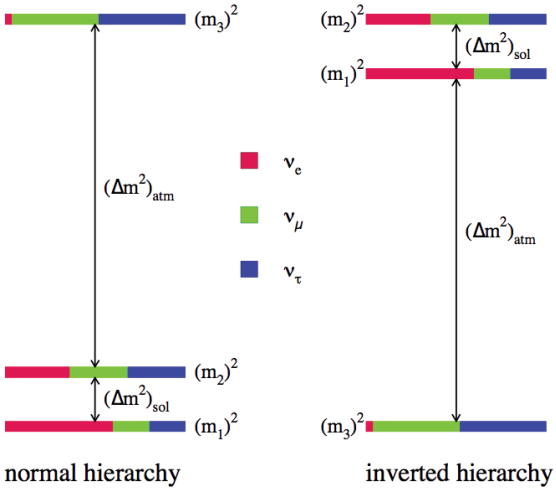

Figure 3.4: Different mass hierarchy scenarios [15]

For the case of three flavors, one can use the matrices

$$O_1 = \begin{pmatrix} 1 & 0 & 0 \\ 0 & \cos\theta_{23} & \sin\theta_{23} \\ 0 & -\sin\theta_{23} & \cos\theta_{23} \end{pmatrix},$$
$$O_2 = \begin{pmatrix} \cos\theta_{13} & 0 & \sin\theta_{13}e^{-i\delta} \\ 0 & 1 & 0 \\ -\sin\theta_{13}e^{i\delta} & 0 & \cos\theta_{13} \end{pmatrix},$$
$$O_3 = \begin{pmatrix} \cos\theta_{12} & \sin\theta_{12} & 0 \\ -\sin\theta_{12} & \cos\theta_{12} & 0 \\ 0 & 0 & 1 \end{pmatrix}, \tag{3.38}$$

with the Dirac phase δ and the Majorana phase matrix

$$F' = \begin{pmatrix} e^{i\varphi_1} & 0 & 0 \\ 0 & e^{i\varphi_2} & 0 \\ 0 & 0 & 1 \end{pmatrix}, \tag{3.39}$$

in the Standard Parametrization to have

$$U_{PMNS} = O_1 \cdot O_2 \cdot O_3 \cdot F' = \begin{pmatrix} c_{12}c_{13} & s_{12}c_{13} & s_{13}e^{-i\delta} \\ -c_{23}s_{12} - s_{23}s_{13}c_{12}e^{i\delta} & c_{23}c_{12} - s_{23}s_{13}s_{12}e^{i\delta} & s_{23}c_{13} \\ s_{23}s_{12} - c_{23}s_{13}c_{12}e^{i\delta} & -s_{23}c_{12} - c_{23}s_{13}s_{12}e^{i\delta} & c_{23}c_{13} \end{pmatrix} \cdot F', \tag{3.40}$$

where, $c_{mn} = \cos\theta_{mn}, s_{mn} = \sin\theta_{mn}$.

The global status of the neutrino mixing parameters is given in Tab. 3.1.

Quantity	Best Fit	3σ Range
Δm^2_{21} (10^{-5} eV^2)	7.60	7.1 – 8.16
Δm^2_{31} (10^{-3} eV^2)	2.46	2.30 – 2.59
θ°_{12}	33.02	30 – 36.5
θ°_{23}	48.9	38 – 51.7
θ°_{13}	8.41	7.82– 9.02

Table 3.1: The global fits for the neutrino mixing parameters [16]

CP and T violating effects

In principle one can assume that the oscillation probability violates CP or T that is

$$\begin{aligned} P(\nu_A \to \nu_B) &\neq P(\bar{\nu}_A \to \bar{\nu}_B)\,, \\ P(\nu_A \to \nu_B) &\neq P(\nu_B \to \nu_A)\,, \end{aligned} \tag{3.41}$$

while CPT is conserved

$$P(\nu_A \to \nu_B) = P(\bar{\nu}_B \to \bar{\nu}_A)\,. \tag{3.42}$$

Now one can calculate the probability $P(\nu_A \to \nu_B)$ for the three flavor case, which, yields

$$\begin{aligned} P(\nu_A \to \nu_B) = |\sum_j U_{Bj} U^*_{Aj} e^{-im_j^2 \frac{L}{2E_\nu}}|^2 &= \sum_j |U_{Bj}|^2 |U_{Aj}|^2 \\ &+ \sum_{j<k} 2Re[U_{Bj} U^*_{Bk} U^*_{Aj} U_{Ak}] \cos\Big(\frac{\triangle m^2_{jk} L}{2E}\Big) \\ &+ \sum_{j<k} 2Im[U_{Bj} U^*_{Bk} U^*_{Aj} U_{Ak}] \sin\Big(\frac{\triangle m^2_{jk} L}{2E}\Big)\,, \end{aligned} \tag{3.43}$$

where $\triangle m^2_{ij} = m^2_j - m^2_i$.

There are some points to be observed in this relation. By making a CP change that is changing $U \to U^*$, the "cos" term does not change sign while the "sin" term does. It means that as long as $\delta = 0$ or $\delta = \pi$, there is no CP violating effect in which case the imaginary part of the mixing matrix vanishes. Studying the time reversal effect, which is the exchange $\nu_B \to \nu_A$ one can come to the same conclusion. And finally, making both changes, $U \to U^*$ and $\nu_B \to \nu_A$ together, which is equal to $\nu \to \bar{\nu}$, one can probe that the CPT invariance holds for the oscillation probability.

Using the unitary property of the matrix U namely

$$\begin{aligned} \sum_i U_{Bi} U^*_{Ai} &= \delta_{AB}\,, \\ \sum_A U_{Ai} U^*_{Aj} &= \delta_{ij}\,, \end{aligned} \tag{3.44}$$

one can find relations between the U dependent coefficients of the above relation, especially for $J^{AB}_{jk} = -Im[U_{Aj}U^*_{Ak}U^*_{Bj}U_{Bk}]$ which deals with the CP and T invariant property. Along with the unitarity one can also use the symmetries

$$J^{AB}_{jk} = -J^{AB}_{kj} = -J^{BA}_{jk} \tag{3.45}$$

and

$$J^{AB}_{jj} = -J^{AA}_{jk} = 0\,, \tag{3.46}$$

to obtain the additional relations

$$J^{AB}_{12} = J^{AB}_{23} = J^{AB}_{31}\,. \tag{3.47}$$

Using these facts one finds that there exist one coefficient

$$\begin{aligned} J = J^{e\mu}_{12} &= -Im[U_{e1}U^*_{\mu 1}U^*_{e2}U_{\mu 2}] \\ &= c^2_{13}s_{13}s_{12}c_{12}s_{23}c_{23}\sin\delta\,, \end{aligned} \tag{3.48}$$

called Jarlskog parameter, in terms of which all other non vanishing coefficients can be written. Putting everything together the transition probability reads

$$\begin{aligned} P_{\nu_A\to\nu_B} = \Lambda^{12}_{AB}\sin\Big(\frac{\triangle m^2_{12}L}{4E_\nu}\Big) + \Lambda^{23}_{AB}\sin\Big(\frac{\triangle m^2_{23}L}{4E_\nu}\Big) + \Lambda^{13}_{AB}\sin\Big(\frac{\triangle m^2_{13}L}{4E_\nu}\Big) \\ \pm 8J\sin\Big(\frac{\triangle m^2_{12}L}{4E_\nu}\Big)\sin\Big(\frac{\triangle m^2_{23}L}{4E_\nu}\Big)\sin\Big(\frac{\triangle m^2_{13}L}{4E_\nu}\Big)\,, \end{aligned} \tag{3.49}$$

where use has been made of the trigonometric relation

$$\sin\alpha + \sin\beta - \sin(\alpha+\beta) = 4\sin(\frac{\alpha}{2})\sin(\frac{b}{2})\sin\Big(\frac{(\alpha+\beta)}{2}\Big)\,, \tag{3.50}$$

and the notation

$$\Lambda^{ij}_{AB} = -4Re[U_{Ai}U^*_{Bi}U^*_{Aj}U_{Bj}]\,. \tag{3.51}$$

In the above relation, the part that controls the CP and T violation effects is the second part, which depends on the Jarlskog parameter. The morals that can be drawn from this relation are first, to have CP and T violation,

δ must be non trivial. Second, the mixing angles θ_{12}, θ_{23} and θ_{13} must be non vanishing and finally, the quantity $\frac{\triangle m^2_{ij} L}{4E}$ must be non vanishing, which means all oscillation modes should be active.

The HSMU Hypothesis

After introducing some features of the neutrino physics in previous sections, here we introduce the main objective of our work in neutrino physics. Due to grand unified theories [17]- [20], quarks and leptons get unified at high scales and appear in the same fundamental representation, therefore one may conclude that their weak interaction properties parametrized by means of the CKM and PMNS matrices will get unified at high scales as well. On the other hand, as experimental results show [21]– [23], the elements of the PMNS matrix are large whereas those of the CKM matrix are close to unity. Indeed, there have been many studies suggesting that this occurs due to the running of the RGE equations of the neutrino mixing parameters, that is, assuming that the elements are small at high scales, their values can change drastically [24]– [27] when running them down to the EW scale. The only assumption needed to realize this scenario is that the neutrino masses are quasi degenerate and hierarchical. Using these facts and assuming that at the unification scale

$$\theta_{12} = \theta^q_{12}, \quad \theta_{13} = \theta^q_{13}, \quad \theta_{23} = \theta^q_{23}\,, \tag{3.52}$$

where θ_{ij} (with $i, j = 1, 2, 3$) are leptonic mixing angles and θ^q_{ij} are the quark mixing angles, Mohapatra et. al. showed that in fact this idea works [28]– [29]. Later on they considered its properties for the case of non zero Dirac and Majorana phases as well [30] and took into account the threshold corrections [55] to bring the solar mass squared difference into the experimental range. Later on this idea, known as high scale mixing unification hypothesis (HSMU), was revised in the light of new experimental data [31,32] and was also extended to the case of Dirac neutrinos as well [33]. This hypothesis nicely explains the pattern of mixings in the neutrino sector including the recent observation of a nonzero small value of θ_{13} [34]– [38].

What we are going to do is to generalise the HSMU hypothesis in the way that the equality of the CKM and PMNS matrices is replaced by proportionality (see next sections).

Minimal Supersymmetric Model

As we are going to discuss the Renormalization Group Equations for neutrino mixing parameters, both in the context of the SM and the Minimal Supersymmetric Model (MSSM), since in our work both parts will be used, we need to comment on the basis of the MSSM to the extent that is relevant to our work. A good review on Supersymmetry (SUSY) can be found in Ref. [39]. SUSY is based on the fact that for every fermion (boson) there exists a boson (fermion), which is its partner and has exactly the same quantum numbers apart from spin. However, since the super partners have not been observed in nature, one introduces the SUSY breaking, which we will talk about later on. The minimal extension of the SM so as to include the supersymmetry is called the MSSM. The particle content of the MSSM is shown in Tab. 3.2.

	spin 0	spin $\frac{1}{2}$	spin 1	$(SU(3), SU(2), U_Y(1))$
quarks(squarks)	$(\tilde{u}_L, \tilde{d}_L)$	(u_L, d_L)	–	$(3, 2, \frac{1}{6})$
	$\tilde{u}_R$	u_R	–	$(3, 1, \frac{2}{3})$
	$\tilde{d}_R$	d_R	–	$(3, 1, -\frac{1}{3})$
leptons(sleptons)	$(\tilde{\nu}, \tilde{e}_L)$	(ν, e_L)		$(1, 2, -\frac{1}{2})$
	$\tilde{e}_R$	e_R	–	$(1, 1, -1)$
higgs(higgsinos)	(h_u^+, h_u^0)	$(\tilde{h}_u^+, \tilde{h}_u^0)$	–	$(1, 2, \frac{1}{2})$
	(h_d^0, h_d^-)	$(\tilde{h}_d^0, \tilde{h}_d^-)$	–	$(1, 2, -\frac{1}{2})$
gluons(gluinos)	–	$\tilde{g}$	g	$(8, 1, 0)$
W-bosons(winos)	–	$\widetilde{W}^{\pm}, \widetilde{W}^0$	$W^{\pm}, W^0$	$(1, 3, 0)$
B-boson (bino)	–	$\widetilde{B}$	B	$(1, 1, 0)$

Table 3.2: The particle content of the MSSM in terms of the chiral and gauge eigenstates and the representation in the SM gauge groups. The transformation property under $SU(3) \times SU(2)$ and the value of $U_Y(1)$ is given in the last column.

As was mentioned before, since the super partners have never been observed, one has to assume that one way or another the SUSY is broken. In our work, we take the scale of SUSY breaking to be at 2 TeV, which is in accordance with the recent SUSY searches in accelerators [40, 41].

The MSSM contains two Higgs doublets which introduces new scalar degrees of freedom. Apart from that, as it is always the case for 2HDM models, it introduces two vevs, ν_1 and ν_2 whose ratio is defined as $\tan\beta = \frac{\nu_2}{\nu_1}$. This becomes important when running the MSSM RGs.

Renormalization Group Equations

After the invention of the renormalization group by Stuckelberg and Petermann [42] in 1953, it was studied by Gell-mann and Low [43] who applied the approach to short distance quantum electrodynamics and also by Bogoliubov and Shirkov [44]. Then, Wilson [45]– [47] applied it to study the critical phenomena in statistical physics and won the Nobel prize of 1982 for his decisive contributions in this field. Finally Callan and Symanzik [48, 49] investigated the energy-scale dependence of Green's functions in general quantum field theories, and were able to conclude the renormalization-group equation, which was also named after them. The basic idea is that when a theory is renormalized at a given scale, μ, it remains so under variation of μ by changing the values of coupling constants and masses, g and m, which are functions of μ themselves. Demanding that a physical quantity like an scattering matrix element is invariant under change of μ, the renormalization group equation as an specific form of the Callan-Symanzik equation reads

$$\mu\frac{\partial S}{\partial \mu} + \beta\frac{\partial S}{\partial g} - \gamma m\frac{\partial S}{\partial m} = 0\,, \tag{3.53}$$

where

$$\beta = \mu\frac{\partial g(\mu)}{\partial \mu}\,, \qquad \gamma = -\frac{\mu}{m}\frac{\partial m(\mu)}{\partial \mu}\,. \tag{3.54}$$

We are especially interested in the β function, which gives the rate of change of the renormalized coupling with respect to the fixed bare charge, at a given scale μ [50]. In our analysis, we are going to study the change of the Yukawa couplings of the given Lagrangian for which we will need to calculate the β

function. As for the Majorana neutrinos, we are dealing with the Weinberg operator (3.55)

$$\mathcal{L}_\kappa = \frac{\kappa_{gf}}{\Lambda}\,\overline{\ell^c_{\mathrm{L}c}}^{g}\varepsilon^{cd}\phi_d\;\ell^f_{\mathrm{L}b}\varepsilon^{ba}\phi_a + \text{h.c.}\,, \tag{3.55}$$

that can be built out of the SM particle content and gives Majorana mass to left handed neutrinos.

For example, if one assumes that the Lagrangian (3.55) is derived via the see–saw type-1 mechanism then, κ can be derived below the scale Λ via the renormalization group equations (RGE), without considering the heavy right handed neutrinos.

This is motivated by the arguments given in the previous chapter on effective field theories. Consequently, one has to integrate out the heavy Majorana neutrinos from the theory when using the effective theory [51] and make sure that heavy particles do not contribute to the β-functions at low energy.

To calculate the RGEs for the coupling constant of the effective operator one has to calculate the relevant loop diagrams. The one–loop diagrams with leptons and scalars that are relevant to this purpose are shown in Fig. 3.5. Also the ones with $U(1)_Y$ gauge bosons, B, are listed in the Fig. 3.6 while those with W_i are the same with B replaced by W_i. At the one-loop level, κ obeys the RGE [52]

$$16\pi^2\frac{\mathrm{d}\kappa}{\mathrm{d}t} = C\left[(Y_eY_e^\dagger)\kappa + \kappa(Y_eY_e^\dagger)^T\right] + \alpha\kappa\,, \tag{3.56}$$

where $t \equiv \ln(\mu/\Lambda)$ and μ is a random scale below the See-saw scale and above the SM scale. The coefficients C are

$$C = -\frac{3}{2}\ \text{in the SM} \tag{3.57}$$

and

$$C = 1\ \text{in the MSSM} \tag{3.58}$$

and the α coefficients read

$$\begin{aligned}
\alpha_{\mathrm{SM}} &= -3g_2^2 + 2(y_\tau^2 + y_\mu^2 + y_e^2) + 6\left(y_t^2 + y_b^2 + y_c^2 + y_s^2 + y_d^2 + y_u^2\right) + \lambda\,,\\
\alpha_{\mathrm{MSSM}} &= -\frac{6}{5}g_1^2 - 6g_2^2 + 6\left(y_t^2 + y_c^2 + y_u^2\right)\,,
\end{aligned} \tag{3.59}$$

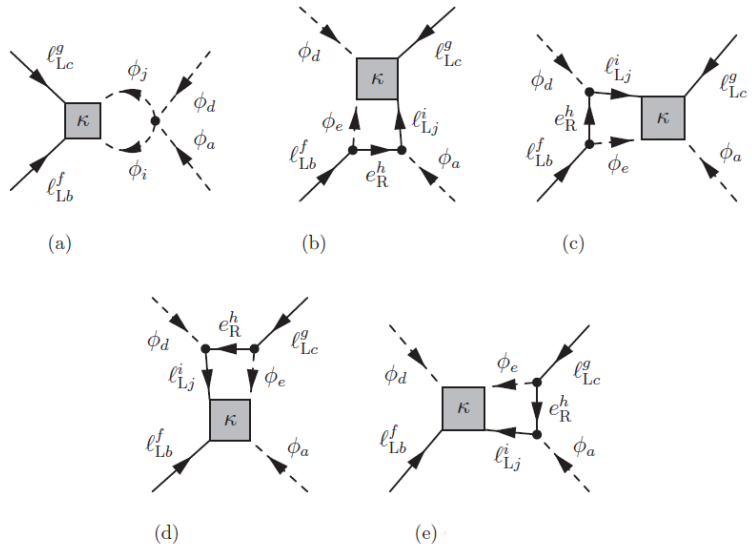

Figure 3.5: One-loop diagrams with leptons and scalars.

where g_1, g_2 and g_3 are the gauge couplings. They satisfy their own RGEs which writes

$$16\pi^2 \frac{\mathrm{d}g_i}{\mathrm{d}t} = a_i g_i^3 \,, \tag{3.60}$$

where $(a_1, a_2, a_3) = (41/10, -19/6, -7)$ in the SM or $(33/5, 1, -3)$ in the MSSM. Also, λ, the Higgs self-coupling, satisfies the RGE

$$\begin{aligned} 16\pi^2 \frac{\mathrm{d}\lambda}{\mathrm{d}t} = 6\lambda^2 - 3\lambda\left(\frac{3}{5}g_1^2 + 3g_2^2\right) + \frac{3}{2}\left(\frac{3}{5}g_1^2 + g_2^2\right)^2 + 3g_2^4 \\ +4\lambda \mathrm{Tr}\left[3(Y_\mathrm{u}Y_\mathrm{u}^\dagger) + 3(Y_\mathrm{d}Y_\mathrm{d}^\dagger) + (Y_l Y_l^\dagger)\right] \\ -8\mathrm{Tr}\left[3(Y_\mathrm{u}Y_\mathrm{u}^\dagger)^2 + 3(Y_\mathrm{d}Y_\mathrm{d}^\dagger)^2 + (Y_l Y_l^\dagger)^2\right] \,, \end{aligned} \tag{3.61}$$

where Y_l, Y_u and Y_d are the charged lepton, up-type quarks, down-type quarks Yukawa coupling matrix, respectively. Using these RGEs one can evaluate the running of the Yukawas of quarks and leptons from the high

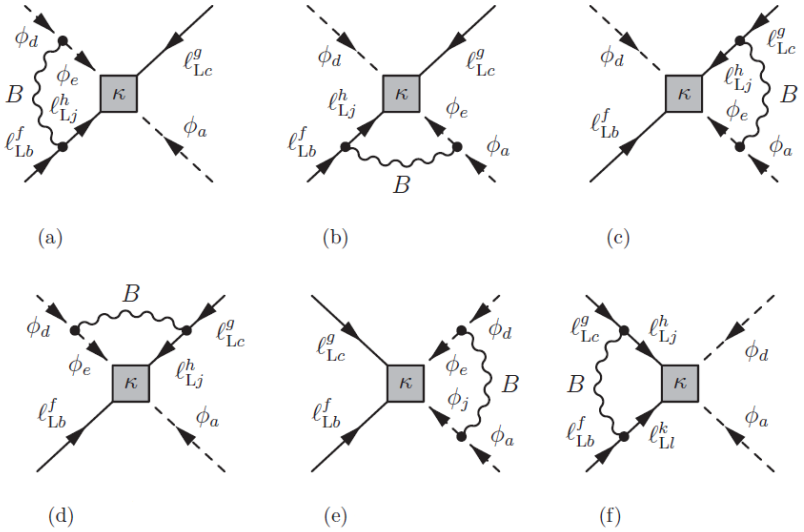

Figure 3.6: One-loop diagrams with $U(1)_Y$ gauge bosons, B

scale to the SM scale and the other way around. Then we are going to examine the behaviour of the neutrino mixing parameters during this running.

Running neutrino mass parameters

Assuming that Y_l is diagonal in the sense that $Y_l = l_d \equiv Diag\{y_e, y_\mu, y_\tau\}$, where y_i is the Yukawa of a given flavor, taking into account that the τ Yukawa is much bigger than the one of the other leptons, defining $\zeta = \frac{\Delta m^2_{21}}{\Delta m^2_{23}}$, with Δm_{21} and Δm_{23} defined in Fig. 3.4, and using the definition of the PMNS matrix (3.40), one finds the running equation of the neutrino

parameters as follows [53], [54]

$$\dot{\theta}_{12} = -\frac{Cy_\tau^2}{32\pi^2}\,\sin 2\theta_{12}\,\sin^2\theta_{23}\,\frac{|m_1\,e^{i\varphi_1}+m_2\,e^{i\varphi_2}|^2}{\Delta m^2_{\rm sol}}+O(\theta_{13})\,, \tag{3.62}$$

$$\begin{aligned}\dot{\theta}_{13} &= \frac{Cy_\tau^2}{32\pi^2}\,\sin 2\theta_{12}\,\sin 2\theta_{23}\,\frac{m_3}{\Delta m^2_{\rm atm}\,(1+\zeta)}\,\times\\ &\times\,[m_1\cos(\varphi_1-\delta)-(1+\zeta)\,m_2\,\cos(\varphi_2-\delta)-\zeta m_3\,\cos\delta]\\ &+\;\; O(\theta_{13})\,,\end{aligned} \tag{3.63}$$

$$\begin{aligned}\dot{\theta}_{23} &= -\frac{Cy_\tau^2}{32\pi^2}\,\sin 2\theta_{23}\,\frac{1}{\Delta m^2_{\rm atm}}\left[c_{12}^2\,|m_2\,e^{i\varphi_2}+m_3|^2+s_{12}^2\,\frac{|m_1\,e^{i\varphi_1}+m_3|^2}{1+\zeta}\right]\\ &+O(\theta_{13})\,,\end{aligned} \tag{3.64}$$

where the dot is the logarithmic derivative with respect to the renormalization scale $\dot{\theta}=\mu\,(d/d\mu)\theta$. The RGE for the Dirac phase is given by

$$\dot{\delta} = \frac{Cy_\tau^2}{32\pi^2}\frac{\delta^{(-1)}}{\theta_{13}}+\frac{Cy_\tau^2}{8\pi^2}\delta^{(0)}+O(\theta_{13})\,, \tag{3.65}$$

where

$$\begin{aligned}\delta^{(-1)} &= \sin 2\theta_{12}\,\sin 2\theta_{23}\,\frac{m_3}{\Delta m^2_{\rm atm}\,(1+\zeta)}\\ &\times\;\;[m_1\sin(\varphi_1-\delta)-(1+\zeta)\,m_2\,\sin(\varphi_2-\delta)+\zeta m_3\,\sin\delta]\;, \qquad (3.66a)\\ \delta^{(0)} &= \frac{m_1 m_2\,s_{23}^2\,\sin(\varphi_1-\varphi_2)}{\Delta m^2_{\rm sol}}\\ &+m_3\,s_{12}^2\left[\frac{m_1\,\cos 2\theta_{23}\,\sin\varphi_1}{\Delta m^2_{\rm atm}(1+\zeta)}+\frac{m_2\,c_{23}^2\,\sin(2\delta-\varphi_2)}{\Delta m^2_{\rm atm}}\right]\\ &+m_3\,c_{12}^2\left[\frac{m_1\,c_{23}^2\,\sin(2\delta-\varphi_1)}{\Delta m^2_{\rm atm}(1+\zeta)}+\frac{m_2\,\cos 2\theta_{23}\,\sin\varphi_2}{\Delta m^2_{\rm atm}}\right] \qquad (3.66b)\end{aligned}$$

For the physical Majorana phases, we obtain

$$\dot{\varphi}_1 = \frac{C y_\tau^2}{4\pi^2}\left\{ m_3 \cos 2\theta_{23} \frac{m_1 s_{12}^2 \sin\varphi_1 + (1+\zeta)\, m_2\, c_{12}^2 \sin\varphi_2}{\Delta m^2_{\rm atm}\,(1+\zeta)} + \frac{m_1 m_2\, c_{12}^2\, s_{23}^2 \sin(\varphi_1-\varphi_2)}{\Delta m^2_{\rm sol}} \right\} + O(\theta_{13}) \,, \tag{3.67}$$

$$\dot{\varphi}_2 = \frac{C y_\tau^2}{4\pi^2}\left\{ m_3 \cos 2\theta_{23} \frac{m_1 s_{12}^2 \sin\varphi_1 + (1+\zeta)\, m_2\, c_{12}^2 \sin\varphi_2}{\Delta m^2_{\rm atm}\,(1+\zeta)} + \frac{m_1 m_2\, s_{12}^2\, s_{23}^2 \sin(\varphi_1-\varphi_2)}{\Delta m^2_{\rm sol}} \right\} + O(\theta_{13}) \,. \tag{3.68}$$

Without loss of accuracy one can neglect ζ against 1 in many cases. For the masses, the results for $y_e = y_\mu = 0$ are

$$16\pi^2\, \dot{m}_1 = \left[\alpha_\kappa + C_\kappa y_\tau^2 \left(2 s_{12}^2\, s_{23}^2 + F_1\right)\right] m_1 \,, \tag{3.69a}$$

$$16\pi^2\, \dot{m}_2 = \left[\alpha_\kappa + C_\kappa y_\tau^2 \left(2 c_{12}^2\, s_{23}^2 + F_2\right)\right] m_2 \,, \tag{3.69b}$$

$$16\pi^2\, \dot{m}_3 = \left[\alpha_\kappa + 2 C_\kappa y_\tau^2\, c_{13}^2\, c_{23}^2\right] m_3 \,, \tag{3.69c}$$

where F_1 and F_2 contain terms proportional to $\sin\theta_{13}$,

$$F_1 = -s_{13} \sin 2\theta_{12} \sin 2\theta_{23} \cos\delta + 2 s_{13}^2\, c_{12}^2\, c_{23}^2 \,, \tag{3.70a}$$

$$F_2 = s_{13} \sin 2\theta_{12} \sin 2\theta_{23} \cos\delta + 2 s_{13}^2\, s_{12}^2\, c_{23}^2 \,. \tag{3.70b}$$

These formulae can be translated into RGEs for the mass squared differences,

$$8\pi^2 \frac{d}{dt}\Delta m^2_{\rm sol} = \alpha_\kappa\, \Delta m^2_{\rm sol} + C_\kappa y_\tau^2 \left[2 s_{23}^2 \left(m_2^2\, c_{12}^2 - m_1^2\, s_{12}^2\right) + F_{\rm sol}\right] \,, \tag{3.71a}$$

$$8\pi^2 \frac{d}{dt}\Delta m^2_{\rm atm} = \alpha_\kappa\, \Delta m^2_{\rm atm} + C_\kappa y_\tau^2 \left[2 m_3^2\, c_{13}^2\, c_{23}^2 - 2 m_2^2\, c_{12}^2\, s_{23}^2 + F_{\rm atm}\right] \,, \tag{3.71b}$$

where

$$F_{\rm sol} = \left(m_1^2 + m_2^2\right) s_{13} \sin 2\theta_{12} \sin 2\theta_{23} \cos\delta + 2 s_{13}^2 c_{23}^2 \left(m_2^2 s_{12}^2 - m_1^2 c_{12}^2\right) , \quad (3.72a)$$

$$F_{\rm atm} = -m_2^2 s_{13} \sin 2\theta_{12} \sin 2\theta_{23} \cos\delta - 2 m_2^2 s_{13}^2 s_{12}^2 c_{23}^2 . \quad (3.72b)$$

Some discussions on the basic features of RGEs of the three neutrino masses, three flavor mixing angles and three CP–violating phases are in order.

(a) The running of neutrino Yukawa couplings κ_i, or masses m_i, are determined by α_κ, unless the y_τ^2-associated term is enhanced by large values of $\tan\beta$. Also they are independent of the CP–violating phase δ.

(b) Taking into account that only the derivative of θ_{12} is proportional to $1/\Delta m_{sol}^2$, regarding the current solar and atmospheric neutrino oscillation data yield, θ_{12} is more sensitive to radiative corrections than θ_{13} and θ_{23}. Although its evolution can be downgraded adjusting the value of $\varphi_1 - \varphi_2$. Also, one can observe that θ_{13} can be radiatively generated even from zero initial value.

(c) The variation of Dirac phase $\dot{\delta}$ is proportional to θ_{13}^{-1} therefore, its running is different from φ_1 and φ_2. For small values of θ_{13}, δ becomes large and divergent in the limit $\theta_{13} \to 0$. Also, δ can be radiatively generated. It is interesting to note that $\dot{\delta}$ can be kept finite even when θ_{13} approaches zero, by fine-tuning of δ, φ_1 and φ_2, which can be used to know the relation between δ and two Majorana phases in this limit.

The Second Paper (see Chapter 5)

Motivation

Inspired by the HSMU hypothesis discussed above, we ask the question, why the CKM and PMNS should be taken exactly equal at the high scale. In fact, there is no symmetry to avoid them to be proportional. From here we postulate the most general relations among the quark and the leptonic mixing angles at the unification scale. In a compactified form the most general relation among the leptonic and the quark mixing angles within the

same generations is as following

$$\theta_{12} = \alpha_1^{k_1}\ \theta_{12}^q, \quad \theta_{13} = \alpha_2^{k_2}\ \theta_{13}^q, \quad \theta_{23} = \alpha_3^{k_3}\theta_{23}^q\,, \tag{3.73}$$

where k_i, with $i = (1, 2, 3)$ are real exponents. We refer to this relation as the, high scale mixing relation, (HSMR). We have chosen (k_1, k_2, k_3) to be $(1, 1, 1)$ for the simplicity of our analysis. The relations within the same generations are the simplest generalization of the HSMU hypothesis.

The Method

The working of the HSMU hypothesis is as follows. The implementation of the HSMU hypothesis requires the minimum supersymmetric standard model (MSSM) as an extension of the standard model (SM). One first evolves the quark mixing angles from the low scale (mass of the Z boson) to the supersymmetry (SUSY) breaking scale using the SM RG equations, discussed before. After that, from the SUSY breaking scale to the unification scale, evolution of quark mixing angles is governed by the MSSM RG equations. In the next step, the quark mixing angles at the unification scale, are put equal to those of the neutrinos following the HSMU hypothesis. The leptonic mixing parameters are then run from the unification scale to the SUSY breaking scale using the MSSM RG equations. From the SUSY breaking scale to the low scale, mixing parameters are evolved through the SM RG equations.

Effects of the Large $\tan\beta$ and Threshold Corrections

We would like to highlight two important effects which the MSSM has in our calculations. The first one is the effect of a large $\tan\beta$. To show the $\tan\beta$ dependence of our results we do some numerics. As in the SM $y_\tau \approx 0.01$, the constant including this factor will amount to

$$\frac{3y_3^2}{64\pi^2} \approx 0.5.10^{-6}\,, \tag{3.74}$$

and in the MSSM it becomes

$$\frac{3y_3^2}{64\pi^2} \approx 0.5.10^{-6}(1 + \tan\beta^2)\,, \tag{3.75}$$

which means the running of angles get enhanced by a factor of $(1+\tan\beta^2)$ and that is why we choose the large value of $\tan\beta = 55$.

Another important contribution of the MSSM to our calculation is called the threshold correction. As it was discussed in the context of effective field theories, the effect of High energy physics demonstrates itself at low energy (at the scale where the heavy degrees of freedom are integrated out) via the Wilson coefficients of the effective Lagrangian. These high energy effects appear order by order that is, in tree level and loops.

Now, the running of the neutrino parameters from high scale to the low scale, happens in two regions. First in the context of MSSM and then SM. This being the case, one would expect that by passing the MSSM breaking scale 2 TeV, where all the heavy super partners are getting integrated out, their effect shows up in the low energy theory, and this is indeed the case. However, a delicacy is involved here. As the super partners can have different masses in general, when approaching the MSSM breaking scale while running down the parameters, one should integrate them out one by one and do the matching accordingly. The corrections imposed this way on the masses and couplings, are called threshold corrections.

In fact, without calculating these corrections and do the matching while assuming all the super partner masses to be degenerate, all parameters can be brought into the experimental range but one, which is the solar mass square Δm^2_{21}. But, after taking into account the MSSM threshold corrections [55] the general mass term for neutrinos can be written as

$$M_\nu(\mu) = I(M_H,\mu) M^0_\nu I^T(M_H,\mu) + \delta M^{th}\,, \tag{3.76}$$

where, μ is the scale of the RG running, M_H is the new physics scale, which can be the See-saw scale and M^{th} defines the threshold corrections to the mass. These corrections read

$$\begin{aligned}
(\Delta m^2_{21})_{th} &= 2\mathrm{m}^2\cos 2\theta_{12}[-2\mathrm{T_e}+\mathrm{T}_\mu+\mathrm{T}_\tau],\\
(\Delta m^2_{32})_{th} &= 2\mathrm{m}^2\sin^2\theta_{12}[-2\mathrm{T_e}+\mathrm{T}_\mu+\mathrm{T}_\tau],\\
(\Delta m^2_{31})_{th} &= 2\mathrm{m}^2\cos^2\theta_{12}[-2\mathrm{T_e}+\mathrm{T}_\mu+\mathrm{T}_\tau]\,,
\end{aligned} \tag{3.77}$$

where m is the mean mass of the Quasi Degenerate (QD) neutrinos and the one loop factor $T_{\hat\alpha}(\hat\alpha = e,\mu,\tau)$ is a function of $y_{\hat\alpha} = 1 - x^2_{\hat\alpha}$ with $x_{\hat\alpha} = M_{\hat\alpha}/M_{\tilde w}$. $M_{\tilde w}$ stands for wino mass and $M_{\hat\alpha}$ represents the mass of charged sleptons [56, 57]. We work with an inverted hierarchy in the

charged–slepton sector where the mass of the selectron is defined through the ratio $R = \frac{M_{\tilde{e}}}{M_{\tilde{\mu},\tilde{\tau}}}$. The mass of the wino is chosen to be 400 GeV following the direct searches at the LHC [40, 41]. In short, the threshold correction effect helps the solar mass squared to come in range.

Different Scenarios for the Proportionality at High Scale

There will be different possibilities depending on the relations among the proportionality factors in relation (3.73). We firstly list below the different possible cases with the maximum and the minimum allowed values of the three independent proportionality factors α_i,

$$\textbf{Case A}: \quad \theta_{12} = \alpha_1^{max}\ \theta_{12}^q, \quad \theta_{13} = \alpha_2^{max}\ \theta_{13}^q, \quad \theta_{23} = \alpha_3^{max}\ \theta_{23}^q, \tag{3.78}$$

$$\textbf{Case B}: \quad \theta_{12} = \alpha_1^{max}\ \theta_{12}^q, \quad \theta_{13} = \alpha_2^{max}\ \theta_{13}^q, \quad \theta_{23} = \alpha_3^{min}\ \theta_{23}^q, \tag{3.79}$$

$$\textbf{Case C}: \quad \theta_{12} = \alpha_1^{max}\ \theta_{12}^q, \quad \theta_{13} = \alpha_2^{min}\ \theta_{13}^q, \quad \theta_{23} = \alpha_3^{max}\ \theta_{23}^q, \tag{3.80}$$

$$\textbf{Case D}: \quad \theta_{12} = \alpha_1^{max}\ \theta_{12}^q, \quad \theta_{13} = \alpha_2^{min}\ \theta_{13}^q, \quad \theta_{23} = \alpha_3^{min}\ \theta_{23}^q, \tag{3.81}$$

$$\textbf{Case E}: \quad \theta_{12} = \alpha_1^{min}\ \theta_{12}^q, \quad \theta_{13} = \alpha_2^{max}\ \theta_{13}^q, \quad \theta_{23} = \alpha_3^{max}\ \theta_{23}^q, \tag{3.82}$$

$$\textbf{Case F}: \quad \theta_{12} = \alpha_1^{min}\ \theta_{12}^q, \quad \theta_{13} = \alpha_2^{max}\ \theta_{13}^q, \quad \theta_{23} = \alpha_1^{min}\ \theta_{23}^q, \tag{3.83}$$

$$\textbf{Case G}: \quad \theta_{12} = \alpha_1^{min}\ \theta_{12}^q, \quad \theta_{13} = \alpha_2^{min}\ \theta_{13}^q, \quad \theta_{23} = \alpha_3^{max}\ \theta_{23}^q, \tag{3.84}$$

$$\textbf{Case H}: \quad \theta_{12} = \alpha_1^{min}\ \theta_{12}^q, \quad \theta_{13} = \alpha_2^{min}\ \theta_{13}^q, \quad \theta_{23} = \alpha_3^{min}\ \theta_{23}^q. \tag{3.85}$$

Then we move on to scenarios where the α_i are related. There can be more general HSMR where two proportionality constants can be identical and the third one is different. However we will discuss in this work more simplified scenarios, where the three proportionality constants are equal.

$$\theta_{12} = \alpha^{k_1}\ \theta_{12}^q, \quad \theta_{13} = \alpha^{k_2}\ \theta_{13}^q, \quad \theta_{23} = \alpha^{k_3}\theta_{23}^q\,. \tag{3.86}$$

As explained before we have restricted the values of k_i as either 0 or 1. We note that the value $(k_1, k_2, k_3) = (0, 0, 0)$ will reduce HSMR to the HSMU hypothesis making Eq. (3.52) a specific form of HSMR, Eq. (3.86). We present below the seven different possible cases, where the quark mixing angles are assumed to be proportional to the corresponding leptonic mixing

angles.

$$\textbf{Case 1}: \quad \theta_{12} = \alpha\ \theta_{12}^q, \quad \theta_{13} = \theta_{13}^q, \quad \theta_{23} = \theta_{23}^q, \tag{3.87}$$

$$\textbf{Case 2}: \quad \theta_{12} = \theta_{12}^q, \quad \theta_{13} = \alpha\ \theta_{13}^q, \quad \theta_{23} = \theta_{23}^q, \tag{3.88}$$

$$\textbf{Case 3}: \quad \theta_{12} = \theta_{12}^q, \quad \theta_{13} = \theta_{13}^q, \quad \theta_{23} = \alpha\ \theta_{23}^q, \tag{3.89}$$

$$\textbf{Case 4}: \quad \theta_{12} = \alpha\ \theta_{12}^q, \quad \theta_{13} = \alpha\ \theta_{13}^q, \quad \theta_{23} = \theta_{23}^q, \tag{3.90}$$

$$\textbf{Case 5}: \quad \theta_{12} = \theta_{12}^q, \quad \theta_{13} = \alpha\ \theta_{13}^q, \quad \theta_{23} = \alpha\ \theta_{23}^q, \tag{3.91}$$

$$\textbf{Case 6}: \quad \theta_{12} = \alpha\ \theta_{12}^q, \quad \theta_{13} = \theta_{13}^q, \quad \theta_{23} = \alpha\ \theta_{23}^q, \tag{3.92}$$

$$\textbf{Case 7}: \quad \theta_{12} = \alpha\ \theta_{12}^q, \quad \theta_{13} = \alpha\ \theta_{13}^q, \quad \theta_{23} = \alpha\ \theta_{23}^q\,. \tag{3.93}$$

The proportionality constant α in the above relations is taken as a real parameter. We have carried out a detailed study for these cases in the second paper. We have used the MATHEMATICA based package REAP [58] for the numerical computation of our results.

Results

We have thoroughly investigated the implications and the phenomenological consequences of all the possible cases, taking into account the latest experimental constraints. The whole analysis has been done with the assumption of normal hierarchy and QD mass pattern. In general, we have discovered three new correlations among Δm^2_{32}, M_{ee}, θ_{12} and the sum of neutrino masses. These correlations were not investigated in previous studies.

The different scenarios of the HSMR can be discriminated through measurements of various observables like M_{ee} and by precise determination of the values of the mixing angles, particularly the θ_{13} and θ_{23} mixing angles. As we have shown in the figures for various cases as well in the tables, the allowed ranges for M_{ee} and the angles are different for different cases and a precise determination of these observables can be used as a way to distinguish various cases of HSMR. In addition to neutrino observables one can also use other processes like lepton–flavor violation to distinguish the different allowed cases. The mass–splitting in the charged–slepton sector is given by the ratio $R = \frac{M_{\tilde{e}}}{M_{\tilde{\mu},\tilde{\tau}}}$. The ratio R almost discriminates every scenario and hence, processes like $\mu \to e\gamma$, $\mu \to eee$ and the anomalous magnetic moment of the electron. For example, the SUSY contribution to the anomalous magnetic moment of the electron directly depends on the

ratio R [59]. The detailed study of this aspect of the work is beyond the scope of this paper.

Finally, in short, the crux of our paper is following.

- We have proposed and studied the HSMR hypothesis which is a more general framework than the HSMU hypothesis.
- The HSMR hypothesis provides a very simple explanation of the observed large neutrino mixing. The present and future neutrino experiments can easily test predictions of our work. If our predictions are confirmed by experiments, like GERDA, it would be a good hint of quark-lepton unification at the high scale.
- We observe that the HSMU hypothesis represents the $\alpha = 1$ limit of the HSMR hypothesis and is constrained by the lowest allowed value of M_{ee} which is 0.384 MeV. Therefore, if the HSMU hypothesis is ruled out by experiments, like GERDA, the other HSMR cases with $\alpha \neq 1$ may survive and their confirmation would be itself a strong hint of the proportionality between quark and leptonic mixing angles which is the basis of the HSMR hypothesis.
- We have done a rigorous, thorough and comprehensive study with the HSMR hypothesis which does not exist in the literature. All results reported in the literature using the HSMU hypothesis, are a very small subset of our results with the HSMR hypothesis presented in our paper. Moreover, we have also thoroughly compared the HSMR hypothesis with respect to the HSMU.
- In our work, we have discovered new strong correlations among different experimental observables for every limit of the HSMR hypothesis. These correlations do not exist in the literature and are easily testable in present ongoing experiments. For example, there is a strong correlation between Δm^2_{32} and M_{ee}. This correlation can be easily tested by the GERDA experiment. There are two more such correlations namely among θ_{12}, $\sum_i m_i$ and M_{ee} discussed in our work which are completely new and unexplored in the literature.
- Furthermore, we have comprehensively studied a strong correlation between θ_{23} and θ_{13} and predictions can be easily tested in present ongoing experiments. This correlation was studied in a previous study in a specific limit. Since we have done a comprehensive full parameter scan, this correlation has become a robust band now.

Results Within the Type-1 See-saw Framework

The dimensional five operator originates from integrating out the heavy degrees of freedom and it can be realized in six different ways [60]. However, regardless of which model is used at the high scale, the shape of the dimensional five operator will be the same. It is worth while to mention that even above the EW scale the mass of the left handed neutrino runs via Yukawas. The same happens to the mass of right handed neutrinos in models like See-saw.

What the REAP package does is to calculate the κ matrix in relation (3.55) at the high scale using the values of the masses which we give as the input. Then, using the RG equation runs it down to the SUSY breaking scale, via the dimensional five operator and finally, from there to the Z mass scale using the standard model RG equations. The difference between the two runnings originates from the different particle content of the models and the fact that SUSY has two Higgs doublets while the SM only has one.

In the first step, we have taken $\Lambda \backsim 10^{14}$ GeV and assumed that whatever new physics which can exist, will show up above this energy range and hence is not covered in our study because, we have taken the HSMU(R) scale to be 10^{14} GeV as well, which makes our work totally model independent. It means, we do not care about which specific model will enter the game (type one, two, three See-saw, etc.) above this scale. On the other hand, if one wants to have the right handed singlets which are then integrated out (as we have considered in our work), one can take the scale of HSMU(R) to be higher, while keeping the scale of new physics below that. Then using the See-saw model, both RGs run, while below that, the right handed field will be integrated out and to run the RGs one only runs the Yukawa of the left handed neutrinos in the context of MSSM. In fact, studies which have included the See-saw mechanism along with the HSMU hypothesis have found a small correction to those of the model independent case [31]. To check the stability of our results, we have also done the calculations in the frame of type one See-saw. To include the right handed singlets at the high scale, we use the package $MSSM$ rather than $MSSM0N$ which does not include the right handed neutrinos and we find that results are in fact stable with small changes as expected.

The Third Paper (see Chapter 6)

Motivation

As it was discussed earlier, the HSMR parametrization can explain the observed pattern of the neutrino mixing assuming they are Majorana in nature. In the third paper, we investigate the consequences of the HSMR parametrization using the RG evolution of Dirac neutrinos. In fact, the nature of neutrinos is still unknown. They could be equally Dirac or Majorana in nature. Hence, from the phenomenological point of view, Dirac neutrinos are as important as Majorana neutrinos. There are many ongoing important experiments to test the nature of neutrinos [5, 61]. Cosmological data do not prefer Majorana or Dirac neutrinos either [62]– [68].

Although, the RG evolution of Majorana neutrinos is extensively studied in the literature, attention is being paid less to the RG evolution of Dirac neutrinos. It was first showed in Ref. [33] that RG evolution for Dirac neutrinos can explain the large neutrino mixing assuming the HSMU hypothesis. However, as we shall show later, these results are ruled out by new updated data [21–23] and due to an improved algorithm used in the package REAP [69].

In this paper we investigate first, if there exists a parameter space with the HSMR parametrization where the RG evolution of Dirac neutrinos can satisfactorily yield an explanation for the large neutrino mixing along with the observation of a small θ_{13}. Second, what is the status of the HSMU hypothesis for Dirac neutrinos? And third, what is the status of the leptonic CP violating phase in this respect?

The Method

The method is quite similar to the one for Majorana neutrinos, described in the previous section. That is, we will need both the SM and the MSSM to run the RG equations apart from the fact that now we use the RG equations describing the evolution of the neutrino mixing parameters for Dirac neutrinos. For the standard parametrization of the leptonic and quark

mixings they can be written as:

$$\dot{\theta}_{12} = \frac{-C\,y_\tau^2}{32\,\pi^2}\,\frac{m_1^2+m_2^2}{m_2^2-m_1^2}\,\sin(2\,\theta_{12})\,\sin^2\theta_{23} + \mathscr{O}(\theta_{13})\,, \tag{3.94}$$

$$\begin{aligned}\dot{\theta}_{13} &= \frac{-C\,y_\tau^2}{32\,\pi^2}\,\frac{1}{(m_3^2-m_1^2)\,(m_3^2-m_2^2)} \\ &\times \Big\{\Big(m_2^2-m_1^2\Big)\,m_3^2\,\cos\delta\,\cos\theta_{13}\,\sin(2\,\theta_{12})\,\sin(2\,\theta_{23}) \\ &\quad + \Big[m_3^4-\Big(m_2^2-m_1^2\Big)\,m_3^2\,\cos(2\,\theta_{12})-m_1^2\,m_2^2\Big] \\ &\times \cos^2\theta_{23}\,\sin(2\,\theta_{13})\Big\}\end{aligned} \tag{3.95}$$

$$\begin{aligned}\dot{\theta}_{23} &= \frac{-C\,y_\tau^2}{32\,\pi^2}\,\frac{[m_3^4-m_1^2\,m_2^2+(m_2^2-m_1^2)\,m_3^2\,\cos(2\,\theta_{12})]}{(m_3^2-m_1^2)\,(m_3^2-m_2^2)}\,\sin(2\,\theta_{23}) \\ &+ \mathscr{O}(\theta_{13})\,,\end{aligned} \tag{3.96}$$

where the dot is the logarithmic derivative with respect to the renormalization scale, and

$$C = \begin{cases} 1\,, & \text{(MSSM)}\,, \\ -3/2\,, & \text{(SM)}\,. \end{cases} \tag{3.97}$$

The RG evolution of the Dirac phase δ is given by the following equation:

$$\dot{\delta} = \dot{\delta}^{(-1)}\theta_{13}^{-1} + \dot{\delta}^{(0)} + \dot{\delta}^{(1)} + \mathscr{O}(\theta_{13}^2)\,. \tag{3.98}$$

The first two coefficients $\dot{\delta}^{(k)}$ read,

$$\begin{aligned}\dot{\delta}^{(-1)} &= \frac{C\,y_\tau^2}{32\,\pi^2}\,\frac{(m_2^2-m_1^2)\,m_3^2}{(m_3^2-m_1^2)\,(m_3^2–m_2^2)}\,\sin(\delta)\,\sin(2\,\theta_{12})\,\sin(2\,\theta_{23})\,, \\ \dot{\delta}^{(0)} &= 0\,.\end{aligned} \tag{3.99a}$$

The third coefficient is given as

$$\begin{aligned}\dot{\delta}^{(1)} &= \frac{C\,y_\tau^2}{16\,\pi^2}\,\frac{m_2^2\,\left(m_3^2–m_1^2\right)^2}{(m_2^2–m_1^2)\,(m_3^2–m_1^2)\,(m_3^2–m_2^2)}\,\cot(\theta_{12})\sin(2\theta_{23})\sin\delta \\ &+ \ \ldots\,.\end{aligned} \tag{3.99b}$$

This term becomes relevant for not too small θ_{13}. The crux of the equations can be captured as following:

$$\begin{aligned} \dot{\theta}_{12} &\propto \frac{m^2}{\Delta m^2_{21}} \\ \dot{\theta}_{13},\, \dot{\theta}_{23} &\propto \frac{m^2}{\Delta m^2_{32}}\,, \end{aligned} \tag{3.100}$$

where $\Delta m^2_{ij} = m^2_i - m^2_j$ $(i, j = 1, 2, 3)$ represents the mass square differences and m is average neutrino mass. We have used the MATHEMATICA based package REAP for the computation of the RG evolution at two-loops [58].

Results

The main achievement of this work is that the RG evolution of Dirac neutrinos could explain the large neutrino mixing including the observation of a small and non–zero value of the mixing angle θ_{13}.

- The mixing angle θ_{23} is non-maximal and lies in the second octant for the SUSY breaking scale 2 TeV and the unification scale at the GUT scale. For the variation of the SUSY breaking scale and the unification scale, the mixing angle θ_{23} is non-maximal and lies in the first octant. The predictions for the mass square difference Δm^2_{31} are also well constrained and testable in experiments.
- The Dirac phase δ is not known from experiments. Hence, any prediction of this important observable is of great interest. Our prediction for this observable is 80 to 287 degrees excluding some part of the allowed parameter space of this quantity. The allowed range for the Jarlskog invariant J_{CP} is -0.27 to 0.27. Thus, a large CP violation is possible in our analysis.
- We predict the Dirac CP phase δ to be zero for the SUSY breaking scale 5 TeV. Furthermore, the Dirac CP phase has a precise range $168.7^\circ - 180^\circ$ at the unification scale 10^{12} GeV.
- The unification scale beyond the GUT scale is ruled out by our investigation. This fact could be useful for the GUT theories having Dirac neutrinos [70]– [78].
- We obtain strong correlations among different experimental observables. Our predictions for the mixing angles θ_{13}, θ_{23}, averaged electron

neutrino mass m_β, Dirac CP phase δ and the sum of the three neutrino masses, $\sum m_i$ are precise and easily testable at some ongoing and future experiments like INO, T2K, NOνA, LBNE, Hyper-K, PINGU and KATRIN [79]– [84].

– We remark that we have investigated the RG evolution of neutrino mixing parameters at two loops. This is a crucial input since the RG evolution at one-loop is insufficient to provide the required enhancement of the mixing angles which in turn, cannot yield the results obtained in this work.

– One of the main consequences of our investigation is that the HSMU hypothesis is not compatible with Dirac neutrinos due to updated experimental data [21–23] and a better algorithm used in the package REAP [69]. The HSMU hypothesis is a particular realization of the HSMR parametrization when we choose $\alpha_1 = \alpha_2 = \alpha_3 = 1$ for $k_1 = k_2 = k_3 = 1$. Hence, the HSMR parametrization is one of the preferable frameworks to study the RG evolution of Dirac neutrinos now.

Bibliography

[1] C.L. Cowan, F. Reines, F.B. Harrison, E.C. Anderson and F.N. Hayes, Science **124** 103 (1956).

[2] K. Kodama *et al.* [DONUT Collaboration], Phys. Lett. B **504** 218 (2001) [hep-ex/0012035].

[3] M. Auger *et al.* [EXO Collaboration], Phys. Rev. Lett. **109**, 032505 (2012), arXiv:1205.5608.

[4] A. Gando *et al.* [KamLAND-Zen Collaboration], Phys. Rev. Lett. **110**, no. 6, 062502 (2013), arXiv:1211.3863.

[5] M. Agostini *et al.* [GERDA Collaboration], Phys. Rev. Lett. **111**, 122503 (2013), arXiv:1307.4720.

[6] P. Lipari., Cern yellow paper (Cern yellow paper 2003-003), pages 115 (2003).

[7] V. N. Aseev *et al.* [Troitsk Collaboration], Phys. Rev. D **84**, 112003 (2011). [arXiv:1108.5034 [hep-ex]].

[8] K.N. Abazajian et al., Astropart. Phys. **35**, 177 (2011).

[9] P.A.R. Ade et al., [Planck Collab.], arXiv:1502.01589.

[10] Neutrino Mass, Mixing and Oscillations, PDG, (2016).

[11] A. Aste, Symmetry **2**, 1776 (2010).

[12] B. Pontecorvo, Sov. Phys. JETP **26**, 984 (1968). [Zh. Eksp. Teor. Fiz. **53**, 1717 (1968)].

[13] N. Cabibbo, Phys. Rev. Lett. 10, 531 (1963); M. Kobayashi and T. Maskawa, Prog. Theor. Phys. **49**, 652 (1973).

[14] Z. Maki, M. Nakagawa and S. Sakata, Prog. Theor. Phys. **28**, 870 (1962).

[15] R. N. Cahn, D. A. Dwyer, S. J. Freedman, W. C. Haxton, R. W. Kadel, Yu. G. Kolomensky, K. B. Luk, P. McDonald, G. D. Orebi Gann, A. W. P. Poon, [hep-ex/1307.5487].

[16] F. Capozzi et al., arXiv:1601.07777.

[17] J. C. Pati and A. Salam, Phys. Rev. **D10**, 275 (1974).

[18] H. Georgi and S. L. Glashow, Phys. Rev. Lett. **32**, 438 (1974).

[19] H. Georgi, Particles and Fields,*Proceedings of APS Division of Particles and Fields,* ed C. Carlson, p575 (1975); (1974); H. Frtzsch, P. Mikowski, Ann. Phys. **93**, 193 (1975).

[20] For a review and references, see S. Raby, in Particle Data Group Book, W. -M. Yao *et al.* J. Phys. **G 33**, 1 (2006).

[21] F. Capozzi, G. L. Fogli, E. Lisi, A. Marrone, D. Montanino and A. Palazzo, Phys. Rev. D **89**, 9 (2014), 093018 [arXiv:1312.2878 [hep-ph]].

[22] M. C. Gonzalez-Garcia, M. Maltoni and T. Schwetz, JHEP **1411**, 052 (2014). [arXiv:1409.5439 [hep-ph]].

[23] D. V. Forero, M. Tortola and J. W. F. Valle, Phys. Rev. D **90**, 9 (2014) [arXiv:1405.7540 [hep-ph]].

[24] K.R.S. Balaji, R.N. Mohapatra, M.K. Parida and E. A. Paschos, Phys. Rev.**D63**, 113002 (2001).

[25] P.H. Chankowski, W. Królikowski and S. Pokorski, hep-ph/9910231; P. H. Chankowski and S. Pokorski, hep-ph/0110249.

[26] J.A. Casas, J.R. Espinosa, A. Ibarra and I. Navarro, Nucl. Phys. **B569**, 82 (2000); hep-ph/9910420.

[27] J. Ellis and S. Lola, hep-ph/9904279; E. Ma, J. Phys. **G25**, L97 (1999); N. Haba, Y. Matsui, N. Okamura and M. Sugiura, hep-ph/9908429; P. Chankowski, A. Ioannisian, S. Pokorski and J. W. F. Valle, Phys. Rev. Lett. **86**, 3488 (2001); M. Frigerio and A. Yu. Smirnov, hep-ph/0212263; J.A. Casas, J.R. Espinosa, A. Ibarra and I. Navarro, Nucl. Phys. **B556**, 3 (1999).

[28] R. N. Mohapatra, M. K. Parida and G. Rajasekaran, Phys. Rev. D **69**, 053007 (2004). [hep-ph/0301234].

[29] R. N. Mohapatra, M. K. Parida and G. Rajasekaran, Phys. Rev. D **72** 013002 (2005). [hep-ph/0504236].

[30] S. K. Agarwalla, M. K. Parida, R. N. Mohapatra and G. Rajasekaran, Phys. Rev. D **75**, 033007 (2007). [hep-ph/0611225].

[31] G. Abbas, S. Gupta, G. Rajasekaran and R. Srivastava, Phys. Rev. D **89**, 093009 (2014). [arXiv:1401.3399 [hep-ph]].

[32] R. Srivastava, arXiv:1503.07964 [hep-ph].

[33] G. Abbas, S. Gupta, G. Rajasekaran and R. Srivastava, arXiv:1312.7384 [hep-ph].

[34] K. Abe *et al.* [T2K Collaboration], Phys. Rev. Lett. **107**, 041801 (2011). [arXiv:1106.2822 [hep-ex]].

[35] P. Adamson *et al.* [MINOS Collaboration], Phys. Rev. Lett. **107**, 181802 (2011). [arXiv:1108.0015 [hep-ex]].

[36] Y. Abe *et al.* [Double Chooz Collaboration], Phys. Rev. D **86**, 052008 (2012). [arXiv:1207.6632 [hep-ex]].

[37] J. K. Ahn *et al.* [RENO Collaboration], Phys. Rev. Lett. **108**, 191802 (2012). [arXiv:1204.0626 [hep-ex]].

[38] F. P. An *et al.* [Daya Bay Collaboration], Phys. Rev. Lett. **108**, 171803 (2012). [arXiv:1203.1669 [hep-ex]].

[39] S. P. Martin, Adv. Ser. Direct. High Energy Phys. **21**, 1 (2010) [Adv. Ser. Direct. High Energy Phys. **18**, 1 (1998)] [hep-ph/9709356].

[40] N. Craig, arXiv:1309.0528 [hep-ph].

[41] ATLAS Supersymmetry (SUSY) searches, ATLAS SUSY Summary 201609.

[42] Stueckelberg, E. C. G., Petermann, A, Helv. Phys. Acta **26**, 499 (1953).

[43] M. Gell-Mann , F. E. Low, Phys. Rev. **95**, 1300 (1954).

[44] N. N. Bogolyubov, D. V. Shirkov, Nuovo Cimento **3**, 845 (1956).

[45] K. G. Wilson, Phys. Rev. B **4**, 3174 (1971).

[46] K. G. Wilson, Phys. Rev. B **4**, 3184 (1971).

[47] K. G. Wilson, J. B. Kogut, Phys. Rep. **12**, 75 (1974).

[48] Jr C. G. Callan, Phys. Rev. D **2**, 1541 (1970).

[49] K. Symanzik, Commun. Math. Phys. 18, 227 (1970).

[50] M. E. Peskin, D. V. Schroeder, Reading, USA: Addison-Wesley, 842 (1995).

[51] A. Pich, hep-ph/9806303.

[52] J. Kersten, Renormalization Group Evolution of Neutrino Masses, Master thesis, November 2001.

[53] Z. Z. Xing, CERN Yellow Report CERN–2014–001, 177 doi:10.5170/CERN-2014–001.177 [arXiv:1406.7739 [hep-ph]].

[54] S. Antusch, J. Kersten, M. Lindner and M. Ratz, Nucl. Phys. B **674** 401 (2003) [hep-ph/0305273].

[55] R. N. Mohapatra, M. K. Parida and G. Rajasekaran, Phys. Rev. D **71**, 057301 (2005) [hep-ph/0501275].

[56] P. H. Chankowski and P. Wasowicz, Eur. Phys. J. C **23**, 249 (2002). [hep-ph/0110237].

[57] E. J. Chun and S. Pokorski, Phys. Rev. D **62** 053001, (2000) . [hep-ph/9912210].

[58] S. Antusch, J. Kersten, M. Lindner, M. Ratz and M. A. Schmidt, JHEP **0503**, 024 (2005), hep-ph/0501272.

[59] D. Stockinger, J. Phys. G **34**, R45 (2007) [hep-ph/0609168].

[60] E. Ma, Phys. Rev. Lett. **81**, 1171 (1998) [hep-ph/9805219].

[61] F. Alessandria, E. Andreotti, R. Ardito, C. Arnaboldi, F. T. Avignone, III, M. Balata, I. Bandac and T. I. Banks *et al.*, arXiv:1109.0494.

[62] K. Dick, M. Lindner, M. Ratz and D. Wright, Phys. Rev. Lett. **84**, 4039 (2000), hep-ph/9907562.

[63] H. Murayama and A. Pierce, Phys. Rev. Lett. **89**, 271601 (2002), hep-ph/0206177.

[64] P. H. Gu and H. J. He, JCAP **0612**, 010 (2006) [hep-ph/0610275].

[65] P. H. Gu, H. J. He and U. Sarkar, JCAP **0711**, 016 (2007) [arXiv:0705.3736 [hep-ph]].

[66] P. H. Gu, H. J. He and U. Sarkar, Phys. Lett. B **659**, 634 (2008) [arXiv:0709.1019 [hep-ph]].

[67] P. H. Gu and U. Sarkar, Phys. Rev. D **77**, 105031 (2008) [arXiv:0712.2933 [hep-ph]].

[68] P. H. Gu, Nucl. Phys. B **872**, 38 (2013) [arXiv:1209.4579 [hep-ph]].

[69] Private communication with Michael A. Schmidt.

[70] E. Ma and R. Srivastava, Phys. Lett. B **741**, 217 (2015) [arXiv:1411.5042 [hep-ph]].

[71] R. N. Mohapatra and J. W. F. Valle, Phys. Rev. D **34**, 1642 (1986).

[72] N. Arkani-Hamed, L. J. Hall, H. Murayama, D. Tucker-Smith and N. Weiner, Phys. Rev. D **64**, 115011 (2001), hep-ph/0006312.

[73] F. Borzumati and Y. Nomura, Phys. Rev. D **64**, 053005 (2001), hep-ph/0007018.

[74] R. Kitano, Phys. Lett. B **539**, 102 (2002), hep-ph/0204164.

[75] S. Abel, A. Dedes and K. Tamvakis, Phys. Rev. D **71**, 033003 (2005), hep-ph/0402287.

[76] H. Murayama, Nucl. Phys. Proc. Suppl. **137**, 206 (2004), hep-ph/0410140.

[77] A. Y. .Smirnov, hep-ph/0411194.

[78] R. N. Mohapatra, S. Antusch, K. S. Babu, G. Barenboim, M. -C. Chen, S. Davidson, A. de Gouvea and P. de Holanda *et al.*, hep-ph/0412099.

[79] G. Drexlin, V. Hannen, S. Mertens and C. Weinheimer, Adv. High Energy Phys. **2013**, 293986 (2013), arXiv:1307.0101.

[80] K. Abe *et al.* [T2K Collaboration], Nucl. Instrum. Meth. A **659**, 106 (2011), arXiv:1106.1238.

[81] R. B. Patterson [NOvA Collaboration], Nucl. Phys. Proc. Suppl. **235-236**, 151 (2013), arXiv:1209.0716.

[82] C. Adams *et al.* [LBNE Collaboration], arXiv:1307.7335.

[83] E. Kearns *et al.* [Hyper-Kamiokande Working Group Collaboration], arXiv:1309.0184.

[84] S. -F. Ge and K. Hagiwara, arXiv:1312.0457.

4. On the Minimality of the Order p^6 Chiral Lagrangian

Pedro Ruiz-Femenía[a] and Mehran Zahiri Abyaneh[b]

[a] *Physik Department T31,*
James-Franck-Straße, Technische Universität München,
D–85748 Garching, Germany

[b] *Instituto de Física Corpuscular (IFIC), CSIC-Universitat de València*
Apdo. Correos 22085, E-46071 Valencia, Spain

[Physics Letters B, Volume 751, Published 17 December 2015]

A method to find relations between the operators in the mesonic Lagrangian of Chiral Perturbation Theory at order p^6 is presented. The procedure can be used to establish if the basis of operators in the Lagrangian is minimal. As an example, we apply the method to the two-flavour case in the absence of scalar and pseudo-scalar sources ($s = p = 0$), and conclude that the minimal Lagrangian contains 27 independent operators.

Introduction

The global chiral symmetry of the QCD Lagrangian for vanishing quark masses, and its spontaneous breaking to the diagonal group, characterize the strong interactions among the lightest hadronic degrees of freedom –the peudoscalar mesons– at low energies. The Nambu-Goldstone nature of these mesons and the mass gap that separates them from the rest of the hadronic spectrum, allows one to build an effective field theory (EFT) containing only these modes, with a perturbative expansion in powers of momenta and masses. The framework, called Chiral Perturbation Theory (ChPT), was introduced in its modern form by Weinberg [1], and Gasser and Leutwyler [2, 3].

At the lowest order, $\mathcal{O}(p^2)$, the effective ChPT Lagrangian $\mathcal{L}_2$ depends only in two low-energy couplings. One-loop contributions built from the lowest-order vertices generate $\mathcal{O}(p^4)$ divergences that are absorbed by the operators of the next-to-leading order $\mathcal{L}_4$ Lagrangian [2], introducing seven (ten) additional coupling constants for the two (three) quark flavours case. In the same way, taking the computations to the next-to-next-to leading order requires the construction of the effective Lagrangian at $\mathcal{O}(p^6)$. This task was first performed systematically in Ref. [4], and later revisited in [5]. Through the use of partial integration, the equations of motion, Bianchi identities and the Cayley-Hamilton relations for SU(n) matrices, the authors of Ref. [5] managed to write down a basis of operators for $\mathcal{L}_6$ in the even-intrinsic-parity sector for $n = 2$ ($n = 3$) light flavours consisting of 53 (90) terms plus 4 (4) contact terms (*i.e.* terms not containing the pseudo-Goldstone fields, which are only needed for renormalization). In recent years, an additional relation among the operators in the basis of [5] for the $n = 2$ case was proven [6], where no additional manipulations but those already used in [5] were required. This showed that the derivation of an algorithm to exhaust all possible algebraic conditions among the $\mathcal{L}_6$ operators imposed by partial integration, equations of motion, Bianchi identities and, particularly, Cayley-Hamilton relations, is a nontrivial task.

Therefore, the question about the minimality of the $\mathcal{O}(p^6)$ chiral Lagrangian is proper and, to the best of our knowledge, remains unanswered. It is the aim of the present work to describe a method that provides necessary conditions for the existence of additional relations between the operators of the $\mathcal{L}_6$ Lagrangian, and to show its application to the two-flavour case when massless quarks are considered. Our approach does not try to exploit the algebraic conditions mentioned above (and used in [5]), but is rather based on the analysis of Green functions built from arbitrary linear combinations of the operators in the basis. The re-

quirement that the matrix elements built from the latter Green functions must vanish for an arbitrary kinematic configuration is a necessary condition for the linear combination to be true at the operator level. From the method one can conclude that the basis is minimal when the necessary conditions provide no freedom for the existence of new relations. On the other hand, if the method allows for new relations, it cannot immediately answer the question about the minimality of the set, but it has the advantage that it gives the precise form that the (potential) new relations among the operator must have. With the latter information at hand, an algebraic proof of the relation at the operator level shall be greatly simplified.

The method involves the computation of tree-level matrix elements of order p^6. Despite being tree-level, the large number of operators in $\mathcal{L}_6$ and their involved Lorentz structure, containing vertices with up to six derivatives, produce rather long expressions. The latter can nevertheless be handled easily with the help of computer tools, and the method lends itself easily to automatization.

The structure of the paper is the following. In Sec. 4.2 we provide the basic ingredients of ChPT needed for our analysis. The method that searches for further relations among the $\mathcal{O}(p^6)$ operators is described in Sec. 4.3, where details about the calculation of the matrix elements which provide the necessary conditions are given through specific examples. Its application to the two-flavour case in the chiral limit with scalar and pseudo-scalar sources set to zero is then presented in Sec. 4.4. Finally, we give our conclusions in Sec. 4.5.

Chiral perturbation theory

The effective Lagrangian that implements the spontaneous breaking of the chiral symmetry $\mathrm{SU}(n)_L \times \mathrm{SU}(n)_R$ to $\mathrm{SU}(n)_V$ in the meson sector is written as an expansion in powers of derivatives and masses of the pseudo-goldstone fields [1–3],

$$\mathcal{L} = \sum_{n \geqslant 1} \mathcal{L}_{2n} \,. \tag{4.1}$$

The lowest order reads

$$\mathcal{L}_2 = \frac{F^2}{4} \langle u_\mu u^\mu + \chi_+ \rangle \,, \tag{4.2}$$

where F is the pion decay constant in the chiral limit and $\langle \dots \rangle$ stands for the trace in flavour space. The chiral tensor u_μ,

$$u_\mu = i \left[u^\dagger \left(\partial_\mu - i r_\mu \right) u - u \left(\partial_\mu - i \ell_\mu \right) u^\dagger \right] \,, \tag{4.3}$$

is built from the Goldstone matrix field

$$u = \exp\left(\frac{i}{\sqrt{2}F}\phi\right) , \tag{4.4}$$

and the left and right $n\times n$-dimensional matrix fields in flavour space, $\ell_\mu = v_\mu - a_\mu$, $r_\mu = v_\mu + a_\mu$, with v_μ, a_μ reproducing the couplings of the quarks to the external vector and axial-vector sources, respectively. On the other hand, the tensor χ_+ in (4.2) is built from $\chi = 2B(s + ip)$, with s and p the scalar and pseudo-scalar external matrix fields and B a low-energy parameter. Quark masses are introduced in the ChPT meson amplitudes through the scalar matrix s. Since we restrict ourselves in the specific examples given later to the chiral limit and in addition set p as well as other contributions to s to zero, we can drop all operators containing the χ tensor in what follows.

In the two flavour-case, which will be used for a specific application of our method, the matrix ϕ collects the pion fields,

$$\phi = \begin{pmatrix} \frac{1}{\sqrt{2}}\pi^0 & \pi^+ \\ \pi^- & -\frac{1}{\sqrt{2}}\pi^0 \end{pmatrix} . \tag{4.5}$$

The vector and axial-vector external fields are general traceless 2×2 matrices,

$$v_\mu = \begin{pmatrix} v_{11} & v_{12} \\ v_{21} & -v_{11} \end{pmatrix}_\mu \qquad \text{and} \qquad a_\mu = \begin{pmatrix} a_{11} & a_{12} \\ a_{21} & -a_{11} \end{pmatrix}_\mu , \tag{4.6}$$

since we do not confine ourselves to the Standard Model vector and axial-vector currents, but allow for the parametrization of other possible beyond-the-Standard-Model currents.

The general structure of the $\mathcal{O}(p^6)$ ChPT Lagrangian was studied in [4, 5]; adopting the notation of the latter reference, in the $n = 2$ case it reads

$$\mathcal{L}_6^{\mathrm{SU}(2)} = \sum_{i=1}^{53} c_i \mathcal{P}_i + 4 \text{ contact terms} , \tag{4.7}$$

where $\mathcal{P}_i$ are the basis elements and c_i are the corresponding low energy constants. In the massless limit with scalar and pseudo-scalar sources set to zero, $27 + 2$ of the $53+4$ operators in (4.7) remain. For completeness, we give their explicit form in the Appendix.

Outline of the method

We describe next the method used to determine the minimal set of monomials of $\mathcal{O}(p^6)$ in the ChPT Lagrangian. It is based on the trivial observation that if a set of operators $\mathcal{P}_i$ from $\mathcal{L}_6$ satisfies a linear relation $\Theta \equiv \sum_i \alpha_i \mathcal{P}_i = 0$, with α_i real or complex numbers, then the matrix elements of (on-shell) pions and currents obtained from the Green functions

$$\langle 0|\, T\, \phi(x_1) \dots \phi(x_n) \dots j_{f_1}(y_1) \dots j_{f_m}(y_m)\, |0\rangle_\Theta \tag{4.8}$$

$$\equiv \frac{(-i)^m}{\mathcal{N}} \frac{\delta^{(m)}}{\delta f_1(y_1) \dots \delta f_m(y_m)} \int [\mathcal{D}\phi]\, \phi(x_1) \dots \phi(x_n) \Big(i \int d^4x\, \Theta(x) \Big) e^{i S_{\rm ChPT}[\phi, f_i]} \Big|_{f_i = 0} ,$$

must also vanish. The Green functions (4.8) are built from $n = 0, 1 \dots$ pion fields (ϕ) and $m = 0, 1 \dots$ vector, axial-vector, scalar or pseudodoscalar currents (j_{f_i}), which derive from the ChPT action by functional differentiation with respect the external field sources ($f_i = v$, a, s, p respectively). The precise definition is given by the path-integral representation provided in the second line of (4.8): the action $S_{\rm ChPT}$, built from the ChPT Lagrangian (4.1), is a functional of the pion fields and the currents, and the term $\int d^4x\, \Theta(x)$ in the integrand entails that the perturbative expansion of the Green function has Θ in one of the interaction vertices. The normalization $\mathcal{N}$ is fixed such that the Green function with $m = n = 0$ equals one. The corresponding matrix elements involving m currents and n pions are obtained by Fourier transforming (4.8) into momentum space and then amputating the external pion lines and putting them on-shell. Let us note that the vanishing of the matrix elements from (4.8) when the relation $\Theta = 0$ has been obtained using the pion-field equation of motion is only guaranteed if the momenta of the pions are taken on the mass shell. This is because the use of the equations of motion at the operator level can be shown to be equivalent to a redefinition of the pion field in the generating functional [4, 5, 7], which leaves on-shell S-matrix elements invariant. For off-shell matrix elements, operators that vanish upon use of the equations of motion can give however a non-zero contribution. For our purposes it is sufficient to consider the perturbative computation of the Green function at the leading order in the momentum expansion, which is $\mathcal{O}(p^6)$ because the $\mathcal{P}_i$ operators in the linear combination Θ are already of that order.

The perturbative calculation consists of tree-level diagrams, of the form of a contact interaction, which we shall refer to as “local" in what follows, as well as with intermediate pion exchange (“non-local"); see Fig. 4.1 for an example.

Local contributions contain an $\mathcal{P}_i$ operator at the vertex, whereas non-local contributions have in addition any number of $\mathcal{O}(p^2)$ vertices, which do not change the chiral order of the amplitude. The amplitudes for the matrix elements are rational functions of the momenta, with a pole structure given by the propagators present in the diagrams and a numerator which is a polynomial in the kinematic invariants. If a relation between operators holds, the matrix element must vanish for any arbitrary momentum configuration of the fields. This requires that all the coefficients of the terms in the polynomial built from the kinematic invariants are zero, and conditions for the α_i are thus obtained. By requiring that a sufficiently large number of matrix elements computed in this way with increasing number of fields vanish, we obtain a set of conditions for the numerical coefficients α_i in Θ; when these conditions yield non-zero solutions, relations between the operators which are fulfilled for all the processes computed are thus found. One may wish to prove that the relations found hold for matrix elements with an arbitrary number of pions and currents. In that case, the fact that we already know the precise numerical coefficients in the relation between the operators simplifies the task of proving it at the operator level using partial integration, equations of motion, and the Bianchi and Cayley-Hamilton identities. Note also that such a proof may be more a formal matter than one of practical relevance; processes with 6 mesons legs or involving more than two vector or axial-vector currents are rather remote experimentally, so just knowing the relations satisfied among the operators for the phenomenologically relevant processes could be enough.

In order to illustrate how the method works let us consider the computation of the matrix element for two specific cases. The first one involves (4.8) with one external vector (v_{11}), one external axial (a_{12}) and one charged pion field (π^-), which is simple enough to provide explicit formulas. We shall refer to the latter with the abridged notation $\langle v_{11} a_{12} \pi^- \rangle$.

The perturbative computation of this matrix element at $\mathcal{O}(p^6)$ is given by the diagrams in Fig. 4.1. The operators in Θ contributing to diagram 4.1a are $\mathcal{P}_{44}, \mathcal{P}_{50}, \mathcal{P}_{51}, \mathcal{P}_{52}$ and $\mathcal{P}_{53}$. For diagram 4.1b, operators $\mathcal{P}_{51}, \mathcal{P}_{52}$ contribute in one of the vertices, whereas the other vertex corresponds to an $\mathcal{O}(p^2)$ interaction. To calculate the amplitude, we take the momenta of the fields incoming and use energy-momentum conservation. We thus have two independent momenta, which we take to be that of the pion, p_1, and that of the axial current, q. In addition we have the "polarization" vectors from the external fields v_{11} and a_{12}, ϵ_v and ϵ_a respectively.[1] Taking into account the on-shell condition for the (massless) pion,

[1] The introduction of polarization vectors for the external fields is not strictly necessary: we could work with the tensor amplitude with Lorentz indices of the external sources μ, ν left open

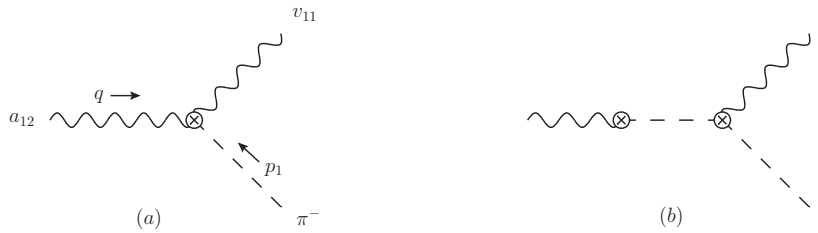

Figure 4.1: *a*) Local and *b*) non-local contributions to the $\langle v_{11} a_{12} \pi^- \rangle$ matrix element.

$p_1^2 = 0$, the amplitude can then be written in terms of seven different kinematic invariants, $p_1 \cdot q$, $p_1 \cdot \epsilon_v$, $p_1 \cdot \epsilon_a$, $q \cdot \epsilon_v$, $q \cdot \epsilon_a$, $\epsilon_v \cdot \epsilon_a$ and q^2. Adding the result from the diagrams with operators $\mathcal{P}_i$ multiplied by corresponding coefficients α_i, the perturbative amplitude reads

$$\begin{aligned}
\mathcal{M} = \frac{1}{q^2}\Big\{ & 4\,(\alpha_{51} - \alpha_{53})\big[\,\epsilon_v \cdot q\,\epsilon_a \cdot q\,(p_1 \cdot q)^2 \\
& - \epsilon_v \cdot p_1\,\epsilon_a \cdot q\,(p_1 \cdot q)^2 + q^2\,\epsilon_v \cdot p_1\,\epsilon_a \cdot p_1\,p_1 \cdot q\,\big] \\
& + (2\alpha_{50} - \alpha_{51} + \alpha_{52} + \alpha_{53})\,q^4\,\epsilon_v \cdot \epsilon_a\,p_1 \cdot q \\
& + (\alpha_{51} - \alpha_{52} - \alpha_{53})\,q^2\,\epsilon_v \cdot q\,\epsilon_a \cdot q\,p_1 \cdot q \\
& + (2\alpha_{44} - 2\alpha_{51} - \alpha_{52} + 3\alpha_{53})\,q^2\,\big[\,\epsilon_v \cdot p_1\,\epsilon_a \cdot q\,p_1 \cdot q - q^2\,\epsilon_v \cdot p_1\,\epsilon_a \cdot p_1\big] \\
& - (2\alpha_{44} + 3\alpha_{51} - 2\alpha_{52} - 2\alpha_{53})\,q^2\,\epsilon_v \cdot \epsilon_a\,(p_1 \cdot q)^2 \\
& + (2\alpha_{44} - \alpha_{51} - 2\alpha_{52} + 2\alpha_{53})\,q^2\,\epsilon_v \cdot q\,\epsilon_a \cdot p_1\,p_1 \cdot q \\
& + 2\,\alpha_{50}\,q^4\,\big[\,q^2\,\epsilon_v \cdot \epsilon_a - \epsilon_v \cdot q\,\epsilon_a \cdot p_1 - \epsilon_v \cdot q\,\epsilon_a \cdot q\big]\Big\}\,,
\end{aligned} \tag{4.9}$$

up to a global constant factor, and we have also dropped the Dirac delta function with the momentum conservation. The $1/q^2$ factor arises from the scalar propagator in diagram Fig. 4.1a; since we have factored out it globally, the resulting polynomial in the numerator is of order z_i^4 in the kinematic invariants $z_i \equiv p_1 \cdot q$, $p_1 \cdot \epsilon_v$, ..., with the restriction that all monomials must contain both polarization vectors ϵ_v and ϵ_a. The resulting amplitude is therefore of chiral or-

and require that the coefficients of all tensor structures vanish. The contraction of the tensor amplitude with arbitrary vectors ϵ_v, ϵ_a allows to work with a scalar function, which simplifies handling the long expressions that are obtained for the amplitudes of Green functions with more fields.

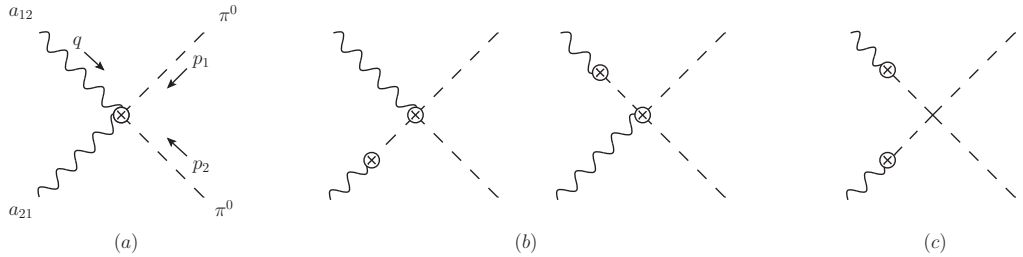

Figure 4.2: (a) Local and $(b), (c)$ non-local contributions to the $\langle a_{12} a_{21} \pi^0 \pi^0 \rangle$ matrix element.

der p^6; recall that the polarization vectors count as $\mathcal{O}(p)$, just like the external fields v_μ, a_μ. The requirement that (4.9) must vanish if a relation between the $\mathcal{O}(p^6)$ operators holds forces the coefficients of all monomials in the numerator to vanish. This translates into the following set of conditions for the α_i:

$$\alpha_{50} = \alpha_{52} = 0 \quad , \quad \alpha_{51} = \alpha_{53} = -2\alpha_{44} \; . \tag{4.10}$$

The first condition in (4.10) implies that no relation involving operators $\mathcal{P}_{50}$ and $\mathcal{P}_{52}$ can be satisfied by the matrix element chosen in this example. Since an operator relation must be true for any process we can already conclude that the operators 50 and 52 belong to the minimal basis of the Lagrangian. The second condition in (4.10) translates into the relation $\mathcal{P}_{44} - 2\mathcal{P}_{51} - 2\mathcal{P}_{53} = 0$ being satisfied for this process. By analysing other processes we shall conclude in Sec. 4.4 that the latter relation is actually part of a larger one involving more terms, that holds exactly for the operators in $\mathcal{L}_6^{\mathrm{SU}(2)}$.

Let us now choose a matrix element with one pion field more, for instance $\langle a_{12} a_{21} \pi^0 \pi^0 \rangle$, which involves two axial-vector currents. This example shall give us an idea of the increasing complexity brought by diagrams with more legs. Fig. 4.2 shows the diagrammatic contributions to the corresponding matrix element. The pure local term, Fig. 4.2a, stems from the operators $1-3, 36-44$ and $50-53$. The non-local contributions include two different type of diagrams: in Figs. 4.2b, an axial-3π vertex from operators $1-3, 36-38$ and $51-53$ of the $\mathcal{O}(p^6)$ Lagrangian is combined with the axial-pion vertex from $\mathcal{L}_2^{\mathrm{SU}(2)}$ [2], whereas in Fig. 4.2c, we need the $\mathcal{O}(p^6)$ 4π vertices from operators $\mathcal{P}_{1-3}$. The amplitudes for $\langle a_{12} a_{21} \pi^0 \pi^0 \rangle$

[2] We note that there is no axial$-\pi$ vertex in $\mathcal{L}_6^{\mathrm{SU}(2)}$ with massless pions.

depend on 11 independent kinematic invariants, namely $p_1\cdot p_2$, q^2, $p_1\cdot q$, $p_2\cdot q$, $p_1\cdot\epsilon_{12}$, $p_2\cdot\epsilon_{12}$, $q\cdot\epsilon_{12}$, $p_1\cdot\epsilon_{21}$, $p_2\cdot\epsilon_{21}$, $q\cdot\epsilon_{21}$ and $\epsilon_{12}\cdot\epsilon_{21}$, and we have again considered massless pions. The number of monomials of order p^6 which can be built out of the kinematic invariants is therefore large, and handling the amplitude in order to find out the conditions for the α_i requires automatisation. For this task, we have implemented the computation of the tree-level matrix elements at $\mathcal{O}(p^6)$ and the extraction of the relations for the α_i in a MATHEMATICA code. In the case at hand, $\langle a_{12}a_{21}\pi^0\pi^0\rangle$, one obtains an amplitude with 132 independent monomials in the numerator, whose coefficients yield the equations for α_i: 50 of these equations are non-trivially identical, but only 10 turn out to be independent. The solution to this system then provides 10 relations among the coefficients α_i of the 16 operators that contribute to $\langle a_{12}\, a_{21}\pi^0\pi^0\rangle$:

$$\begin{aligned}
&\alpha_{38}=\alpha_{50}=0 \quad , \quad \alpha_1=-4\alpha_2=\frac{4}{3}\alpha_3=\alpha_{36}=-\alpha_{37} \quad , \quad \alpha_{51}=\alpha_{53}\\
&3\alpha_1-2\alpha_{41}-2\alpha_{42}+4\alpha_{43}-4\alpha_{51}=0\\
&\alpha_1+8\alpha_{39}-8\alpha_{40}+6\alpha_{41}+6\alpha_{42}-12\alpha_{43}-8\alpha_{44}=0\\
&\alpha_1+2\alpha_{39}-2\alpha_{40}+\alpha_{41}+\alpha_{42}-2\alpha_{43}-\alpha_{52}=0\ .
\end{aligned} \tag{4.11}$$

Taking into account these conditions together, one thus finds that the linear combination

$$\begin{aligned}
\Theta =&\alpha_1\Big(\mathcal{P}_1-\frac{1}{4}\,\mathcal{P}_2+\frac{3}{4}\,\mathcal{P}_3+\mathcal{P}_{36}-\mathcal{P}_{37}-\frac{3}{4}\,\mathcal{P}_{40}-\mathcal{P}_{41}-\mathcal{P}_{42}+\frac{1}{4}\,\mathcal{P}_{43}\\
&-\mathcal{P}_{44}+2\mathcal{P}_{51}+2\mathcal{P}_{53}\Big)\\
&+\alpha_{39}\Big(\mathcal{P}_{39}-\mathcal{P}_{40}-2\,\mathcal{P}_{41}+\mathcal{P}_{43}-\mathcal{P}_{44}+2\,\mathcal{P}_{51}+2\,\mathcal{P}_{53}\Big)
\end{aligned} \tag{4.12}$$

makes the amplitude $\langle a_{12}a_{21}\pi^0\pi^0\rangle$ vanish for arbitrary values of α_1 and α_{39}, implying that the two relations among the $\mathcal{P}_i$ operators between parenthesis in (4.12) are equal to zero for this particular process. We can proceed in the same way for other matrix elements and require a simultaneous vanishing of all of them by solving for the α_i. The latter is a necessary condition for the existence of a relation between the $\mathcal{O}(p^6)$ operators. In the next section we show that the procedure eventually allows for just two relations in the SU(2) case without scalar and pseudo-scalar external fields.

SU(2) case with $s = p = 0$

As a proof of concept we show in this section how the method described above applies to the two-flavour ChPT Lagrangian in the chiral limit and without additional external scalar or pseudo-scalar sources ($s = p = 0$) but $v_\mu, a_\mu \neq 0$. This simplified framework does not lack of phenomenological relevance: it provides a very good approximation to the low-energy interaction of the pions in the presence of electroweak currents, since mass corrections in the u, d quark sector are small and there are no other contributions to the external sources s and p in the Standard Model[3].

Within this framework, we have computed the matrix elements from (4.8) with the generic field content as listed in the first column of Tab. 6.1. The notation $\langle va\, 3\pi\rangle$, for instance, stands for all processes involving three pion fields (charged or neutral) and one vector and one axial-vector field component, and similarly for the rest. The second column indicates which $\mathcal{O}(p^6)$ operators contribute to the Green functions. The relations among the operators satisfied for each process, obtained as in the examples of Sec. 4.3 by solving a system of equations for the coefficients α_i, are then given in the third column. We have not written the equations for the α_i for each process except for the cases where they require some of the α_i to vanish; the condition $\alpha_i = 0$ obtained for a given matrix element already implies that the corresponding operator $\mathcal{P}_i$ cannot be part of any relation, which is an important information. We note that the relations written in Tab. 6.1 guarantee that all matrix elements with arbitrary charge (or isospin) configuration of the pion and ChPT currents vanish. For a given charge (isospin) channel additional relations among the operators that contribute can exist, which we do not provide in Tab. 6.1.

The relations satisfied for a set of processes can be obtained by combining the equations for the coefficients α_i from each process and looking for a compatible solution. From the table one sees that the combination of matrix elements $\langle vv\rangle$, $\langle vaa\rangle$, $\langle vv\, 2\pi\rangle$, $\langle aa\, 2\pi\rangle$, $\langle v\, 4\pi\rangle$ and $\langle 6\pi\rangle$ already involve all the operators in the SU(2) ChPT Lagrangian with $s = p = 0$. The fact that operators $\mathcal{P}_{45}$ and $\mathcal{P}_{55}$ only appear in $\langle vaa\rangle$ requires a further matrix element depending on $\mathcal{P}_{45}$ in order to fix it completely. That is why the matrix element $\langle vva\pi\rangle$ is also computed. The results for the rest of processes in Tab. 6.1 is given for completeness; their computation also serves us as a check of the relations found with the minimal set of processes.

[3]Let us recall that at low energies the scalar $q\bar{q}$ interaction with the Higgs produces terms in the amplitude suppressed by $1/m_h^2$.

Green function	$\mathcal{P}_i$	Operator relations
$\langle vv \rangle$	56	$\alpha_{56}=0$
$\langle v\,2\pi \rangle$	51, 53	$\mathcal{P}_{51} + \mathcal{P}_{53} = 0$
$\langle va\pi \rangle$	44, 50−53	$\alpha_{50}=\alpha_{52}=0$ $\mathcal{P}_{44} - 2\mathcal{P}_{51} - 2\mathcal{P}_{53} = 0$
$\langle vaa \rangle$	44, 45, 50−53, 55	$\alpha_{50}=\alpha_{52}=0$ $3\mathcal{P}_{45} + 8\mathcal{P}_{55} = 0$ $\mathcal{P}_{44} - \mathcal{P}_{45} - 2\mathcal{P}_{51} - 2\mathcal{P}_{53} = 0$
$\langle 4\pi \rangle$	1−3	$4\mathcal{P}_1 - \mathcal{P}_2 + 3\mathcal{P}_3 = 0$
$\langle vv\,2\pi \rangle$	29−33, 44, 50−53	$\alpha_{50}=\alpha_{52}=0$ $\mathcal{P}_{29} - \mathcal{P}_{30} + 2\mathcal{P}_{31} - 4\mathcal{P}_{32} + \mathcal{P}_{33} - \mathcal{P}_{44} + 2\mathcal{P}_{51} + 2\mathcal{P}_{53} = 0$
$\langle aa\,2\pi \rangle$	1−3, 36−44, 50−53	$\alpha_{38} = \alpha_{50} = \alpha_{52} = 0$ $\mathcal{P}_{39} - \mathcal{P}_{40} - 2\mathcal{P}_{41} + \mathcal{P}_{43} - \mathcal{P}_{44} + 2\mathcal{P}_{51} + 2\mathcal{P}_{53} = 0$ $4\mathcal{P}_1 - \mathcal{P}_2 + 3\mathcal{P}_3 + 4\mathcal{P}_{36} - 4\mathcal{P}_{37} - 4\mathcal{P}_{39} + \mathcal{P}_{40} + 4\mathcal{P}_{41}$ $-4\mathcal{P}_{42} - 3\mathcal{P}_{43} = 0$
$\langle a\,3\pi \rangle$	1−3, 36−38, 51, 53	$\alpha_{38} = 0$ $4\mathcal{P}_1 - \mathcal{P}_2 + 3\mathcal{P}_3 + 4\mathcal{P}_{36} - 4\mathcal{P}_{37} = 0$ $\mathcal{P}_{51} + \mathcal{P}_{53} = 0$
$\langle vva\,\pi \rangle$	29−33, 44, 45, 50−53	$\alpha_{50} = \alpha_{52} = 0$ $\mathcal{P}_{29} - \mathcal{P}_{30} + 2\mathcal{P}_{31} - 4\mathcal{P}_{32} + \mathcal{P}_{33} - \mathcal{P}_{44} + \mathcal{P}_{45}$ $+2\mathcal{P}_{51} + 2\mathcal{P}_{53} = 0$
$\langle v\,4\pi \rangle$	1−3, 27−28 36−38, 51−53	$\alpha_{38} = 0$ $4\mathcal{P}_1 - \mathcal{P}_2 + 3\mathcal{P}_3 - 6\mathcal{P}_{27} - 14\mathcal{P}_{28} + 4\mathcal{P}_{36} - 4\mathcal{P}_{37} = 0$ $2\mathcal{P}_{27} + 2\mathcal{P}_{28} - \mathcal{P}_{51} - \mathcal{P}_{53} = 0$
$\langle va\,3\pi \rangle$	1−3, 27−44, 50−53	$\alpha_{38} = \alpha_{50} = \alpha_{52} = 0$ $\mathcal{P}_{29} + \mathcal{P}_{39} = 0$ $\mathcal{P}_{31} + \mathcal{P}_{32} + \mathcal{P}_{41} + \mathcal{P}_{42} = 0$ $8\mathcal{P}_1 - 2\mathcal{P}_2 + 6\mathcal{P}_3 - 12\mathcal{P}_{27} - 28\mathcal{P}_{28} + 8\mathcal{P}_{36} - 8\mathcal{P}_{37}$ $-8\mathcal{P}_{39} + 2\mathcal{P}_{40} + 8\mathcal{P}_{41} - 8\mathcal{P}_{42} - 6\mathcal{P}_{43} = 0$ $4\mathcal{P}_{27} + 4\mathcal{P}_{28} + \mathcal{P}_{30} - 2\mathcal{P}_{31} + 4\mathcal{P}_{32} - \mathcal{P}_{33} + \mathcal{P}_{40} + 2\mathcal{P}_{41}$ $-\mathcal{P}_{43} + \mathcal{P}_{44} - 2\mathcal{P}_{51} - 2\mathcal{P}_{53} = 0$
$\langle 6\pi \rangle$	1−3, 24−26	$4\mathcal{P}_1 - \mathcal{P}_2 + 3\mathcal{P}_3 - 10\mathcal{P}_{24} + 4\mathcal{P}_{25} + 6\mathcal{P}_{26} = 0$

Table 4.1: Relations among $\mathcal{O}(p^6)$ operators satisfied for each of the Green functions computed. The second column lists the operators that contribute in each case.

Combining the equations for α_i found for the different matrix elements we get that all the latter vanish provided

$$\begin{aligned}
&\alpha_{38} = \alpha_{50} = \alpha_{52} = \alpha_{55} = \alpha_{56} = 0\,,\\
&\alpha_1 \Big(8\,\mathcal{P}_1 - 2\,\mathcal{P}_2 + 6\,\mathcal{P}_3 - 20\,\mathcal{P}_{24} + 8\,\mathcal{P}_{25} + 12\,\mathcal{P}_{26} - 16\,\mathcal{P}_{28} - 3\,\mathcal{P}_{29} + 3\,\mathcal{P}_{30} - 6\,\mathcal{P}_{31}\\
&\qquad + 12\,\mathcal{P}_{32} - 3\,\mathcal{P}_{33} + 8\,\mathcal{P}_{36} - 8\,\mathcal{P}_{37} - 11\,\mathcal{P}_{39} + 5\,\mathcal{P}_{40} + 14\,\mathcal{P}_{41} - 8\,\mathcal{P}_{42} - 9\,\mathcal{P}_{43}\\
&\qquad + 3\,\mathcal{P}_{44} - 3\,\mathcal{P}_{45} - 6\,\mathcal{P}_{51} - 6\,\mathcal{P}_{53} \Big)\\
+\ &\alpha_{27} \Big(8\,\mathcal{P}_{27} + 8\,\mathcal{P}_{28} - 2\,\mathcal{P}_{29} + 2\,\mathcal{P}_{30} - 4\,\mathcal{P}_{31} + 8\,\mathcal{P}_{32} - 2\,\mathcal{P}_{33} - 2\,\mathcal{P}_{39} + 2\,\mathcal{P}_{40}\\
&\qquad + 4\,\mathcal{P}_{41} - 2\,\mathcal{P}_{43} + 2\,\mathcal{P}_{44} - 2\,\mathcal{P}_{45} - 4\,\mathcal{P}_{51} - 4\,\mathcal{P}_{53} \Big) = 0\,, \qquad (4.13)
\end{aligned}$$

which holds for whatever values of α_1 and α_{27}, meaning that the two linear combinations among the operators $\mathcal{P}_i$ between parenthesis must vanish independently. The relations obtained can be simplified if one uses the second linear combination into the first one. In this way we find:

$$\begin{aligned}
&4\,\mathcal{P}_{27} + 4\,\mathcal{P}_{28} - \mathcal{P}_{29} + \mathcal{P}_{30} - 2\,\mathcal{P}_{31} + 4\,\mathcal{P}_{32} - \mathcal{P}_{33} - \mathcal{P}_{39} + \mathcal{P}_{40} + 2\,\mathcal{P}_{41}\\
&\qquad - \mathcal{P}_{43} + \mathcal{P}_{44} - \mathcal{P}_{45} - 2\,\mathcal{P}_{51} - 2\,\mathcal{P}_{53} = 0\,, \qquad (4.14)
\end{aligned}$$

$$\begin{aligned}
&8\,\mathcal{P}_1 - 2\,\mathcal{P}_2 + 6\,\mathcal{P}_3 - 20\,\mathcal{P}_{24} + 8\,\mathcal{P}_{25} + 12\,\mathcal{P}_{26} - 12\,\mathcal{P}_{27} - 28\,\mathcal{P}_{28} + 8\,\mathcal{P}_{36} - 8\,\mathcal{P}_{37}\\
&\qquad - 8\,\mathcal{P}_{39} + 2\,\mathcal{P}_{40} + 8\,\mathcal{P}_{41} - 8\,\mathcal{P}_{42} - 6\,\mathcal{P}_{43} = 0\,. \qquad (4.15)
\end{aligned}$$

The result (6.3) agrees with a relation which is known to hold among the $\mathcal{O}(p^6)$ operators when the scalar and pseudo-scalar sources are set to zero [8][4]. Likewise, (6.4) matches the additional relation found for the SU(2) case in [6], once the operators depending on scalar and pseudo-scalar tensor source χ are neglected in the latter. Since relations (6.3,6.4) were proven algebraically in these references, they are of course satisfied for all matrix elements with any number of pions and currents. We can moreover state that these are the only two relations between the SU(2) ChPT operators of $\mathcal{O}(p^6)$ in the limit $s = p = 0$; otherwise any further relation of the form $\sum \alpha_i' \mathcal{P}_i = 0$ would have been obtained from the analysis of the functions of Tab. 6.1 with our method (let us recall that the vanishing

[4]Ref. [8] provided relation (6.3) for a number of flavors $n = 3$ using the SU(3) operator numbering introduced in [5]. The corresponding relation for SU(2) can be obtained by translating into the SU(2) numbering scheme for the operators, and further using that the operator $\mathcal{P}_{52}$ in the two-flavor case is equal to $-\mathcal{P}_{50} - \mathcal{P}_{51}$ (*i.e.* to $-\mathcal{P}_{27} - \mathcal{P}_{28}$ in the SU(2) numbering scheme).

of any matrix element with an insertion of $\sum \alpha_i' \mathcal{P}_i$ is a necessary condition for the existence of the relation). We therefore conclude that the set of minimal operators of the SU(2) ChPT Lagrangian of $\mathcal{O}(p^6)$ with scalar and pseudo-scalar sources set to zero reduces from the 27+2 operators initially written down in [5] to 25+2 (note that the contact terms do not take part in any of the relations above). Eqs. (6.3,6.4) can be used to drop two of the 27 basis elements of the set of [5].

The application of our method to the general two- and three-flavour cases is straightforward. For SU(2) including scalar and pseudo-scalar sources, if a similar analysis does not yield additional relations to that of Ref. [6], it would ascertain that the basis of $\mathcal{O}(p^6)$ operators from [5] is minimal up to one term. The case of SU(3) is more involved at the technical level, since we have to consider an octet of pseudo-goldstone bosons and many more matrix elements can be built. Starting the analysis of processes with less number of fields, one could expect that the space of solutions for the coefficients α_i is either very much constrained, and eventually no solution is allowed after computing a few matrix elements, or that it actually allows for one (or more) relations among the operators. In the former case one could already conclude that the basis of $\mathcal{L}_6^{\mathrm{SU(3)}}$ is minimal. In the latter, one may try to check if the relations found from the analysis of the simpler processes also hold at the level of the operators (*i.e.* for any matrix element with an arbitrary number of fields) by using the same algebraic manipulations as in [5], with the great advantage that one would know beforehand the coefficients that the operators participating in the relation must have. The study of the general two- and three-flavour cases with the automated tools developed in this work will be the subject of future investigation.

Summary

The large number of low-energy constants in the mesonic chiral Lagrangian of order p^6 makes their determination by direct comparison with the experiment rather difficult. To simplify this task, one would like to eliminate possible redundancies by establishing the minimal set of independent operators in $\mathcal{L}_6$, that parametrize the rational part of the $\mathcal{O}(p^6)$ chiral amplitudes.

We have described in this paper a method to search for additional relations among the basis operators that build the $\mathcal{O}(p^6)$ SU(n) chiral Lagrangian. It relies on the computation of tree-level amputated Green functions with insertions of the $\mathcal{L}_6$ operators, which are then required to vanish on-shell for an arbitrary kinematic configuration. The method can be used to establish the minimal basis of operators

in the Lagrangian. This has been done in the present work for the two-flavour $\mathcal{O}(p^6)$ Lagrangian without scalar and pseudo-scalar external sources. For this case we have shown that the original basis of 27 measurable terms plus 2 contact terms written in [5] in the even-intrinsic-parity sector has 25+2 independent terms, where the two additional relations between operators that emerge from our method had been already noticed in the literature [6, 8].

As a next step, the method shall be applied to determine the minimal basis of operators in the SU(2) case with general scalar and pseudo-scalar sources, as well as in SU(3). Furthermore, one can expect that the method extends naturally to other relevant effective actions containing a large number of operators, and in particular to the linear and non-linear effective theories that describe the breaking of the electroweak symmetry.

Acknowledgments

We thank J. Sanz-Cillero for pointing us to the operator relation in Ref. [8] and for his comments on the draft. We also thank G. Ecker for useful communication regarding the functionality of the code Ampcalculator [9], used for cross-checks, and J. Portolés for comments on the draft. MZA wants to thank A.Pich and J. Portolés for helpful discussions. This work is partially supported by MEC (Spain) under grants FPA2007-60323 and FPA2011-23778 and by the Spanish Consolider-Ingenio 2010 Programme CPAN (CSD2007-00042).

Appendix

We provide in this appendix the explicit form of the operators in the $\mathcal{O}(p^6)$ ChPT Lagrangian in the SU(2) case (4.7) without scalar and pseudo-scalar sources. The expressions are read off from the list given in the appendix C of Ref. [5] by discarding terms containing the χ tensor.

Besides the chiral tensors already written in Sec. 4.2, the following building blocks are needed to construct the operators in Tab. 4.2:

$$\begin{aligned} h_{\mu\nu} &= \nabla^\mu u_\nu + \nabla^\nu u_\mu \,, \\ f_\pm^{\mu\nu} &= u F_L^{\mu\nu} u^\dagger \pm u^\dagger F_R^{\mu\nu} u \,, \quad \nabla_\rho f_\pm^{\mu\nu} \,, \end{aligned} \tag{4.16}$$

with the non-abelian field strength tensor built from the right and left external fields,

$$F_L^{\mu\nu} = \partial^\mu \ell^\nu - \partial^\nu \ell^\mu - i\,[\ell^\mu, \ell^\nu]\ ,$$
$$F_R^{\mu\nu} = \partial^\mu r^\nu - \partial^\nu r^\mu - i\,[r^\mu, r^\nu] \tag{4.17}$$

and the covariant derivative defined as

$$\nabla_\mu X = \partial_\mu X + [\Gamma_\mu, X]\,, \tag{4.18}$$

where

$$\Gamma_\mu = \frac{1}{2}\{u^\dagger(\partial_\mu - ir_\mu)u + u(\partial_\mu - i\ell_\mu)u^\dagger\}\,. \tag{4.19}$$

i	$\mathcal{P}_i$	Matrix element
1	$\langle u\cdot u h_{\mu\nu}h^{\mu\nu}\rangle$	$\langle 4\pi\rangle$
2	$\langle h_{\mu\nu}u_\rho h^{\mu\nu}u^\rho\rangle$	$\langle 4\pi\rangle$
3	$\langle h_{\mu\nu}\left(u_\rho h^{\mu\rho}u^\nu + u^\nu h^{\mu\rho}u_\rho\right)\rangle$	$\langle 4\pi\rangle$
24	$\langle (u\cdot u)^3\rangle$	$\langle 6\pi\rangle$
25	$\langle u\cdot u u_\mu u_\nu u^\mu u^\nu\rangle$	$\langle 6\pi\rangle$
26	$\langle u_\mu u_\nu u_\rho u^\mu u^\nu u^\rho\rangle$	$\langle 6\pi\rangle$
27	i $\langle f_{+\mu\nu}u_\rho u^\mu u^\nu u^\rho\rangle$	$\langle v\,4\pi\rangle$
28	i $\langle f_{+\mu\nu}u^\mu u\cdot u u^\nu\rangle$	$\langle v\,4\pi\rangle$
29	$\langle u\cdot u f_{+\mu\nu}f_+^{\mu\nu}\rangle$	$\langle vv\,2\pi\rangle$
30	$\langle f_{+\mu\nu}u_\rho f_+^{\mu\nu}u^\rho\rangle$	$\langle vv\,2\pi\rangle$
31	$\langle f_{+\mu\nu}f_+^{\mu\rho}u^\nu u_\rho\rangle$	$\langle vv\,2\pi\rangle$
32	$\langle f_{+\mu\nu}f_+^{\mu\rho}u_\rho u^\nu\rangle$	$\langle vv\,2\pi\rangle$
33	$\langle f_{+\mu\nu}\left(u_\rho f_+^{\mu\rho}u^\nu + u^\nu f_+^{\mu\rho}u_\rho\right)\rangle$	$\langle vv\,2\pi\rangle$
36	$\langle f_{-\mu\nu}\left(h^{\nu\rho}u_\rho u^\mu + u^\mu u_\rho h^{\nu\rho}\right)\rangle$	$\langle a\,3\pi\rangle$
37	$\langle f_{-\mu\nu}h^{\nu\rho}\rangle\langle u^\mu u_\rho\rangle$	$\langle a\,3\pi\rangle$
38	$\langle f_{-\mu\nu}\left(u^\mu h^{\nu\rho}u_\rho + u_\rho h^{\nu\rho}u^\mu\right)\rangle$	$\langle a\,3\pi\rangle$
39	$\langle u\cdot u f_{-\mu\nu}f_-^{\mu\nu}\rangle$	$\langle aa\,2\pi\rangle$
40	$\langle f_{-\mu\nu}u_\rho f_-^{\mu\nu}u^\rho\rangle$	$\langle aa\,2\pi\rangle$
41	$\langle f_{-\mu\nu}f_-^{\mu\rho}u^\nu u_\rho\rangle$	$\langle aa\,2\pi\rangle$
42	$\langle f_{-\mu\nu}f_-^{\mu\rho}u_\rho u^\nu\rangle$	$\langle aa\,2\pi\rangle$
43	$\langle f_{-\mu\nu}\left(u_\rho f_-^{\mu\rho}u^\nu + u^\nu f_-^{\mu\rho}u_\rho\right)\rangle$	$\langle aa\,2\pi\rangle$
44	i $\langle f_{+\mu\nu}[f_-^{\nu\rho}, h_\rho^\mu]\rangle$	$\langle va\,\pi\rangle$
45	i $\langle f_{+\mu\nu}[f_-^{\nu\rho}, f_{-\rho}^{\mu}]\rangle$	$\langle vaa\rangle$
50	$\langle \nabla_\rho f_{-\mu\nu}\nabla^\rho f_-^{\mu\nu}\rangle$	$\langle aa\rangle$
51	i $\langle \nabla_\rho f_{+\mu\nu}[h^{\mu\rho}, u^\nu]\rangle$	$\langle v\,2\pi\rangle$
52	i $\langle \nabla^\mu f_{+\mu\nu}[f_-^{\nu\rho}, u_\rho]\rangle$	$\langle va\,\pi\rangle$
53	i $\langle \nabla^\mu f_{+\mu\nu}[h^{\nu\rho}, u_\rho]\rangle$	$\langle v\,2\pi\rangle$
contact terms		
55	i $\langle F_{L\mu\nu}F_L^{\mu\rho}F_{L\rho}^{\nu}\rangle + L\to R$	$\langle vaa\rangle$
56	$\langle D_\rho F_{L\mu\nu}D^\rho F_L^{\mu\nu}\rangle + L\to R$	$\langle vv\rangle$

Table 4.2: $\mathcal{O}(p^6)$ operators for SU(2) with $s = p = 0$, in the basis of [5]. The label in the first column refers to the SU(2) numbering scheme used in the latter reference. The last column indicates the simplest process to which the operator contributes.

Bibliography

[1] S. Weinberg, Physica A **96** (1979) 327.

[2] J. Gasser and H. Leutwyler, Annals Phys. **158** (1984) 142.

[3] J. Gasser and H. Leutwyler, Nucl. Phys. B **250** (1985) 465.

[4] H. W. Fearing and S. Scherer, Phys. Rev. D **53** (1996) 315 [hep-ph/9408346].

[5] J. Bijnens, G. Colangelo and G. Ecker, JHEP **9902** (1999) 020 [hep-ph/9902437].

[6] C. Haefeli, M. A. Ivanov, M. Schmid and G. Ecker, arXiv:0705.0576 [hep-ph].

[7] C. Arzt, Phys. Lett. B **342** (1995) 189 [hep-ph/9304230].

[8] P. Colangelo, J. J. Sanz-Cillero and F. Zuo, JHEP **1211** (2012) 012 [arXiv:1207.5744 [hep-ph]].

[9] http://homepage.univie.ac.at/Gerhard.Ecker/CPT-amp.html

5. High Scale Mixing Relations as a Natural Explanation for Large Neutrino Mixing

Gauhar Abbas[a], Mehran Zahiri Abyaneh[a], Aritra Biswas[b], Saurabh Gupta[c], Monalisa Patra[d], G. Rajasekaran[e], Rahul Srivastava[f]

[a] *Instituto de Física Corpuscular (IFIC), CSIC-Universitat de Valèncía Apdo. Correos 22085, E-46071 Valencia, Spain*

[b] *The Institute of Mathematical Sciences, Chennai 600 113, India*

[c] *Instituto de Física, Universidade de São Paulo, C. Postal 66318, 05314-970 São Paulo, Brazil*

[d] *Physik-Institut, Universität Zürich, CH-8057 Zürich, Switzerland*

[e] *The Institute of Mathematical Sciences, Chennai 600 113, India*

[e] *Chennai Mathematical Institute, Siruseri 603 103, India*

[f] *The Institute of Mathematical Sciences, Chennai 600 113, India*

[International Journal of Modern Physics A, Volume 31, Issue 17, Published 20 June 2016]

The origin of small mixing among the quarks and a large mixing among the neutrinos has been an open question in particle physics. In order to answer this question, we postulate general relations among the quarks and the leptonic mixing angles at a high scale, which could be the scale of Grand Unified Theories. The central idea of these relations is that the quark and the leptonic mixing angles can be unified at some high scale either due to some quark-lepton symmetry or some other underlying mechanism and as a consequence, the mixing angles of the leptonic sector are proportional to that of the quark sector. We investigate the phenomenology of the possible relations where the leptonic mixing angles

are proportional to the quark mixing angles at the unification scale by taking into account the latest experimental constraints from the neutrino sector. These relations are able to explain the pattern of leptonic mixing at the low scale and thereby hint that these relations could be possible signatures of a quark-lepton symmetry or some other underlying quark-lepton mixing unification mechanism at some high scale linked to Grand Unified Theories.

14.60.Pq, 11.10.Hi, 11.30.Hv, 12.15.Lk

Introduction

The quark mixing matrix, V_{CKM}, parametrizes the misalignment in the diagonalisation of the *up* and *down* type quark mass matrices. It is well known that V_{CKM} is almost close to a unit matrix. This implies that the quark mixing angles are small. On the other hand, analogous misalignment in the leptonic sector is encoded in the neutrino mixing matrix, U_{PMNS}. It turns out that U_{PMNS} is not close to a unit matrix. The mixing angles in the neutrino sector are large except θ_{13} [52–54]. The origin of small mixing among quarks and a large mixing in the neutrino sector poses an intriguing open question.

Among many approaches to explain the mixing pattern of the leptons, the assumption of family or flavor symmetries is a popular one. These symmetries differentiate among the members of different families and are usually discrete, finite and non-abelian, for reviews see Refs. [4, 5]. This approach has been intensively used to study the mixing in the leptonic sector [4, 5, 9, 30]. In addition to the leptonic mixing, there are also considerable efforts to understand the quark mixing through family symmetries [6–8]. The family symmetries can also be a built-in characteristic of the Grand Unified Theories (GUT) [9].

The quark-lepton unification is one of the most attractive features of the GUT theories [1–3]. The GUT symmetry group contains quarks and leptons in a joint representation. The weak interaction properties of the quarks and the leptons therefore get correlated. Hence it is possible in these theories, to derive the origin of the small and the large mixing in the quark and the lepton sectors respectively, along with any relation between them, if it exists.

There are also reasons to speculate about the quark-lepton unification even on the experimental side. The so-called quark-lepton complementarity (QLC) relation [17, 18] between the leptonic mixing angle θ_{12} and the Cabibbo angle θ_C

$$\theta_{12} + \theta_C \approx \frac{\pi}{4}, \tag{5.1}$$

can be a footprint of a high scale quark-lepton unification [17–21]. Another interesting observation is due to the recent non-zero measurement of leptonic mixing angle θ_{13} [22–26] which is

$$\theta_{13} \approx \frac{\theta_C}{\sqrt{2}}. \tag{5.2}$$

This relation also hints a possible link between the quark and leptonic mixing, and it can be an artifact of some high scale quark-lepton symmetry in an underlying GUT theory [27].

Therefore, the present state of the measured leptonic mixing angles provide the theoretical motivation for a common origin of the quark and leptonic mixing at some high scale. In fact, the idea that the quark and lepton mixing can be unified at some high scale, referred to as "high scale mixing unification" (HSMU) hypothesis, was first proposed in Ref. [11–14]. In recent studies [15, 17, 33] it has been shown that HSMU hypothesis 'naturally' leads to nonzero and a small value for the leptonic mixing angle θ_{13} and predicts a non-maximal θ_{23} (cf. [15, 17] for details). This hypothesis has been studied in the context of Dirac neutrinos as well (cf. [16] for details). The central idea of this hypothesis is that the quark mixing angles become identical to that of the leptons at some high scale (referred to as the unification scale) which is typically taken as GUT scale (cf. [15, 16, 33] for details). In other words, at the unification scale

$$\theta_{12} = \theta^q_{12}, \quad \theta_{13} = \theta^q_{13}, \quad \theta_{23} = \theta^q_{23}, \tag{5.3}$$

where θ_{ij} (with $i, j = 1, 2, 3$) are leptonic mixing angles and θ^q_{ij} are the quark mixing angles. This hypothesis nicely explains the pattern of mixing in the neutrino sector including the recent observation of nonzero and a small value of θ_{13} [22–26]. The large leptonic mixing angles at the low scale are obtained through the renormalization group (RG) evolution of the corresponding mixing parameters from the unification scale to the low scale.

The implementation of the HSMU hypothesis requires the minimum supersymmetric standard model (MSSM) as an extension of the standard model (SM). The working of the HSMU hypothesis is as follows. We first evolve the quark mixing angles from the low scale (mass of the Z boson) to the supersymmetry (SUSY) breaking scale using the SM RG equations. After that, from the SUSY breaking scale to the unification scale, evolution of quark mixing angles is governed by the MSSM RG equations. In the next step, the quark mixing angles at the unification scale, are put equal to that of the neutrinos following the HSMU

hypothesis. The leptonic mixing parameters are then run from the unification scale to the SUSY breaking scale using the MSSM RG equations. From the SUSY breaking scale to the low scale, mixing parameters are evolved through the SM RG equations.

In addition to SUSY, we also need a large $\tan\beta$ to realize the HSMU hypothesis [15, 33]. The only free parameters during the top-down running of the leptonic mixing parameters are masses of the three light neutrinos. They are chosen at the unification scale in such a manner that we recover all the mixing parameters at the low scale within the 3σ limit of the global fit. It turns out that the chosen masses of neutrinos must be quasi-degenerate (QD) and normal hierarchical [15, 33]

In this work, inspired by the HSMU hypothesis, we postulate the most general relations among the quark and the leptonic mixing angles at the unification scale. In a compactified form the most general relation among the leptonic and the quark mixing angles within the same generations is as following

$$\theta_{12} = \alpha_1^{k_1}\ \theta_{12}^q, \quad \theta_{13} = \alpha_2^{k_2}\ \theta_{13}^q, \quad \theta_{23} = \alpha_3^{k_3}\theta_{23}^q. \tag{5.4}$$

where k_i, with $i = (1, 2, 3)$ are real exponents. We refer to this relation as the "high scale mixing relation" (HSMR). We have chosen (k_1, k_2, k_3) to be $(1, 1, 1)$ for the simplicity of our analysis. The relations within the same generations are the simplest generalization of the HSMU hypothesis. In principle, we can also construct the most general HSMR relations among different generations completely independent of the HSMU hypothesis. The analysis of these relations is beyond the scope of this work and could be studied elsewhere.

There will be different possibilities depending on the relations among the proportionality factors. We firstly list below the different possible cases with the maximum and the minimum allowed values of the three independent proportion-

ality factors α_i,

$$\begin{aligned}
\textbf{Case A}: &\quad \theta_{12} = \alpha_1^{max}\ \theta_{12}^q, \quad \theta_{13} = \alpha_2^{max}\ \theta_{13}^q, \quad \theta_{23} = \alpha_3^{max}\ \theta_{23}^q, && (5.5)\\
\textbf{Case B}: &\quad \theta_{12} = \alpha_1^{max}\ \theta_{12}^q, \quad \theta_{13} = \alpha_2^{max}\ \theta_{13}^q, \quad \theta_{23} = \alpha_3^{min}\ \theta_{23}^q, && (5.6)\\
\textbf{Case C}: &\quad \theta_{12} = \alpha_1^{max}\ \theta_{12}^q, \quad \theta_{13} = \alpha_2^{min}\ \theta_{13}^q, \quad \theta_{23} = \alpha_3^{max}\ \theta_{23}^q, && (5.7)\\
\textbf{Case D}: &\quad \theta_{12} = \alpha_1^{max}\ \theta_{12}^q, \quad \theta_{13} = \alpha_2^{min}\ \theta_{13}^q, \quad \theta_{23} = \alpha_3^{min}\ \theta_{23}^q, && (5.8)\\
\textbf{Case E}: &\quad \theta_{12} = \alpha_1^{min}\ \theta_{12}^q, \quad \theta_{13} = \alpha_2^{max}\ \theta_{13}^q, \quad \theta_{23} = \alpha_3^{max}\ \theta_{23}^q, && (5.9)\\
\textbf{Case F}: &\quad \theta_{12} = \alpha_1^{min}\ \theta_{12}^q, \quad \theta_{13} = \alpha_2^{max}\ \theta_{13}^q, \quad \theta_{23} = \alpha_1^{min}\ \theta_{23}^q, && (5.10)\\
\textbf{Case G}: &\quad \theta_{12} = \alpha_1^{min}\ \theta_{12}^q, \quad \theta_{13} = \alpha_2^{min}\ \theta_{13}^q, \quad \theta_{23} = \alpha_3^{max}\ \theta_{23}^q, && (5.11)\\
\textbf{Case H}: &\quad \theta_{12} = \alpha_1^{min}\ \theta_{12}^q, \quad \theta_{13} = \alpha_2^{min}\ \theta_{13}^q, \quad \theta_{23} = \alpha_3^{min}\ \theta_{23}^q. && (5.12)
\end{aligned}$$

In this work, we have presented our results for the maximum and minimum allowed values of α_i for all the above cases, Eqs. (5.5-5.12). We then move on to scenarios, assuming relations among the α_i's. There can be more general HSMR where two proportionality constants can be identical and the third one is different. However we will discuss in this work more simplified scenerios, where the three proportionality constants are equal.

$$\theta_{12} = \alpha^{k_1}\ \theta_{12}^q, \quad \theta_{13} = \alpha^{k_2}\ \theta_{13}^q, \quad \theta_{23} = \alpha^{k_3}\theta_{23}^q. \tag{5.13}$$

As explained before we have restricted to values of k_i as either 0 or 1. We note that the value $(k_1, k_2, k_3) = (0, 0, 0)$ will reduce HSMR to HSMU hypothesis making Eq. (5.3) a specific form of HSMR, Eq. (5.13). We present below the seven different possible cases, where the quark mixing angles are assumed to be proportional to the corresponding leptonic mixing angles.

$$\begin{aligned}
\textbf{Case 1}: &\quad \theta_{12} = \alpha\ \theta_{12}^q, \quad \theta_{13} = \theta_{13}^q, \quad \theta_{23} = \theta_{23}^q, && (5.14)\\
\textbf{Case 2}: &\quad \theta_{12} = \theta_{12}^q, \quad \theta_{13} = \alpha\ \theta_{13}^q, \quad \theta_{23} = \theta_{23}^q, && (5.15)\\
\textbf{Case 3}: &\quad \theta_{12} = \theta_{12}^q, \quad \theta_{13} = \theta_{13}^q, \quad \theta_{23} = \alpha\ \theta_{23}^q, && (5.16)\\
\textbf{Case 4}: &\quad \theta_{12} = \alpha\ \theta_{12}^q, \quad \theta_{13} = \alpha\ \theta_{13}^q, \quad \theta_{23} = \theta_{23}^q, && (5.17)\\
\textbf{Case 5}: &\quad \theta_{12} = \theta_{12}^q, \quad \theta_{13} = \alpha\ \theta_{13}^q, \quad \theta_{23} = \alpha\ \theta_{23}^q, && (5.18)\\
\textbf{Case 6}: &\quad \theta_{12} = \alpha\ \theta_{12}^q, \quad \theta_{13} = \theta_{13}^q, \quad \theta_{23} = \alpha\ \theta_{23}^q, && (5.19)\\
\textbf{Case 7}: &\quad \theta_{12} = \alpha\ \theta_{12}^q, \quad \theta_{13} = \alpha\ \theta_{13}^q, \quad \theta_{23} = \alpha\ \theta_{23}^q. && (5.20)
\end{aligned}$$

The proportionality constant α in the above Eqs. (5.14-5.20) is taken as real parameter. We have carried out a detailed study for these cases in this work.

We note that there exist GUT models in the literature where proportionality between the quark and the leptonic mixing angles are explicitly shown. For example, the proportionality relation observed between the leptonic mixing angle θ_{13} and the Cabibbo angle θ_C in Eq. (5.2) can arise naturally in $SU(5)$ GUTs and Pati- Salam models. For more details, see [27]. Further more, it is shown in Ref. [18] that the relations between the quark and the leptonic mixing angles are possible and they support the idea of grand unification. However, non-abelian and abelian flavor symmetries are essential to make this happen [18] .

There is two-fold importance of the HSMR hypothesis. The first remarkable feature is that these relations provide a very simple way to achieve a large neutrino mixing. We shall see that predictions of these relations are easily testable in present and forthcoming experiments. The second importance is that if predictions of HSMR hypothesis are confirmed by experimets, like neutrinoless double beta decay, this would be a strong hint of quark-lepton unification at high scale.

The plan of the paper is as follows. In section 6.3, we present the required RG equations for the running of the neutrino mixing parameters. The SUSY threshold corrections and the neutrino mass scale are discussed in section 6.4. The results are presented in section 5.4 using dimensional-5 operator as well as in the framework of type-1 seasaw. In section 5.5, for the sake of illustration, we discuss two models where HSMR hypothesis can be realised. We summarize our results and conclude in section 5.6.

RG evolution of the leptonic mixing parameters

In this section, we briefly discuss the RG evolution of the leptonic mixing parameters.The most often studied scenario is the one where the Majorana mass term for the left handed neutrinos is given by the lowest dimensional operator [36]

$$\mathscr{L}_\kappa = \frac{1}{4}\kappa_{gf}\,\overline{\ell^{\rm C}_{\rm L}}{}^{g}_{c}\varepsilon^{cd}\phi_d\;\ell^{f}_{{\rm L}b}\varepsilon^{ba}\phi_a + \text{h.c.}\,, \tag{5.21}$$

in the SM. In the MSSM, it is given by

$$\mathscr{L}^{\rm MSSM}_\kappa \;=\; \mathscr{W}_\kappa\big|_{\theta\theta} + \text{h.c.} = -\tfrac{1}{4}\kappa_{gf}\,L^{g}_{c}\varepsilon^{cd}h^{(2)}_{d}\;L^{f}_{b}\varepsilon^{ba}h^{(2)}_{a}\big|_{\theta\theta} + \text{h.c.}\,, \tag{5.22}$$

where κ_{gf} has mass dimension -1, $\ell^C_{\rm L}$ is the charge conjugate of a lepton doublet and $a, b, c, d \in \{1, 2\}$ are $\mathrm{SU}(2)_{\rm L}$ indices. The double-stroke letters L and h denote

the lepton doublets and the up-type Higgs superfield in the MSSM. Using this mass operator, we introduce neutrino masses in a rather model independent way since it does not depend on the underlying mass mechanism.

The evolution of the above dimensional-5 operator below the scale where it is generated is provided by its RG equation. The one loop equation is as follows [37–40]

$$16\pi^2\,\dot{\kappa} \;=\; C\,(Y_e^\dagger Y_e)^T\,\kappa + C\,\kappa\,(Y_e^\dagger Y_e) + \hat{\alpha}\,\kappa\;, \tag{5.23}$$

where $\dot{\kappa} = \frac{d\kappa}{dt}$, $t = \ln(\mu/\mu_0)$ and μ is the renormalization scale and

$$\begin{aligned} C &= 1 \qquad \text{in the MSSM}\;, \\ C &= -\frac{3}{2} \quad \text{in the SM}\;. \end{aligned} \tag{5.24}$$

The parameter $\hat{\alpha}$ in the SM and MSSM is given by

$$\begin{aligned} \hat{\alpha}_{\rm SM} &= -3g_2^2 + 2(y_\tau^2 + y_\mu^2 + y_e^2) + 6\left(y_t^2 + y_b^2 + y_c^2 + y_s^2 + y_d^2 + y_u^2\right) + \lambda\;, \\ \hat{\alpha}_{\rm MSSM} &= -\frac{6}{5}g_1^2 - 6g_2^2 + 6\left(y_t^2 + y_c^2 + y_u^2\right)\;. \end{aligned} \tag{5.25}$$

The quantities y_f ($f \in \{e, d, u\}$) represent the Yukawa coupling matrices of the charged leptons, down- and up-type quarks respectively, g_i ($i = 1, 2$) denote the gauge couplings and λ is the Higgs self coupling. For more details see Ref. [36].

We are interested in the RG evolution of parameters that are the masses, the mixing angles and the physical phases. The mixing angles and the physical phases are described by the PMNS matrix. This matrix is parameterized as follows

$$U_{PMNS} \;=\; V \cdot U, \tag{5.26}$$

where

$$V = \begin{pmatrix} c_{12}c_{13} & s_{12}c_{13} & s_{13}e^{-\delta} \\ -c_{23}s_{12} - s_{23}s_{13}c_{12}e^{\delta} & c_{23}c_{12} - s_{23}s_{13}s_{12}e^{\delta} & s_{23}c_{13} \\ s_{23}s_{12} - c_{23}s_{13}c_{12}e^{\delta} & -s_{23}c_{12} - c_{23}s_{13}s_{12}e^{\delta} & c_{23}c_{13} \end{pmatrix}, \tag{5.27}$$

and

$$U = \begin{pmatrix} e^{-\varphi_1/2} & 0 & 0 \\ 0 & e^{-\varphi_2/2} & 0 \\ 0 & 0 & 1 \end{pmatrix},$$

with c_{ij} and s_{ij} defined as $\cos\theta_{ij}$ and $\sin\theta_{ij}$ $(i,j=1,2,3)$, respectively. The quantity δ is the Dirac phase and φ_1, φ_2 are the Majorana phases. The global experimental status of the leptonic mixing parameter is summarized in Table 6.1.

Quantity	Best Fit	3σ Range
Δm^2_{21} $(10^{-5}$ eV$^2)$	7.54	6.99 – 8.18
Δm^2_{32} $(10^{-3}$ eV$^2)$	2.39	2.20 – 2.57
θ°_{12}	33.71	30.59 – 36.81
θ°_{23}	41.38	37.7 – 52.3
θ°_{13}	8.8	7.63 – 9.89

Table 5.1: The global fits for the neutrino mixing parameters [53].

Here we would like to remark that the RG equations (5.23) for Yukawa couplings matrices are parametrization independent. The main aim is to probe if there is any connection between the quark and the leptonic mixing. For this purpose, we have chosen the standard parametrization which is the most studied and also commonly used in the literature. In principle, one could use an alternative parameterization to work and test the reality of HSMR. The results can be always interpreted as a possible indication of a connection between quark and leptonic mixing.

We now summarize the RG equations used for running the leptonic mixing parameters from high to the low scale. For a detailed discussion of these equations, see Ref. [36]. These equations are derived using the lowest dimensional neutrino mass operator as discussed above and are given by the following analytical expressions [36]

$$\dot{\theta}_{12} = -\frac{Cy_\tau^2}{32\pi^2}\,\sin 2\theta_{12}\,s_{23}^2\,\frac{|m_1\,e^{\varphi_1}+m_2\,e^{\varphi_2}|^2}{\Delta m^2_{21}}+\mathscr{O}(\theta_{13})\,, \tag{5.28}$$

$$\begin{aligned}\dot{\theta}_{13} &= \frac{Cy_\tau^2}{32\pi^2}\,\sin 2\theta_{12}\,\sin 2\theta_{23}\,\frac{m_3}{\Delta m^2_{32}\,(1+\zeta)}\times \\ &\quad\times\left[m_1\cos(\varphi_1-\delta)-(1+\zeta)\,m_2\,\cos(\varphi_2-\delta)-\zeta m_3\,\cos\delta\right] \\ &\quad+\mathscr{O}(\theta_{13})\,,\end{aligned} \tag{5.29}$$

$$\dot{\theta}_{23} = -\frac{Cy_\tau^2}{32\pi^2}\sin 2\theta_{23}\,\frac{1}{\Delta m_{32}^2}\left[c_{12}^2\,|m_2\,e^{\varphi_2}+m_3|^2+s_{12}^2\,\frac{|m_1\,e^{\varphi_1}+m_3|^2}{1+\zeta}\right] + \mathscr{O}(\theta_{13})\,, \tag{5.30}$$

where $\dot{\theta}_{ij} = \frac{d\theta_{ij}}{dt}$ (with $i,j = 1,\,2,\,3$), $t = \ln(\mu/\mu_0)$, μ being the renormalization scale and

$$\zeta := \frac{\Delta m_{21}^2}{\Delta m_{32}^2}\,, \quad \Delta m_{21}^2 := m_2^2 - m_1^2, \quad \Delta m_{32}^2 := m_3^2 - m_2^2. \tag{5.31}$$

For the masses, the results for $y_e = y_\mu = 0$ but arbitrary θ_{13} are

$$16\pi^2\,\dot{m}_1 = \left[\hat{\alpha} + Cy_\tau^2\left(2s_{12}^2\,s_{23}^2 + F_1\right)\right] m_1\,, \tag{5.32a}$$

$$16\pi^2\,\dot{m}_2 = \left[\hat{\alpha} + Cy_\tau^2\left(2c_{12}^2\,s_{23}^2 + F_2\right)\right] m_2\,, \tag{5.32b}$$

$$16\pi^2\,\dot{m}_3 = \left[\hat{\alpha} + 2Cy_\tau^2\,c_{13}^2\,c_{23}^2\right] m_3\,, \tag{5.32c}$$

where $\dot{m}_i = \frac{dm_i}{dt}$ (i =1, 2, 3) and F_1, F_2 contain terms proportional to $\sin\theta_{13}$,

$$F_1 = -s_{13}\,\sin 2\theta_{12}\,\sin 2\theta_{23}\,\cos\delta + 2s_{13}^2\,c_{12}^2\,c_{23}^2\,, \tag{5.33a}$$

$$F_2 = s_{13}\,\sin 2\theta_{12}\,\sin 2\theta_{23}\,\cos\delta + 2s_{13}^2\,s_{12}^2\,c_{23}^2\,. \tag{5.33b}$$

In this work, we are working in the CP conserving limit which means Majorana and Dirac phases are assumed to be zero. Therefore, we have not provided the RG equations for them. The non-zero phases are expected to have non-trivial impact on the parameter space. However, this study is beyond the scope of the present work and will be presented in a future investigation. Furthermore, we also study the effect of the new physics which could generate the above dimensional-5 operator. For this purpose, we present our analysis within the framework of type-1 seesaw.

Now, we briefly discuss the evolution of the leptonic mixing angles. In the SM as can be seen from Eq. (5.25), only tau Yukawa coupling will dominate the evolution which is already very small. Hence the running of the neutrino masses is governed by a common scaling factor and the evolution of leptonic mixing angles can only be enhanced for QD mass pattern. In the MSSM the value of tau Yukawa coupling can be larger with respect to the value in the SM for a large value of $\tan\beta$. Hence the evolution of the leptonic mixing parameters can be enhanced in addition to the enhancement coming from the QD neutrino mass pattern as discussed below.

It is interesting to note from Eqs. (5.28, 5.29 and 5.30) that the major contribution to RG evolution of the mixing angles arises due to following enhancement factors

$$\dot{\theta}_{12} \propto \xi_1, \qquad \dot{\theta}_{13},\, \dot{\theta}_{23} \propto \xi_2, \tag{5.34}$$

where

$$\xi_1 \;=\; \frac{m^2}{\Delta m^2_{21}}, \qquad \xi_2 = \frac{m^2}{\Delta m^2_{32}}, \tag{5.35}$$

and m is the average neutrino mass with $m = (m_1 + m_2 + m_3)/3$. It is clear that we need masses of the neutrinos to be QD to explain the largeness of mixing angles at the low scale.

The low energy SUSY threshold corrections and the absolute neutrino mass scale

We discuss the required low energy SUSY threshold corrections for the mass square differences and the significance of the absolute neutrino mass scale in this section.

The low energy SUSY threshold corrections

It is well established in the previous works on HSMU hypothesis that among the five mixing parameters, one of the mass square differences (Δm^2_{21}) lies outside the 3σ global range [11–15]. As shown in the previous works, this mass square difference can be brought well within the 3σ global limit, if the low energy SUSY threshold corrections are incorporated to the mass square differences [11–15]. The importance of SUSY threshold corrections for QD neutrinos is discussed in Refs. [41–44]. These corrections are given by the following equations [12]

$$\begin{aligned}
(\Delta m^2_{21})_{th} &= 2\mathrm{m}^2 \cos 2\theta_{12}[-2\mathrm{T_e} + \mathrm{T}_\mu + \mathrm{T}_\tau], \\
(\Delta m^2_{32})_{th} &= 2\mathrm{m}^2 \sin^2\theta_{12}[-2\mathrm{T_e} + \mathrm{T}_\mu + \mathrm{T}_\tau], \\
(\Delta m^2_{31})_{th} &= 2\mathrm{m}^2 \cos^2\theta_{12}[-2\mathrm{T_e} + \mathrm{T}_\mu + \mathrm{T}_\tau].
\end{aligned} \tag{5.36}$$

where m is the mean mass of the QD neutrinos and the one loop factor $T_{\hat{\alpha}}(\hat{\alpha} = e, \mu, \tau)$ is given by [41, 44]

$$T_{\hat{\alpha}} = \frac{g_2^2}{32\pi^2}\left[\frac{x_\mu^2 - x_{\hat{\alpha}}^2}{y_\mu y_{\hat{\alpha}}} + \frac{(y_{\hat{\alpha}}^2 - 1)}{y_{\hat{\alpha}}^2} ln(x_{\hat{\alpha}}^2) - \frac{(y_\mu^2 - 1)}{y_\mu^2} ln(x_\mu^2)\right], \quad (5.37)$$

where g_2 is the $SU(2)$ coupling constant and $y_{\hat{\alpha}} = 1 - x_{\hat{\alpha}}^2$ with $x_{\hat{\alpha}} = M_{\hat{\alpha}}/M_{\tilde{w}}$; $M_{\tilde{w}}$ stands for wino mass, $M_{\hat{\alpha}}$ represents the mass of charged sleptons. We work with an inverted hierarchy in the charged-slepton sector where the mass of selectron is defined through the ratio $R = \frac{M_{\tilde{e}}}{M_{\tilde{\mu},\tilde{\tau}}}$. The mass of the wino is chosen to be 400 GeV following the direct searches at the LHC [58].

The absolute neutrino mass scale

The scale of the neutrino mass is one of the open questions, ever since it has been confirmed that the neutrinos are massive. In case of QD and the normal hierarchical spectra, we have

$$m_1 \lesssim m_2 \lesssim m_3 \simeq m_0 \quad (5.38)$$

with

$$m_0 \gg \sqrt{\Delta m_{32}^2} \approx 5 \times 10^{-2}\,\text{eV}. \quad (5.39)$$

There are three complementary ways to measure the neutrino mass scale. The first one, a model independent method, is to use the kinematics of β-decay to determine the effective electron (anti) neutrino mass (m_β). It is given by

$$m_\beta \equiv \sqrt{\sum |U_{ei}|^2\, m_i^2}\,. \quad (5.40)$$

The m_β has an upper bound of 2 eV from tritium beta decay [66, 67]. In future, the KATRIN experiment has sensitivity to probe m_β as low as 0.2 eV at 90% CL [65]. We note that m_0 in the QD regime for CP conservation is approximately equal to the effective beta decay mass m_β. Hence QD mass pattern is well within the sensitivity of the KATRIN.

The second method to extract the neutrino mass is neutrinoless double beta decay which assumes that neutrinos are Majorana particles [49, 50]. The observable parameter M_{ee}, the double beta decay effective mass is given as following

$$\begin{aligned} M_{ee} &= \left|\sum U_{ei}^2\, m_i\right|, \\ &= \left|m_1 c_{12}^2\, c_{13}^2 e^{-i\varphi_1} + m_2 s_{12}^2\, c_{13}^2\, e^{-i\varphi_2} + m_3 s_{13}^2\, e^{-i2\delta}\right|. \end{aligned} \tag{5.41}$$

For quasi-degenerate neutrinos

$$M_{ee} \approx m_0 \left|c_{12}^2\, c_{13}^2 e^{-i\varphi_1} + s_{12}^2\, c_{13}^2\, e^{-i\varphi_2} + s_{13}^2\, e^{-i2\delta}\right|. \tag{5.42}$$

Since the contribution of m_3 is suppressed by the small $\sin^2\theta_{13}$ coefficient, we obtain

$$M_{ee} \simeq m_0 \sqrt{1 - \sin^2 2\theta_{12} \frac{(1-\cos(\varphi_1 - \varphi_2))}{2}}. \tag{5.43}$$

For CP conserving case where the Majorana and Dirac phases are zero, $M_{ee} \simeq m_0$. For $M_{ee} \simeq 0.1$ eV, the above expression corresponds approximately to half-life in the range of 10^{25} to 10^{26} yrs [49] which makes the QD mass scheme testable in present and future experiments . In the QD regime, the neutrino mass can be written as [49]

$$m_0 \leq (M_{ee})^{\rm exp}_{\rm max} \frac{1 + \tan^2\theta_{12}}{1 - \tan^2\theta_{12} - 2\,|U_{e3}|^2} \equiv (M_{ee})^{\rm exp}_{\rm max}\, f(\theta_{12}, \theta_{13})\,. \tag{5.44}$$

Using inputs from Table 6.1, the function $f(\theta_{12}, \theta_{13})$ has a range from 2.2 to 4.1 at 3σ. The most stringent upper limit on the effective mass M_{ee} provided by the GERDA experiment is 0.4 eV [23]. Hence $m_0 \leq 1.64$ eV and sum of the neutrino masses $\Sigma m_i = 3m_0 \leq 4.91$ eV.

The third determination of neutrino masses is provided by the cosmological and astrophysical observations. The sum of the neutrino masses, Σm_i, has a range for upper bound to be $0.17 - 0.72$ eV at 95% CL [68]. This limit is not model independent and depends on the cosmological model applied to the data.

Results

We present our results in this section for the different cases listed in Eqs. (5.14 - 5.20) and for limiting cases of the most general HSMR as shown in Eqs. (5.5 - 5.11). As discussed earlier, we need MSSM as an extension of the SM for the implementation of HSMR and HSMU hypothesis. In the first step, we run

quark mixing angles, gauge couplings, Yukawa couplings of quarks and charged leptons from the low scale to the SUSY breaking scale. The evolution from the SUSY breaking scale to the unification scale is done through the MSSM RG equations. After evolving up to the unification scale, we obtain quark mixing angles $\theta_{12}^q = 13.02^\circ$, $\theta_{13}^q = 0.17^\circ$ and $\theta_{23}^q = 2.03^\circ$. In the next step, quark mixing angles are used to calculate the leptonic mixing angles using HSMR at the unification scale. After this, we run down the MSSM RG equations up to the SUSY breaking scale. The SM RG equations take over the evolution of mixing parameters beyond the SUSY breaking scale. The SUSY breaking scale is chosen to be 2 TeV following the direct LHC searches [58]. We also need a large $\tan\beta$ which is chosen to be 55. The unification scale where HSMR can exist is chosen to be 10^{14} GeV which is consistent with present experimental observations [53]. We have used the MATHEMATICA based package REAP [57] for the numerical computation of our results. We have done a rigorous, thorough and comprehensive in this work. For this pupose, we have written an interface code which together with public code can be used to scan whole parameter space.

RG evolution of HSMR

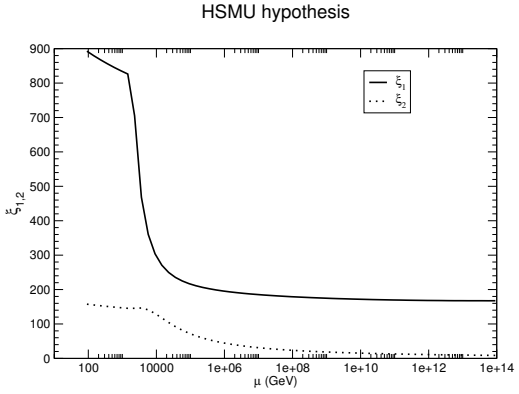

Figure 5.1: The change in the RG evolution of the enhancement factors ($\xi_{1,2}$), 5.35, for the HSMU case as a function of the RG scale μ when α deviates from unity.

We study the RG evolution of HSMR as given in Eqs. (5.14 - 5.20) and compare our results with respect to the HSMU hypothesis. In Fig. 5.1, we show how enhancement factors ξ_1 and ξ_2 evolve from the unification scale to the low

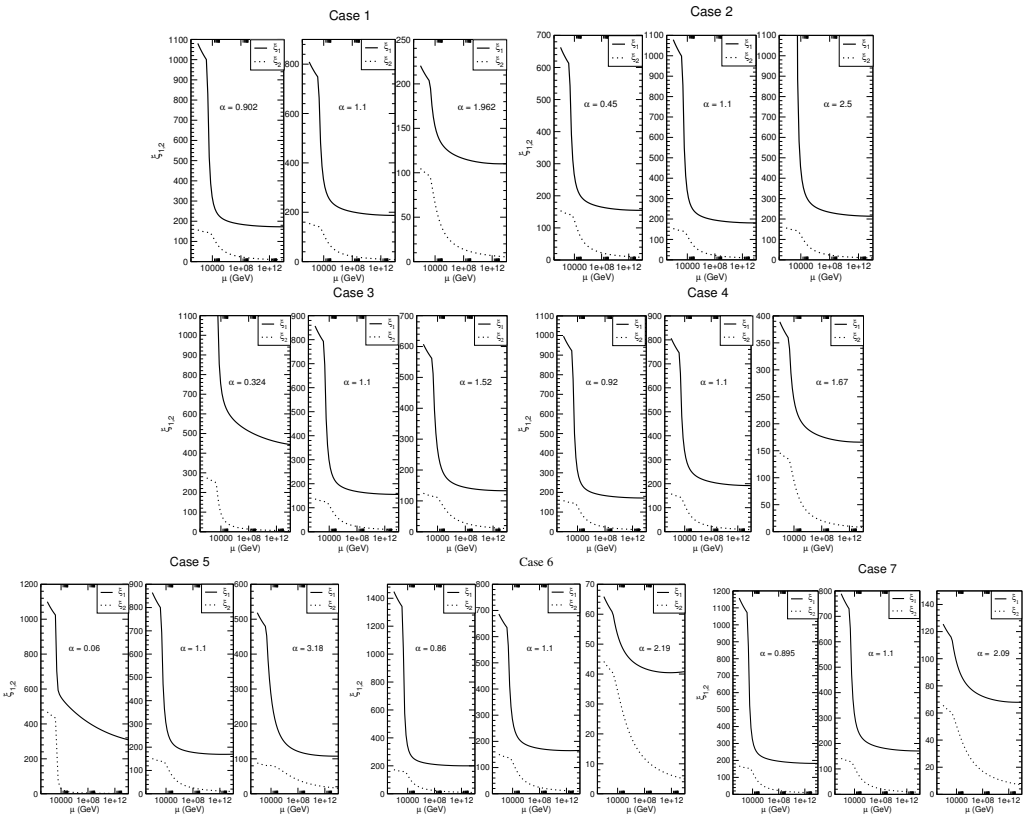

Figure 5.2: The change in the RG evolution of the enhancement factors ($\xi_{1,2}$), 5.35, for the different cases of HSMR as a function of the RG scale μ when α deviates from unity.

scale, as α deviates from unity for the HSMU. The results are displayed for all the HSMR cases in Fig. 5.2. It can be seen from Fig. 5.2 that the evolution in Case 1 at $\alpha = 1.1$ is similar to HSMU hypothesis. However, as α approaches to lowest value on the left panel of Case 1, ξ_1 changes sufficiently. Similarly for the upper limit of $\alpha = 1.962$, the evolution again becomes very different from the HSMU hypothesis. This explains why the RG evolution of the PMNS mixing angles change when α deviates from unity. The same argument follows for all the other cases of HSMR and can be checked from Fig. 5.2.

We next show the evolution of the mixing angles for the HSMU in Fig. 5.3. The results are displayed for all the HSMR cases in Fig. 5.4. We observe from

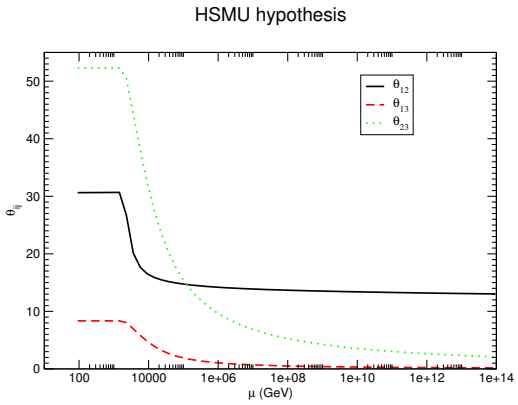

Figure 5.3: The evolution of the mixing angles for the HSMU case

Figs. 5.1 and 5.2 along with Figs. 5.3 and 5.4, that the evolution of HSMR is similar to the HSMU hypothesis when α deviates slightly from unity. However, when α is very far from unity, RG evolution undergoes dramatic changes. There is another interesting phenomenon that can be observed from Fig. 5.4. It can be easily seen that the RG evolution of the mixing angles, for Cases 3 and 5 are similar, with θ_{12} and θ_{23} almost similar at the low scale at the lower end of α. The difference between them at the low scale increases with the increase in value of α. The pattern is exactly opposite in the other cases of HSMR, with the difference between θ_{12} and θ_{23} at the low scale decreasing as one goes from the lower to the upper end of α. This in a way tells us beforehand that the phenomenology of Case 3 and 5 will be similar, which will be discussed in detail afterwards.

Phenomenology of HSMR

In this subsection, we discuss in details the phenomenological implications of HSMR. Our aim is to investigate the behavior of α as it deviates from unity and its phenomenological consequences taking into account all the experimental constraints of Table 6.1 and the GERDA limit [23]. The common observation among all HSMR is the emergence of the strong correlations among Δm^2_{32}, M_{ee}, θ_{23}, θ_{13} and Σm_i.

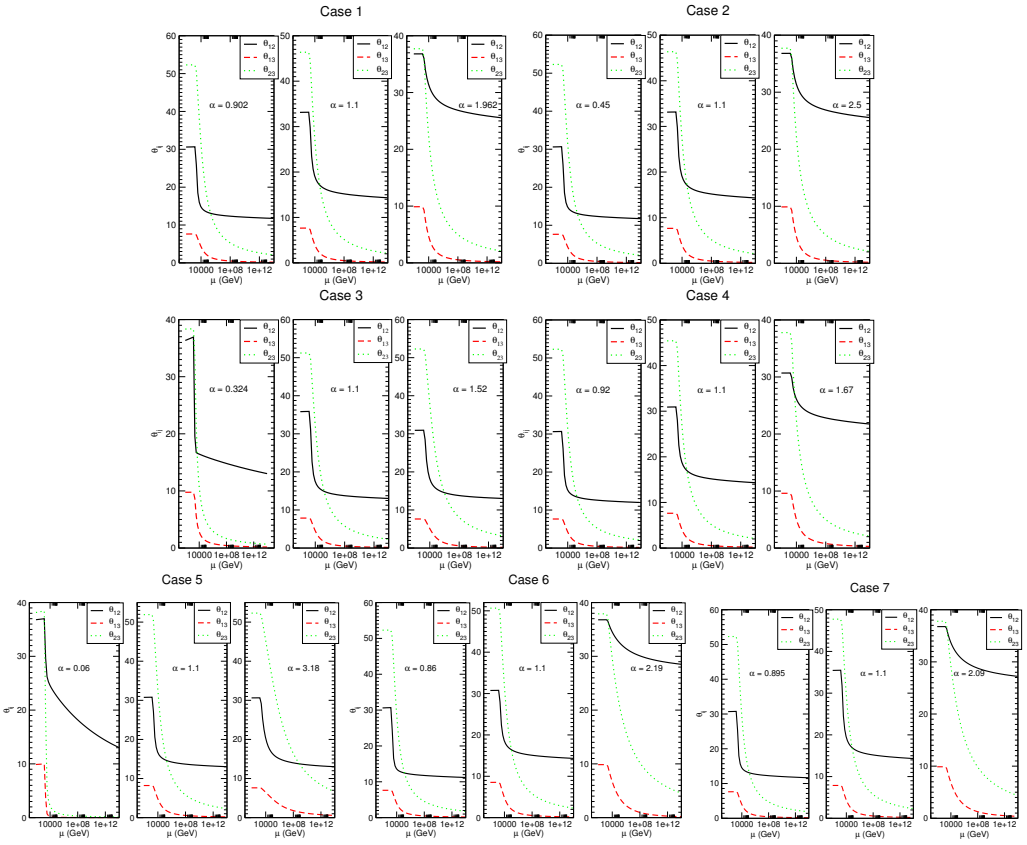

Figure 5.4: The evolution of the mixing angles for the different HSMR cases

HSMU hypothesis

As observed earlier, the value $\alpha = 1$ will reduce all cases of HSMR to HSMU hypothesis. We present a full parameter scan of the HSMU hypothesis using dimensional-5 operator. It should be noted that this analysis was absent in the previous works on HSMU hypothesis [15, 17, 33] and is reported in this work for the first time. We present a correlation in Fig. 6.1, which is not studied in the previous investigations. We show here the variation of Δm^2_{32} with respect to M_{ee}. The M_{ee} has an upper bound of 0.4 eV from the GERDA experiment [23]. Using this limit, we are able to put an upper bound on the allowed range of Δm^2_{32}. The allowed range for Δm^2_{32} is $(2.21 - 2.45) \times 10^{-3}$ eV^2 as observed from Fig. 6.1. The lower bound on M_{ee} is 0.384 eV for the HSMU hypothesis. Hence, our

work on the HSMU hypothesis will be ruled out if GERDA crosses this number in the future. The effective β decay mass m_β is another interesting observable since it does not depend on whether the neutrinos are Majorana or Dirac. The prediction for m_β coincides with the effective double beta decay mass M_{ee} in the QD regime and for CP conservation. Hence, the allowed range for m_β is identical to that of M_{ee} in our work.

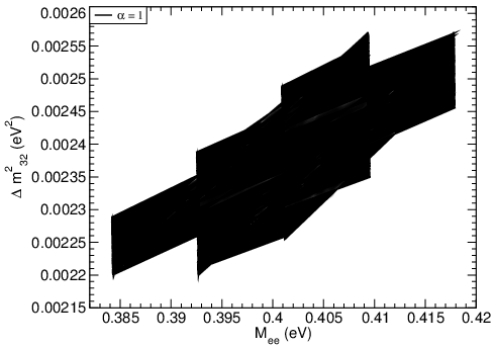

Figure 5.5: The variation of Δm^2_{32} with respect to M_{ee}, in the context of the HSMU hypothesis, with α =1.

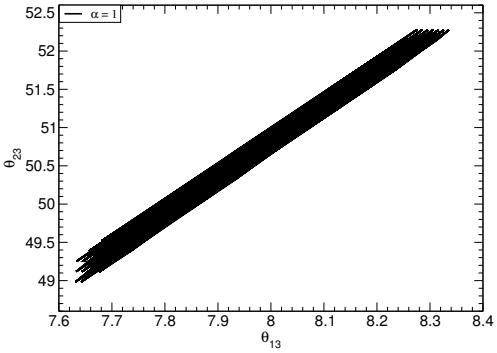

Figure 5.6: The variation of θ_{23} with respect to θ_{13}, in the context of the HSMU hypothesis, with α =1.

In Fig. 6.2, we show the variation of θ_{23} with respect to θ_{13}. We observe a strong correlation between θ_{13} and θ_{23}. The difference between this investigation and that of presented in Ref. [15] is the variation of θ_{12}. In the previous work, this correlation was reported for a chosen value of the angle θ_{12} at the low scale in the context of type 1 seesaw. In this work, we do not choose any particular value of θ_{12} at the low scale. We obtain a band for this correlation and previous results are a specific case of our present results. We observe that θ_{23} is non maximal and always lies in the second octant. This confirms the predictions of our earlier work [15]. The allowed range of θ_{13} is $7.63^\circ - 8.34^\circ$ and that of θ_{23} is $49^\circ - 52.3^\circ$.

We next present variation of θ_{12} against M_{ee} in Fig. 6.3. This correlation is also a new prediction of our work and do not exist in previous studies. The whole 3σ global range for the angle θ_{12} is allowed for the $M_{ee} \leq 0.4$ eV, However, as can be observed from Fig. 6.3, the range $34.4^\circ \leq \theta_{12} \leq 36.81^\circ$ is ruled out for 0.384 eV $\leq M_{ee} \leq$ 0.393 eV. The precise predictions for all observables are provided in Table 6.2. In the end, we also have a new correlation between the sum of neutrino masses and M_{ee} which is not studied previously. This correlation

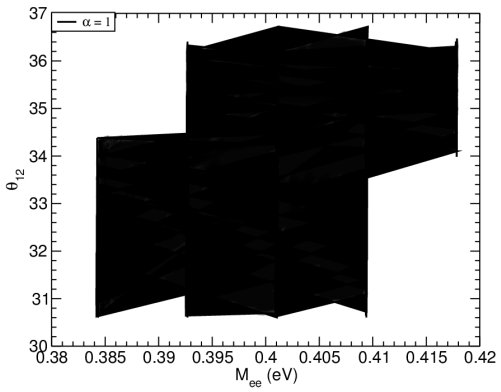

Figure 5.7: The variation of θ_{12} with respect to M_{ee}, in the context of the HSMU hypothesis, with α =1.

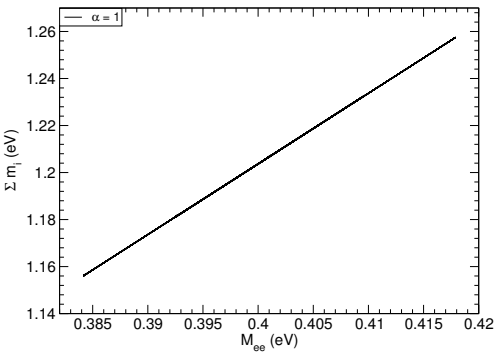

Figure 5.8: The variation of Σm_i with respect to M_{ee}, in the context of the HSMU hypothesis, with α =1.

is shown in Fig. 6.4. Our prediction for sum of neutrino masses is $1.16 - 1.2$ eV using the upper bound on M_{ee} given by the GERDA.

The most general HSMR within the same generations

The most general HSMR within the same generations for $(k_1, k_2, k_3) = (1, 1, 1)$ as defined before is given by the following equation

$$\theta_{12} = \alpha_1 \ \theta_{12}^q, \quad \theta_{13} = \alpha_2 \ \theta_{13}^q, \quad \theta_{23} = \alpha_3 \ \ \theta_{23}^q. \tag{5.45}$$

We present the results for the maximum and the minimum values of α_i for Eqs. (5.5-5.12), taking into account all the experimental constriants. In the Table 5.2, we present the allowed values of α_i along with the the respective physical masses and the mixing angles.

It is remarkable that in the Case E, all the mixing parameters are within 3σ global range without adding threshold corrections. If we add threshold corrections, the predictions are $\Delta m^2_{32} = 2.35 \times (10^{-3}\text{eV}^2)$ and $\Delta m^2_{21} = 7.01 \times (10^{-5}\text{eV}^2)$ for $R = 1.0$. Thus, threshold corrections at this point are effectively negligible. We further notice that the different combinations of the allowed end points of α_i, leads to M_{ee} around 0.35 eV - 0.4 eV. This most general case with different α_i, alone will not suffice, when the value of M_{ee} will be further constrained by the future experiments. We then have to look for more specific cases, where the

	α_1	α_2	α_3	Masses at unification scale (eV)			Σm_i (eV)	θ_{12}°	θ_{13}°	θ_{23}°	Δm_{32}^2 (10^{-3}eV^2)	Δm_{21}^2 (10^{-5}eV^2)	M_{ee} (eV)	m_1 (eV)	R
				m_1	m_2	m_3									
Case A	1.46	2.54	1.19	0.458	0.461	0.519	1.16	36.52	9.88	41.14	2.5	8.06	0.385	0.385	2.29
Case B	1.45	1.68	0.91	0.4757	0.478	0.538	1.20	30.61	8.79	37.97	2.25	8.12	0.40	0.399	1.8
Case C	1.38	0.71	1.28	0.489	0.493	0.5527	1.24	36.8	9.87	50.83	2.22	8.14	0.411	0.411	5.3
Case D	1.14	0.92	0.94	0.475	0.478	0.537	1.20	31.18	7.70	45.31	2.20	8.14	0.40	0.399	1.69
Case E	0.8	2.2	1.15	0.41	0.412	0.462	1.04	32.77	7.65	48.13	2.35	7.01	0.344	0.344	-
Case F	0.89	1.61	0.82	0.475	0.477	0.5361	1.20	30.6	7.65	43.66	2.22	7.37	0.40	0.399	1.06
Case G	0.92	0.98	1.03	0.442	0.445	0.499	1.12	32.37	7.64	52.19	2.22	7.86	0.372	0.371	1.48
Case H	0.88	0.95	0.86	0.476	0.479	0.537	1.20	30.99	7.63	51.97	2.22	7.55	0.40	0.4	1.29

Table 5.2: The allowed predictions for the different cases of the most general HSMR for minimum and maximum allowed values of α_i, Eqs. (5.5-5.11).

α_i's will not be different, but have some relations among them. We consider the simplified scenario, where the α_i's are equal. We have carried out a detailed analysis for all the possible seven cases in this scenario in the next subsections.

Case 1: $\theta_{12} = \alpha\ \theta_{12}^q, \quad \theta_{13} = \theta_{13}^q, \quad \theta_{23} = \theta_{23}^q$

The first case of HSMR is the one where leptonic mixing angle θ_{12} is proportional to θ_{12}^q and the other two angles are identical. In Fig. 6.5, we show how the correlation between Δm_{32}^2 and M_{ee} changes as α deviates from unity. We observe on the left panel of Fig. 6.5 that the lowest allowed value of α is 0.902. This value is derived by the 3σ global limit of the leptonic mixing angles. On the right panel of Fig. 6.5, the upper bound on α is shown. For the upper bound on α, in principle, one can go up to 1.962 with all mixing parameters within the global range. This value of α belongs to $M_{ee} > 0.4$ eV and hence is ruled out by the GERDA limit. The allowed upper bound on α is 1.28 which is derived using the GERDA limit.

We compare Fig. 6.5 with Fig. 6.1 of the HSMU hypothesis ($\alpha = 1$) to study the phenomenological behavior of α. As obvious from the left panel of Fig. 6.5 , M_{ee} has its maximum allowed range at the lowest value of α. This is because the absolute neutrino mass decreases for $\alpha < 1$ and increases for $\alpha > 1$ in the case under study. Hence, at $\alpha = 0.902$ on the left panel of Fig. 6.5, we obtain 0.365 eV $\leq$

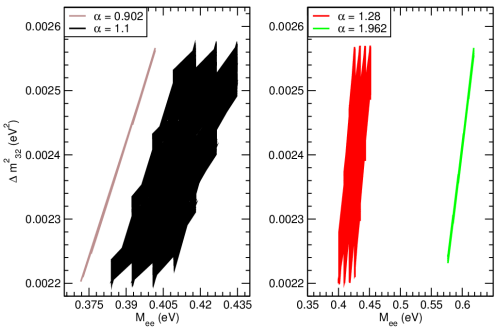

Figure 5.9: The variation of Δm^2_{32} with respect to M_{ee} for Case 1 of HSMR.

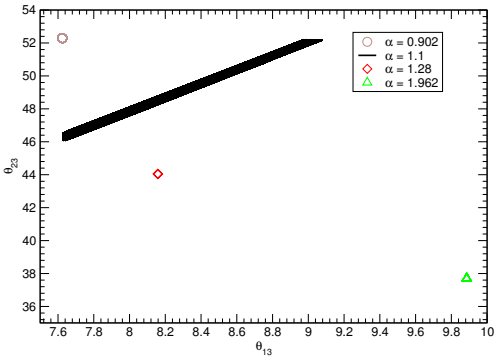

Figure 5.10: The variation of θ_{23} with respect to θ_{13} for Case 1 of HSMR.

$M_{ee} \leq 0.40$ eV corresponding to whole 3σ global range of Δm^2_{32}. The same prediction for the HSMU hypothesis in Fig. 6.1, ($\alpha = 1$) is 0.385 eV $\leq M_{ee} \leq 0.418$ eV which belongs to $\Delta m^2_{32} = (2.21 - 2.45) \times 10^{-3}$ eV^2. The prediction when α slightly deviates from unity ($\alpha = 1.1$) is 0.384 eV $\leq M_{ee} \leq 0.435$ eV corresponding to $\Delta m^2_{32} = (2.22 - 2.57) \times 10^{-3}$ eV^2. At the upper allowed value of $\alpha = 1.28$, we have 0.4 eV $\leq M_{ee} \leq 0.45$ eV which belongs to $\Delta m^2_{32} = (2.20 - 2.57) \times 10^{-3}$ eV^2. We observe that the uppermost value of $\alpha = 1.962$ has 0.571 eV $\leq M_{ee} \leq 0.625$ eV belonging to $\Delta m^2_{32} = (2.23 - 2.57) \times 10^{-3}$ eV^2. This value of α is already ruled out by the GERDA limit.

This case can be ruled out if GERDA reaches $M_{ee} < 0.365$ eV. There is an apparent overlap between predictions of the case under study and the HSMU hypothesis. This can be discriminated using the SUSY ratio R. For a clear picture of the phenomenological consequences, we provide values of mixing parameters and other observables belonging to minimum and maximum allowed values of α for each case and the HSMU hypothesis in Table 6.2.

The variation of θ_{23} with respect to θ_{13} is shown in Fig. 5.10. The mixing angles reach their 3σ limits at their lower and upper ends. For example, at $\alpha = 0.902$, θ_{13} is at its minimum of the 3σ global limit while θ_{23} is at its maximum independent of the upper bound of M_{ee}. On the other hand, at $\alpha = 1.962$, the predictions are reversed but this value is already rejected by the GERDA limit of M_{ee}. The allowed ranges of θ_{13} and θ_{23}, at $\alpha = 1.1$, are $7.62^\circ - 9.1^\circ$ and $46.09^\circ - 52.2^\circ$ respectively. Compared to Fig. 6.2 for the HSMU hypothesis where the allowed range of θ_{23} is always in the second octant, θ_{23} has its minimum value

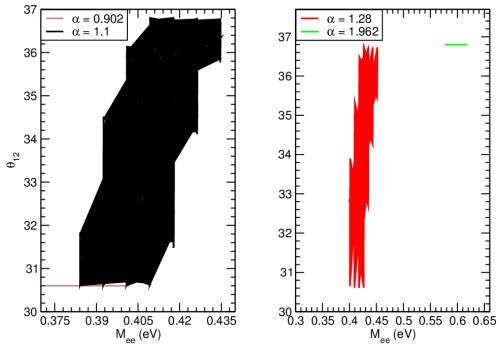

Figure 5.11: The variation of θ_{12} with respect to M_{ee} for Case 1 of HSMR.

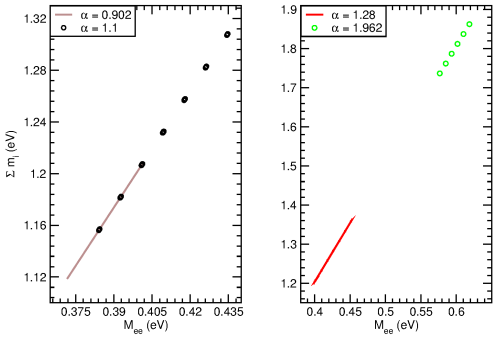

Figure 5.12: The variation of Σm_i with respect to M_{ee} for Case 1 of HSMR.

$44.04°$ at $\alpha = 1.28$ which belongs to $M_{ee} = 0.4$ eV and lies in the first octant. The corresponding value of θ_{13} is $8.16°$.

We next show the behavior of θ_{12} with respect to M_{ee} in Fig. 5.11. We observe that at $\alpha = 0.902$, θ_{12} is at its global minimum $30.6°$. On the left panel of Fig. 5.11, at $\alpha = 1.1$, θ_{12} has an allowed range of $30.6° - 35.65°$ for $M_{ee} \leq 0.4$ eV. For the HSMU hypothesis in Fig. 6.3, θ_{12} has the whole 3σ global range with some higher values ruled out for $M_{ee} \leq 0.393$ eV. For $\alpha = 1.28$, the value of θ_{12} is $32.82°$ for $M_{ee} = 0.4$ eV as can be seen from the right panel of the figure. For $\alpha = 1.962$, θ_{12} reaches to the maximum of its 3σ global limit.

Finally in Fig. 5.12, the variation of sum of the neutrino masses with respect to M_{ee} is presented. For lowest value of $\alpha = 0.902$, on the left panel, the range of Σm_i is $1.12 - 1.2$ eV for $M_{ee} \leq 0.4$ eV. At $\alpha = 1.1$, it is $1.16 - 1.2$ eV for $M_{ee} \leq 0.4$ eV. On the right panel, the value of sum at $\alpha = 1.28$ is 1.2 eV and the region $\Sigma m_i > 1.2$ eV belongs to $M_{ee} > 0.4$ eV.

Case 2: $\theta_{12} = \theta_{12}^q, \quad \theta_{13} = \alpha\ \theta_{13}^q, \quad \theta_{23} = \theta_{23}^q$

The second case which we consider has leptonic mixing angle θ_{13} proportional to θ_{13}^q. In this case, the lower bound on α is 0.45 which is derived using global limits on the mixing angles. The α on the upper side, however, is remarkably bounded by the ratio R. This theoretical bound arises because we work with an inverted hierarchy in the charged-slepton sector and at $\alpha = 2.5$, we have $R = 1$.

In principle, α has a range up to 3.5 satisfying all experimental constraints with $R < 1$.

In Fig. 5.13, we show the behavior of Δm^2_{32} versus M_{ee} for different values of α. For the $\alpha = 0.45$ on the right panel, we have 0.382 eV $\leq M_{ee} \leq$ 0.418 eV which corresponds to the whole 3σ global range of Δm^2_{32}. In case of $\alpha = 1.1$ on the left panel, 0.38 eV $\leq M_{ee} \leq$ 0.428 eV belongs to $\Delta m^2_{32} = (2.2 - 2.57) \times 10^{-3}$ eV^2. The range of M_{ee} at the upper end $\alpha = 2.5$ is 0.342 eV $\leq M_{ee} \leq$ 0.378 eV corresponding to $\Delta m^2_{32} = (2.2 - 2.53) \times 10^{-3}$ eV^2. A remarkable feature emerges in this case. Unlike case 1, the absolute neutrino mass scale increases for $\alpha < 1$ and decreases for $\alpha > 1$. Now, at the upper allowed value of $\alpha = 2.5$, M_{ee} is sufficiently below the GERDA limit. We would emphasize that one of the main observations of this case is that α is not constrained by the GERDA limit on either side. These results can easily be tested by GERDA in the near future.

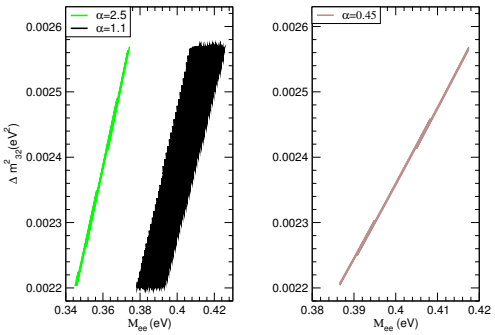

Figure 5.13: The variation of Δm^2_{32} with respect to M_{ee} for Case 2 of HSMR.

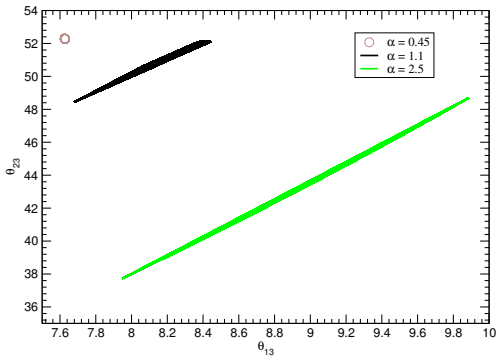

Figure 5.14: The variation of θ_{23} with respect to θ_{13} for Case 2 of HSMR.

We show the variation of θ_{23} with respect to θ_{13} in Fig. 5.14. As can be seen, for the lowest possible value of $\alpha = 0.45$, the allowed range is just a point which is located at $\theta_{13} = 7.65^\circ$ and $\theta_{23} = 52.5^\circ$. As $\alpha = 1.1$, the range of θ_{13} is $7.65^\circ - 8.4^\circ$ and that of θ_{23} is $48.5^\circ - 52.5^\circ$. Finally for the highest value of $\alpha = 2.5$, θ_{13} has almost the whole 3σ range $7.92^\circ - 9.88^\circ$ and the range of θ_{23} is $36.8^\circ - 48^\circ$. These results can be contrasted to case 1 where the minimum of the mixing angle $\theta_{23} = 44.04^\circ$ also happens for the upper value of α namely $\alpha = 1.28$ and in both cases, the value of θ_{23} can be in the first octant, contrary to the HSMU hypothesis. Also in both cases, the maximum of the mixing angle of θ_{23} corresponds to the lower value of alpha.

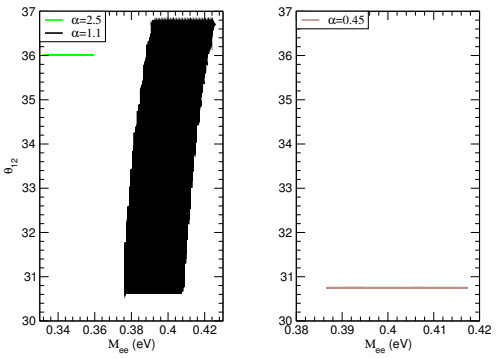

Figure 5.15: The variation of θ_{12} with respect to M_{ee} for Case 2 of HSMR.

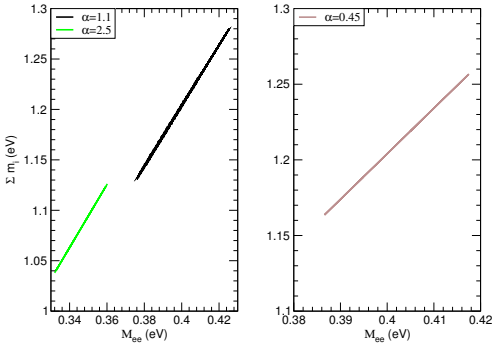

Figure 5.16: The variation of Σm_i with respect to M_{ee} for Case 2 of HSMR.

The next to be considered is the variation of θ_{12} versus M_{ee} as is shown in Fig. 5.15. In the right panel it can be observed that $\alpha = 0.45$ corresponds to the minimum $\theta_{12} = 30.8^\circ$ and 0.384 eV $\leq M_{ee} \leq$ 0.42 eV. For $\alpha = 1.1$ on the left panel, the whole 3σ range for θ_{12} is allowed for 0.39 eV $\leq M_{ee} \leq$ 0.4 eV and for $M_{ee} \leq$ 0.39 eV the allowed range of θ_{12} decreases. The upper value of $\alpha = 2.5$, on the left panel, corresponds $\theta_{12} = 36.02^\circ$ while 0.344 eV $\leq M_{ee} \leq$ 0.366 eV.

In Fig. 5.16, we show the behavior of the sum of the neutrino masses with respect to M_{ee}. As can be seen in the right panel, for the lowest value of $\alpha = 0.45$, Σm_i lies in the range $1.16-1.2$ eV which corresponds to 0.383 eV $\leq M_{ee} \leq$ 0.4 eV. For $M_{ee} > 0.4$, the range of Σm_i is $1.2 - 1.26$ eV. For the upper value of $\alpha = 2.5$, we have $\Sigma m_i = 1.05-1.12$ eV while 0.342 eV $\leq M_{ee} \leq$ 0.366 eV. On the left panel, for $\alpha = 1.1$, the range of Σm_i is $1.13 - 1.2$ eV which corresponds to 0.36 eV $\leq M_{ee} \leq$ 0.4 eV and the rest of the data point corresponds to $M_{ee} >$ 0.4 eV.

Case 3: $\theta_{12} = \theta_{12}^q, \quad \theta_{13} = \theta_{13}^q, \quad \theta_{23} = \alpha\ \theta_{23}^q$

We now consider the final case where two of the leptonic mixing angles θ_{12}, θ_{13} are identical to the quark mixing angle θ_{12}^q, θ_{13}^q and the third leptonic mixing angle θ_{23} is proportional to the quark mixing angle θ_{23}^q. The correlation between Δm_{32}^2 and M_{ee} is shown in Fig. 5.17. The minimum allowed value of α, with all the mixing parameters within the global range, is 0.324. However in this case as can be seen from the right panel of Fig. 5.17, we have 0.62 eV $\leq M_{ee} \leq$ 0.66 eV. This value of α corresponds to the entire 3σ range of Δm_{32}^2 and violates the upper

limit from GERDA. Therefore we also consider the lower value of $\alpha = 0.89$, with all the mixing parameters within the global range and 0.4 eV $\leq M_{ee} \leq$ 0.43 eV. This value corresponds to the entire 3σ range of Δm^2_{32}. The prediction of M_{ee} at $\alpha = 1.1$ is 0.372 eV $\leq M_{ee} \leq$ 0.41 eV corresponding to the entire 3σ range of Δm^2_{32}. The upper allowed value of α in this case is 1.52, (left panel of Fig. 5.17) with 0.3 eV $\leq M_{ee} \leq$ 0.34 eV and having the entire 3σ range of Δm^2_{32}. Hence, the allowed range of α in this case covers the entire 3σ range of Δm^2_{32}. The absolute neutrino mass scale increases for $\alpha < 1$ and decreases for $\alpha > 1$ similar to Case 2. The behavior of α in this case, Fig. 5.17 is different from Case 1, Fig. 6.5, with the lower end of α constraining M_{ee}. In this case it is possible to reach values of M_{ee} as low as 0.3 eV compared to Cases 1, 2 and the HSMU hypothesis, and will only be ruled out if the limit from GERDA reaches $M_{ee} < 0.3$ eV.

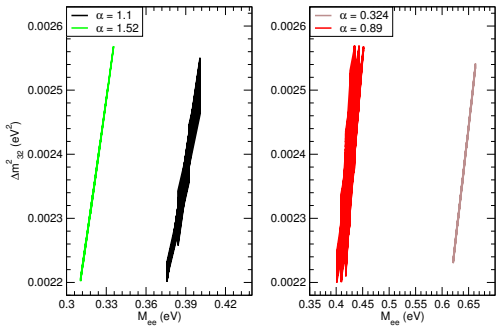

Figure 5.17: The variation of Δm^2_{32} with respect to M_{ee} for Case 3 of HSMR.

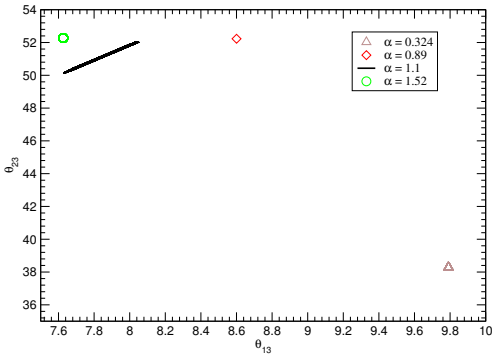

Figure 5.18: The variation of θ_{23} with respect to θ_{13} for Case 3 of HSMR.

We next show the correlation of θ_{23} with respect of θ_{13} in Fig. 5.18. The θ_{23} and θ_{13} reach their 3σ global limits at the lowest and upper most end of α. The value of θ_{13} is 8.56° and that of θ_{23} is 52.4° for lower allowed value of $\alpha = 0.89$, corresponding to $M_{ee} = 0.4$ eV. The allowed ranges of θ_{13} and θ_{23} for $\alpha = 1.1$ in this case are much more constrained compared to Cases 1, 2 and the HSMU hypothesis. They are $7.62° - 8.05°$ and $50.1° - 52.1°$ respectively. The upper end of $\alpha = 1.52$, results in a minimum value of θ_{13}, whereas θ_{23} is at maximum with $\theta_{23} = 52.4°$. The behavior of α here is different from Cases 1 and 2 with the lower end of α resulting in the upper end point of θ_{13} and lower end point of θ_{23}.

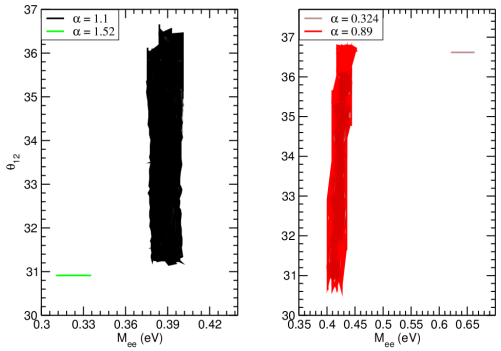

Figure 5.19: The variation of θ_{12} with respect to M_{ee} for Case 3 of HSMR.

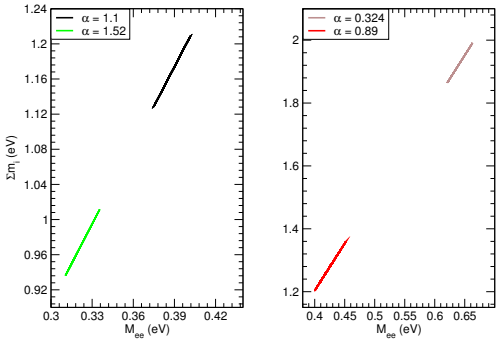

Figure 5.20: The variation of Σm_i with respect to M_{ee} for Case 3 of HSMR.

In Fig. 5.19, we show the variation of θ_{12} with M_{ee}. We observe that the lower (30.78°) and upper (36.7°) 3σ global limits of θ_{12}, are reached at the upper most and the lowest ends of α respectively. In case of $\alpha = 0.89$, the value of θ_{12} is 30.62° which belongs to $M_{ee} = 0.4$. The whole 3σ global range of θ_{12} is allowed for $\alpha = 1.1$.

Finally we show in Fig. 5.20, the variation of the sum of the neutrino masses with respect to M_{ee}. The region with $M_{ee} \geq 0.4$ eV for $\alpha = 0.324$, has Σm_i in the range of $1.84 - 2$ eV and for $\alpha = 0.89$ it is in the range $1.2 - 1.38$ eV. In case of $\alpha = 1.1$, with $M_{ee} < 0.4$ eV, Σm_i is in the range $1.12 - 1.2$ eV. The upper end of $\alpha = 1.52$ has the sum in the range of $0.93 - 1.01$ eV. It is seen that Σm_i and M_{ee} is much more relaxed compared to the HSMU and Cases 1, 2.

Case 4: $\theta_{12} = \alpha\ \theta^q_{12}, \quad \theta_{13} = \alpha\ \theta^q_{13}, \quad \theta_{23} = \theta^q_{23}$

We now consider the case where the leptonic mixing angles θ_{12}, θ_{13} are proportional to the corresponding quark mixing angles $\theta^q_{12}, \theta^q_{13}$ and the leptonic mixing angle θ_{23} is identical to the quark mixing angle θ^q_{23}. The lowest allowed value of α for Case 4 is 0.92 which is derived using the 3σ global limits on mixing angles. The upper allowed value of α, respecting the GERDA limit, is 1.67. When we relax the GERDA limit then α turns out to be 1.77 satisfying the 3σ global limits. We show, the correlation between Δm^2_{32} and M_{ee} in Fig. 5.21. The lowest value of $\alpha = 0.92$, covers the range 0.38 eV $\leq M_{ee} \leq 0.4$ eV which corresponds to $\Delta m^2_{32} = (2.30 - 2.50) \times 10^{-3}$ eV^2 (cf. left panel of Fig. 5.21). The prediction

of M_{ee} for $\alpha = 1.1$ is 0.384 eV $\leq M_{ee} \leq$ 0.41 eV corresponding to the whole 3σ global range of Δm^2_{32}. On the right panel, the upper allowed end of $\alpha = 1.67$ has 0.4 eV $\leq M_{ee} \leq$ 0.42 eV with $\Delta m^2_{32} = (2.30 - 2.49) \times 10^{-3}$ eV^2. The upper most end $\alpha = 1.77$ where the GERDA limit is not satisfied, has 0.46 eV $\leq M_{ee} \leq$ 0.48 eV corresponding to $\Delta m^2_{32} = (2.37 - 2.53) \times 10^{-3}$ eV^2, as shown in the right panel of Fig. 5.21. The behavior of α is similar to Case 1 with the upper values of α being constrained by the GERDA limit. The first distinction that this case offers, with the others considered before is that the whole 3σ range of Δm^2_{32} is not covered in Case 4 for all the allowed values of α.

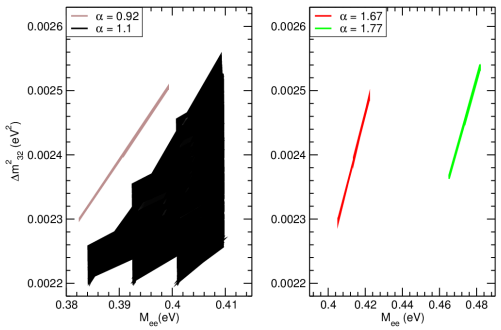

Figure 5.21: The variation of Δm^2_{32} with respect to M_{ee} for Case 4 of HSMR.

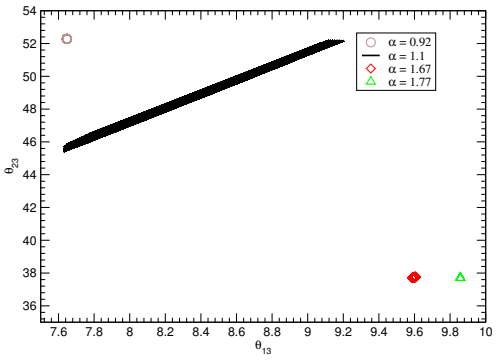

Figure 5.22: The variation of θ_{23} with respect to θ_{13} for Case 4 of HSMR.

Next, we show the correlation between θ_{23} and θ_{13} as illustrated in Fig. 5.22. The lower end of $\alpha = 0.92$ reaches to the minimum of its 3σ global limit for θ_{13} and the maximum of the 3σ limit for θ_{23}. The situation for the upper most end of $\alpha = 1.77$, is just opposite to the lower end, i.e. θ_{13} is at the maximum of the 3σ global limit whereas θ_{23} is at its global minimum. This observation is just opposite to Case 3, where θ_{13} (θ_{23}) reaches the global minimum (maximum), at the upper end of α. The allowed ranges of θ_{13} and θ_{23}, at $\alpha = 1.1$ for this case are $7.62^\circ - 9.2^\circ$ and $45.41^\circ - 52.17^\circ$, respectively. The value of θ_{13} is 9.59° and that of θ_{23} is $37.71^\circ - 37.76^\circ$, for $\alpha = 1.67$.

The variation of θ_{12} with respect to M_{ee} is shown in Fig. 5.23. The lower and upper 3σ global limits of θ_{12} are obtained at the lower and upper most end of α respectively. This observation is in contrast with Case 3 and Case 5 (to be discussed later). We get the full range of θ_{12} (cf. Fig. 5.23 for details) for $\alpha = 1.1$,

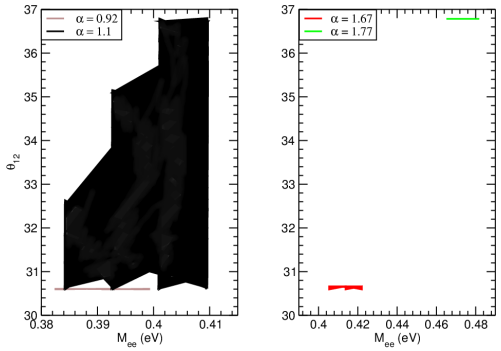

Figure 5.23: The variation of θ_{12} with respect to M_{ee} for Case 4 of HSMR.

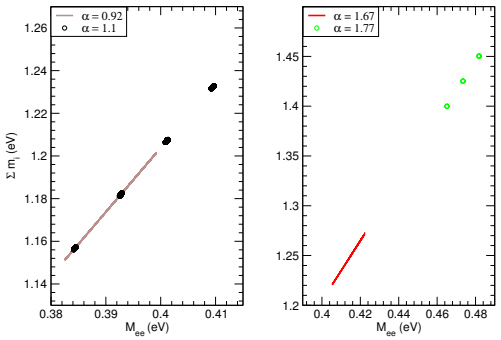

Figure 5.24: The variation of Σm_i with respect to M_{ee} for Case 4 of HSMR.

with some higher values of θ_{12} being ruled out for $M_{ee} \leq 0.394$ eV. The value of θ_{12} at $\alpha = 1.67$ is $30.59° - 30.66°$.

Finally, we show the variation of the sum of neutrino masses with respect to M_{ee} in Fig. 5.24. We find that for the lowest value of $\alpha = 0.92$, the sum of neutrino mass ranges between $1.15-1.20$ eV for 0.38 eV $\leq M_{ee} \leq 0.4$ eV. In case of $\alpha = 1.1$, Σm_i has a range of $1.157 - 1.23$ eV corresponding to 0.38 eV $\leq M_{ee} \leq 0.41$ eV as can be seen from the left panel of Fig. 5.24. A close look at the right panel of Fig. 5.24 reveals that for $\alpha = 1.67$, Σm_i is in the range $1.22 - 1.27$ eV corresponding to 0.4 eV $\leq M_{ee} \leq 0.42$ eV. The range for Σm_i turns out to be $1.4 - 1.45$ eV for $\alpha = 1.77$ which corresponds to $M_{ee} > 0.4$ eV.

Case 5: $\theta_{12} = \theta_{12}^q, \quad \theta_{13} = \alpha\ \theta_{13}^q, \quad \theta_{23} = \alpha\ \theta_{23}^q$

We now look at the case of the leptonic mixing angle θ_{12} being identical with its CKM counterpart and the other two leptonic mixing angles being proportional to the quark mixing angles. The correlation between Δm^2_{32} and M_{ee} is shown in Fig. 5.25 as α deviates from unity. The minimum allowed value of α, with all the mixing parameters within the global range, is 0.06. However in this case as can be seen from the right panel of Fig. 5.25, we have 2.24 eV $\leq M_{ee} \leq 2.28$ eV, which violates the upper limit from GERDA. Therefore including the constraints of GERDA, the lowest possible value of α becomes 0.89. For $\alpha = 0.89$, as can be seen from the right panel of Fig. 5.25, we obtain 0.40 eV $\leq M_{ee} \leq 0.42$ eV corresponding to $\Delta m^2_{32} = (2.20 - 2.48) \times 10^{-3}$ eV^2. The prediction of M_{ee} for

α=1.1 from the left panel of Fig. 5.25 is 0.36 eV $\leq M_{ee} \leq$ 0.41 eV which belongs to the whole 3σ range of Δm^2_{32}. The upper allowed value of α in this case is 3.18, (left panel of Fig. 5.25) with 0.214 eV $\leq M_{ee} \leq$ 0.223 eV corresponding to $\Delta m^2_{32} = (2.28 - 2.46) \times 10^{-3}$ eV^2. The absolute neutrino mass scale increases for $\alpha < 1$ and decreases for $\alpha > 1$ similar to Cases 2 and 3. The behavior of α in this case is similar to Cases 2 and 3, with the lower end of α being constrained by the GERDA limit. It can also be seen from Fig. 5.25, that as we move towards the upper and lower ends of α, the whole 3σ range of Δm^2_{32} is not covered.

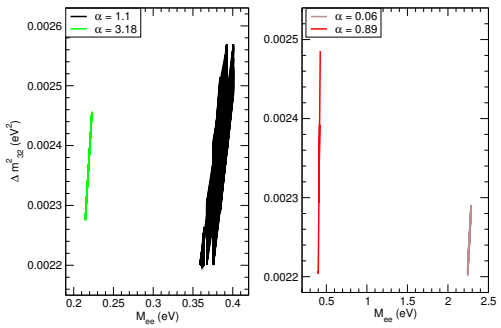

Figure 5.25: The variation of Δm^2_{32} with respect to M_{ee} for Case 5 of HSMR.

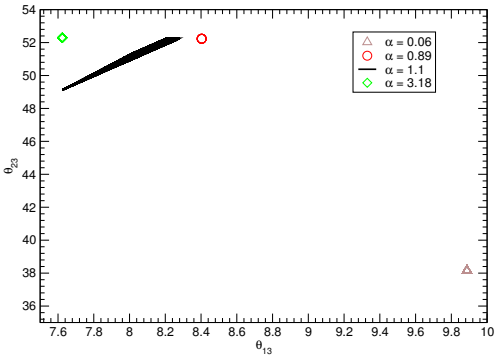

Figure 5.26: The variation of θ_{23} with respect to θ_{13} for Case 5 of HSMR.

We next show the correlation of θ_{23} with respect of θ_{13} in Fig. 5.26. The 3σ global end point limits of θ_{23} and θ_{13}, are reached at the lowest and upper ends of α. The values of θ_{13} and θ_{23} for lowest value of $\alpha = 0.89$ are 8.40° and 52.23° respectively. These values belong to $M_{ee} = 0.4$ eV. The allowed ranges of θ_{13} and θ_{23}, at $\alpha = 1.1$ for this case are $7.62° - 8.31°$ and $49.0° - 52.3°$ respectively. The upper end of $\alpha = 3.18$, results in a global minimum value of θ_{13} and a global maximal value of θ_{23}, similar to Case 3. The lower end of α results in a global maximum value of θ_{13} and a global minimum value of θ_{23}.

We next show the variation of θ_{12} with M_{ee} in Fig. 5.27. The lower (30.62°) and the upper (36.81°) 3σ global limits of θ_{12}, correspond to the upper and the lowest ends of α. However, for case of $\alpha = 1.1$, the whole 3σ range of θ_{12} ($30.62° - 36.81°$) is covered.

Finally we show in Fig. 5.28, the variation of the sum of the neutrino masses with respect to M_{ee}. The region with $M_{ee} \geq 0.4$ eV, for $\alpha = 0.06$, has Σm_i in the range of $6.73 - 6.85$ eV and for $\alpha = 0.89$ it is in the range $1.20 - 1.28$ eV.

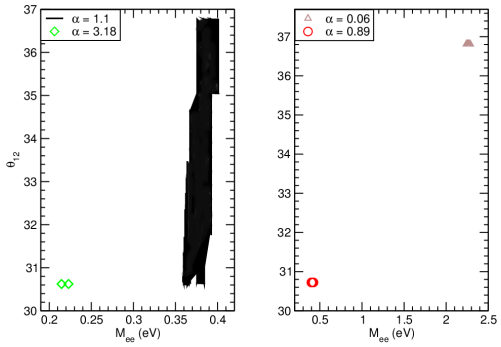

Figure 5.27: The variation of θ_{12} with respect to M_{ee} for Case 5 of HSMR.

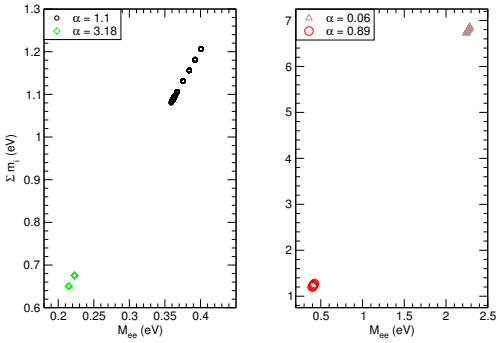

Figure 5.28: The variation of Σm_i with respect to M_{ee} for Case 5 of HSMR.

For $\alpha = 1.1$, with $M_{ee} < 0.4$ eV, Σm_i is in the range $1.07 - 1.22$ eV. The upper end of $\alpha = 3.18$ has the sum in the range of $0.65 - 0.67$ eV which is remarkably lower than the previous cases. We note that the Σm_i is below the cosmological upper bound [68]. The further discussion on the cosmological constraints on our work will be provided in the last section of this paper. It is observed that Case 5 behaves almost similarly to Case 3, and is the most relaxed one in terms of M_{ee}. We can go to values of M_{ee} as low as 0.21 eV, consistent with the upper end of α. Hence, this case is partially beyond the reach of GERDA sensitivity which is maximum 0.3 eV. However, this is well within the reach of KATERIN experiment [65].

Case 6: $\theta_{12} = \alpha\ \theta_{12}^q, \quad \theta_{13} = \theta_{13}^q, \quad \theta_{23} = \alpha\ \theta_{23}^q$

We next consider the case where the leptonic mixing angle θ_{13} is identical with its CKM counterpart and the other two leptonic mixing angles are proportional to the quark mixing angles. The correlation between Δm^2_{32} and M_{ee} is shown in Fig. 5.29. The minimum allowed value of α, with all the mixing parameters within the global range, is 0.86. It can be seen from the left panel of Fig. 5.29, for this value of α, M_{ee} has a range 0.397 eV $\leq$ M_{ee} $\leq$ 0.42 eV corresponding to $\Delta m^2_{32} = (2.20 - 2.48) \times 10^{-3}$ eV^2. In case of $\alpha = 1.1$, we have 0.36 eV $\leq$ $M_{ee} \leq 0.424$ eV which corresponds to the whole 3σ range of Δm^2_{32}. At the upper allowed value of $\alpha = 2.11$ as seen from the right panel of Fig. 5.29, we have 0.41 eV $\leq M_{ee} \leq$ 0.45 eV with the whole 3σ range of Δm^2_{32} covered. We have

0.64 eV $\leq M_{ee} \leq$ 0.67 eV corresponding to $\Delta m^2_{32} = (2.22 - 2.54) \times 10^{-3}$ eV^2 for the uppermost value of $\alpha = 2.19$. This end is already rejected by the GERDA limit. In this case, it is worth mentioning that the absolute neutrino mass scale increases for both $\alpha < 1$ and $\alpha > 1$.

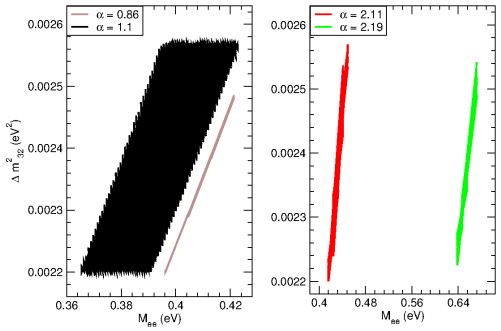

Figure 5.29: The variation of Δm^2_{32} with respect to M_{ee} for Case 6 of HSMR.

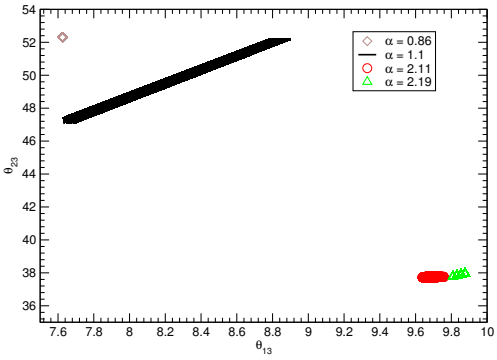

Figure 5.30: The variation of θ_{23} with respect to θ_{13} for Case 6 of HSMR.

The behavior of α in this case Fig. 5.29 is different from Case 5, Fig. 5.25. Unlike Case 5 considered before, in this case for both lower and upper end values of α we get M_{ee} close to its upper limit. This is because unlike the previous cases, in this case the limit on lower value of α comes not from M_{ee} but from the neutrino oscillation parameters. Also, although the upper limit of $\alpha = 2.11$ is constrained by M_{ee} but this value is quite close to the upper limit of 2.19 obtained without the M_{ee} constraint.

In Fig. 5.30, we show the correlation of θ_{23} with respect of θ_{13}. The 3σ global end point limits of θ_{23} and θ_{13}, are reached at the lowest and uppermost end of α. The allowed ranges of θ_{13} and θ_{23}, at $\alpha = 1.1$ for this case are $7.62° - 8.90°$ and $47.0° - 52.3°$ respectively. At $\alpha = 2.11$, the value of θ_{13} is $9.4° - 9.76°$ and that of θ_{23} is $38.7° - 38.8°$.

We next show the variation of θ_{12} with M_{ee} in Fig. 5.31. The lower ($30.60°$) and upper ($36.81°$) 3σ global limits of θ_{12}, is reached at the lowest and the uppermost end of α. This behavior is quite the opposite of the behavior shown in Fig. 5.27 for Case 5. In case of $\alpha = 1.1$, the whole 3σ range of θ_{12} ($30.60° - 36.81°$) is covered. The value of θ_{12} at $\alpha = 2.11$ is $34.57° - 35.02°$.

Finally we show in Fig. 5.32, the variation of the sum of the neutrino masses with respect to M_{ee}. In case of $\alpha = 0.86$ the sum of neutrino masses Σm_i is in

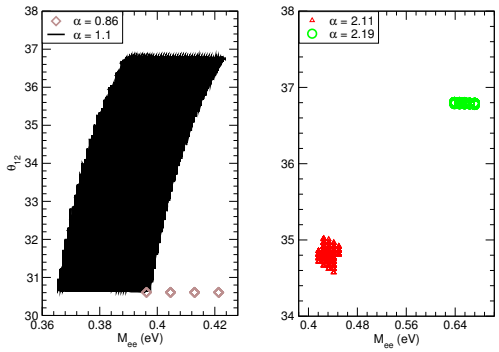

Figure 5.31: The variation of θ_{12} with respect to M_{ee} for Case 6 of HSMR.

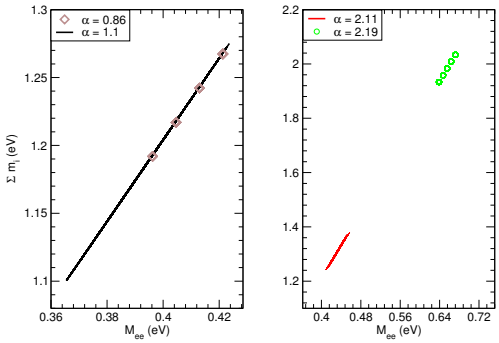

Figure 5.32: The variation of Σm_i with respect to M_{ee} for Case 6 of HSMR.

the range of $1.19 - 1.27$ eV. Next for $\alpha = 1.1$, Σm_i has a range of $1.1 - 1.27$ eV for $M_{ee} \leq 0.4$ eV and when $\alpha = 2.11$ it is in the range $1.26 - 1.36$ eV for 0.4 eV $\leq M_{ee} \leq 0.48$ eV.

Case 7: $\theta_{12} = \alpha\ \theta_{12}^q, \quad \theta_{13} = \alpha\ \theta_{13}^q, \quad \theta_{23} = \alpha\ \theta_{23}^q$

We finally consider the case where all the leptonic mixing angles are proportional to the quark mixing angle by the same proportionality constant (α). We find that the upper bound on α, is constrained by the mass limit (M_{ee}) from GERDA, whereas the lower limit on α is constrained by the 3σ global limit of the leptonic mixing angles. The lowest value of α is 0.89 and the highest value of α relaxing the GERDA limit is 2.09, whereas by taking into account the M_{ee} limit, the highest value is 2.

We next discuss the behavior of the neutrino mass and mixing parameters in Case 7, with the variation of α in the allowed range. Firstly like all the previous cases, the variation of Δm^2_{32} with M_{ee} is shown in Fig. 5.33. As seen from the left panel of Fig. 5.33, for the lowest value of $\alpha = 0.895$, we have 0.391 eV $\leq M_{ee} \leq 0.425$ eV which corresponds to the whole 3σ global range of Δm^2_{32}. At $\alpha = 1.1$, the range of M_{ee} is 0.362 eV $\leq M_{ee} \leq 0.405$ eV which again corresponds to the whole 3σ global range of Δm^2_{32}. The range of M_{ee} at $\alpha = 2$ is 0.4 eV $\leq M_{ee} \leq 0.42$ eV which corresponds to the whole 3σ global range of Δm^2_{32}. The uppermost end of $\alpha = 2.09$ has 0.42 eV $\leq M_{ee} \leq 0.452$ eV which corresponds to the whole 3σ global range of Δm^2_{32} and is rejected by the GERDA

limit. Hence, the entire allowed range of α covers the whole 3σ range of m^2_{32}. The absolute neutrino mass scale increases for both $\alpha < 1$ and $\alpha > 1$ similar to Case 6. The behavior of α resembles to Case 6 with the upper and lower ends of α having values close to M_{ee}.

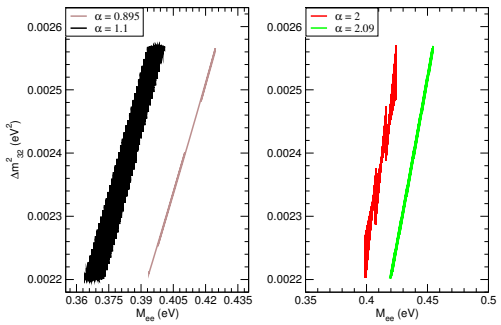

Figure 5.33: The variation of Δm^2_{32} with respect to M_{ee} for Case 7 of HSMR.

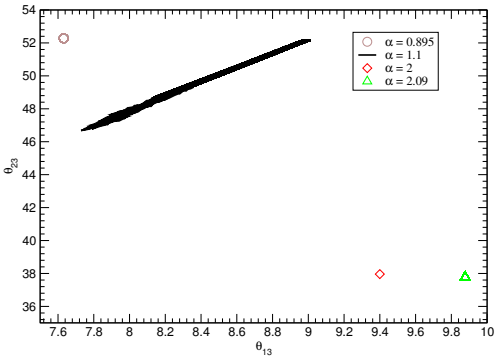

Figure 5.34: The variation of θ_{23} with respect to θ_{13} for Case 7 of HSMR.

We show the range of θ_{23} and θ_{13} covered by the different allowed values of α in Fig. 5.34. The 3σ global limits on the mixing angles are reached at the lower and uppermost ends of α. The allowed ranges of θ_{13} and θ_{23} for $\alpha = 1.1$ are $7.76^\circ - 9.02^\circ$ and $46.3^\circ - 52.26^\circ$ respectively. For $\alpha = 2.0$, the value of θ_{13} is 9.44° and that of θ_{23} is 37.8° which belongs to $M_{ee} = 0.4$ eV. The uppermost end of $\alpha = 2.09$, gives the value of θ_{13} at its global upper limit, whereas θ_{23} is kept at its global lower limit. The converse is true for the lower end of α with θ_{13}, θ_{12} at its lower value and θ_{23} at its maximum.

The variation of the third mixing angle θ_{12} with respect to M_{ee} is next plotted in Fig. 5.35. The pattern obtained is similar to Case 6, with the lower and upper end of α giving the 3σ global end points of θ_{12} respectively. The whole 3σ global range of θ_{12} is allowed, for $\alpha = 1.1$. The value of θ_{12} at $\alpha = 2$ is 36.6°.

Finally we plot the sum of the neutrino masses as a function of M_{ee} in Fig. 5.36. For $\alpha = 0.895$, range of Σm_i is $1.18 - 1.28$ eV corresponding to $0.391 \leq M_{ee} \leq 0.425$ eV. The range of Σm_i at $\alpha = 1.1$ is $1.09 - 1.18$ eV for $M_{ee} \leq 0.4$ eV. At the upper allowed value of $\alpha = 2.0$, it is $1.2 - 1.28$ eV for $0.4 \leq M_{ee} \leq 0.425$ eV. The sum of the neutrino masses is $1.27 - 1.38$ eV for $0.42 \leq M_{ee} \leq 0.452$ eV, in case of the uppermost value of $\alpha = 2.09$. This range is not allowed by the GERDA limit.

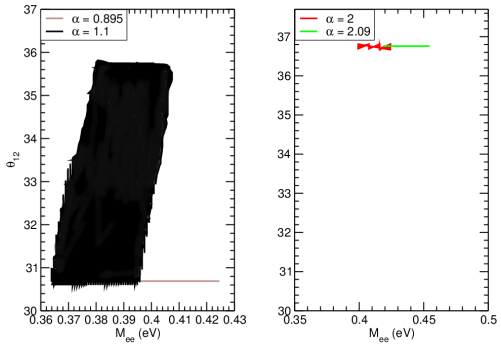

Figure 5.35: The variation of θ_{12} with respect to M_{ee} for Case 7 of HSMR.

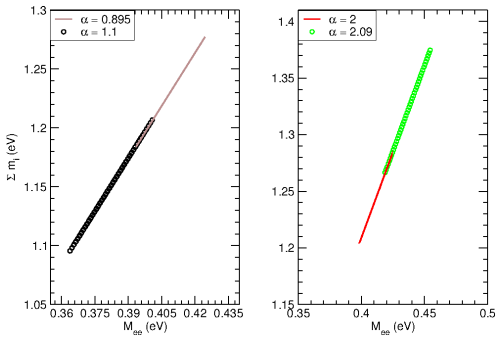

Figure 5.36: The variation of Σm_i with respect to M_{ee} for Case 7 of HSMR.

Lastly as a completion, in order to give a clear picture of all the cases discussed here along with their phenomenological consequences, we summarize our results in Table 6.2. The upper and lower ends of α allowed by the experiments for all the cases are presented along with the corresponding values of masses and mixing angles of the neutrino sector.

The effects of new physics within type-1 seesaw framework

In this sub-section, we discuss the possible effects of the new physics which could generate dimensional-5 operator. For sake of illustration we take type-1 seesaw as the mechanism responsible for generating the effective dimensional-5 operator. The RG equations for type-1 seesaw can be found in the Ref. [57]. In table 6.3, we show results for different cases of HSMR with a seesaw scale equals 4×10^{13} GeV which is slightly lower than the scale of the dimensional-5 operator. We have chosen this scale to demonstrate and differentiate the effects of type-1 mechanism from the results obtained using dimesional-5 operator. Since the major part of RG magnification happens at scales much lower than the typical seesaw scales, the results obtained from dimension-5 operator and those obtained form type-I seesaw mechanism are not very different over a large range of parameters [11–16]. Our results for type-I seesaw are as shown in Table 6.3. To take the effect of type-I seesaw thoroughly, we have done the RG running from the GUT scale (2×10^{16}) GeV to the seesaw scale using the full RG equation for type-I seesaw mechanism. Below the seesaw scale the right handed neutrinos

	α	Masses at unification scale (eV)			Σm_i (eV)	θ_{12}°	θ_{13}°	θ_{23}°	Δm_{32}^2 (10^{-3}eV^2)	Δm_{21}^2 (10^{-5}eV^2)	M_{ee} (eV)	m_1 (eV)	R
		m_1	m_2	m_3									
HSMU	1	0.457-0.476	0.46-0.48	0.515-0.538	1.16-1.2	30.59-36.81	7.63-8.34	49-52.3	2.21-2.45	6.99-8.18	0.384-0.4	0.383	1.5-1.8
2*Case 1	0.902	0.442-0.478	0.445-0.481	0.498- 0.539	1.12-1.2	30.6	7.62	52.29	2.20-2.55	6.99-8.18	0.365-0.4	0.40155	1.39-1.42
	1.28	0.476	0.478	0.538	1.2	32.82	8.16	44.05	2.20	7.196	0.4	0.399	2.1
2*Case 2	0.45	0.41 - 0.445	0.411 - 0.448	0.464 - 0.54	1.16-1.2	30.8	7.65	52.3	2.20-2.57	7.00-8.18	0.38-0.42	0.345-0.375	1.70-1.95
	2.5	0.415 - 0.444	0.416 - 0.445	0.468 - 0.5	1.05-1.12	31.89-36.6	7.92-9.88	37.7-48	2.20-2.53	7.00-8.18	0.342-0.378	0.348-0.373	1
2*Case 3	0.89	0.48	0.48	0.5384	1.2	30.6	8.56	52.3	2.20	6.99	0.4	0.401	1.44
	1.52	0.369-0.399	0.373-0.403	0.418-0.451	0.93-1.01	30.78	7.62	52.3	2.20-2.56	6.99-8.18	0.31-0.336	0.310-0.335	2.16-2.21
2*Case 4	0.92	0.455-0.475	0.458-0.478	0.513-0.536	1.15-1.20	30.6	7.65	52.28	2.30-2.50	6.99-8.01	0.382-0.40	0.3823-0.399	1.463-1.479
	1.67	0.482-0.502	0.485-0.505	0.546-0.568	1.22 -1.27	30.59-30.66	9.59	37.71-37.76	2.29-2.49	7.08-8.18	0.405-0.422	0.405-0.422	2.82-2.86
2*Case 5	0.89	0.475-0.505	0.478-0.508	0.536-0.570	1.20-1.28	30.72	8.40	52.23	2.20-2.48	7.00-7.97	0.4-0.42	0.399-0.424	1.465-1.485
	3.18	0.255-0.265	0.26-0.27	0.29-0.30	0.65-0.67	30.62	7.62	52.3	2.27-2.45	6.99-8.12	0.214-0.223	0.214-0.222	3.542-3.672
2*Case 6	0.86	0.47-0.50	0.474-0.504	0.531-0.565	1.19-1.27	30.61	7.62	52.3	2.20-2.48	6.99-8.17	0.396-0.421	0.396-0.421	1.241-1.268
	2.11	0.494-0.533	0.502-0.542	0.567-0.612	1.26-1.36	34.57-35.02	9.64-9.76	37.70-37.8	2.20-2.57	6.99-8.18	0.416-0.450	0.414-0.448	246.94-251.84
2*Case 7	0.895	0.468-0.505	0.471-0.508	0.528-0.57	1.185-1.22	30.68	7.63	52.28	2.20-2.31	6.99-8.18	0.393-0.4	0.393-0.404	1.34-1.37
	2	0.474	0.48	0.5413	1.18	36.6	9.44	37.8	2.20	7.248	0.39	0.398	81.7-82.11

Table 5.3: The allowed predictions for HSMU and the different cases of the HSMR for lower and upper allowed values of α, Eqs. (5.14-5.20).

are integrated out and as before, the subsequent RG running is done with effect dimension-5 operator. Here we will like to remark that since in this case the RG running is done from a higher scale i.e. GUT scale so we expect small deviations from the previous results primarily due to the larger range of RG running. The dependence of RG evolution on the chosen high scale is studied in [15, 16].

We observe from comparing Tables 6.3 and 6.2 that for case 1 of the HSMR, the lower allowed end of α effectively does not change. As expected, there are slight changes in the value of the observables. For example, the M_{ee} decreases and reaches to the value 0.349 eV compare to the prediction given in table 6.2. Similar observation for the mass of the lightest neutrino. The upper end of α changes after introducing seesaw scale, primarily due to increased RG running range. In Table 6.2, the upper allowed end for case 1 is 1.28. As we observe in Table 6.3, it is now 1.71 and parameter space is bit expanded. However, there is no significant qualitative change in our results which are same as before.

Similarly, for case 2, one can observe from the Tables 6.3 and 6.2 that the lower end of α does not change much. The results are stable and similar to Table 6.2. The upper end of α changes slightly and is 2.59 now. Again as before, there is no significant qualitative change in our results which are same as before.

In case 3 of Table 6.3, the lower value of α has shifted a bit from that of Table6.2, that is from 0.89 to 0.75, but the higher value remains intact being

1.52. The parameters also cover more or less the same span as before and show a stable situation .

The observed pattern in case 4 is same as the case 1, as we see that the lower end does not change while the upper end changes from 1.67 to 1.76 after the inclusion of type-I seesaw (see Table 6.3 and Table 6.2 for comparison). The value of M_{ee} and the mass of lightest neutrino decreases compare to the values given in Table 6.2 and attain the values 0.3508 eV and 0.3506 eV, respectively.

The observed pattern in case 5 is also same as that obtained in Table 6.2. Comparing the results with Table 6.2, we find that the value of α at the lower end changes slightly. The lower end saturates the bound for M_{ee}, whereas at the upper end the value of M_{ee} turns out to be 0.205 eV, which is slightly smaller than the value quoted in Table 6.2.

In case 6, the upper value of α changes very slightly compared to Table 6.2, whereas the lower value remains the same. In this case both the lower and upper end saturates the bound for M_{ee}.

As expected, the results for case 7 are stable as can be observed from Tables 6.2 and 6.3, where the lower end of α is now 0.896 instead of 0.895 and the higher end remains the same, namely $\alpha = 2$.

	α	Masses at unification scale (eV)			Σm_i (eV)	θ_{12}°	θ_{13}°	θ_{23}°	Δm_{32}^2 (10^{-3}eV^2)	Δm_{21}^2 (10^{-5}eV^2)	M_{ee} (eV)	m_1 (eV)	R
		m_1	m_2	m_3									
2*Case 1	0.903	0.465	0.469	0.538	1.04	31.06	7.63	52.30	2.209	8.00	0.349	0.344	1.48
	1.71	0.540-0.542	0.545-0.546	0.628-0.63	1.203- 1.205	30.82 - 33.38	8.68 - 9.87	37.75 - 40.25	2.201-2.26	7.05-7.96	0.399-0.4	0.39815	4.89
2*Case 2	0.47	0.486-0.486	0.49	0.562 - 0.562	1.08-1.08	30.66-30.92	7.62	52.15-52.19	2.2-2.23	7.65-8	0.359	0.359-0.359	1.96-1.99
	2.59	0.478-0.480	0.481- 0.483	0.55 - 0.554	1.06	30.68-31.2	9.1-9.16	42.96-43.51	2.5-2.56	7-7.24	0.354	0.353-0.354	1
2*Case 3	0.75	0.542 - 0.5429	0.545 - 0.546	0.625782 - 0.627092	1.20171 - 1.204	30.607 - 32.73	8.746 - 8.952	51.33 - 52.285	2.2-2.24	6.99-8.16	0.399 - 0.4	0.399 - 0.4	1.351 - 1.374
	1.52	0.392	0.397	0.455	0.88	30.7133	7.639	52.298	2.28	7.05	0.292	0.291	2.52
2*Case 4	0.92	0.4744	0.478	0.5487	1.06	30.98	7.64	52.27	2.266	8.081	0.351	0.3506	1.55
	1.76	0.548-0.5544	0.552-0.558	0.636-0.6435	1.22-1.23	36.09-36.55	9.80-9.87	37.71-37.83	2.204-2.207	7.101-7.837	0.4045-0.4088	0.4039-0.4083	4.7-4.85
2*Case 5	0.80	0.537	0.540	0.621	1.191	32.68	7.79	49.17	2.20	8.09	0.396	0.396	1.532
	3.18	0.274	0.280	0.321	0.623	30.65	7.63	52.3	2.45	7.22	0.205	0.205	4.582
2*Case 6	0.86	0.497	0.500	0.574	1.104	31.09	7.62	52.3	2.20	7.86	0.367	0.367	1.301
	2.14	0.544	0.555	0.642	1.22	35.06	9.88	37.77	2.21	8.18	0.402	0.400	957
2*Case 7	0.896	0.49	0.50	0.57	1.104	30.65 - 31.41	7.62	52.26	2.24	7.1-8.1	0.36	0.36	1.42
	2	0.5	0.49-0.51	0.58	1.12	34.30 - 36.69	9.52 - 9.84	37.80 - 38.07	2.28 - 2.47	7.08 - 7.21	0.37	0.37	155.5

Table 5.4: The allowed predictions for the different cases of the HSMR for lower and upper allowed values of α, Eqs. (5.14-5.20) within the framework of type-1 seesaw for sea-saw scale 4×10^{13} GeV. It should be noted that RG evolution begins from GUT scale which is 2×10^{16} GeV.

Thus, as expected the results obtained with the framework of type-I seesaw mechanism are qualitatively same as those obtained using only dimension-5 effective operator. The general observation is that the absolute mass scale is de-

creasing due to the RG evolution starting from GUT scale (2×10^{16} GeV) which is higher than the scale of dimensional-5 operator. This leads to a slight change in the allowed end of α that is constrained by the observable M_{ee}. That is why, we observe a slight change in the values of mixing angles. We remark that if the high scale from where RG evolution begins, is chosen to be 10^{14} GeV with a seesaw scale equals 4×10^{13} GeV, we recover the results obtained with dimensional-5 operator which is naturally expected.

Theoretical models for high scale mixing relations

In this section, we address the theoretical implementation of HSMR hypothesis from the model building point of view. The only aim of this section is to illustrate that the HMSR hypothesis can be simply realized in models based on flavor symmetries. We follow the same line of argument as presented in Ref. [11].

Now we discuss a simple realization of HSMR relations using abelian Z_7 flavor symmetry. To realize the HSMR relations we add three $SU(2)$ triplet scalars ξ_i; $i = 1, 2, 3$ to the particle content of MSSM. The smallness of neutrino masses can then be explained by the type-2 seesaw mechanism. Let the quarks and leptons and scalars transform under Z_7 as follows

$$\begin{aligned} Q_L^1 &\sim 1, \quad Q_L^2 \sim \omega, \quad Q_L^3 \sim \omega^3, \quad u_R, d_R \sim 1, \quad c_R, s_R \sim \omega, \quad t_R, b_R \sim \omega^3 \\ L_L^1 &\sim 1, \quad L_L^2 \sim \omega, \quad L_L^3 \sim \omega^3, \quad e_R \sim 1, \quad \mu_R \sim \omega, \quad \tau_R \sim \omega^3 \\ H_u, H_d &\sim 1, \quad \xi_1 \sim 1, \quad \xi_2 \sim \omega^2, \quad \xi_3 \sim \omega^6 \end{aligned} \tag{5.46}$$

where $\omega = e^{\frac{2\pi i}{7}}$ is the seventh root of unity. In the above equation Q_L^i, L_L^i; $i = 1, 2, 3$ are the quark and the lepton doublets respectively whereas u_R, d_R, $c_R, s_R, t_R, b_R, e_R, \mu_R, \tau_R$ are the quark and the charged lepton singlets. Moreover, H_u, H_d are the two scalar doublets required to give mass to the up and down type quarks respectively.

It is easy to see from Eq. (5.46) that the Z_7 symmetry leads to diagonal mass matrices for both the quarks and the leptons leading to $U_{CKM} = U_{PMNS} = I$. To obtain the realistic CKM and PMNS matrices as well as the HSMR relations, we allow for small Z_7 symmetry breaking terms as done in Ref. [71] albeit for A_4 symmetry. Such corrections can arise from soft supersymmetry breaking sector as shown in Ref. [72–74]. Allowing for symmetry breaking terms of the form $|h_i'''| << |h_i''| << |h_i'| << |h_i|$ where h_i are the terms invariant under Z_7 symmetry and h_i', h_i'' and h_i''' are the symmetry breaking terms transforming as ω, ω^2 and

ω^3 respectively under Z_7 symmetry. Following the approach of Ref. [71] one can then easily realize the HSMR relations. Here we want to emphasize that owing to quite different masses of quarks and charged leptons, this analysis will in general lead to HSMR relations and not to HSMU relations. To obtain HSMU relations from such an approach one has to invoke a symmetry or mechanism to ensure that the symmetry breaking terms are exactly same in both quark and lepton sectors.

Before, ending this section we would like to further remark that although we have only discussed realization of HSMR relations through the Z_7 symmetry, they can also be quite easily and naturally realized using other flavor symmetries and also using other type of seesaw mechanisms. For example, one can also realize HSMR relations within the framework of type-1 seesaw mechanism using Z_7 symmetry. For this, instead of adding triplet scalars we add three right handed neutrinos which transform as $N_{1R} \sim 1, N_{2R} \sim \omega, N_{3R} \sim \omega^3$ under the Z_7 symmetry. We also add three heavy singlet scalars ϕ_i; $i = 1, 2, 3$ transforming as $\phi_i \sim 1, \phi_2 \sim \omega^5, \phi_3 \sim \omega$ under Z_7 symmetry. Following computations analogous to those done above, one can again easily obtain the HSMR relations. Thus, it is clear that HSMR relations are very natural and can be easily realized using discreet flavor symmetries. In this work we do a model independent analysis of the consequences of the HSMR relations assuming they are realized at the high scale by appropriate flavor symmetries.

Summary

The very small mass of the neutrinos along with a large mixing among them is arguably a remarkable observation. This phenomenon is starkly different from the mixing in the quark sector which is small in the SM. The quest to understand the origin of a large mixing among the neutrinos and a small mixing among the quarks has led to many interesting theoretical ideas. Many beyond the standard model scenarios have been constructed, trying to understand the major theoretical challenge posed by the neutrino mixing. GUT theories with the quark-lepton unification have been extensively used in the literature to understand the neutrino sector at low energies. The postulated HSMR in this work is another effort to understand this extraordinary observation of neutrino mixing. We have shown from a model building point of view, how the HSMR can be naturally realized using different flavor symmetries and seesaw mechanisms. We have first considered the most general relation among the leptonic and the quark mixing angles, with different proportionality constants (α_i). We then list the different possible cases

which arise, for the maximum and minimum allowed values of α_i. It is found that for the allowed range of α_i, M_{ee} is between 0.35 eV - 0.4 eV. The future experiments from GERDA will severely constrain these scenarios. We then look into more simplified cases to have a clear physical picture and therefore consider the α_i to be equal for the three generations and vary k_i to 0 or 1. We then list the seven possible ways the quark and the leptonic mixing angles can be proportional to each other (cf. Eqs. (5.14- 5.20)). It is remarkable that these relations naturally explain the difference between V_{CKM} and U_{PMNS} at the low scale. Furthermore, the QLC relation and the observation in Eq. (5.2) can be easily recovered by these relations.

We have thoroughly investigated the implications and the phenomenological consequences of all the possible cases, taking into account the latest experimental constraints. The whole analysis has been done with the assumption of normal hierarchy and QD mass pattern. In general, we have discovered three new correlations among Δm^2_{32}, M_{ee}, θ_{12} and sum of neutrino masses. These correlations are not investigated in previous studies.

We first discuss about the HSMU scenario, which is a special case of all the HSMR scenarios in the α =1 limit. The behavior of the neutrino masses and the mixing parameters at the low energy scale is discussed in detail for all the cases in HSMR with the value of α deviating from unity in the allowed range. The allowed range of α is bounded by the recent experimental results listed in Table 6.1 and the upper limit on M_{ee} provided by GERDA [23]. It is seen that for all the cases except Case 2, the M_{ee} constraint from the GERDA results in either upper (Cases 1, 4, 6 and 7) or lower (Cases 3 and 5) limit of α. Otherwise the allowed value of α is mostly constrained by the 3σ global limits on neutrino mixing parameters.

An interesting feature is observed in Case 2, where the lower end is constrained by the 3σ global limits of neutrino mixing parameters but the upper end is constrained by the value of the ratio R, which contributes through threshold corrections. We have worked here in the inverted hierarchy scheme in the charged slepton sector, forcing the ratio to be either greater than or equal to one. A common behavior has been observed for all the cases, where we always find a strong correlation between θ_{23} and θ_{13}, for all the allowed values of α except at the end points which corresponds to a point in the $\theta_{23} - \theta_{13}$ plane. It is also seen that among all the experimental constraints M_{ee} is the most interesting one as it mostly constrains the different cases as well as differentiates among them. If in the future the upper limit from GERDA goes down to 0.35 eV, then HSMU, Case 1, Case 4, Case 6 and Case 7 will be ruled out. The ones who will survive

will be Cases 2, 3 and 5 which allows M_{ee} as low as 0.2 eV but with the value of $\alpha > 1$. The constraint on M_{ee} can automatically be reverted to the sum of the neutrino masses. It will show a similar behavior while discriminating the various cases. We also notice that if we take into account the GERDA limit of 0.4 eV, then the allowed range of α in Cases 1, 3 and 5 is limited to a small region in the $\theta_{23} - \theta_{13}$ plane (Figs. 5.10, 5.18, 5.26). Therefore these cases along with HSMU will be ruled out, if the best fit value of θ_{23} becomes less than 44° or that of θ_{13} becomes greater than 8.55° in the future. We further see that Cases 2 and 5 can survive longer, and the region of $M_{ee} = 0.2$ eV is beyond the sensitivity of GERDA which is maximum 0.3 eV. The region of $M_{ee} = 0.2$ eV will easily be probed by KATRIN [65] since m_β is approximately identical to M_{ee} in this work. Here, we pause to comment on the cosmological limit on the sum of the neutrino masses [68]. Our predictions in all cases except Case 5 are slightly above the upper cosmological bound of 0.72 eV. As commented earlier, this bound is model dependent. Hence, it is preferred to test predictions of this work in a laboratory based experiment, like GERDA [23].

We also observe that Cases 3 and 5 show similar behavior, this is mainly because both consider the framework, where the neutrino mixing angle θ_{23} is equal to the quark mixing angle by a proportionality constant $\alpha\theta_{23}^q$. Although Case 5 also has the condition of $\theta_{13} = \alpha\, \theta_{13}^q$, but at the GUT scale $\theta_{13}^q \ll \theta_{23}^q$, therefore the effect of θ_{23}^q dominates. The same pattern can be observed for Case 1 and Case 4, explained through the same argument, $\theta_{13}^q \ll \theta_{12}^q$ at the GUT scale. Continuing the same argument as expected we find that Case 7 displays similar behavior as Case 6. The effect of the neutrino mixing angle θ_{13} being proportional to the quark mixing has many interesting results, as it leads to the most optimistic case. However once the other angles become proportional, this effect is subdued. Finally we note that all these interpretations have been done with the assumption that the Dirac and the Majorana phases of the PMNS matrix are zero and phenomenological consequences can change with nonzero phases. The overall scenario depicting a quark-lepton symmetry at a high scale through HSMR can be narrowed down to a particular case or completely ruled out, only from the future improved experimental constraints. These constraints can be from the neutrinoless double beta decay [23], or the LHC constraints on the SUSY spectrum.

The different scenarios of the HSMR can be discriminated through measurement of various observables like M_{ee} and by precise determination of the values of the mixing angles, particularly θ_{13} and θ_{23} mixing angles. As we have shown in the figures for various cases as well in the tables, the allowed ranges for M_{ee}

and the angles are different for different cases and a precise determination of these observables can be used as a way to distinguish various cases of HSMR. In addition to neutrino observables one can also use other process like lepton-flavor violation to distinguish the different allowed cases. The mass-splitting in the charged-slepton sector is given by the ratio $R = \frac{M_{\tilde{e}}}{M_{\tilde{\mu},\tilde{\tau}}}$. We observe from tables 5.2 and 6.2 that the ratio R almost discriminate every scenario. Hence the processes like $\mu \to e\gamma$, $\mu \to eee$ and anomalous magnetic moment of the electron. For example, the SUSY contribution to the anomalous magnetic moment of the electron directly depends on the ratio R [58]. The detail study of this aspect of the work is not possible in this paper.

Furthermore, for sake of completion, we also present our results in the framework of the type-1 seesaw. The aim is to show how the predictions do not change in any significant way and that the analysis done with effective dimension-5 operator is quite robust. As argued before, this is not surprising as the major part of RG magnification happens only at much lower scales closer to SUSY breaking scale. At such low scales, the effective dimension-5 operator provides a very good approximation to the high scale seesaw mechanisms. The mass scale of the right-handed neutrinos is chosen 4×10^{13} GeV which is close to the scale of the dimensional-5 operator. We notice that parameter space increases very slowly as we decrease the scale of new physics primarily due to increased span of RG running. However predictions do not change in any significant manner and are quite robust.

We also comment on a general theoretical view which is more general than the HSMU hypothesis and the HSMR. Assuming that at some high scale, both the mixing matrices (CKM and PMNS) are approximately unit matrices, but some perturbation can mix the generations leading to the Wolfenstein form of the mixing in both the quark and lepton sectors. This results in the mixing between the first and the second generations to be λ (a small number of order 0.2), the second and the third generations mixing to be second order in λ i.e. $\sin\theta_{23} \sim \lambda^2$ while the first and the third generations mixing to be third order order in λ i.e. $\sin\theta_{13} \sim \lambda^3$. Now after RG evolution the CKM mixing angles do not change much but the PMNS mixing angles are dramatically magnified for the reasons already mentioned in this as well as our earlier papers [15, 17, 33].

Finally, in short, crux of our paper is following.

- We have proposed and studied the HSMR hypothesis which is a more general framework than the HSMU hypothesis.
- The HSMR hypothesis provides a very simple explanation of the observed large neutrino mixing. The present and future neutrino experiments can

easily test predictions of our work. If our predictions are confirmed by experiments, like GERDA, it would be a good hint of quark-lepton unification at high scale.

- We observe that the HSMU hypothesis represents $\alpha = 1$ limit of the HSMR hypothesis and is constrained by the lowest allowed value of M_{ee} which is 0.384 MeV. Therefore, if the HSMU hypothesis is ruled out by experiments, like GERDA, the other HSMR cases with $\alpha \neq 1$ may survive and their confirmation would be itself a strong hint of the proportinality between quark and leptonic mixing angles which is the basis of the HSMR hypothesis.
- We have done a rigorous, thorough and comprehensive study with the HSMR hypothesis which does not exist in the literature. All results reported in the literature using the HSMU hypothesis, are very small subset of our results with the HSMR hypothesis presented in our paper. Moreover, we have also thoroughly compared HSMR hypothesis with respect to the HSMU.
- In our work, we have discovered new strong correlations among different experimental observables for every limit of the HSMR hypthesis. These correlations do not exist in the literature and are easily testable in present ongoing experiments. For example, there is a strong correlation between Δm^2_{32} and M_{ee}. This correlation can be easily tested by GERDA experiment. There are two more such correlations namely among θ_{12}, M_{ee}, Σm_i and M_{ee} discussed in our work which are completely new and unexplored in the literature.
- Furthermore, we have comprehensively studied a strong correlation between θ_{23} and θ_{13} and predictions can be easily tested in present ongoing experiments. This correlation was studied in a previous study in a specific limit. Since we have done a comprehensive full parameter scan, this correlation has become a robust band now.

It is a pleasure to thank Antonio Pich for his valuable suggestions and comments on the manuscript. GA dedicates this paper to I. Sentitemsu Imsong. The work of GA has been supported in part by the Spanish Government and ERDF funds from the EU Commission [Grants No. FPA2011-23778, FPA2014-53631-C2-1-P No. and CSD2007-00042 (Consolider Project CPAN)]. The work of SG is supported by Conselho Nacional de Desenvolvimento Científico e Tecnológico (CNPq) Brazil grant 151112/2014-2.

Bibliography

[1] F. Capozzi, G. L. Fogli, E. Lisi, A. Marrone, D. Montanino and A. Palazzo, Phys. Rev. D **89** (2014) 9, 093018 [arXiv:1312.2878 [hep-ph]].

[2] M. C. Gonzalez-Garcia, M. Maltoni and T. Schwetz, JHEP **1411** (2014) 052 [arXiv:1409.5439 [hep-ph]].

[3] D. V. Forero, M. Tortola and J. W. F. Valle, Phys. Rev. D **90** (2014) 9, 093006 [arXiv:1405.7540 [hep-ph]].

[4] H. Ishimori, T. Kobayashi, H. Ohki, Y. Shimizu, H. Okada and M. Tanimoto, Prog. Theor. Phys. Suppl. **183** (2010) 1 [arXiv:1003.3552 [hep-th]].

[5] W. Grimus and P. O. Ludl, J. Phys. A **45** (2012) 233001 [arXiv:1110.6376 [hep-ph]].

[6] G. Altarelli and F. Feruglio, Rev. Mod. Phys. **82** (2010) 2701 [arXiv:1002.0211 [hep-ph]].

[7] S. F. King and C. Luhn, Rept. Prog. Phys. **76** (2013) 056201 [arXiv:1301.1340 [hep-ph]].

[8] E. Ma and R. Srivastava, Phys. Lett. B **741** (2015) 217 [arXiv:1411.5042 [hep-ph]].

[9] E. Ma and R. Srivastava, Mod. Phys. Lett. A **30** (2015) 26, 1530020 [arXiv:1504.00111 [hep-ph]].

[10] M. Holthausen and K. S. Lim, Phys. Rev. D **88** (2013) 033018 [arXiv:1306.4356 [hep-ph]].

[11] T. Araki, H. Ishida, H. Ishimori, T. Kobayashi and A. Ogasahara, Phys. Rev. D **88** (2013) 096002 [arXiv:1309.4217 [hep-ph]].

[12] H. Ishimori and S. F. King, Phys. Lett. B **735** (2014) 33 [arXiv:1403.4395 [hep-ph]].

[13] C. S. Lam, Phys. Rev. D **89** (2014) 9, 095017 [arXiv:1403.7835 [hep-ph]].

[14] J. C. Pati and A. Salam, Phys. Rev. D **10** (1974) 275 [Erratum-ibid. D **11** (1975) 703].

[15] H. Georgi and S. L. Glashow, Phys. Rev. Lett. **32** (1974) 438.

[16] H. Fritzsch and P. Minkowski, Annals Phys. **93** (1975) 193.

[17] A. Y. Smirnov, hep-ph/0402264.

[18] M. Raidal, Phys. Rev. Lett. **93** (2004) 161801 [hep-ph/0404046].

[19] H. Minakata and A. Y. Smirnov, Phys. Rev. D **70** (2004) 073009 [hep-ph/0405088].

[20] P. H. Frampton and R. N. Mohapatra, JHEP **0501** (2005) 025 [hep-ph/0407139].

[21] S. K. Kang, C. S. Kim and J. Lee, Phys. Lett. B **619** (2005) 129 [hep-ph/0501029].

[22] K. Abe *et al.* [T2K Collaboration], Phys. Rev. Lett. **107** (2011) 041801 [arXiv:1106.2822 [hep-ex]].

[23] P. Adamson *et al.* [MINOS Collaboration], Phys. Rev. Lett. **107** (2011) 181802 [arXiv:1108.0015 [hep-ex]].

[24] Y. Abe *et al.* [Double Chooz Collaboration], Phys. Rev. D **86** (2012) 052008 [arXiv:1207.6632 [hep-ex]].

[25] J. K. Ahn *et al.* [RENO Collaboration], Phys. Rev. Lett. **108** (2012) 191802 [arXiv:1204.0626 [hep-ex]].

[26] F. P. An *et al.* [Daya Bay Collaboration], Phys. Rev. Lett. **108** (2012) 171803 [arXiv:1203.1669 [hep-ex]].

[27] S. Antusch, C. Gross, V. Maurer and C. Sluka, Nucl. Phys. B **866** (2013) 255 [arXiv:1205.1051 [hep-ph]].

[28] R. N. Mohapatra, M. K. Parida and G. Rajasekaran, Phys. Rev. D **69** (2004) 053007 [hep-ph/0301234].

[29] R. N. Mohapatra, M. K. Parida and G. Rajasekaran, Phys. Rev. D **71** (2005) 057301 [hep-ph/0501275].

[30] R. N. Mohapatra, M. K. Parida and G. Rajasekaran, Phys. Rev. D **72** (2005) 013002 [hep-ph/0504236].

[31] S. K. Agarwalla, M. K. Parida, R. N. Mohapatra and G. Rajasekaran, Phys. Rev. D **75** (2007) 033007 [hep-ph/0611225].

[32] G. Abbas, S. Gupta, G. Rajasekaran and R. Srivastava, Phys. Rev. D **89** (2014) 9, 093009 [arXiv:1401.3399 [hep-ph]].

[33] G. Abbas, S. Gupta, G. Rajasekaran and R. Srivastava, Manuscript under preparation

[34] R. Srivastava, arXiv:1503.07964 [hep-ph].

[35] G. Abbas, S. Gupta, G. Rajasekaran and R. Srivastava, arXiv:1312.7384 [hep-ph].

[36] S. Antusch, J. Kersten, M. Lindner and M. Ratz, Nucl. Phys. B **674** (2003) 401 [hep-ph/0305273].

[37] P. H. Chankowski and Z. Pluciennik, Phys. Lett. B **316** (1993) 312 [hep-ph/9306333].

[38] K. S. Babu, C. N. Leung and J. T. Pantaleone, Phys. Lett. B **319** (1993) 191 [hep-ph/9309223].

[39] S. Antusch, M. Drees, J. Kersten, M. Lindner and M. Ratz, Phys. Lett. B **519** (2001) 238 [hep-ph/0108005].

[40] S. Antusch, M. Drees, J. Kersten, M. Lindner and M. Ratz, Phys. Lett. B **525** (2002) 130 [hep-ph/0110366].

[41] E. J. Chun and S. Pokorski, Phys. Rev. D **62** (2000) 053001 [hep-ph/9912210].

[42] P. H. Chankowski, A. Ioannisian, S. Pokorski and J. W. F. Valle, Phys. Rev. Lett. **86** (2001) 3488 [hep-ph/0011150].

[43] E. J. Chun, Phys. Lett. B **505** (2001) 155 [hep-ph/0101170].

[44] P. H. Chankowski and P. Wasowicz, Eur. Phys. J. C **23** (2002) 249 [hep-ph/0110237].

[45] N. Craig, arXiv:1309.0528 [hep-ph].

[46] C. Kraus, B. Bornschein, L. Bornschein, J. Bonn, B. Flatt, A. Kovalik, B. Ostrick and E. W. Otten *et al.*, Eur. Phys. J. C **40** (2005) 447 [hep-ex/0412056].

[47] V. N. Aseev *et al.* [Troitsk Collaboration], Phys. Rev. D **84** (2011) 112003 [arXiv:1108.5034 [hep-ex]].

[48] G. Drexlin, V. Hannen, S. Mertens and C. Weinheimer, Adv. High Energy Phys. **2013** (2013) 293986 [arXiv:1307.0101 [physics.ins-det]].

[49] W. Rodejohann, J. Phys. G **39** (2012) 124008 [arXiv:1206.2560 [hep-ph]].

[50] S. M. Bilenky and C. Giunti, Int. J. Mod. Phys. A **30** (2015) 04n05, 1530001 [arXiv:1411.4791 [hep-ph]].

[51] M. Agostini *et al.* [GERDA Collaboration], Phys. Rev. Lett. **111** (2013) 12, 122503 [arXiv:1307.4720 [nucl-ex]].

[52] P. A. R. Ade *et al.* [Planck Collaboration], arXiv:1502.01589 [astro-ph.CO].

[53] S. Antusch, J. Kersten, M. Lindner, M. Ratz and M. A. Schmidt, JHEP **0503** (2005) 024 [hep-ph/0501272].

[54] E. Ma, Mod. Phys. Lett. A **17**, 627 (2002) [hep-ph/0203238].

[55] K. S. Babu, E. Ma and J. W. F. Valle, Phys. Lett. B **552**, 207 (2003) [hep-ph/0206292].

[56] K. S. Babu, B. Dutta and R. N. Mohapatra, Phys. Rev. D **60**, 095004 (1999) [hep-ph/9812421].

[57] F. Gabbiani, E. Gabrielli, A. Masiero and L. Silvestrini, Nucl. Phys. B **477**, 321 (1996) [hep-ph/9604387].

[58] D. Stockinger, J. Phys. G **34**, R45 (2007) doi:10.1088/0954-3899/34/2/R01 [hep-ph/0609168].

6. Precise Predictions For Dirac Neutrino mixing

Gauhar Abbas , Mehran Zahiri Abyaneh, Rahul Srivastava

[a] *Instituto de Física Corpuscular (IFIC), CSIC-Universitat de València*
Apdo. Correos 22085, E-46071 Valencia, Spain

[Physical Review D 95, Published 5 April 2017]

The neutrino mixing parameters are thoroughly studied using renormalization-group evolution of Dirac neutrinos with recently proposed parametrization of the neutrino mixing angles referred as 'high-scale mixing relations'. The correlations among all neutrino mixing and CP violating observables are investigated. The predictions for the neutrino mixing angle θ_{23} are precise, and could be easily tested by ongoing and future experiments. We observe that the high scale mixing unification hypothesis is incompatible with Dirac neutrinos due to updated experimental data.

14.60.Pq, 11.10.Hi, 11.30.Hv, 12.15.Lk

Introduction

Neutrino mixing is one of the most fascinating and challenging discoveries. This is starkly different from quark mixing which is small in the standard model (SM). There are a number of ways to explain these two very different phenomena. The quark-lepton unification, which is one of the main attractive features of the grand unified theories (GUT) [1–3], could provide an explanation of the origin of neutrino and quark mixing since quarks and leptons live in a joint represenation of the symmetry group. Another interesting approach is to use flavor symmetries [4–8]. These symmetries could also naturally appear in GUT theories [9].

To explain the origin of neutrino and quark mixing, recently a new parametrization of the neutrino mixing angles in terms of quark mixing angles was proposed in Ref. [10]. The varoius simplified limits of this prameterization are referred as 'high-scale mixing relations'(HSMR). The parametrization is inspired by the high scale mixing unification (HSMU) hypothesis which states that at certain high scales the neutrino mixing angles are identical to that of the quark mixing angles [11–14]. This hypothesis is studied in detail in Refs. [15–19] .

The HSMR parametrization of the neutrino mixing angles assumes that the neutrino mixing angles are proportional to those of quarks due to some underlying theory which could be a quark-lepton unification or models based on flavor symmetries. In fact, such models are also presented in Ref. [10]. The scale where the HSMR parametrization could be realized is referred as unification scale. In its most general form, the HSMR parametrization can be written as follows:

$$\theta_{12} = \alpha_1^{k_1}\ \theta_{12}^q, \quad \theta_{13} = \alpha_2^{k_2}\ \theta_{13}^q, \quad \theta_{23} = \alpha_3^{k_3}\theta_{23}^q. \tag{6.1}$$

where θ_{ij} (with $i, j = 1, 2, 3$) denotes leptonic mixing angles and θ_{ij}^q are the quark mixing angles. Exponents k_i with $i = (1, 2, 3)$ are real. Predictions of the HSMR parametrization could be a strong hint of the quark-lepton unification, some flavor symmetry or both.

The HSMR parametrization is studied in the framework of the SM extended by the minimum supersymmetric standard model (MSSM). The beginning point is to run the quark mixing angles from the low scale (mass of the Z boson) to the supersymmetry (SUSY) breaking scale using the renormalization-group (RG) evolution of the SM. The RG equations of the MSSM govern the evolution of quark mixing angles from the SUSY breaking scale to the unification scale. After obtaining quark mixing angles at the unification scale, the HSMR parametrization is used to run neutrino mixing parameters from the unification scale to the SUSY breaking scale via RG evolution of the MSSM. From the SUSY breaking scale to the low scale, the SM RG equations are used to evolve the neutrino mixing parameters. The free parameters controlling the top-down evolution of the neutrino mixing parameters are masses of the three light neutrinos, Dirac CP phase and parameters α_i. Masses of neutrinos must be quasidegenerate and normal hierarchical. Furthermore, the large value of $\tan\beta$ is required [10].

On the other hand, the nature of neutrinos is still unknown. They could be equally Dirac or Majorana in nature. Hence, from the phenomenological point of view, Dirac neutrinos are as important as Majorana neutrinos. There are many ongoing important experiments to test the nature of neutrinos [20–23]. However, for the Dirac mass of neutrinos, the Yukawa couplings for neutrinos seem to

be unnaturally small. The elegant way to explain this fine-tuning is see-saw mechanism which assumes that neutrinos are Majorana in nature [24–28].

The smallness of masses for Dirac neutrinos could be explained in many models using heavy degrees of freedom [29–38]. There are also models based on extra dimensions which explain the smallness of Dirac neutrino mass by a small overlapping of zero-mode profiles along extra dimensions [39–41]. Dirac neutrinos seem to be a natural choice in certain orbifold compactifications of the heterotic string where the standard see-saw mechanism is difficult to realize [42]. Cosmological data do not prefer Majorana or Dirac neutrinos either. For instance, the baryon asymmetry of the Universe can also be explained for Dirac neutrinos in various theoretical models [43–49].

Although the RG evolution of Majorana neutrinos is extensively studied in the literature [11–17, 50, 51], less attention is being paid to the RG evolution of Dirac neutrinos. In fact, as far as we know, it was shown for the first time in Ref. [16] that RG evolution for Dirac neutrinos can explain the large neutrino mixing assuming the HSMU hypothesis. However, as we show later, these results are ruled out by new updated data [52–54] and due to an improved algorithm used in the package REAP [55].

It is established that the HSMR parametrization can explain the observed pattern of the neutrino mixing assuming they are Majorana in nature [10]. In this paper, we investigate the consequences of the HSMR parametrization using the RG evolution of Dirac neutrinos.

This paper is organized in the following way: In Sec. 6.2, we present our results on the RG evolution of the neutrino mixing parameters. In Sec. 6.3 we present a model with naturally small Dirac neutrino masses, where the HSMR parametrization discussed in Eq.6.1 can be explicitly realized. We summarize our work in Sec. 6.4.

RG evolution of the neutrino mixing parameters for Dirac neutrinos

Now we present our results. The RG equations describing the evolution of the neutrino mixing parameters for Dirac neutrinos are derived in Ref. [56]. We have used Mathematica- based package REAP for the computation of the RG evolution at two loops [57]. The first step is to evolve quark mixing angles, gauge couplings, Yukawa couplings of quarks, and charged leptons from the low scale to the SUSY breaking scale. From the SUSY breaking scale to the unification scale, evolution undergoes the MSSM RG equations. The quark mixing angles at the unification

scale after evolution are $\theta_{12}^q = 13.02^\circ$, $\theta_{13}^q = 0.17^\circ$ and $\theta_{23}^q = 2.03^\circ$. Now, quark-mixing angles are used by the HSMR parametrization at the unification scale and neutrino mixing parameters are evolved down to the SUSY breaking scale using the MSSM RG equations. After this, the evolution of mixing parameters are governed by the SM RG equation. The value of $\tan\beta$ is chosen to be 55. For simplification, we have assumed $k_1 = k_2 = k_3 = 1$ in the HSMR parametrization. The global status of the neutrino mixing parameters is given in Table 6.1.

Quantity	Best fit	3σ range
Δm^2_{21} (10^{-5} eV^2)	7.60	7.11 – 8.18
Δm^2_{31} (10^{-3} eV^2)	2.48	2.30 – 2.65
θ°_{12}	34.6	31.8 – 37.8
θ°_{23}	48.9	38.8 – 53.3
θ°_{13}	8.6	7.9– 9.3

Table 6.1: The global fits for the neutrino mixing parameters [52]

Results for the SUSY breaking scale at 2 TeV

In this subsection, we present our results for the SUSY breaking scale at 2 TeV following the direct LHC searches [58]. The unification scale where the HSMR parametrization could be realized is chosen to be GUT scale (2×10^{16} GeV). The free parameters of the analysis are shown in Table 6.2.

Quantity	Range at the unification scale
α_1	$0.7 - 0.8$
α_2	$2.12 - 2.78$
α_3	$1.002 - 1.01$
m_1(eV)	$0.49227 - 0.49825$
m_2 (eV)	$0.494 - 0.5$
m_3 (eV)	$0.52898 - 0.53542$
δ_{Dirac}	$(-14^\circ, 14^\circ)$

Table 6.2: The free parameters of the analysis chosen at the unification scale.

In Fig. 6.1, we show a correlation between mixing angles θ_{13} and θ_{23}. It is obvious that our prediction for θ_{23} is precise. The allowed range of θ_{13} is

$7.94^\circ - 9.3^\circ$. The corresponding range of θ_{23} is $51.5^\circ - 52.64^\circ$. It is important to note that the predictions for θ_{13} include the best fit value. Another important prediction is that θ_{23} is nonmaximal and lies in the second octant. Being precise, this correlation is easily testable in future and ongoing experiments such as INO, T2K, NOνA, LBNE, Hyper-K, and PINGU [59–64].

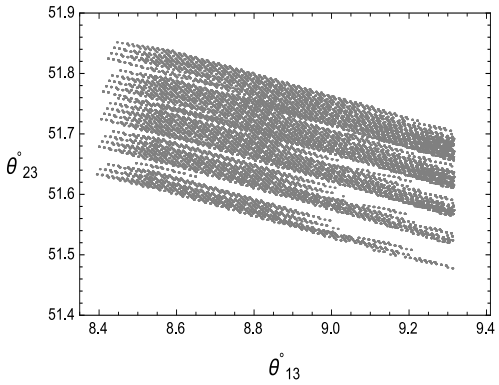

Figure 6.1: The variation of θ_{23}° with respect to θ_{13}°.

In Fig. 6.2, we show the variation of "averaged electron neutrino mass" m_β [65] with respect to Δm_{31}^2. The allowed range of m_β is $0.4633 - 0.4690$ eV which is precise. The upper bound on m_β is 2 eV from tritium beta decay [66, 67]. The KATRIN experiment is expected to probe m_β as low as 0.2 eV at 90% C.L. [65]. Hence, our prediction for m_β is well within the reach of the KATRIN experiment. The allowed range for Δm_{31}^2 is $(2.30 - 2.37) \times 10^{-3}\text{eV}^2$ which is bounded with respect to the 3σ range given by the global fit in Table 6.1. It should be noted that the best fit value of Δm_{31}^2 given in Table 6.1 is excluded by our results.

We show in Fig.6.3 another important predictions of this work. This is the variation of the CP violating Dirac phase δ_{Dirac} with respect to θ_{13}. The Dirac phase δ_{Dirac} is not known from experiments. Hence, any prediction of this important observable is of great interest. Our prediction for δ_{Dirac} is 80.01° to 287.09° excluding a sufficient part of the allowed parameter space of this quantity. In Fig.6.4, we show the behavior of the Jarlskog invariant J_{CP} with respect to Dirac phase δ_{Dirac}. The allowed range for this observable is -0.266 to 0.266. Thus, a large CP violation is possible in our analysis.

The variation of the sum of three neutrino masses, Σm_i with respect to Δm_{31}^2 is shown in Fig.6.5. The allowed range of Σm_i is $1.393 - 1.410$ eV, which is precise. We comment that our prediction for Σm_i is a little higher than that provided by the cosmological and astrophysical observations which is 0.72 eV at

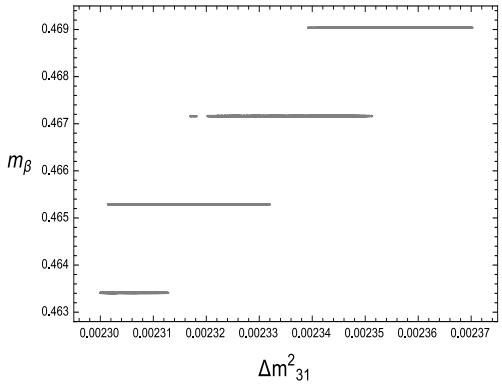

Figure 6.2: The variation of m_β with respect to Δm^2_{31}.

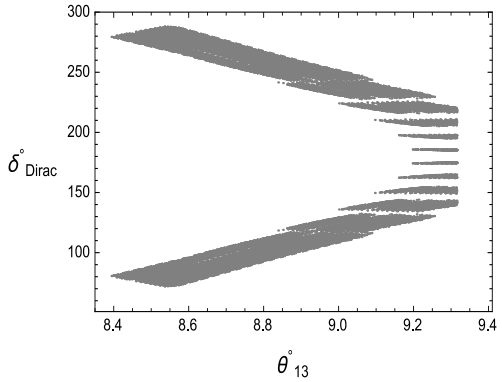

Figure 6.3: The variation of δ°_{Dirac} with respect to θ°_{13}.

95%C.L. [68]. However, cosmological limit on Σm_i is highly model dependent. For example, as shown in Fig. 29 of Ref. [68] this could be as large as 1.6eV. Furthermore, Ref. [68] assumes degenerate neutrinos ignoring the observed mass splittings whereas their model (ΛCDM) assumes two massless and one massive neutrino with $\Sigma m_i = 0.06$eV. Moreover, ΛCDM is facing several challenges in explaining structures on galaxy scales [69]. Hence, our predictions are aimed to test in laboratory-based experiments like KATRIN [65].

We do not obtain any constraints on the mixing angle θ_{12} and mass square difference Δm^2_{21}. The whole 3σ ranges of global fit are allowed in this case for these quantities.

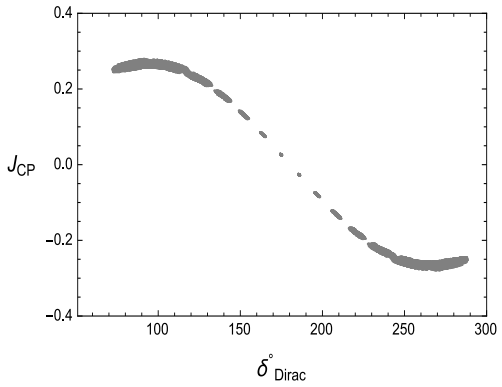

Figure 6.4: The variation of J_{CP} with respect to δ°_{Dirac}.

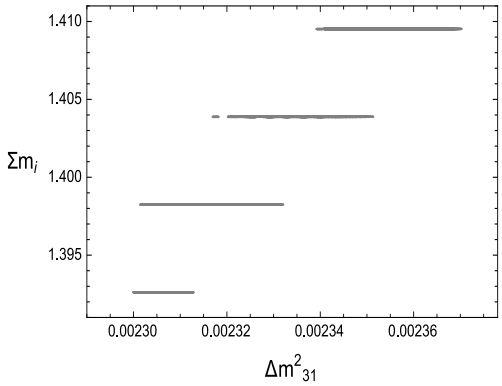

Figure 6.5: The variation of Σm_i with respect to Δm^2_{31}.

Variation of the SUSY breaking scale

Now, we discuss the effect of variation of the SUSY breaking scale on our predictions. In this case, we change the SUSY breaking scale to 5 TeV. However, the unification scale is still at the GUT scale. Our results are summarized in Tables 6.3 and 6.4. In Table 6.3, we provide our free parameters which are chosen at the GUT scale. Our predictions at the low scale are given in Table 6.4.

We observe that the mixing angle θ_{12} and mass square difference Δm^2_{21} were unconstrained for the SUSY breaking scale at 2 TeV in the previous subsection. Now, we observe that these quantities are bounded with respect to the 3σ range given by the global fit. The mixing angle θ_{23}, unlike the investigation for SUSY breaking scale 2 TeV, lies in the first octant and is non-maximal.

Quantity	Range
α_1	$0.88 - 1.012$
α_2	$2.72 - 2.85$
α_3	1.095
m_1(eV)	$0.46878 - 0.47380$
m_2 (eV)	$0.47 - 0.475$
m_3 (eV)	$0.50321 - 0.50857$
δ_{Dirac}	$(-14^\circ, 14^\circ)$

Table 6.3: The free parameters of the analysis chosen at the unification scale for the SUSY breaking scale at 5 TeV. The first column showes the parameters and the second column showes their range at the unification scale.

Quantity	Range
θ_{12}	$32.85^\circ - 37.74^\circ$
θ_{13}	$7.94^\circ - 8.20^\circ$
θ_{23}	$38.86^\circ - 39.45^\circ$
m_1(eV)	$0.44458 - 0.44932$
Δm^2_{21} (10^{-5} eV^2)	$7.15 - 8.15$
Δm^2_{31} (10^{-3} eV^2)	$2.30 - 2.34$
m_β (eV)	$0.4447 - 0.4468$
Σm_i (eV)	$1.337 - 1.351$
δ_{Dirac}	$281.28^\circ - 355.49^\circ$ and $0 - 89.14^\circ$
J_{CP}	-0.2511 to 0.2511

Table 6.4: Predictions of neutrino mixing parameters and other observables at the low scale for the SUSY breaking scale at 5 TeV. The first column showes the parameters and the second column showes their range at the low scale.

Variation of the unification scale

In this subsection, we investigate the variation of the unification scale. In Tables 6.5 and 6.6, we show our results when we choose the unification scale to be 10^{12} GeV which is well below the GUT scale. However, the SUSY breaking scale is kept to 2 TeV. We show in Table 6.5, the values of the free parameters chosen at the unification scale. In Table 6.6, we present our results. The first remarkable prediction is the sum of neutrino masses which is well below the cosmological bound. The Dirac CP phase has a precise range. The mixing angle θ_{12} and mass square difference Δm^2_{21} are now relatively constrained. The mixing angle θ_{23} lies in the first octant, and is nonmaximal.

We conclude that there is no parameter space beyond the GUT scale for Dirac neutrinos so that we could recover the experimental data at the low scale using the RG evolution. This is a strong prediction and could be useful in construction of models (particularly GUT models) where Dirac neutrinos are the natural choice [30–38].

Quantity	Range
α_1	$0.67 - 0.85$
α_2	$19.9 - 20.92$
α_3	$7.41 - 7.42$
m_1(eV)	$0.19815 - 0.20311$
m_2 (eV)	$0.2 - 0.205$
m_3 (eV)	$0.21100 - 0.21628$
δ_{Dirac}	$(-10°, 18°)$

Table 6.5: The free parameters of the analysis chosen at the unification scale of 10^{12} GeV and SUSY breaking scale of 2 TeV. The first column showes the parameters and the second column showes their range at the unification scale.

Quantity	Range
θ_{12}	$32.35° - 37.34°$
θ_{13}	$7.94° - 8.45°$
θ_{23}	$38.83° - 39.18°$
m_1(eV)	$0.18321 - 0.18801$
Δm^2_{21} (10^{-5} eV^2)	$7.77 - 8.17$
Δm^2_{31} (10^{-3} eV^2)	$2.30 - 2.42$
m_β (eV)	$0.1834 - 0.1880$
Σm_i (eV)	$0.556 - 0.570$
δ_{Dirac}	$182.66° - 203.43°$ and $0 - 120°$
J_{CP}	-0.1020 to 0.2336

Table 6.6: Predictions of neutrino mixing parameters and other observables for the unification scale of 10^{12} GeV and the SUSY breaking scale at 2 TeV. The first column showes the parameters and the second column showes their range at the low scale.

Model for the HSMR parametrization

We have investigated the HSMR parametrization for Dirac neutrinos in a model independent way. However, for the sake of completeness, in this section we discuss theoretical implementation of the HSMR parametrization in a specific model for Dirac neutrinos. Our model is based on a model presented in Ref. [19,70] which provides Dirac neutrinos with naturally small masses. This model is a type of neutrinophilic SUSY extension of the SM which can easily be embedded in a class of $SU(5)$ models.

To obtain HSMR parametrization in the model given in Ref. [70], we impose a Z_3 discrete symmetry on this model. Under the Z_3 symmetry the first generation of both left- and right-handed quarks and leptons transforms as 1, while the second generation transforms as ω and the third generation transforms as ω^2, where ω denotes cube root of unity with $\omega^3 = 1$. All other fields transform trivially as 1 under the Z_3 symmetry. The Z_3 symmetry ensures that the mass matrices for both up and down quarks as well as for charged leptons and neutrinos

are all simultaneously diagonal. This in turn implies that the $V_{\rm CKM}$ as well as $V_{\rm PMNS}$ are both unity and there is no generation mixing in either quark or lepton sectors.

To allow for the mixing, we break Z_3 in a way as done in Ref. [71]. Such corrections can arise from the soft SUSY breaking sector [72–74]. For this purpose, we allow symmetry breaking terms of the form $|y_i''| << |y_i'| << |y_i|$ where $|y_i|$ are the terms invariant under Z_3 symmetry, and $|y_i'|, |y_i''|$ are the symmetry breaking terms transforming as ω, ω^2 under the Z_3 symmetry. This symmetry breaking pattern is well established and is known to explain the CKM structure of the quark sector [71]. Here, we have imposed this pattern on quarks as well as leptons simultaneously.

Including these symmetry breaking terms, the mass matrices for quarks and leptons become

$$M_{u,d,l} = \begin{pmatrix} y_1 v & y_2' v & y_3'' v \\ y_1'' v & y_2 v & y_3' v \\ y_1' v & y_2'' v & y_3 v \end{pmatrix} , \qquad M_\nu = \begin{pmatrix} y_1 u & y_2' u & y_3'' u \\ y_1'' u & y_2 u & y_3' u \\ y_1' u & y_2'' u & y_3 u \end{pmatrix} , \tag{6.2}$$

where v stands for the vacuum expectation value (vev) of the usual H_u, H_d doublet scalars of MSSM and u is the vev of the neutrinophilic scalar H_ν as discussed in Ref. [70]. Also, for the sake of brevity we have dropped the sub- and superscripts on the various terms. The mass matrix in (6.2) is exactly same as the mass matrix obtained in Ref. [71] and can be diagonalized in the same way as done in Ref. [71]. The mass matrices of (6.2) lead to a "Wolfenstein-like structure" for both CKM and Pontecorvo-Maki-Nakagawa-Sakata (PMNS) matrices, thus leading to the HSMR parametrization given in Eq.6.1. Since this model is a modification of model given in Ref. [70] which can be embedded in a class of $SU(5)$ GUT models, therefore, it can also be easily embedded in the $SU(5)$ GUT model in a quite similar way as done in Ref. [70].

Summary

Neutrino mixing is remarkably different from small quark mixing. The aim of the present work is to provide an insight into a common origin of neutrino as well as quark mixing for Dirac neutrinos. Furthermore, we show that smallness of neutrino masses can be explained through the RG evolution of Dirac neutrinos. The HSMR parametrization of neutrino mixing angles is one among many other theoretical frameworks constructed for this purpose. The origin of this

parametrization lies in the underlying concept of the quark-lepton unification or flavor symmetries or both. Hence, the confirmation of predictions provided by the HSMR parametrization would be a strong hint of the quark-lepton unification or a grand symmetry operating at the unification scale.

As far as our knowledge is concerned, it was shown for the first time in Ref. [16] that the RG evolution can also explain the large neutrino mixing for Dirac neutrinos. However, as we have shown in this work, these results are no longer valid due to updated experimental data [52–54] and the improved algorithm used in the package REAP [55].

In the present work, we have investigated the RG evolution of Dirac neutrinos in the framework of the HSMR parametrization. To our knowledge, this is the first thorough study on the RG behavior of Dirac neutrinos. The main achievement is that the RG evolution of Dirac neutrinos could explain the large neutrino mixing including the observation of a small and nonzero value of the mixing angle θ_{13}. We obtain strong correlations among different experimental observables. Our predictions for the mixing angles θ_{13}, θ_{23}, averaged electron neutrino mass m_β, Dirac CP phase δ_{Dirac} and the sum of three neutrino masses, Σm_i are precise and easily testable at ongoing and future experiments like INO, T2K, NOνA, LBNE, Hyper-K, PINGU and KATRIN [59–65]. The mixing angle θ_{23} is nonmaximal and lies in the second octant for the SUSY breaking scale 2 TeV and unification scale at the GUT scale. For the variation of the SUSY breaking scale and the unification scale, the mixing angle θ_{23} is nonmaximal and lies in the first octant. The predictions for the mass square difference Δm^2_{31} are also well constrained and testable in experiments. Furthermore, the Dirac CP phase is found to be lying in precise ranges in our analysis. The unification scale beyond the GUT scale is ruled out in our investigation. This fact could be useful for the GUT theories having Dirac neutrinos [30–38]. We remark that we have investigated the RG evolution of neutrino mixing parameters at two loops. This is a crucial input since the RG evolution at one loop is insufficient to provide the required enhancement of the mixing angles which in turn, cannot yield the results obtained in this work.

One of the main consequences of our investigation is that the HSMU hypothesis is not compatible with Dirac neutrinos due to updated experimental data [52–54] and a better algorithm used in the package REAP [55]. The HSMU hypothesis is a particular realization of the HSMR parametrization when we choose $\alpha_1 = \alpha_2 = \alpha_3 = 1$ for $k_1 = k_2 = k_3 = 1$. As can be observed from Tables 6.2, 6.3 and 6.5 the allowed range for α_i excludes the $\alpha_1 = \alpha_2 = \alpha_3 = 1$ case. This result is rigorous and robust in the sense that changing the SUSY breaking

scale and the unification scale does not change this conclusion. Hence, the HSMR parametrization is one of the preferable frameworks to study the RG evolution of Dirac neutrinos now.

The work of G. A. and M. Z. A. is supported by the Spanish Government and ERDF funds from the EU Commission [Grants No. FPA2011-23778, FPA2014-53631-C2-1-P and No. CSD2007-00042 (Consolider Project CPAN)]. RS is funded by the Spanish grants FPA2014-58183-P, Multidark CSD2009-00064, SEV-2014-0398 (MINECO) and PROMETEOII/2014/084 (Generalitat Valenciana).

Bibliography

[1] J. C. Pati and A. Salam, Phys. Rev. D **10** (1974) 275 [Erratum-ibid. D **11** (1975) 703].

[2] H. Georgi and S. L. Glashow, Phys. Rev. Lett. **32** (1974) 438.

[3] H. Fritzsch and P. Minkowski, Annals Phys. **93** (1975) 193.

[4] G. Altarelli and F. Feruglio, Rev. Mod. Phys. **82** (2010) 2701 [arXiv:1002.0211 [hep-ph]].

[5] S. F. King and C. Luhn, Rept. Prog. Phys. **76** (2013) 056201 [arXiv:1301.1340 [hep-ph]].

[6] M. Holthausen and K. S. Lim, Phys. Rev. D **88** (2013) 033018 [arXiv:1306.4356 [hep-ph]].

[7] T. Araki, H. Ishida, H. Ishimori, T. Kobayashi and A. Ogasahara, Phys. Rev. D **88** (2013) 096002 [arXiv:1309.4217 [hep-ph]].

[8] H. Ishimori and S. F. King, Phys. Lett. B **735** (2014) 33 [arXiv:1403.4395 [hep-ph]].

[9] C. S. Lam, Phys. Rev. D **89** (2014) 9, 095017 [arXiv:1403.7835 [hep-ph]].

[10] G. Abbas, M. Z. Abyaneh, A. Biswas, S. Gupta, M. Patra, G. Rajasekaran and R. Srivastava, Int. J. Mod. Phys. A **31**, no. 17, 1650095 (2016) doi:10.1142/S0217751X16500950 [arXiv:1506.02603 [hep-ph]].

[11] R. N. Mohapatra, M. K. Parida and G. Rajasekaran, Phys. Rev. D **69** (2004) 053007 [hep-ph/0301234].

[12] R. N. Mohapatra, M. K. Parida and G. Rajasekaran, Phys. Rev. D **71** (2005) 057301 [hep-ph/0501275].

[13] R. N. Mohapatra, M. K. Parida and G. Rajasekaran, Phys. Rev. D **72** (2005) 013002 [hep-ph/0504236].

[14] S. K. Agarwalla, M. K. Parida, R. N. Mohapatra and G. Rajasekaran, Phys. Rev. D **75** (2007) 033007 [hep-ph/0611225].

[15] G. Abbas, S. Gupta, G. Rajasekaran and R. Srivastava, Phys. Rev. D **89** (2014) 9, 093009 [arXiv:1401.3399 [hep-ph]].

[16] G. Abbas, S. Gupta, G. Rajasekaran and R. Srivastava, Phys. Rev. D **91**, no. 11, 111301 (2015) doi:10.1103/PhysRevD.91.111301 [arXiv:1312.7384 [hep-ph]].

[17] R. Srivastava, Pramana **86**, no. 2, 425 (2016) [arXiv:1503.07964 [hep-ph]].

[18] R. Srivastava, Springer Proc. Phys. **174**, 369 (2016).

[19] N. Haba and R. Takahashi, Europhys. Lett. **100**, 31001 (2012) doi:10.1209/0295-5075/100/31001 [arXiv:1206.2793 [hep-ph]].

[20] F. Alessandria, E. Andreotti, R. Ardito, C. Arnaboldi, F. T. Avignone, III, M. Balata, I. Bandac and T. I. Banks *et al.*, arXiv:1109.0494.

[21] M. Auger *et al.* [EXO Collaboration], Phys. Rev. Lett. **109**, 032505 (2012), arXiv:1205.5608.

[22] A. Gando *et al.* [KamLAND-Zen Collaboration], Phys. Rev. Lett. **110**, no. 6, 062502 (2013), arXiv:1211.3863.

[23] M. Agostini *et al.* [GERDA Collaboration], Phys. Rev. Lett. **111**, 122503 (2013), arXiv:1307.4720.

[24] P. Minkowski, Phys. Lett. B **67**, 421 (1977).

[25] M. Gell-Mann, P. Ramond and R. Slansky, Conf. Proc. C **790927**, 315 (1979), arXiv:1306.4669.

[26] T. Yanagida, Conf. Proc. C **7902131**, 95 (1979).

[27] S. L. Glashow, NATO Adv. Study Inst. Ser. B Phys. **59**, 687 (1980).

[28] R. N. Mohapatra and G. Senjanovic, Phys. Rev. Lett. **44**, 912 (1980).

[29] G. Abbas, arXiv:1609.02899 [hep-ph].

[30] E. Ma and R. Srivastava, Phys. Lett. B **741**, 217 (2015) [arXiv:1411.5042 [hep-ph]].

[31] R. N. Mohapatra and J. W. F. Valle, Phys. Rev. D **34**, 1642 (1986).

[32] N. Arkani-Hamed, L. J. Hall, H. Murayama, D. Tucker-Smith and N. Weiner, Phys. Rev. D **64**, 115011 (2001), hep-ph/0006312.

[33] F. Borzumati and Y. Nomura, Phys. Rev. D **64**, 053005 (2001), hep-ph/0007018.

[34] R. Kitano, Phys. Lett. B **539**, 102 (2002), hep-ph/0204164.

[35] S. Abel, A. Dedes and K. Tamvakis, Phys. Rev. D **71**, 033003 (2005), hep-ph/0402287.

[36] H. Murayama, Nucl. Phys. Proc. Suppl. **137**, 206 (2004), hep-ph/0410140.

[37] A. Y. .Smirnov, hep-ph/0411194.

[38] R. N. Mohapatra, S. Antusch, K. S. Babu, G. Barenboim, M. -C. Chen, S. Davidson, A. de Gouvea and P. de Holanda *et al.*, hep-ph/0412099.

[39] P. Q. Hung, Nucl. Phys. B **720**, 89 (2005) doi:10.1016/j.nuclphysb.2005.05.023 [hep-ph/0412262].

[40] P. Ko, T. Kobayashi and J. h. Park, Phys. Rev. D **71**, 095010 (2005) doi:10.1103/PhysRevD.71.095010 [hep-ph/0503029].

[41] S. Antusch, O. J. Eyton-Williams and S. F. King, JHEP **0508**, 103 (2005) doi:10.1088/1126-6708/2005/08/103 [hep-ph/0505140].

[42] J. Giedt, G. L. Kane, P. Langacker and B. D. Nelson, Phys. Rev. D **71**, 115013 (2005) doi:10.1103/PhysRevD.71.115013 [hep-th/0502032].

[43] K. Dick, M. Lindner, M. Ratz and D. Wright, Phys. Rev. Lett. **84**, 4039 (2000), hep-ph/9907562.

[44] H. Murayama and A. Pierce, Phys. Rev. Lett. **89**, 271601 (2002), hep-ph/0206177.

[45] P. H. Gu and H. J. He, JCAP **0612**, 010 (2006) doi:10.1088/1475-7516/2006/12/010 [hep-ph/0610275].

[46] P. H. Gu, H. J. He and U. Sarkar, JCAP **0711**, 016 (2007) doi:10.1088/1475-7516/2007/11/016 [arXiv:0705.3736 [hep-ph]].

[47] P. H. Gu, H. J. He and U. Sarkar, Phys. Lett. B **659**, 634 (2008) doi:10.1016/j.physletb.2007.11.061 [arXiv:0709.1019 [hep-ph]].

[48] P. H. Gu and U. Sarkar, Phys. Rev. D **77**, 105031 (2008) doi:10.1103/PhysRevD.77.105031 [arXiv:0712.2933 [hep-ph]].

[49] P. H. Gu, Nucl. Phys. B **872**, 38 (2013) doi:10.1016/j.nuclphysb.2013.03.014 [arXiv:1209.4579 [hep-ph]].

[50] J. A. Casas, J. R. Espinosa and I. Navarro, JHEP **0309**, 048 (2003) [hep-ph/0306243].

[51] J. A. Casas, J. R. Espinosa, A. Ibarra and I. Navarro, Nucl. Phys. B **573**, 652 (2000) doi:10.1016/S0550-3213(99)00781-6 [hep-ph/9910420].

[52] D. V. Forero, M. Tortola and J. W. F. Valle, Phys. Rev. D **90**, no. 9, 093006 (2014) doi:10.1103/PhysRevD.90.093006 [arXiv:1405.7540 [hep-ph]].

[53] F. Capozzi, G. L. Fogli, E. Lisi, A. Marrone, D. Montanino and A. Palazzo, Phys. Rev. D **89** (2014) 9, 093018 [arXiv:1312.2878 [hep-ph]].

[54] M. C. Gonzalez-Garcia, M. Maltoni and T. Schwetz, JHEP **1411** (2014) 052 [arXiv:1409.5439 [hep-ph]].

[55] Private communication with Michael A. Schmidt.

[56] M. Lindner, M. Ratz and M. A. Schmidt, JHEP **0509**, 081 (2005), hep-ph/0506280.

[57] S. Antusch, J. Kersten, M. Lindner, M. Ratz and M. A. Schmidt, JHEP **0503**, 024 (2005), hep-ph/0501272.

[58] N. Craig, arXiv:1309.0528 [hep-ph].

[59] M. S. Athar *et al.* [INO Collaboration], INO-2006-01.

[60] K. Abe *et al.* [T2K Collaboration], Nucl. Instrum. Meth. A **659**, 106 (2011), arXiv:1106.1238.

[61] R. B. Patterson [NOvA Collaboration], Nucl. Phys. Proc. Suppl. **235-236**, 151 (2013), arXiv:1209.0716.

[62] C. Adams *et al.* [LBNE Collaboration], arXiv:1307.7335.

[63] E. Kearns *et al.* [Hyper-Kamiokande Working Group Collaboration], arXiv:1309.0184.

[64] S. -F. Ge and K. Hagiwara, arXiv:1312.0457.

[65] G. Drexlin, V. Hannen, S. Mertens and C. Weinheimer, Adv. High Energy Phys. **2013**, 293986 (2013), arXiv:1307.0101.

[66] C. Kraus, B. Bornschein, L. Bornschein, J. Bonn, B. Flatt, A. Kovalik, B. Ostrick and E. W. Otten *et al.*, Eur. Phys. J. C **40** (2005) 447 [hep-ex/0412056].

[67] V. N. Aseev *et al.* [Troitsk Collaboration], Phys. Rev. D **84** (2011) 112003 [arXiv:1108.5034 [hep-ex]].

[68] P. A. R. Ade *et al.* [Planck Collaboration], arXiv:1502.01589 [astro-ph.CO].

[69] B. Famaey and S. McGaugh, J. Phys. Conf. Ser. **437**, 012001 (2013) doi:10.1088/1742-6596/437/1/012001 [arXiv:1301.0623 [astro-ph.CO]].

[70] N. Haba, Europhys. Lett. **96**, 21001 (2011) doi:10.1209/0295-5075/96/21001 [arXiv:1107.4823 [hep-ph]].

[71] E. Ma, Mod. Phys. Lett. A **17**, 627 (2002) doi:10.1142/S0217732302006722 [hep-ph/0203238].

[72] K. S. Babu, E. Ma and J. W. F. Valle, Phys. Lett. B **552**, 207 (2003) doi:10.1016/S0370-2693(02)03153-2 [hep-ph/0206292].

[73] K. S. Babu, B. Dutta and R. N. Mohapatra, Phys. Rev. D **60**, 095004 (1999) doi:10.1103/PhysRevD.60.095004 [hep-ph/9812421].

[74] F. Gabbiani, E. Gabrielli, A. Masiero and L. Silvestrini, Nucl. Phys. B **477**, 321 (1996) doi:10.1016/0550-3213(96)00390-2 [hep-ph/9604387].

Conclusions

Spontaneous Symmetry Breaking (SSB) is a phenomenon where a symmetry in the basic laws of physics appears to be broken. In the language of Quantum Field Theory (QFT), a system is said to possess a symmetry that is spontaneously broken if the Lagrangian describing the dynamics of the system is invariant under these symmetry transformations, but the vacuum is not.

SSB is the corner stone of the Standard Model (SM) of particle physics, which is based on the gauge group $SU(3)_C \times SU(2)_L \times U(1)_Y$. It includes strong interactions under $SU(3)_C$, and weak interactions and the electromagnetic interactions, unified in the Electroweak interaction under the gauge group $SU(2)_L \times U(1)_Y$. Another building block of the SM is the Higgs mechanism through which, the would–be Goldstone bosons associated to the SSB combine with the massless gauge bosons and as result, the gauge bosons become massive. Furthermore, the fermions of the SM also get mass via the Yukawa interaction with the Higgs field. The only exception are neutrinos, which in the SM remain massless.

On the other hand, the Higgs mechanism is at work when the broken symmetry is a local symmetry however, this does not need always to be the case. When the symmetry is a global one, the Goldstone theorem takes the center stage which states that: *if a theory has a global symmetry of the Lagrangian, which is not a symmetry of the vacuum, then there must exist one massless boson, scalar or pseudoscalar, associated to each generator which does not annihilate the vacuum and having its same quantum numbers. These modes are referred to as Nambu-Goldstone bosons or simply as Goldstone bosons.*

In part one of the thesis we have worked on an example of the Goldstone theorem. Due to the fact that the QCD Lagrangian in the limit $m_u, m_d, m_s \to 0$ has an $SU(3)_L \times SU(3)_R$ or chiral global symmetry in the flavor space, which is spontaneously broken in nature to the subgroup $H = SU(3)_V$, one expects 8 Nambu-Goldstone bosons to appear. These bosons can be recognized as the pseudo–scalar mesons, which have acquired a small mass from the explicit symmetry breaking due to the small quark masses. As the dynamics of the pseudo–scalar mesons occurs in the energy range where the QCD coupling becomes non–perturbative, one needs to use effective field theory methods to deal with their dynamics. One such theory is ChPT. We have described ChPT and given an example of ChPT

at order p^6 that is, as the number of $O(p^6)$ operators increases dramatically, compared to the lower order Lagrangians, we have investigated if this Lagrangian is minimal or there is redundancy in its basis, in the chiral $SU(2)$ limit, without external scalar and pseudo–scalar sources. We have concluded that out of 27 measurable terms plus 2 contact terms in the even-intrinsic-parity sector, 25+2 terms are independent. The relations we have found are

$$4\,\mathcal{P}_{27} + 4\,\mathcal{P}_{28} - \mathcal{P}_{29} + \mathcal{P}_{30} - 2\,\mathcal{P}_{31} + 4\,\mathcal{P}_{32} - \mathcal{P}_{33} - \mathcal{P}_{39} + \mathcal{P}_{40} + 2\,\mathcal{P}_{41} - \mathcal{P}_{43} + \mathcal{P}_{44} - \mathcal{P}_{45} - 2\,\mathcal{P}_{51} - 2\,\mathcal{P}_{53} = 0\,, \tag{6.3}$$

$$8\,\mathcal{P}_1 - 2\,\mathcal{P}_2 + 6\,\mathcal{P}_3 - 20\,\mathcal{P}_{24} + 8\,\mathcal{P}_{25} + 12\,\mathcal{P}_{26} - 12\,\mathcal{P}_{27} - 28\,\mathcal{P}_{28} + 8\,\mathcal{P}_{36} - 8\,\mathcal{P}_{37} - 8\,\mathcal{P}_{39} + 2\,\mathcal{P}_{40} + 8\,\mathcal{P}_{41} - 8\,\mathcal{P}_{42} - 6\,\mathcal{P}_{43} = 0\,. \tag{6.4}$$

Also, the fact that these relations were already shown to exist analytically, confirms our method. Even if using this method, one finds relations which are not proved analytically, one can be sure that up to the given approximation, these are the only relations, which may or may not hold at the operator level. This simplifies a lot the task of the analytical proof, as these relations give a clue of what the coefficients of the would–be–analytical relations should be.

As we mentioned, in the SM neutrinos remain massless however, observations suggest that neutrinos oscillate in flavor space, and one introduces the PMNS matrix, in parallel to the CKM matrix for quarks, to quantify this oscillation. This on the other hand, dictates that neutrinos are massive and hence, one has to find a manner to give them mass by extending the SM. This has been done in two ways, assuming neutrinos are Dirac or Majorana particles and using the Higgs mechanism.

In part two of this thesis, we have considered an example of each type of neutrinos, namely Dirac and Majorana, in the context of the high scale mixing relation (HSMR), which states that the PMNS matrix and the CKM matrix are proportional at the high scale. In a compactified form a general relation among the leptonic and the quark mixing angles within the same generations is as following

$$\theta_{12} = \alpha_1^{k_1}\ \theta_{12}^q, \quad \theta_{13} = \alpha_2^{k_2}\ \theta_{13}^q, \quad \theta_{23} = \alpha_3^{k_3}\theta_{23}^q\,, \tag{6.5}$$

where k_i, with $i = (1, 2, 3)$ are real exponents. We refer to this relation as the HSMR. This is a generalization of the HSMU hypothesis, which suggest that these two matrices are unified at high scale. The HSMU hypothesis is a particular realization of the HSMR parametrization when we choose $\alpha_1 = \alpha_2 = \alpha_3 = 1$ for

$k_1 = k_2 = k_3 = 1$. Then, running the RG equations for the parameters of the PMNS and CKM matrices, we have been able to make some predictions for what the value of these parameters should be at low scale, both for the case of Dirac and Majorana neutrinos.

For the case when neutrinos are Majorana particles, we have some distinct predictions for correlations among the parameters of the PMNS matrix, which can be tested in the present and future neutrino experiments easily. If our predictions are confirmed by experiments, like GERDA, it would be a good hint of quark-lepton unification at high scale. Also, our analysis suggest that all results reported in the literature using the HSMU hypothesis, are a very small subset of our results with the HSMR hypothesis presented in our paper. In short the gist of our work on Majorana neutrinos is:

The HSMR parametrization that we have proposed and studied is a more general framework than the HSMU hypothesis which provides a very simple explanation of the observed large neutrino mixing. It can be tested by ongoing and future neutrino experiments, and if it is confirmed, it would be a good hint of quark-lepton unification at the high scale.

More specifically, we observe that the HSMU hypothesis represents the $\alpha = 1$ limit of the HSMR hypothesis and is constrained by the lowest allowed value of M_{ee} which is 0.384 MeV. Therefore, if the HSMU hypothesis is ruled out by experiments, the other HSMR cases with $\alpha \neq 1$ may survive.

All results reported in the literature using the HSMU hypothesis, are a very small subset of our results with the HSMR hypothesis presented in our paper. Apart from that, we have discovered new strong correlations among different experimental observables for every limit of the HSMR hypothesis which are easily testable in present ongoing experiments. For example, there is a strong correlation between Δm^2_{32} and M_{ee}. This correlation can be easily tested by the GERDA experiment. There are two more such correlations namely among θ_{12}, $\sum_i m_i$ and M_{ee} discussed in our work which are completely new and unexplored in the literature.

Furthermore, we have comprehensively studied a strong correlation between θ_{23} and θ_{13}, which was studied in a previous study in a specific limit. Since we have done a comprehensive full parameter scan, this correlation has become a robust band now. We have also repeated the calculation including the type one seesaw mechanism and showed that the previous results are stable.

For the case when neutrinos are Dirac particles, apart from precise predictions for the parameters of the PMNS matrix, our main achievement is that, the HSMU hypothesis is not compatible with Dirac neutrinos. Hence, the HSMR

parametrization as a more general realization of the HSMU hypothesis is the preferable framework to study the RG evolution of Dirac neutrinos. Also, the unification scale beyond the GUT scale is ruled out in our investigation, which can be useful for the GUT theories having Dirac neutrinos. In short our results can be summarized as follows:

We obtain strong correlations among different experimental observables. Our predictions for the mixing angles θ_{13}, θ_{23}, the averaged electron neutrino mass m_β, the Dirac CP phase δ and the sum of the three neutrino masses, $\sum m_i$ are precise and easily testable at some ongoing and future experiments.

The mixing angle θ_{23} is non-maximal and lies in the second octant for the SUSY breaking scale 2 TeV and the unification scale at the GUT scale. For the variation of the SUSY breaking scale and the unification scale, the mixing angle θ_{23} is non-maximal and lies in the first octant. The predictions for the mass square difference Δm^2_{31} are also well constrained and testable in experiments.

Furthermore, the Dirac CP phase has a precise range $168.7^\circ - 180^\circ$ at the unification scale 10^{12} GeV. At low scale our prediction for this observable is 80 to 287 degrees excluding some part of the allowed parameter space of this quantity. Since the phase δ is not known from experiments, any prediction of this important observable is of great interest. For the SUSY breaking scale 5 TeV, the Dirac CP phase δ is zero. The allowed range for the Jarlskog invariant J_{CP} is -0.27 to 0.27. Thus, a large CP violation is possible in our analysis.

And the last but not the least, the unification scale beyond the GUT scale is ruled out by our investigation. This fact could be useful for the GUT theories having Dirac neutrinos

7. Resumen de la Tesis

Física de ChPT

Objetivos

Debido al hecho de que los quarks y los gluones están confinados en el interior de los hadrones, son los hadrones los grados de libertad asintóticos que se observan en la física macroscópica. Por lo tanto, los estados inicial y final en nuestros experimentos de bajas energías no van a ser quarks y gluones sino hadrones sin carga de color.

Todavía no se sabe una transformacion del lagrangiano de QCD y sus parámetros y las propiedades de los hadrones. Un método ampliamente utilizado de afrontar el problema ha sido a través de teorías efectivas. En el caso de QCD, se llama ChPT.

Hay un teorema atribuido a Weinberg que dice [22]: Para un conjunto dado de estados asintóticos, el Lagrangiano más general que contiene todos los términos permitidos por las simetrías asumidas dará los elementos más generales de la matriz S consistentes con la analiticidad, la descomposición del cluster de unitaridad perturbativa y las simetrías asumidas. En otras palabras, independientemente de la teoría subyacente, cuando se conocen los grados de libertad y las simetrías relevantes para la escala de energía real, el lagrangiano efectivo construido a partir de ellos abordará la misma física de la teoría subyacente [23]. Así, al estudiar un fenómeno específico, es necesario aislar los ingredientes más relevantes del resto, de modo que se pueda obtener una descripción simple sin tener que entender todo [24]. Si un pequeño parámetro λ, también se realiza en la teoría efectiva, se pueden realizar cálculos perturbativos sobre este parámetro.

Sabiendo esto, uno seguiría adelante con la construcción de una teoría efectiva de interacciones fuertes a energías bajas donde el lagrangiano original de QCD se encuentra con el problema de que en el régimen, $p^2 \ll 1\ GeV^2$, donde la dinámica de los mesones tiene lugar, la constante de acoplamiento de QCD excede la unidad. En este régimen energético, las partículas fundamentales son hadrones en lugar de quarks y gluones. Para construir un Lagrangiano para un proceso que ocurre a una escala $p \ll \Lambda$, se puede utilizar una expansión en potencias de

p/Λ donde Λ es la energía de corte del modelo. Entonces, el Lagrangiano podría organizarse como una serie de potencias crecientes, es como

$$\mathcal{L} = \mathcal{L}_2 + \mathcal{L}_4 + ...\mathcal{L}_{2n}\,, \tag{7.1}$$

donde, el subíndice indica el orden del lagrangiano.

Se dice que el lagrangiano de QCD tiene una simetría aproximada $SU(3)_L \times SU(3)_R = G$ o simetría quiral. Por supuesto, los quarks son masivos y la simetría quiral no se realiza plenamente en la naturaleza sin embargo, para los tres quarks más ligeros u, d, s, se podría suponer que se mantiene de forma aproximada. Pero como esta simetría no es visible en el espectro de los hadrones ligeros [25], debe estar espontáneamente rota en la naturaleza debido a algún mecanismo de ruptura de simetría espontánea (SSB). Esto lleva a que la simetría global $SU(3)_L \times SU(3)_R = G$ se reduzca al subgrupo $H = SU(3)_V$.

Siendo este el caso, el teorema de Goldstone dicta que la diferencia entre el número original y el final de generadores, debería haberse convertido en bosones de Goldstone. En el caso que nos ocupa, el número de bosones de Goldstone es de 8. Como la simetría quiral también se rompe explícitamente debido a las masas de quarks en el lagrangiano de QCD, los bosones podrían ser reconocidos como los mesones pseudo escalares, que han adquirido una pequeña masa debido a esta ruptura de simetría explícita.

En QCD la simetría quiral global se rompe a través de las fuertes interacciones subyacentes, que conducen a un condensado de quarks. Este condensado formado por un quark y un antiquark es el parámetro de orden y se dice que el SSB correspondiente es una ruptura de simetría dinámica.

Considerando tres sabores de quarks, u, d y s, el lagrangiano de QCD restringido a estas condiciones es

$$\mathcal{L} = \sum_{j=u,d,s} \bar{\psi_j}(i\gamma^\mu\partial_\mu + g_s\mathbf{G}^\mu\gamma_\mu - m_i)\psi_j - \frac{1}{4}G_{\mu\nu}G^{\mu\nu}\,, \tag{7.2}$$

donde ψ es un vector en el espacio de sabores (u,d,s). Su descomposición en helicidades left y right responde a

$$\psi_L = \frac{1}{2}(1-\gamma_5)\psi \qquad \psi_R = \frac{1}{2}(1+\gamma_5)\psi\,. \tag{7.3}$$

En primer lugar este lagrangiano es invariante bajo las simetrias discretas siguientes: paridad (P), conjugación de carga (C), inversión del tiempo (T). Pero

lo importante es que también presenta invariancia bajo la simetría quiral global en el espacio de sabor $SU(3)_L \times SU(3)_R$.

Como ChPT es la teoría efectiva de QCD, su lagrangiano debe satisfacer las mismas simetrías. Es decir, invariancia bajo paridad, conjugación de carga, inversión temporal e invariancia bajo transformaciones, $SU(3)_L \times SU(3)_R$.

Con estas simetrías podemos construir el lagrangiano invariante más general posible y organizarlo como una serie de potencias en momentos (i.e. en número de derivadas). Debido a la invariancia bajo paridad los términos de la serie corresponderán siempre a números de potencias pares. El primer término de este desarrollo en serie es

$$\mathcal{L}_2 = \frac{F^2}{4} Tr(D_\mu U^\dagger D^\mu U) + \frac{F^2}{4} Tr(U\chi^\dagger + \chi U^\dagger) \tag{7.4}$$

Los diagramas a un loop con vértices de $\mathcal{L}_2$ dan lugar a contribuciones de orden p^4. Pero también tendremos contribuciones de orden p^4 provenientes directamente de $\mathcal{L}_4$. Imponiendo las mismas simetrías que en el caso de $\mathcal{L}_2$ el lagrangiano más general posible de orden p^4 es el siguiente:

$$\begin{aligned}
\mathcal{L}_4 \;=\; & L_1\langle D_\mu U^\dagger D^\mu U\rangle^2 + L_2\langle D_\mu U^\dagger D_\nu U\rangle\langle D^\mu U^\dagger D^\nu U\rangle + L_3\langle D^\mu U^\dagger D_\mu U D^\nu U^\dagger D_\nu U\rangle \\
& + L_4\langle D^\mu U^\dagger D_\mu U\rangle\langle \chi^\dagger U + \chi U^\dagger\rangle + L_5\langle D^\mu U^\dagger D_\mu U(\chi^\dagger U + U^\dagger\chi)\rangle \\
& + \; L_6\langle \chi^\dagger U + \chi U^\dagger\rangle^2 + L_7\langle \chi^\dagger U - \chi U^\dagger\rangle^2 + L_8\langle \chi^\dagger U\chi^\dagger U + \chi U^\dagger\chi U^\dagger\rangle \\
& - \; iL_9\langle F^R_{\mu\nu} D^\mu U D^\nu U^\dagger + F^L_{\mu\nu} D^\mu U^\dagger D^\nu U\rangle + L_{10}\langle U^\dagger F^R_{\mu\nu} U F^{L\mu\nu}\rangle\,,
\end{aligned} \tag{7.5}$$

donde

$$\begin{aligned}
F^R_{\mu\nu} &= \partial^\mu r^\nu - \partial^\nu r^\mu - i[r^\mu, r^\nu]\,, \\
F^L_{\mu\nu} &= \partial^\mu \ell^\nu - \partial^\nu \ell^\mu - i[\ell^\mu, \ell^\nu]\,.
\end{aligned} \tag{7.6}$$

Como puede verse, el lagrangiano de $O(p^2)$ depende de dos acoplamientos de baja energía, mientras que el lagrangiano de $O(p^4)$ introduce (siete) diez constantes de acoplamiento para dos (tres) sabores de los quarks. Las predicciones de los lagrangios anteriores están en buen acuerdo con los experimentos. Por ejemplo, las predicciones de $O(p^4)$ para las constantes de desintegración del mesón y el radio electromagnético del mesón están en bastante buen acuerdo con las observaciones experimentales [24]. Además, las divergencias de las contribuciones de un lazo se absorben con el lagrangiano de $O(p^4)$. Sin embargo, la precisión requerida

en las aplicaciones fenomenológicas lleva a tomar en cuenta las correcciones del orden siguiente, $O(p^6)$.

El lagrangiano de $O(p^6)$ para 2(3) sabores introduce 53(90) nuevos términos y 4(4) términos de contacto, que en comparación con los Lagrangianos de orden inferior es un gran número y los patrones muestran que al ir a órdenes superiores, este número aumentará aún más. Por completitud hemos mostrado los términos de lagrangiano $O(p^6)$ en el Apéndice. La cuestión es, ahora que uno tiene que lidiar con un número tan grande de términos, ¿se sabe con seguridad que no hay redundancia en la base del lagrangiano?

El objetivo del presente trabajo es presentar un método para encontrar relaciones entre los operadores del lagrangiano mesónico de la Teoría de Perturbación Quiral de orden p^6. El procedimiento se puede utilizar para establecer si la base de los operadores en el Lagrangiano es mínima. Como ejemplo, aplicamos el método al caso de dos sabores en ausencia de fuentes escalares y pseudo-escalares ($s = p = 0$), y concluimos que el Lagrangiano mínimo contiene 27 operadores independientes.

Metodología

Para decirlo simplemente, calculamos las funciones de Green para una configuración cinemática arbitraria, a la cual contribuyen todos o algunos de los operadores dados, es decir, los operadores que están incluidos en la base elegida. Entonces, exigimos que la función de Green desaparezca y por lo tanto, la base es mínima cuando no existe relación entre los coeficientes de los operadores. Si se encuentran nuevas relaciones para un proceso, sólo son válidas para ese proceso. Al resolver las relaciones para todos los procesos juntos, se llega a relaciones generales que incluyen a todos los operadores involucrados. Pero, aun así, no hay garantía de que esos operadores pertenezcan al subconjunto mínimo hasta que se dé la prueba analítica. Sin embargo, la ventaja es que la prueba algebraica se simplifica grandemente, cuando los coeficientes son conocidos.

$$\langle 0|\, T\, \phi(x_1)\phi(x_2)\ldots f_1(y_1)f_2(y_2)\ldots \Big(\int d^4x \sum_i \alpha_i\, \mathcal{P}_i(x)\Big)|0\rangle = 0\,, \tag{7.7}$$

donde α_i son números reales o complejos, ϕ un número arbitrario de campos piónicos y $f_i = v,\ a,\ s,\ p$ fuentes externas.

Uno necesita calcular siete funciones de Green, a saber

$$\langle vv\rangle,\ \langle vaa\rangle,\ \langle vv\,2\pi\rangle,\ \langle aa\,2\pi\rangle, \langle v\,4\pi\rangle, \langle 6\pi\rangle, \langle vva\pi\rangle\,. \tag{7.8}$$

Resultados del Primer Artículo (el Capítulo 4)

Combinando las ecuaciones para α_i encontradas para las diferentes funciones de Green obtenemos

$$\begin{aligned} 4\,\mathcal{P}_{27} + 4\,\mathcal{P}_{28} - \mathcal{P}_{29} + \mathcal{P}_{30} - 2\,\mathcal{P}_{31} + 4\,\mathcal{P}_{32} - \mathcal{P}_{33} - \mathcal{P}_{39} + \mathcal{P}_{40} + 2\,\mathcal{P}_{41} \\ - \mathcal{P}_{43} + \mathcal{P}_{44} - \mathcal{P}_{45} - 2\,\mathcal{P}_{51} - 2\,\mathcal{P}_{53} = 0\,, \end{aligned} \tag{7.9}$$

$$\begin{aligned} 8\,\mathcal{P}_1 - 2\,\mathcal{P}_2 + 6\,\mathcal{P}_3 - 20\,\mathcal{P}_{24} + 8\,\mathcal{P}_{25} + 12\,\mathcal{P}_{26} - 12\,\mathcal{P}_{27} - 28\,\mathcal{P}_{28} + 8\,\mathcal{P}_{36} - 8\,\mathcal{P}_{37} \\ -8\,\mathcal{P}_{39} + 2\,\mathcal{P}_{40} + 8\,\mathcal{P}_{41} - 8\,\mathcal{P}_{42} - 6\,\mathcal{P}_{43} = 0\,. \end{aligned} \tag{7.10}$$

Pero, estas relaciones ya se demostró que existen analíticamente en Refs. [26, 27] en el límite quiral $SU(2)$. Por lo tanto, utilizando nuestro método hemos concluido que éstas son las únicas relaciones de operador que pueden existir en el límite que hemos estudiado y la base original de 27 términos medibles más 2 términos de contacto, tiene $25+2$ términos independientes. Además, el hecho de que sean probados analíticamente también, confirma nuestro método. El punto es que, incluso si las dos relaciones no hubiesen sido probadas analíticamente, nuestro método debería ser útil para asegurar que hasta esta aproximación hay dos relaciones y para asegurarse de que se mantienen en el nivel del operador.

También vale la pena mencionar que, los procesos con más de 6 patas de mesones o que implican más de dos vectores o vector y axial no son realizables experimentalmente. Por lo tanto, el método puede utilizarse para reducir el número de operadores que se utilizan para calcular funciones específicas de Green, sin exigir la prueba analítica de las relaciones a nivel de operador.

Física de los Neutrinos

Objetivos

El Modelo Estándar (SM) de la física de partículas es uno de los modelos más exitosos de la física moderna, basado en el grupo $SU(3)_C \times SU(2)_L \times U(1)_Y$, que describe las partículas fundamentales y sus interacciones. Incluye interacciones fuertes bajo $SU(3)_C$, interacciones débiles y las interacciones electromagnéticas,

unificadas en la interacción Electrodébil bajo el grupo $SU(2)_L \times U(1)_Y$. Una revisión pedagógica de SM se puede encontrar en la referencia [1]. También, contiene tres familias de quarks y leptones, tres bosones masivos $W^{\pm}$, Z y el fotón para el caso electrodébil, y ocho gluones sin masa para la interaccion fuerte. El fotón y los gluones no tienen masa, pero el resto de las partículas son masivas y obtienen la masa a traves de sus interacciones con el campo escalar del Higgs.

Aunque el SM es muy exitoso, sabemos que no puede ser la descripción final de la naturaleza. A pesar de sus predicciones muy precisas, hay una serie de observaciones que no entran dentro del alcance de lo que el SM puede describir. El problema más abrumador del SM es el hecho de que no contiene gravedad.

Otro tema que es más relevante para nuestro trabajo es que no hay masas de neutrinos en el modelo. Por otra parte, es necesario dar masas a los neutrinos para describir las oscilaciones. Como predijo Bruno Pontecorvo [2] hace muchos años, cuando los neutrinos son masivos, la oscilación del sabor ocurrirá para los neutrinos en el vacío. Esto significa que los autoestados del Hamiltoniano libre no son los mismos que los del Hamiltoniano de interacciones. La probabilidad de oscilación es

$$P(\nu_A \to \nu_B; L) \simeq \sum_{j,k} U^*_{Aj} U_{Bj} U_{Ak} U^*_{Bk} e^{-i\frac{\Delta m^2_{jk} L}{2E}} . \tag{7.11}$$

Este probabilidad depende del matriz de mezcla Pontecorvo-Maki-Nakagawa-Sakata [2, 3]. Para el caso de dos sabores de neutrinos se escribe como

$$P(\nu_e \to \nu_\mu; L) = \sin^2 2\,\theta \sin^2[\frac{\Delta m^2_{12}}{4E} L]\} \tag{7.12}$$

Eso depende de las diferencias de masas de los neutrinos ($\Delta m^2_{12} = m^2_1 - m^2_2$) y de la energia E. Se ve que la probabilidad de oscilaciones de neutrinos no es sensible a las masas absolutas de los neutrinos sino solo a sus diferencias. Los resultados de varios experimentos demuestran que, $\Delta m^2_{Sol} = \Delta m^2_{12} = 10^{-5}$ eV, $\Delta m^2_{atm} = \Delta m^2_{23} = 10^{-3}$ eV. Ademas, los tres ángulos ya han sido medidos pero la fase de CP permanece indeterminada. Aparte de esto, no se sabe cual es la jerarquia de las masas, normal (NH) e invertida (IH), representadas en la Fig. 7.1

Muchos experimentos han sido planeados y construidos para medir estos parámetros y los resultados actuales se ven en la Tabla 7.1. De los experimentos

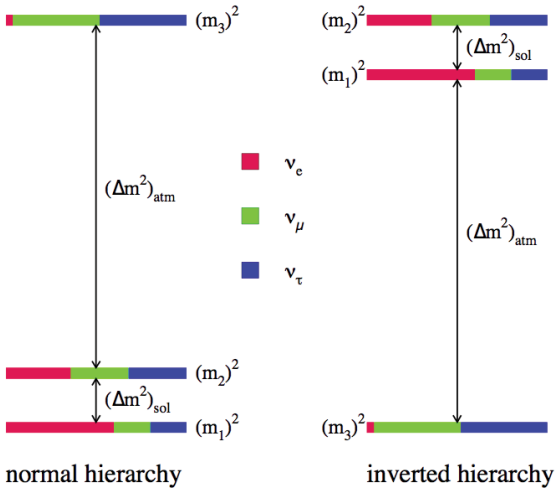

Figure 7.1: Representacion de las jerarquías normal (NH), invertida (IH).

Quantity	Best Fit	3σ Range
Δm^2_{21} $(10^{-5}$ eV$^2)$	7.60	7.1 – 8.16
Δm^2_{31} $(10^{-3}$ eV$^2)$	2.46	2.30 – 2.59
θ°_{12}	33.02	30 – 36.5
θ°_{23}	48.9	38 – 51.7
θ°_{13}	8.41	7.82– 9.02

Table 7.1: Datos globales de ocilacion de neutrinos [4].

como la desintegración beta, se puede medir la masa absoluta de los neutrinos.

$$m_{\nu_e} < 2.2 \text{ eV} \qquad [5] \text{ a} \qquad 2\sigma\,, \tag{7.13}$$

Si son de Majorana, $M_{e\,e} \leq 0.4$ eV [8].

El límite que proviene de análisis cosmológicos para la suma de masas de los neutrinos es [9]

$$\sum_j m_j \leq 0.57 \text{ eV}\,. \tag{7.14}$$

Este límite es más fuerte pero depende de los modelos que se usan.

Hay dos maneras de dar masa a los neutrinos, dependiendo de si son partículas de Majorana o Dirac. El término de masa de Majorana se permite sólo para partículas elćtricamente neutras ya que de lo contrario violaría la conservación de la carga. Por lo tanto, se cree comúnmente que los únicos candidatos a tener una masa de Majorana en el SM son los neutrinos. Por otra parte, en el contexto del SM la masa de Majorana para los neutrinos zurdos no está permitida debido a la invariancia $SU(2)$. Esto se puede resolver mediante el mecanismo de Higgs y la introducción del operador de Weinberg

$$\mathcal{L}_\kappa = \frac{1}{4}\kappa_{gf}\,\overline{\ell^{\rm c}_{{\rm L}c}}^{g}\varepsilon^{cd}\phi_d\;\ell^{f}_{{\rm L}b}\varepsilon^{ba}\phi_a + \text{h.c.}\,. \tag{7.15}$$

Este operador no es renormalizable. Por lo tanto para altas energías, se usa el modelo seesaw que tiene varios tipos.

El lagrangiano que describe la masa de los neutrinos se escribe como

$$\mathcal{L}_{Mass} = -\frac{1}{2}M_R\overline{\psi^{\rm c}_R}\psi_R - M_D\overline{\psi_R}\psi_L + h.c.\,, \tag{7.16}$$

donde el último término es de masa de Dirac, y se genera cuando el campo de Higgs obtiene su valor esperado de vacío, v, o sea, cuando se rompe la simetría electrodébil. Sin embargo, la masa de Majorana puede existir, independintemente de ello. De este lagrangiano se obtienen las masas M_1 y M_2

$$M_{1,2} = \frac{M_R}{2} \pm \sqrt{\frac{M_R^2}{4} + M_D^2}\,, \tag{7.17}$$

y asumiendo que $M_R \gg M_D$, los neutrinos ligeros tienen la masa:

$$M_1 \simeq \frac{M_D^2}{M_R}\,, \tag{7.18}$$

y los neutrinos pesados la masa

$$M_2 \simeq M_R\,. \tag{7.19}$$

Este es el mechanismo seesaw y significa que si la masa de Majorana M_R , es suficientemente alta, se pueden explicar las masas tan pequeñas de los neutrinos, mientras que los acoplamientos de Yukawa pueden ser de $O(1)$. Existe un experi-

mento para saber si los neutrinos son de Majorana, que es la desintegración beta doble sin neutrinos ($0\nu\beta\beta$), Fig. 7.2.

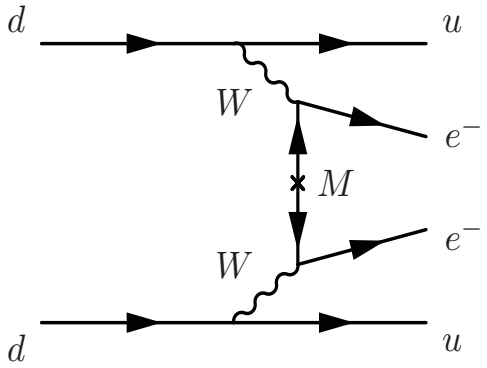

Figure 7.2: La desintegracion beta doble sin neutrinos

Utilizando la analogía con el caso de los quarks, donde los autoestados débiles son diferentes de los autoestados masivos y por lo tanto

$$\begin{pmatrix} d' \\ s' \\ b' \end{pmatrix} = V^{CKM} \begin{pmatrix} d \\ s \\ b \end{pmatrix} \quad . \tag{7.20}$$

uno puede escribir

$$\begin{pmatrix} \nu_e \\ \nu_\mu \\ \nu_\tau \end{pmatrix} = U^{PMNS} \begin{pmatrix} \nu_1 \\ \nu_2 \\ \nu_3 \end{pmatrix} \quad . \tag{7.21}$$

con

$$U_{PMNS} = = \begin{pmatrix} c_{12}c_{13} & s_{12}c_{13} & s_{13}e^{-i\delta} \\ -c_{23}s_{12} - s_{23}s_{13}c_{12}e^{i\delta} & c_{23}c_{12} - s_{23}s_{13}s_{12}e^{i\delta} & s_{23}c_{13} \\ s_{23}s_{12} - c_{23}s_{13}c_{12}e^{i\delta} & -s_{23}c_{12} - c_{23}s_{13}s_{12}e^{i\delta} & c_{23}c_{13} \end{pmatrix} \cdot F' \tag{7.22}$$

donde, $c_{mn} = \cos\theta_{mn}, s_{mn} = \sin\theta_{mn}$ y δ es el fase de Dirac. La matriz $F' = Diag\{e^{i\varphi_1}, e^{i\varphi_2}, 1\}$ introduce las fases de Majorana.

Sabiendo todo eso, se puede preguntar, si U_{PMNS} y V_{CKM} están relacionadas de alguna manera. En el Refs. [6, 7], suponiendo que la masa de los neutrinos es

casi degenerada y jerárquica, sugirieron que en la escala de unificación existe la siguiente relación entre los ángulos de mezcla de los quarks y los neutrinos

$$\theta_{12} = \theta^q_{12},\ \theta_{13} = \theta^q_{13},\ \theta_{23} = \theta^q_{23}, \tag{7.23}$$

donde θ_{ij} (with $i, j = 1, 2, 3$) son los ángulos leptónicos y θ^q_{ij} los de los quarks. Luego, usando las écuaciones de RG, corriendo los parámetros hasta la M_Z, obtienen sus valores, los cuales se pueden comparar con los datos experimentales actuales.

Aquí, inspirados por la hipótesis HSMU, hacemos la pregunta: ¿por qué la relación entre CKM y PMNS debería ser exactamente igual en la escala alta? De hecho, no hay simetría para evitar que sean proporcionales. A partir de aquí postulamos relaciones más generales entre los ángulos de mezcla en la escala de unificación. La relación más general es

$$\theta_{12} = \alpha_1^{k_1}\ \theta^q_{12},\quad \theta_{13} = \alpha_2^{k_2}\ \theta^q_{13},\quad \theta_{23} = \alpha_3^{k_3}\theta^q_{23}. \tag{7.24}$$

Donde k_i, con $i = (1, 2, 3)$ son exponentes reales. Nos referimos a esta relación como la "relación de mezcla a gran escala" (HSMR). Hemos elegido $(k_1, k_2, k_3) = (1, 1, 1)$ para nuestro análisis.

Metodología

El funcionamiento de la hipótesis HSMR es el siguiente: La implementación de la hipótesis HSMR requiere el modelo estándar supersimétrico mínimo (MSSM) como una extensión del modelo estándar (SM). Primero se desarrollan los ángulos de mezcla de los quark desde la escala baja (masa del bosón Z) hasta la escala de ruptura de supersimetría (SUSY) usando las ecuaciones de RG de SM. Después de eso, desde la escala de ruptura SUSY hasta la escala de unificación, la evolución de los ángulos de mezcla de los quarks se rige por las ecuaciones de RG de MSSM. En el siguiente paso, los ángulos de mezcla de quarks en la escala de unificación, se ponen proporcionales a los de los neutrinos siguiendo la hipótesis HSMR. Los parámetros de mezcla leptónica corren desde la escala de unificación hasta la escala de ruptura SUSY usando las ecuaciones de RG de MSSM. Desde la escala de ruptura SUSY hasta la escala baja, los parámetros de mezcla se desarrollan a través de las ecuaciones de RG de SM.

De hecho, la naturaleza de los neutrinos es aún desconocida. Podrían ser igualmente Dirac o Majorana en naturaleza. Por lo tanto, desde el punto de vista fenomenológico, los neutrinos de Dirac son tan importantes como los neutrinos de Majorana. Hay muchos experimentos importantes en curso para probar la

naturaleza de los neutrinos [8, 11]. Los datos cosmológicos tampoco prefieren los neutrinos de Majorana o Dirac [12]– [13].

En el primer trabajo, utilizando la parametrización de HSMR hemos explicado el patrón observado de la mezcla de neutrinos asumiendo que son de naturaleza Majorana. Para los neutrinos de Majorana, hemos investigado los casos:

$$\textbf{Case 1}: \quad \theta_{12} = \alpha\ \theta^q_{12}, \quad \theta_{13} = \theta^q_{13}, \quad \theta_{23} = \theta^q_{23}, \tag{7.25}$$
$$\textbf{Case 2}: \quad \theta_{12} = \theta^q_{12}, \quad \theta_{13} = \alpha\ \theta^q_{13}, \quad \theta_{23} = \theta^q_{23}, \tag{7.26}$$
$$\textbf{Case 3}: \quad \theta_{12} = \theta^q_{12}, \quad \theta_{13} = \theta^q_{13}, \quad \theta_{23} = \alpha\ \theta^q_{23}, \tag{7.27}$$
$$\textbf{Case 4}: \quad \theta_{12} = \alpha\ \theta^q_{12}, \quad \theta_{13} = \alpha\ \theta^q_{13}, \quad \theta_{23} = \theta^q_{23}, \tag{7.28}$$
$$\textbf{Case 5}: \quad \theta_{12} = \theta^q_{12}, \quad \theta_{13} = \alpha\ \theta^q_{13}, \quad \theta_{23} = \alpha\ \theta^q_{23}, \tag{7.29}$$
$$\textbf{Case 6}: \quad \theta_{12} = \alpha\ \theta^q_{12}, \quad \theta_{13} = \theta^q_{13}, \quad \theta_{23} = \alpha\ \theta^q_{23}, \tag{7.30}$$
$$\textbf{Case 7}: \quad \theta_{12} = \alpha\ \theta^q_{12}, \quad \theta_{13} = \alpha\ \theta^q_{13}, \quad \theta_{23} = \alpha\ \theta^q_{23}. \tag{7.31}$$

En el segundo trabajo, investigamos las consecuencias de la parametrización de HSMR utilizando la evolución RG de los neutrinos de Dirac y se investiga en primer lugar si existe un espacio de parámetros con la parametrización de HSMR donde la evolución RG de los neutrinos de Dirac puede dar una explicación satisfactoria para la mezcla de neutrinos grandes con la observación de θ_{13}. En segundo lugar, ¿cuál es el estado de la hipótesis de HSMU para los neutrinos de Dirac? Y en tercer lugar, ¿cuál es el estado de la fase leptónica de CP a este respecto?

Para los neutrinos de Dirac no hay mucho espacio de parámetros en la escala alta.

Resultados del Segundo Artículo (el Capítulo 5)

- Hemos propuesto y estudiado la hipótesis HSMR que es más general que la hipótesis HSMU.
- La hipótesis de HSMR ofrece una explicación muy simple de los parámetros de la mezcla de neutrinos observada. Los actuales y futuros experimentos con neutrinos pueden fácilmente probar las predicciones de nuestro trabajo. Si nuestras predicciones son confirmadas por experimentos, como GERDA, sería un buen indicio de unificación de quark-lepton a gran escala.
- Observamos que la hipótesis HSMU representa el límite $\alpha = 1$ de la hipótesis HSMR y está limitada por el valor más bajo permitido de M_{ee} que es $0.384\ \mathrm{M}eV$. Por lo tanto, si la hipótesis de HSMU es descartada por experimentos, como GERDA, los otros casos de HSMR con $\alpha \neq 1$ pueden

sobrevivir y su confirmación sería un fuerte indicio de la proporcionalidad de ángulos de mezcla, que es el base de la hipótesis HSMR.

- Hemos hecho un estudio riguroso, exhaustivo y completo con la hipótesis HSMR que no existe en la literatura. Todos los resultados publicados en la literatura usando la hipótesis de HSMU, son un subconjunto muy pequeño de nuestros resultados con la hipótesis de HSMR presentada en nuestro artículo. Además, también hemos comparado a fondo la hipótesis HSMR con respecto a la HSMU.
- En nuestro trabajo, hemos descubierto nuevas correlaciones fuertes entre diferentes observables experimentales para cada límite de la hipótesis de HSMR. Estas correlaciones no existen en la literatura y son fácilmente comprobables en los actuales experimentos en curso. Por ejemplo, existe una fuerte correlación entre Δm^2_{32} y M_{ee}. Esta correlación puede ser fácilmente probada por el experimento GERDA. Hay dos correlaciones más, a saber, entre θ_{12}, Σm_i y M_{ee} discutidas en nuestro trabajo que son completamente nuevas.
- Además, hemos estudiado exhaustivamente una fuerte correlación entre θ_{23} y θ_{13} y las predicciones pueden ser fácilmente probadas en los actuales experimentos en curso. Esta correlación se estudió en un estudio previo en un límite específico. Dado que hemos hecho un análisis completo de parámetros completo, esta correlación se ha convertido en una banda robusta ahora.

Resultados del Tercer Artículo (el Capítulo 6)

- El principal logro de este trabajo es que la evolución RG de los neutrinos de Dirac podría explicar la mezcla de neutrinos incluyendo la observación del valor pequeño y no nulo del ángulo de mezcla θ_{13}. Se obtienen correlaciones fuertes entre diferentes observables experimentales.
- Nuestras predicciones para los ángulos de mezcla θ_{13}, θ_{23}, "promedio de masa de neutrino de electrones" m_β, Dirac CP fase δ y las suma de tres masas de neutrinos, Σm_i son precisas y fácilmente comprobables en los experimentos en curso y futuros como INO, T2K, NOVA, LBNE, Hyper-K, PINGU y KATRIN [14], [15]. El ángulo de mezcla θ_{23} no es máximo y se encuentra en el segundo octante para la escala de ruptura SUSY 2 TeV y la escala de unificación en la escala GUT.
- Para la variación de la escala de ruptura SUSY y la escala de unificación, el ángulo de mezcla θ_{23} no es máximo y se encuentra en el primer octante. Las predicciones para la diferencia cuadrática de masa Δm^2_{31} también están

bien restringidas y son comprobables en experimentos. Proponemos que la fase δ_{Dirac} sea cero para la escala de ruptura SUSY 5 TeV. Además, la fase de Dirac CP tiene un rango preciso de $168.7° - 180°$ en la escala de unificación 10^{12} GeV. La escala de unificación más allá de la escala GUT está descartada en nuestra investigación. Este hecho podría ser útil para las teorías de GUT que tienen neutrinos de Dirac [16]- [17].

- Observamos que hemos investigado la evolución RG de los parámetros de mezcla de neutrinos. Es crucial ya que la evolución de RG de un bucle es insuficiente para proporcionar la mejora requerida de los ángulos de mezcla que a su vez, no pueden producir los resultados obtenidos en este trabajo.
- Una de las principales consecuencias de nuestra investigación es que la hipótesis HSMU no es compatible con los neutrinos de Dirac debido a los datos experimentales actualizados [18–20] y un mejor algoritmo utilizado en el paquete REAP [21]. La hipótesis HSMU es una realización particular de la parametrización HSMR cuando elegimos $\alpha_1 = \alpha_2 = \alpha_3 = 1$ para $k_1 = k_2 = k_3 = 1$. Por lo tanto, la parametrización HSMR es uno de los marcos preferibles para estudiar la evolución RG de los neutrinos de Dirac ahora.

Bibliography

[1] A. Pich, arXiv:0705.4264 [hep-ph].

[2] B. Pontecorvo, Sov. Phys. JETP **26** 984 (1968) [Zh. Eksp. Teor. Fiz. **53**, 1717 (1968)].

[3] Z. Maki, M. Nakagawa and S. Sakata, Prog. Theor. Phys. **28**, 870 (1962).

[4] F. Capozzi et al.,arXiv:1601.07777.

[5] V. N. Aseev *et al.* [Troitsk Collaboration], Phys. Rev. D **84** 112003 (2011) [arXiv:1108.5034 [hep-ex]].

[6] R. N. Mohapatra, M. K. Parida and G. Rajasekaran, Phys. Rev. D **69** 053007 (2004) [hep-ph/0301234].

[7] R. N. Mohapatra, M. K. Parida and G. Rajasekaran, Phys. Rev. D **72** 013002 (2005) [hep-ph/0504236].

[8] M. Agostini *et al.* [GERDA Collaboration], Phys. Rev. Lett. **111**, 122503 (2013), arXiv:1307.4720.

[9] P.A.R. Ade et al., [Planck Collab.], arXiv:1502.01589.

[10] Z. Maki, M. Nakagawa and S. Sakata, Prog. Theor. Phys. **28**, 870 (1962).

[11] F. Alessandria, E. Andreotti, R. Ardito, C. Arnaboldi, F. T. Avignone, III, M. Balata, I. Bandac and T. I. Banks *et al.*, arXiv:1109.0494.

[12] K. Dick, M. Lindner, M. Ratz and D. Wright, Phys. Rev. Lett. **84**, 4039 (2000), hep-ph/9907562.

[13] P. H. Gu, Nucl. Phys. B **872**, 38 (2013) doi:10.1016/j.nuclphysb.2013.03.014 [arXiv:1209.4579 [hep-ph]].

[14] G. Drexlin, V. Hannen, S. Mertens and C. Weinheimer, Adv. High Energy Phys. **2013**, 293986 (2013), arXiv:1307.0101.

[15] K. Abe *et al.* [T2K Collaboration], Nucl. Instrum. Meth. A **659**, 106 (2011), arXiv:1106.1238.

[16] E. Ma and R. Srivastava, Phys. Lett. B **741**, 217 (2015) [arXiv:1411.5042 [hep-ph]].

[17] R. N. Mohapatra, S. Antusch, K. S. Babu, G. Barenboim, M. -C. Chen, S. Davidson, A. de Gouvea and P. de Holanda *et al.*, hep-ph/0412099.

[18] F. Capozzi, G. L. Fogli, E. Lisi, A. Marrone, D. Montanino and A. Palazzo, Phys. Rev. D **89**, 9 (2014) [arXiv:1312.2878 [hep-ph]].

[19] M. C. Gonzalez-Garcia, M. Maltoni and T. Schwetz, JHEP **1411** 052 (2014). [arXiv:1409.5439 [hep-ph]].

[20] D. V. Forero, M. Tortola and J. W. F. Valle, Phys. Rev. D **90** 9 (2014), 093006 [arXiv:1405.7540 [hep-ph]].

[21] Private communication with Michael A. Schmidt.

[22] S. Weinberg, Physica A **96**, 327 (1979).

[23] M. Z. Abyaneh, arXiv:1208.2554 [hep-ph].

[24] A. Pich, Chiral Perturbation Theory, Rept. Prog. Phys. **58**, 563 (1995).

[25] S. Scherer , Adv. Nucl. Phys. **27** 277 (2003).

[26] C. Haefeli, M. A. Ivanov, M. Schmid and G. Ecker, arXiv:0705.0576 [hep-ph].

[27] P. Colangelo, J. J. Sanz-Cillero and F. Zuo, JHEP **1211** 012 (2012). [arXiv:1207.5744 [hep-ph]].

Acknowledgements

I would like to thank my supervisor for very helpeful comments about my questions, his liberal approach and all his support. I would like to thank Jorge Portolés for his useful comments on my questions and all his help from the first day. Many thanks to my colleague Pedro Ruiz-Femenía, for his collaboration in the paper on Chiral Perturbation Theory, and all I learned from him. Many thanks to Gauhar Abbas for collaboration in two of the papers of this work about the Neutrino Physics and all I learned from him. I would like to thank my colleages Aritra Biswas, Saurabh Gupta, Monalisa Patra, G. Rajasekaran and Rahul Srivastava with whom I collaborated in papers on Neutrino Physics. I would like to thank all my family, especially my dear mother for her infinite patience and support that helped me get here. Last, but not least, I would like to thank all my friends and colleagues Alejandro Celis, Javier Fuentes, Marija Kekić and of course Victor Ilisie, for very helpful descussions and so many helps they gave to me.

This work has been supported in part by the Spanish Government, by ERDF funds from EU Commission [grants FPA2011-23778, FPA2014-53631-C2-1-P] and a Grisolia fellowship from GV.